Mass Balance and 3D Model of PAHs in Boston's Inner Harbor

by

Ricardo N. Petroni
Ingeniero Hidráulico, 1993
Ingeniero Civil, 1994
Universidad Nacional de La Plata, Argentina

Peter H. Israelsson
Environmental Engineering , B.A., 1995
English, B.A., 1995
Lafayette College

Submitted to the Department of Civil and Environmental Engineering
In Partial Fulfillment of the Requirements for the Degree of

MASTER OF ENGINEERING
IN CIVIL AND ENVIRONMENTAL ENGINEERING
at the
MASSACHUSETTS INSTITUTE OF TECHNOLOGY
June 1998

Signature of the Authors_____
Department of Civil and Environmental Engineering
May 20, 1998

Certified by_____
E. Eric Adams
Senior Research Engineer
Thesis Supervisor

Certified by_____
Joseph M. Sussman
Chairman, Departmental Committee on Graduate Studies

Mass Balance and 3D Model of PAHs in Boston's Inner Harbor

by

Ricardo N. Petroni **Peter H. Israelsson**

Submitted to the Department of Civil and Environmental Engineering
In Partial Fulfillment of the Requirements for the Degree of
Master of Engineering in Civil and Environmental Engineering
June, 1998

ABSTRACT

The present study focuses on predicting the long term changes in water column concentrations of polycyclic aromatic hydrocarbons (PAHs) in Boston's Inner Harbor which may result from the sediment dredging scheduled to occur in conjunction with the Navigation Improvement Project. It has been suggested that sediment flux is one of the primary sources of PAH loading to the water column. Three representative PAHs were selected based on their spectrum of molecular weights, including naphthalene, pyrene, and benzo[a]pyrene.

Two types of models were created to establish present conditions and predict future changes in PAH concentrations. A simple "box" model was constructed to predict an average steady-state concentration for the entire study area. This model provided a useful tool by which the relative importance of various sources and sinks of PAHs could be evaluated. The physical and chemical processes incorporated into the model included river, combined sewer overflow (CSO), and stormwater advective loadings; atmospheric deposition; diffusive sediment-water and air-water exchange; hydrodynamic flushing; and direct photolysis. Only winter conditions were simulated. The predicted steady state concentrations were 1.2×10^3 ng/l, 21 ng/l, and 1.5 ng/l for naphthalene, pyrene, and benzo[a]pyrene, respectively. In order to resolve spatial variations in PAH distribution in the Inner Harbor, a 3D model was also constructed, incorporating the same processes as the box model. While overall predicted concentrations were in general of similar magnitude as the box model, elevated concentrations were observed locally in the Fort Point Channel and the Mystic and Chelsea Rivers. The Charles River was shown to have a significant impact on two of the PAHs. Model accuracy for pyrene was substantiated by water quality measurements taken concurrently with the study (Flores, 1998). The models are believed to accurately simulate the transport of pyrene and benzo[a]pyrene. The model prediction for naphthalene is believed to be an overestimation based on sensitivity analysis.

The removal of contaminated sediments was simplified to assume a perfect removal in all dredged areas. For each compound, a substantial decrease in concentration was predicted, particularly in the areas scheduled for dredging.

ACKNOWLEDGEMENTS

We would like to begin by thanking the other members of the Master of Engineering group project team who contributed to this report, namely Amparo E. Flores and Sharon W. Ho.

We are also extremely grateful to our advisor, E. Eric Adams, for all his support and advice in this process. His thoughtful insights and constant attention made this study possible.

We would also like to extend our thanks to the MIT Sea Grant College Program for supporting our efforts and providing us with equipment and the use of the *R/V Penelope*. We enjoyed the opportunity to have our research incorporated into a larger group.

We also want to thank Alan F. Blumberg of HydroQual, Inc., for allowing us to use the ECOMsi model.

Scott Fitzgerald was instrumental in assisting us in carrying out the field work for the project, and Rachel Adams provided assistance and advice on a variety of issues. We are grateful to both of them for their efforts.

From Ricardo:

Thank you, Maria Jose for all the unconditional support and happiness you gave me during this adventure. Thank you also, for giving me the best news of this year, our baby. To him/her (we don't know the gender yet), I dedicate this work.

Thank you, Mom and Dad for your lifetime support and for giving me all the tools to be here today. Thank you Dad for teaching me honesty and how to think. Thank you Mom for loving me so much and being who you are. You are an important part of each of my accomplishments.

I would also like to give a special thanks to the really nice people I've met in the M.Eng. program (I hope we keep going for chickens.) Specially, I would like to mention among them the ones who are part of this thesis: of course Peter, thank you for your nice easygoing mood and most important of all thank you for your friendship; Amparo, thank you for helping us and sharing your work and knowledge; and Sharon, thanks for the help in writing.

John, Karen, Conny, Charles, Ana, Amparo, Scott, Amy and Peter, thank you very much for your friendship. It really helped me to survive all the changes that occur during this short period of time.

From the faculty, I would like to thank again Eric Adams (talking to you was always productive) and Phil Gschwend for being an outstanding professor (you made me remember the joy of learning.)

Lastly, I would like to thank all the musicians that filled my ears while working. They made my life through huge quantities of work easier.

From Peter:

I will begin by thanking the person who has stood by my side throughout this whole process, my fiancée Janani. She has helped me in ways that I cannot even begin to count or explain. From making me smile to reminding me that there is more to life than work and school, she is a constant source of inspiration and a very important part of my life.

I would of course not be where I am today without a tremendous amount of love and care from my parents. Thank you for supporting me in all my endeavors and giving me the confidence and strength to pursue my dreams. I would also like to thank my brother, Johan, and my sisters, Lena and Monica, for breaking Mom and Dad in for me. Let me also take this opportunity to dissuade Caroline, Robbie, Michelle, Maria, Susanna, and Daniel from ever taking a nine month Master's program if you value your sleep. I am very grateful for my family.

I would like to thank Ricardo for being a pleasure to work with. In addition to being one of the best engineers I have worked with, he is also a good friend. Honorable mention should also be extended to the MEng gang – you know who you are – especially the late night ones who kept the MEng room a "happening place" even at 4:30 a.m..

I dedicate this thesis to my Mother and Father, to the rest of my family, and to Janani.

TABLE OF CONTENTS

LIST OF FIGURES

LIST OF TABLES

1 EXECUTIVE SUMMARY

Boston's Inner Harbor has been scheduled to be dredged within the near future in order to deepen the shipping lanes which are so vital to commerce in the area. While the motivating factor behind the dredging project is economic, it has the potential to offer long term environmental benefit by removing contaminated sediment from the bottom of the harbor. This could have a substantial effect since it has been suggested that sediment flux is one of the primary sources of pollution to the water column for a number of contaminants. The present study focuses on predicting long term changes in water concentrations of polycyclic aromatic hydrocarbons (PAHs), a group of compounds that tend to sorb readily to sediment particles. In particular, naphthalene, pyrene, and benzo[a]pyrene were selected based on their spectrum of molecular weights and thus environmental transport characteristics.

In order to predict long term changes in water column concentrations, it was first necessary to model the current conditions of PAH distribution within the harbor. This effort took the form of two separate models, each of which provided valuable information to the understanding of PAH behavior in the study area. The first model was a simple mass balance or "box model" which yielded an average steady-state concentration for the entire inner harbor. While this simplified formulation neglected spatial variations in PAH concentration, it provided a valuable tool for evaluating the relative importance of the sources and sinks for each compound. The physical and chemical processes considered in the model included river, combined sewer overflow (CSO), and stormwater advective loadings; atmospheric deposition; diffusive sediment-water and air-water exchange, and direct photolysis. Only winter conditions were modeled for each compound. The resulting steady state concentrations for this time period were 1.2×10^3 ng/l, 21 ng/l, and 1.5 ng/l for naphthalene, pyrene, and benzo[a]pyrene, respectively.

One major drawback to the box model was that it failed to resolve the spatial distribution of PAHs within the system. Because sediment PAH concentrations and CSO discharges

are not uniformly distributed throughout the study area, spatial variability was assumed to be an important consideration. Therefore, a 3D model was also constructed. Each of the source and sink processes from the box model were incorporated into a grid constructed for the ECOMsi hydrodynamic model. Simulations were run for seven day periods and such that an apparent steady state was reached within the system. Spatial distributions of each compound were plotted along with vertical profiles from a number of selected locations. On average, the results from the 3D model were of the same order as predicted by the box model. However, substantial local peaks of PAH concentration were observed in the areas of the Fort Point Channel and the Mystic and Chelsea Rivers. Also of noteworthy was the dominant impact of the Charles River (during relatively high flow conditions) on the flow regime of the study area as well as the concentration distribution of pryrene and benzo[a]pyrene. Vertical profiles demonstrated that the highest concentrations of these two compounds were found in the top layers, mostly due to the impact of the freshwater sources. Thus the 3D representation of the distribution allowed surface decay processes (air-water exchange and photodegradation) to play larger roles in these areas. It is believed that both models correctly simulate the transport of pyrene and benzo[a]pyrene within the system to varying degrees of accuracy. The model prediction for naphthalene is believed to be an overestimation based on the results of the sensitivity analysis in Chapter 7 of the report.

Model predictions for pyrene were confirmed by water quality measurements taken concurrently with the present study. The measurements were taken with an innovative technique which involved the use of semi-permeable membrane devices (SPMDs). Chapter 5 of this study, which describes the measurement methodology and results, has been included courtesy of Amparo Flores (Flores, 1998). Measured pyrene concentrations were on the same order of magnitude as predicted by both models. One sampling station provided two measurements at different elevations in the water column. As predicted by the 3D model, pyrene concentrations were observed to be lower at the bottom than at the surface.

Once the models were established, the post-dredging scenario was evaluated. In this analysis, dredging was assumed to be perfectly efficient in completely removing all PAHs from the sediments in the dredged areas. Both models predict substantial water column concentration decreases in the post-dredge scenario. Once a more thorough understanding of the selected sediment disposal option (subaqueous capping within the harbor) is obtained, these models can be applied to simulate a more accurate long term concentration distribution.

2 OVERVIEW

For centuries, Boston Harbor has served as a receptacle for human waste (MWRA, 1996b). Over the past decades, the public has become increasingly concerned with the impact of sewage disposal on the harbor. In the 1980's, litigation over the pollution of Boston Harbor resulted in the development of a Federal court-ordered schedule to plan and build proper sewage treatment facilities for the over five hundred million gallons of sewage generated by 2.5 million people and 5,500 businesses in Boston and surrounding areas (MWRA, 1991). In 1985, the Massachusetts Water Resources Authority (MWRA) was created for the purpose of managing water and sewer services in the area. One of the MWRA's biggest projects is the Boston Harbor Project, the goal of which is the improvement of water quality in the harbor. Upon completion, the project is expected to cost an estimated 4 billion dollars (Sea Grant, 1996). Since the development of the MWRA, extensive work has been done to try to abate the pollution in Boston Harbor.

Currently, the metropolitan of Boston is attempting to fix a different sort of problem in the harbor. Much of the region's economy depends on the area's accessibility to the waters of the Atlantic Ocean. As of 1996, harbor commerce was generating $8 billion annually in revenue (MWRA, 1996b). However, as rivers and sewage outfalls empty into the harbor, sediments carried by these sources settle to the harbor floor. Eventually, sediment build-up raises the harbor floor (USACOE, 1988). Recently, it was discovered that some of the shipping lanes in the Inner Harbor were too shallow for larger boats to navigate. Although the harbor's principal channels and main entrance are more than 40 feet deep, the tributaries are often less than 35 feet deep. Most of the port terminals in the Inner Harbor are located along these tributaries. The resulting delays and loading restrictions to these areas provide a loss of revenue for the city of Boston (USACE, 1997).

As a solution to this problem, Boston has proposed to dredge portions of the Inner Harbor of sediment (authorized in the Water Resources Development Act of 1990). By dredging accumulated and native sediment, shipping lanes in the harbor will be deepened and better access will result. The sections of the Inner Harbor which will be dredged include

portions of the Mystic and Chelsea Rivers, the area of the Inner Confluence, and portions of the Reserved Channel. A map of the Inner Harbor, along with the areas that will be dredged, is shown in Figure 2.1. It has been estimated that over 2,535,600 cubic yards of sediment will be removed from the various shipping channels through this project (USACE, 1997 and USACOE, 1988).

Unfortunately, the sediments of Boston Harbor have been demonstrated to contain high concentrations of toxic metals and organic compounds (USGS, 1994). As such, they must be treated as hazardous waste if they are removed from the harbor. Since the complete on-land treatment and disposal of hazardous waste can be extremely expensive so an alternate plan was conceived. The United States Army Corps of Engineers (USACOE) proposed to bury the contaminated sediments in the harbor itself. Disposal cells will be dug in the northern area of the Inner Harbor and filled with the dredged material. The cleaner sediments that are excavated to make the cells will be dumped offshore in Massachusetts Bay. The cells will then be "capped" with approximately three feet of clean sand, which is intended to eliminate (or at least drastically reduce) the chemical impact of the dredged materials.

The dredging and capping of these contaminated sediments could have a significant positive impact on the harbor's water quality. Chemical concentrations in the sediment are so high that it is suspected that there is a flux of contaminants to the harbor water column from this source (Stolzenbach *et al.*, 1998). By removing and isolating this possible source of contaminants, the water column concentrations of these chemicals may be significantly reduced. If so, dredging could actually improve the water quality in the harbor.

Both dredging and capping have been used in other areas as a means of remediation, but they have not been demonstrated to be effective in an area such as Boston Harbor. In order to evaluate the impact of the dredging and capping processes on the water quality of the harbor, it is necessary to first determine the pre-dredging conditions.

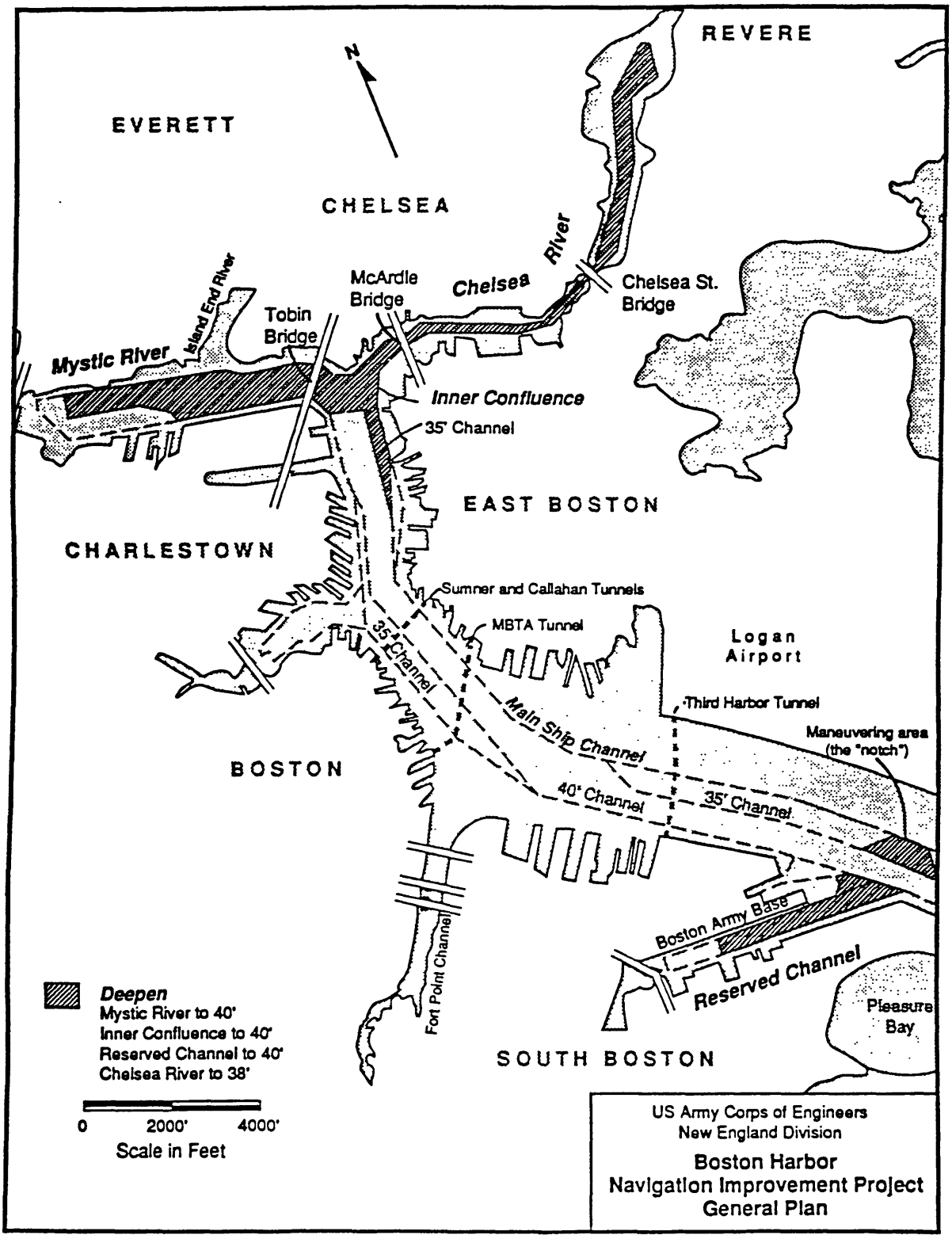

Figure 2.1 - Map of Boston Inner Harbor. Areas proposed for dredging are shaded in. (Adapted from USACOE, 1996)

It has been recognized for many years that some PAHs can cause cancer in laboratory mammals and possibly humans, and occupational exposures to PAHs have been correlated with the incidence of human cancer (International Agency for Research on Cancer, 1973; National Academy of Sciences, 1972; Bridboard *et al.*, 1976) so PAHs are of major concern to regulators and the general public. As a consequence, sixteen PAH compounds are on the EPA priority pollutant list (MWRA, 1994).

The overall purpose of this study is to evaluate the potential impact dredging will have on the water quality of Boston's Inner Harbor with respect to PAHs. There are many steps in this evaluation process. First, an assessment of current conditions in the Boston Harbor must be performed. This includes taking PAH concentration measurements in the water column. This process also involves implementing a model that simulates current conditions, and is consistent with water quality measurements. Once a model have been successfully constructed, predictions can be made of the effect sediment removal will have on the Harbor's water quality.

This study begins with a brief overview of PAHs and the study area in question, followed by a discussion of the water quality measurements is given. These measurements were made using an experimental technique involving semi-permeable membrane devices (SPMDs). Next, the theoretical basis for describing the transport of PAHs is presented. Following an estimation of sources and sinks of PAHs, a box model is constructed to give an overall estimate of concentrations in the harbor. Since it has been noted that the Inner Harbor is not very well mixed (Adams *et al*, 1993), the spatial distribution of PAHs may be important. Therefore, a 3D model was implemented and is presented in Chapter 8. The results of the box and 3D models were compared to the measurements made by the SPMDs. Finally, the models were adjusted to simulate the long-term effects of dredging on the Harbor's long-term water quality.

3 GENERAL BACKGROUND

This section is intended to give a the reader a brief background about Polycyclic Aromatic Hydrocarbons (PAHs) and the area of the study, Boston's Inner Harbor.

3.1 POLYCYCLIC AROMATIC HYDROCARBONS

3.1.1 Chemical Structure and Properties

Polycyclic aromatic hydrocarbons or polyarenes, commonly referred to as PAHs, are composed of two or more aromatic benzenoid rings. The term "aromatic" was originally used to describe these compounds because of their fragrant odor. Over time, the term aromatic has evolved to mean the stable nature of a particular group of organic compounds. Polycyclic aromatic hydrocarbons have greater stability and lower reactivity than similar, acyclic conjugated compounds because of resonance stabilization.

PAHs are planar hydrocarbons, i.e., composed of carbon and hydrogen atoms only. The smallest and lightest PAH is naphthalene ($C_{10}H_8$), a PAH composed of two fused benzene rings. On the other extreme is graphite, a form of elemental carbon. The structures of some of the most common PAHs found in the environment are shown in Figure 3.1

Physical and chemical characteristics of PAHs generally vary in a regular fashion with molecular weight (Neff, 1979). For example, resistance to oxidation and reduction tends to decrease with increasing molecular weight. Vapor pressure and aqueous solubility decrease almost logarithmically with increasing molecular weight. In general, PAHs have very low solubilities in water because of their nonpolar, hydrophobic structures. Table 3.1.1 lists physical constants for some representative PAHs. There is a wide range in the behavior, distribution in the environment, and the effects on biological systems of individual compounds. Toxicities of individual PAHs vary widely and are of concern because some are carcinogenic, tumorigenic and/or mutagenic compounds (Crunkilton and DeVita, 1997).

In general, polycyclic aromatic hydrocarbons undergo the following reactions to varying degrees: electrophilic and nucleophilic substitutions, free radical reactions, addition reactions, reduction and reductive alkylations, oxidation, rearrangements of the aromatic ring system, and complex formations (Harvey, 1997). The transformation of PAHs through oxidation is an important and fundamental reaction of PAHs. The oxidative metabolism of PAHs (e.g., benzo(a)pyrene) by the cytochrome P-450 microsomal enzymes is responsible for their carcinogenic potential in organisms (Harvey, 1991).

3.1.2 Sources and Fate in the Environment

Polycyclic aromatic hydrocarbons are ubiquitous in the environment. Significant levels are found in the atmosphere, in the soil, and in the aquatic environment. The PAHs present in the atmosphere are primarily derived from the fossil fuels used in heat and power generation, refuse burning, and coke ovens. These sources together contribute more than 50% of the nationwide emissions of benzo(a)pyrene, a hydrocarbon that is widely employed as a standard for PAH emissions (Harvey, 1997). Vehicle emissions are another major source of PAHs, particularly in the urban areas of industrialized countries, contributing as much as 35% to the total PAH emissions in the USA (Bjorseth *et al.*, 1985). Natural sources, such as forest fires and volcanic activity, also contribute to the input of PAHs into the atmosphere, but anthropogenic sources are considered to be the most significant sources of PAHs in atmospheric pollution. Because of their high melting points and low vapor pressures, atmospheric PAHs are generally considered to be associated with particulate matter, either as pure material or adsorbed to other particulate matter (National Academy of Sciences, 1972).

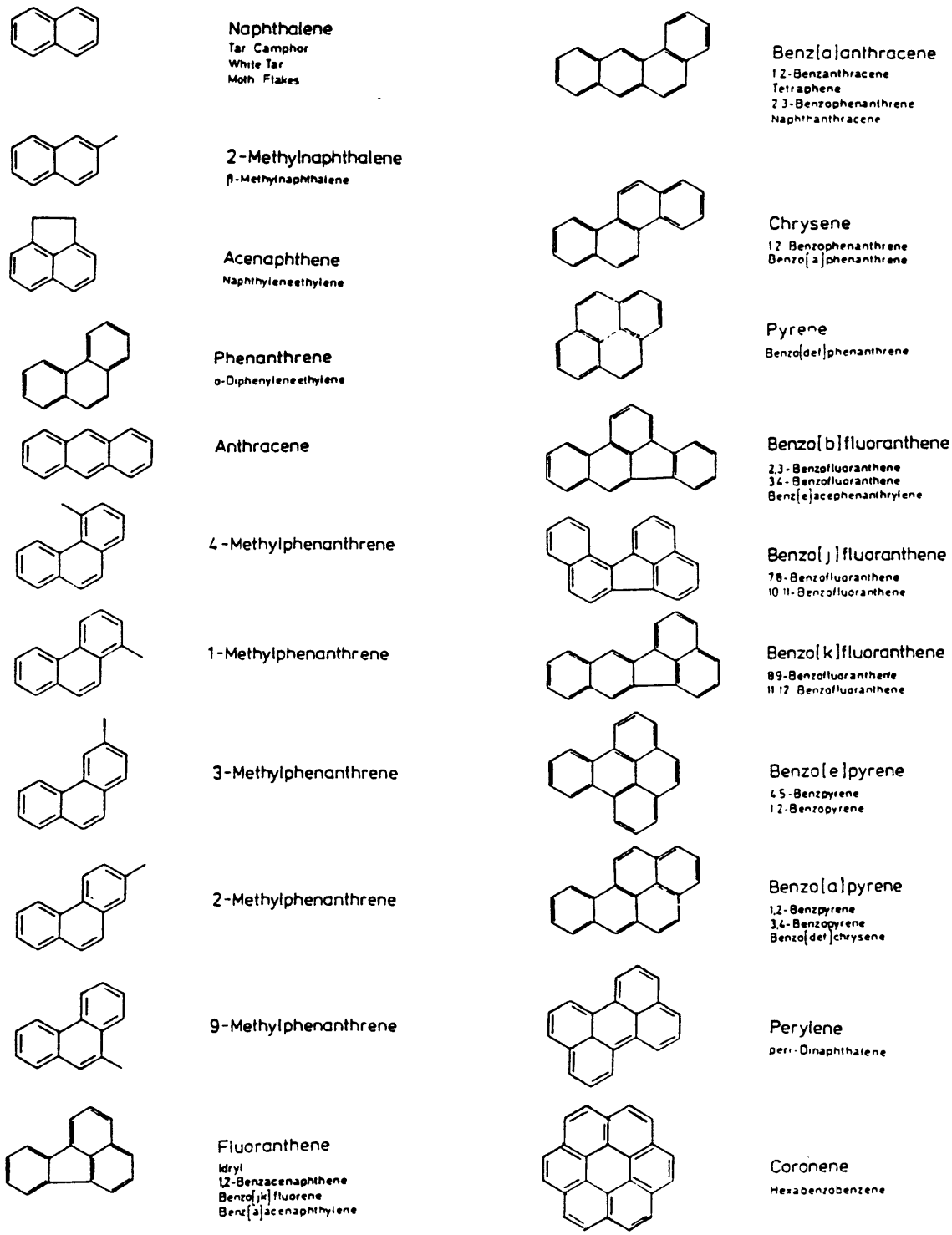

Figure 3.1 - The structures of some polycyclic aromatic hydrocarbons commonly found in the environment (Bjorseth, 1983).

The combinations of PAHs produced in pyrolytic reactions vary according to the temperature of combustion. High temperatures result in relatively simple mixtures of unsubstituted PAHs. At intermediate temperatures, such as that of smoldering wood, complex mixtures of alkyl-substituted and unsubstituted PAHs are formed (Harvey, 1997). Lower temperatures lead to products predominantly composed of methyl- and other alkyl-substituted PAHs. Crude oils formed from the fossilization of plants exhibit characteristic patterns of aromatic hydrocarbon components in which alkyl-substituted PAHs are found in a much higher percentage than unsubstituted ones (Harvey, 1997). The ratio of alkyl-substituted (e.g., methylnaphthalene) to unsubstituted compounds (e.g., naphthalene) present in a sample can actually be used as an indicator of the source. Petrogenic (derived from petroleum) sources exhibit abundance patterns high in alkylated forms while pyrogenic (derived from combusted products, including petroleum) sources are characterized by the dominance of the unsubstituted forms in which the substituents have been oxidized.

Besides being found in the atmosphere and in the soil, PAHs are widely distributed in the aquatic environment because of various pathways of transport. PAHs, bound to particulate matter carried through the air, can deposit onto aquatic surfaces; PAHs in water undergo exchange with the air through dissolution and evaporation; runoff of PAH-polluted ground sources drain into rivers and other water bodies; and municipal and industrial effluents containing PAHs are discharged into receiving waters. Direct spillage of petroleum into water also serves as a major source of PAHs (Neff, 1985). In the aquatic environment, PAHs can then enter the food chain by being absorbed or ingested by plankton, mollusks, and fish which may eventually be consumed by human populations. Because of their hydrophobicity and low solubility in water, PAHs tend to be associated with the complex matrix of organic matter in particulate matter which eventually settle to the bottom. Thus, relative concentrations of PAHs are usually highest in the sediments, intermediate in the aquatic biota, and lowest in the water column (Neff, 1985).

PAH concentrations in natural waters are primarily a function of the sources. In most cases, there is a direct correlation between PAH concentrations in rivers and the degree of industrialization and other human activity along the banks and the rest of the watershed. Groundwater and well water contain PAH concentrations which are lower than those in river water by a factor of ten or more (Neff, 1979). PAHs in groundwater are thought to be derived from the leaching of surface waters through soils contaminated with PAHs (Borneff and Kunte, 1969; Hellmann, 1974; Suess, 1976). Purified tap water and reservoir water contain a PAH concentration similar to, or slightly higher than, that of ground water (Neff, 1979). Table 3.1 lists typical concentration ranges of benzo(a)pyrene and total PAHs in various aquatic systems.

In general, PAHs are quite stable and persistent, especially once they have become incorporated into the anoxic environment of bottom sediments. Under certain conditions, they can be subjected to various chemical transformations and degradative processes. In the natural environment, the most important processes are photoxidation, chemical oxidation, and biological transformation (Neff, 1985). The delocalized pi-electron orbital system in PAHs makes them susceptible to direct photolysis (the absorption of light energy directly) and indirect photolysis (absorption of light energy from light-excited compounds like singlet oxygen ($^1O_2$), hydroxyl radicals ($^{\cdot}OH$), and organic peroxy radicals ($^{\cdot}OOR$)). Direct photolysis is the more dominant mechanism for photodegradation of PAHs (Neff, 1985). In high salinity waters, PAHs can undergo electrophilic substitution reactions with chlorine ions to produce chlorinated aromatic compounds (Neff, 1985). PAHs can also be transformed or metabolized by microorganisms such as bacteria, fungi, and algae (Warshawsky *et al.*, 1995). In aquatic systems, biodegradation occurs in oxidized, surficial sediments (Shiaris, 1989). The rates of PAH degradation tend to decrease with increasing molecular weight (Neff, 1985).

Table 3.1
Typical concentration ranges of benzo(a)pyrene and total PAHs in various aquatic systems.

Source	Concentration in ng/L or pptr	
	Benzo(a)pyrene	Total PAH
River Rhine at Mainz, Germany	50-110	730-1500
River Rhine at Koblenz, Germany	10-60	500-3000
River Aach at Stockach, Germany	4-43	1440-3100
Pskov Region, former USSR (remote from human activity)	0.01-0.1	no data
Sunzha River, former USSR (below discharge of an oil refinery)	50-3500	no data
Thames River, England	170-280	800-2350
Trent River, England	5.3-504	25-3790
Oyster River, Connecticut, USA	78-150	no data
Ohio River at Huntington, West Virginia, USA	5.6	57.9
Lake Constance, Germany	0.2-11.5	25-234
Lake Erie at Buffalo, NY, USA	0.3	4.7
Groundwater (Germany)	0.4-7.0	10.9-123.5
Goundwater (USA)	0.2	8.3
Well water (Germany)	2-15	100-750
Well water (England)	0.2-0.6	3.6-5.8
Tap water (Germany)	0.5-9.0	29.2-125.5
Tap water (9 US Cities)	0.2-1.6	0.9-14.9

These values were taken from Tables 33 and 34, pp. 67-68 of Polycyclic Aromatic Hydrocarbons in the Aquatic Environment, Neff, 1979. For exact references of individual measurements, see Neff, 1979.

Starting in 1991, a major study estimated PAH inputs into the near shore regions of Massachusetts Bay, including Boston Harbor, using site-specific non-point and point source PAH concentration data from waterborne sources (MWRA, 1994). A study by Golomb *et al.* (1996) looked into atmospheric PAH loadings into Massachusetts Bay. The study by the MWRA found that the major waterborne sources for different PAH

compounds varied. The greatest loadings of low molecular weight and total (low+heavy) PAH compounds were from sewage and sludge discharges from publicly-owned treatment works or POTWs while the greatest source of high molecular weight and carcinogenic compounds were from non-point sources including rivers (Cura and Studer, 1996). The difference in sources, and therefore discharge points, may have important implications for the distribution of PAH compounds over Boston Harbor. Since PAHs vary in their toxicity (National Academy of Sciences, 1972), it is important to identify and quantify the individual PAHs found in the water column of different regions of the harbor.

3.2 BOSTON HARBOR BACKGROUND

3.2.1 Physical and Hydrographic Characteristics

Boston Harbor is located in the Northwest corner of Massachusetts Bay, which is itself a part of the Gulf of Maine. Boston Harbor comprises an area of about 50 square miles, bounded by 180 miles of shoreline. It can be divided into sub-regions easily defined by topographical boundaries. The regions north and south of the boundary between Dorchester Bay and Quincy Bay are referred to as the North Harbor and South Harbor, respectively. The North Harbor can further be divided into the Inner Harbor and the Northwest Harbor while the South Harbor can further be divided into the Central Harbor and the Southeast Harbor.

The focus of this study is the Boston Inner Harbor region (Figure 2.1). The Inner Harbor is bound by the confluence of the Mystic and Chelsea Rivers up north and the entrance to Massachusetts Bay down south. Its volume varies from approximately 7.8×10^7 m^3 at high tide to 5.6×10^7 m^3 at low tide. The Inner Harbor is relatively shallow, with a nearly constant mean water depth of 10 m.

Boston Harbor is only slightly stratified by salinity gradients because its freshwater input is relatively small compared to tidal flushing. The Inner Harbor receives freshwater inputs from the Charles River, Mystic River, and Chelsea River. The largest input is from the Charles River with an annual average flow (1931-1992) of 8×10^5 m^3/day (USGS, 1992). In the summer months, Boston Harbor becomes thermally-stratified. The density currents that result from the thermal stratification contribute to surface and bottom water exchange with Massachusetts Bay but, overall, this mechanism is minor relative to tidal flushing (Stolzenbach *et al.*, 1998).

3.2.2 Sources of Contamination in Boston Harbor

Contaminants have both point and non-point sources in Boston Harbor. These include tributary rivers and groundwater flows, runoff from stormwater drains and combined sewer overflows, industrial discharges, ship and boat traffic, sewage and sludge discharges from treatment plants, and the atmosphere.

Each of the six major tributaries (Charles River, Neponset River, Weymouth Back River, Mystic River, Weymouth Fore River, and Weir River) which empty into the harbor carry with them varying levels of contaminants. The identities and the concentrations of these contaminants vary according to the domestic and industrial activities within the corresponding watersheds. Groundwater flowing into the harbor's shoreline also carries with it contaminants resulting from current human activities and leachate from wastes in old landfills.

In the 1800s, combined sewer-storm drains (commonly referred to as combined sewer overflows or CSOs) were constructed by the surrounding towns of Boston, Cambridge, Chelsea, and Somerville (MWRA, 1993) to handle both sewage and rainwater flows. During heavy rain, some of these drains still discharge directly into the harbor along the shoreline or into tributaries which ultimately flow into Boston Harbor. Outflows from CSOs can carry significant loads of contaminants into Boston Harbor. Stormwater runoff

will carry contaminants that have been washed away from the ground surface. Spilled motor oil on roadways and driveways, for example, may enter storm drains after being washed away by the rain. Of the over 80 CSOs that discharge a combination of storm water and raw or partially-treated sewage into Boston Harbor, 35 CSO's discharge directly into the Inner Harbor. As of 1992, the average flow from these CSOs corresponded to about 1% of the average Charles River input (Chan-Hilton *et al.*, 1998).

Many industries developed along the harbor shoreline in the late 1800's. Historically, these industries were able to discharge their raw wastes directly into the harbor. Even in this era of heavy regulation, industries are still allowed to discharge controlled concentrations of chemical wastes into the water. Industrial (commercial) and private boat and ship traffic also contribute to contamination in the harbor through fuel leaks and motor emissions.

Sewage effluent and associated sludge discharges have, by far, been the largest sources of contaminant input into Boston Harbor. Starting in 1878, sewage vats on Moon Island with a capacity of 50 million gallons discharged raw waste into the harbor twice daily with the outgoing tide (MWRA, 1996). Raw sewage pump stations were constructed in East Boston in 1889 and on Deer Island in 1899. It was not until 1952 that the first primary wastewater treatment plant was constructed on Nut Island. This facility provided screening and sedimentation of solids and chlorination to reduce bacterial levels which had become a recognized health risk within the harbor (Stolzenbach *et al.*, 1998). Starting in 1968, primary treatment was begun at Deer Island and the Moon Island outfall was reserved for wet weather flows only (ceased in 1992). A new primary treatment plant was constructed in 1995 at Deer Island and was upgraded to secondary treatment in 1997 (MWRA, 1997). A new outfall discharging 9.5 miles out into Massachusetts Bay is expected to be in operation at the end of 1998. As of 1991, the Boston sewer system was transporting an average of 500 million gallons of sewage per day from Boston and surrounding communities to the Deer Island and Nut Island sewage plants (MWRA, 1991).

According to Menzie *et al.* (MWRA, 1994), the total PAH input into Boston Harbor is approximately 20,000 kg/yr. Most of this total PAH input originates from sewage effluent and sludge discharge. However, the major source of low molecular weight PAHs like 2-methylnaphthalene (total loading of 1,760 kg/yr) was found to be sewage while that of high molecular weight compounds like benzo(a)pyrene (total loading of 22 kg/yr) was found to be tributaries. Their study also estimated that 89% of the 2-methynaphthalene discharged into the harbor is added to the North Harbor and 73% of the benzo(a)pyrene is added to the South Harbor (MWRA, 1994).

4 PREVIOUS STUDIES

4.1 REVIEW OF DREDGING STUDIES

R. N. Bray (1997) wrote "Dredging is an ancient art but a relatively young science." Historical signs of dredging which date back several thousands of years have been discovered on archeological expeditions. In those times the tools of use were on the technological level of a raft and bucket. Though the tools have changed significantly since then, our understanding of the processes which occur has not advanced as quickly.

There are many reasons that prompt the need for dredging. Initially, dredging projects resulted from various engineering needs. Dredging sediment provides a way to deepen channels for navigation, obtain material needed for other construction, and win valuable minerals. More recently, the environmental applications of dredging practices have been recognized. Dredging has been used to create or improve habitats such as wetlands, and dredging and disposing of contaminated sediments may improve the water quality of a system.

Little is known about the various environmental impacts dredging has on an aquatic environment. Only recently has this topic been investigated to any large extent. Most studies investigate the potential negative impacts the dredging process has on the environment. Dredging temporarily increases the water's turbidity around the dredge site. This may decrease oxygen levels by increasing the organic content of the water, interfere with fish navigation in the area, increase the concentration of harmful chemicals in the water, and affect the benthos of the sediment floor. If the dredging is occurring in an estuarine area, the process could increase salt intrusion into the freshwater. In addition, the deepening of channels causes some areas of a water body to become anaerobic. Many of these effects are of greater concern if "maintenance," or recurrent, dredging is performed.

However, there are some benefits to dredging sediments. In areas where the sediments are heavily contaminated, the removal of the large contamination source can improve water quality. Additionally, stirring up the sediment floor may release much needed nutrients to the surrounding waters. When considering dredging, it is important to weigh the various negative and positive impacts the process will have on the environment (Bray, 1997 and ICE, 1995).

There are increasingly more cases where dredging is used as an environmental solution to improve water quality. For instance, hydraulic dredging and fill techniques were used in an attempt to restore a 40-acre fishing lake in Memphis, Tennessee (Schellbach and Van Veen, 1997). This fishing lake bordered a former municipal landfill that contained several contaminants including arsenic, lead, copper, nickel, and pesticides such as chlordane, endrin, and heptachlor. These substances enter the lake, and concentrate in the sediments.

Fish in this lake contained high concentrations of contaminants. Since nearby residents frequently went to the lake to catch and eat fish, this contamination was deemed a serious problem. Recently, the bottom of the lake was dredged with the hopes that removing the source would decrease the ambient water concentrations to acceptable levels, thereby decreasing the amount of contamination in the fish. Although monitoring will not start until sometime this year, expectations are that a significant decrease in pollutant concentrations will be observed (Schellbach and Van Veen, 1997).

Sometimes dredging is not the best solution to a contamination problem. When it was discovered that the Hudson River was contaminated with PCBs, an environmental advocacy group pressed the need for dredging the sediments to remove the contamination. General Electric performed an extensive study and concluded that sediment dredging would not significantly change the concentration of PCBs in the water column. Further investigation found that other measures were needed, and dredging did not take place (GE, 1998).

Another study demonstrates the potential impact sediment removal can have on PAH concentrations in the water column. Contaminated sediments in the Commencement Bay Nearshore Tideflats Superfund Site in Tacoma, Washington, were isolated via a capping procedure as part of the St. Paul Waterway Area Remedial Action and Habitat Restoration Project. The sediments of this region were heavily contaminated with phenolic compounds and several low molecular weight PAHs.

One of the primary purposes of the St. Paul project was to completely isolate the chemical contamination in the sediment. A layer of clean material was placed as a "cap" over the contaminated sediments. Habitat features were provided to encourage the recolonization of the tideflats by various species. A ten-year monitoring program was established to monitor the cap's effectiveness. Of the 2010 possible chemicals that could have been detected, there were only three instances where concentrations rose above EPA's early warning levels at the surface of the sediment. The monitoring also showed a steady increase in the ecology of the area after the contaminated sediments were isolated (Stivers and Sullivan, 1994).

The St. Paul study demonstrates the benefits that come from isolating a sediment floor that is heavily contaminated with PAHs. Although no dredging took place, by covering the sediments with a new layer of "clean" material the end effect was somewhat similar. Unfortunately, the study only examined the impact of capping on the floor of the tideflat. It did not examine the effect sediment isolation had on chemical concentrations in the rest of the water column.

There are very few, if any, documented studies investigating the impact dredging will have on the long term concentration of chemicals in a body of water. Most studies focus on ways to increase dredging efficiency or investigate more short-term environmental changes caused by stirring up sediment. For this reason, a study such as the one presented here is important to provide a framework in which others can investigate the impact dredging will have on overall water quality.

4.2 REVIEW OF CAPPING STUDIES

Once sediments are removed from the bottom of a water body, the dredged material must be disposed of. Generally, options include disposal at sea, disposal in shoreline enclosures, and onshore disposal. Sediment disposal at sea presents one of the most widely used methods since it is relatively easy to employ. However, such disposal can be environmentally detrimental. Ocean dumping elevates TSS, releases pollutants, may damage fisheries, and changes the natural sediment floor. The removal, transport, and treatment of sediments on land can be extremely expensive due to the large volumes and high water content of the dredged material. Therefore, disposal of contaminated material into seabed depressions is an attractive solution in many cases.

Capping contaminated sediments in situ has immediate benefits over other disposal options. It immediately isolates the contamination by increasing the transport length between the contaminated zone and the water column. It is less expensive that on-shore disposal in many cases, and does not have the same detrimental environmental impacts that ocean dumping presents.

There are several things to consider when capping contaminated sediments. Cap performance depends on the cap's method of placement, location, thickness, and composition. If the cap is placed too soon, the dredged material may settle and porewater may flush through the cap. Not only does contaminated porewater enter the aquatic system, the sediment cap becomes contaminated as well (Thibodeaux, 1994 and Bray, 1997).

The act of dredging Boston Harbor's sediments will have little beneficial environmental impact if the sand cap does not isolate the contamination from the water column. For this reason, it is important to consider the effectiveness of the capping layer when evaluating the dredging process on PAH concentration in Boston's Inner Harbor

5 PAH MEASUREMENTS

In order to validate the mathematical models, actual measurements of the concentration of PAH in the area of interest were required. These measurements were performed using Semipermeable Membrane Devices or SPMDs. These devices are still in a development stage; therefore, some background information is provided. The field work will then be presented followed by the lab procedures and the results.

5.1 SEMIPERMEABLE MEMBRANE DEVICES

This section is intended to give the reader a description of the development of the SPMDs, followed by the theory behind these sampling devices.

5.1.1 Historical Development

The use of organic solvents to extract hydrophobic organic compounds from aqueous solutions is a well-established procedure. Chemists often use so-called liquid-liquid extractions to transfer organic compounds in water to a water-immiscible organic solvent for which the target compound has greater affinity. Typically, the water sample is vigorously mixed with the solvent (e.g., methylene chloride) to allow the target compounds to dissolve into the solvent. The water and the organic solvent are then allowed to separate and the solvent is extracted. These procedures employ the organic solvent-water partitioning properties of hydrophobic compounds which, at equilibrium, can be described by their K_{sw}:

$$K_{SW} = \frac{C_S}{C_W} \left[\frac{mol/L_S}{mol/L_W} \right]$$

As the equation demonstrates, the greater the K_{sw} for the analyte, the greater the concentration in the solvent as compared to water. One way of interpreting the physical meaning of the K_{sw} is by thinking in terms of volumes; for a given number of moles of a

compound in one liter of a particular solvent, K_{sw} liters of water will be required to hold the same number of moles. In the case of a highly hydrophobic compound like benzo(a)pyrene which has a *log* K_{sw} of 6.50 in octanol at 25°C (Schwarzenbach *et al.*, 1993), 1 liter of octanol in contact with water will hold a mass of benzo(a)pyrene equivalent to that dissolved in 3,160,000 liters of the water.

The low aqueous solubilities of many organic compounds, especially hydrocarbons, result in low concentrations that are difficult to quantify. For example, benzo(a)pyrene has an aqueous solubility of only $10^{-8.22}$ mol/L or 1.52 µg/L at 25°C. The capacity of certain solvents for dissolving organic compounds out of water can thus be used to concentrate them to levels that can be more easily measured. This concept has been used extensively in laboratory settings but has been applied to *in-situ* field sampling only recently. Field deployment requires a convenient means of separating the solvent from the water so that the solvent can later be collected and analyzed, while still allowing for the transfer of targeted compounds from the water and into the solvent. In the last couple of decades, various groups have developed the use of semipermeable membranes for this specific application.

Huckins *et al.* (1990) credit a group led by Miere (1977) as the first investigators of the use of polyethylene film for dialysis of nonpolar organic contaminants from water into organic solvents. Their work suggested that nonporous, synthetic polymeric films, including low density polyethylene and polypropylene, could serve as semipermeable membranes allowing for diffusion and concentration of organic molecules from water into relatively nonpolar organic solvents. This process is governed by solvent-water partitioning coefficients which, in the case of hydrophobic compounds, strongly favors concentration into the organic solvents.

In 1980, a pair of investigators from the United Kingdom obtained a patent for a device consisting of a nonpolar organic solvent contained in a semipermeable membrane such as regenerated cellulose, vinyl chloride, polyvinylidene fluoride, or polytetrafluoroethylene. As stated in the patent, the device was to be used as a concentrator for removing organic

contaminants from aqueous systems (Byrne and Aylott, 1980). Their design represented a new application of dialysis to liquid-liquid extraction of organic compounds from an aqueous environment.

In 1987, Sodergren used solvent-filled dialysis membranes to simulate uptake of pollutants by aquatic organisms (Sodergren, 1987). In his study, he used dialysis membranes to crudely mimic biological cell membranes and 3 mL of *n*-hexane as the lipid pool capable of collecting lipophilic organic compounds. The solvent-filled bags were exposed to organochlorine aqueous solutions (*p,p'*-DDE, *p,p'*-DDT, Clophen A50) in the lab for 8-10 days and various aquatic environments in the field (e.g., a 4-day exposure to a bleach pulp plant effluent and a 2-week exposure to an activated sludge basin of a sewage treatment plant) to examine uptake behavior. The samples were analyzed by using a syringe to penetrate the membrane and extract the solvent and shooting the extract directly into a gas chromatograph or GC without any clean-up procedure.

Johnson extended this study by using bigger volumes of *n*-hexane (40 mL) and performing a 32-day exposure of the bags to well water to examine the uptake kinetics of Arochlor 1248 into the bag (Johnson, 1991). As in Sodergren's study, the *n*-hexane was shot directly into the GC after extraction from the bags. He also used fugacity-based bioconcentration kinetics, interpreted with respect to Fickian diffusion, to provide a theoretical basis for the observed behavior of the solvent-filled bags.

In the early 1990's, researchers led by Huckins at the US Geological Survey's Midwest Science Center developed a design based on the organic solvent-water partitioning concept used in the previous studies (Sodergren, 1987; Johnson, 1991). Their design, which they named Semipermeable Membrane Device or SPMD, consists of a 91-cm long strip of low density polyethylene (LDPE) film as the membrane and the lipid, triolein, as the organic solvent. Huckins and his group also developed a mathematical model of the uptake and dissipation kinetics of the SPMDs. While Johnson used his solvent-filled bags for qualitative monitoring only, these SPMDs are designed to quantitatively

determine analyte concentrations in the field based on measured concentrations in the triolein after a given exposure time. The design and the kinetics model of these standardized and commercially-available SPMDs are discussed in more detail in the following sections. Huckins and his group also patented a new procedure for performing the analysis on these devices (US Patents #5,098,573 and 5,395,426). Unlike Sodergren's and Johnson's procedure, where the lipid was shot directly into the GC, a dialysis is performed on SPMDs to first extract the analytes from the triolein. The dialyzing solvent, e.g. cyclopentane, is then concentrated using volume reduction techniques and fractionated into various groups (e.g. PAHs, halogenated compounds, etc.) before analysis by a GC.

Since their development, these devices have been used and tested for a wide variety of purposes in diverse environmental settings. In recent years, SPMDs have been used to measure freely-dissolved concentrations of organic contaminants in urban streams (Crunkilton and DeVita, 1997), to determine contaminant residence times in an irrigation water canal (Prest *et al.*, 1997), to evaluate the bioavailability of contaminants associated with sediments (Cleveland *et al.*, 1997), to quantify organic contaminant concentrations in compost (Strandberg *et al.*, 1997), to simulate uptake by bivalves, the traditional biomonitors (Hofelt *et al.*, 1997), and to develop a spatial distribution of PAH concentrations in urban streams (Moring and Rose, 1997).

SPMDs have been deployed in the waters of Dorchester and Duxbury Bays in Massachusetts (Peven *et al.*, 1996), the metropolitan areas of Texas (Moring and Rose, 1997), the Upper Mississippi River (Ellis *et al.*, 1995), the San Joaquin and Sacramento Rivers in California (Prest *et al.*, 1992), Corio Bay in Australia (Prest, Richardson *et al.*, 1995), and Central Finland (Herve *et al.*, 1995), among others. They have also been used for toxicity testing of sediments from Antarctica (Cleveland *et al.*, 1997). Note that SPMDs are also capable of extracting organic compounds from the air and have been used as passive air samplers (Petty *et al.*, 1993 and Prest, Huckins *et al.*, 1995) for organic contaminants.

5.1.2 Design of SPMDs

A semipermeable membrane device consists of two components: the membrane and the solvent or sequestration phase. The membrane is typically a thin-walled (50-250 micrometers) nonporous polymer like LDPE, plasma-treated silicone or silastic, polypropylene, polyvinylchloride, or other similar materials (Huckins' tutorial, 1997). Although the membranes used in SPMDs are typically referred to as "nonporous", they actually have cavities up to approximately 10 angstroms in diameter. The cavities are transitory and are formed by the random thermal motions of the polymer chains. For the membrane to serve its purpose well, it needs to retain the sequestering phase within the membrane while allowing for the diffusion of target compounds. The lower limit of the molecular size of the sequestration phase or solvent is such that the solvent molecules are not able to cross the membrane and escape to the surrounding water to a significant extent.

Besides containing the solvent within the device, the small diameters of these cavities dictate an upper limit for the sizes of the compounds that can penetrate the membrane and reach the solvent. Huckins pointed out that the diameters of many environmental contaminants of interest approach the maximum size of the cavities in nonporous membranes; therefore it is likely that analytes associated with aqueous particulates and dissolved organic carbon, such as humic acids, cannot penetrate the membrane (Huckins, 1993). The use of nonpolar membranes will also impede the passage of ions into the membrane. SPMDs can therefore be expected to sequester only freely-dissolved, non-ionic compounds, an advantage over conventional PAH sampling procedures.

Studies have shown that polar nonporous membranes such as cellulose can reduce or eliminate solvent losses to the surrounding environment, but a corresponding reduction in the uptake rates of nonpolar analytes were also observed (Huckins, 1993). A study by Gray and Spacie (1991) compared the concentration potential of lipid-containing polyethylene membranes to hexane-filled cellulose dialysis bags (Sodergren, 1987) and

found that lindane and trifluralin were sequestered to a much a greater extent in the former.

The sequestration phase is typically a large molecular weight (≥ 600 Daltons) nonpolar liquid such as a neutral lipid, silicone fluid, or other lipid-like organic fluid (Huckins' tutorial, 1997). Various investigators have used relatively low molecular weight, nonpolar compounds like hexane, but this resulted in losses to the surrounding water because of their membrane solubility and permeability. Huckins *et al.* (1993) noted that the diffusion of the sequestration phase out of the membrane may also impede analyte uptake because the analyte will have to diffuse against an outward solvent flux leading to concentration polarization at or near the membrane exterior surface. Obviously, this problem is eliminated when a solvent is chosen such that the molecules are too large to significantly diffuse through the membrane.

Huckins' commercially-available standardized SPMDs consists of LDPE layflat tubing and high-purity synthetic triolein (≥ 95%). The SPMDs are 2.5 cm wide by 91.4 cm long flat tubes which contain 1 mL (0.915 g) of triolein as a thin film spread over the entire tube. The LDPE tubing is 75-90 micrometers thick. The SPMDs are heat-sealed at both ends.

Triolein or glyceryl trioleate is *9-octadecenoic acid, 1,2,3-propanetriyl ester*. It has a molecular weight of 885.45 g and consists of 57 C's, 104 H's, and 6 O's (Budavari (ed.) *et al.*, 1996). Triolein is approximately 27 angstroms in length and approximately 28 angstroms in breadth so it should not be able to diffuse through the 10-angstrom cavities in the membrane to a significant extent. Triolein is the major neutral lipid in many aquatic organisms and was chosen as the sequestration phase because SPMDs are designed to simulate bioaccumulation in aquatic organisms. Chiou's work (1985) demonstrated that when the published bioconcentration factors (BCF) of organic compounds in water, that is, the ratio of the steady-state concentration of a compound in the organism (or a part of it) compared to that in water, are based on lipid content rather than on total mass, they are approximately equal to the equilibrium triolein-water

partition coefficients, K_{tw}. This suggests that partitioning of organic compounds between fish and the surrounding water are determined by the near equilibrium partitioning between triolein and water. The uptake of organic contaminants by SPMDs can therefore simulate passive, that is, non-metabolic, uptake of organic contaminants by fish and, perhaps, other aquatic organisms.

Besides minimizing solvent loss and simulating bioconcentration, the use of pure triolein as the sequestering media for SPMDs has other major advantages. Chiou demonstrated that there is a close correlation between K_{tw}'s and the corresponding octanol-water partition coefficients, K_{ow}'s, for many organic compounds (Chiou, 1985). Figure 5.1 shows a plot of the log K_{tw}'s versus the log K_{ow}'s of a wide range of organic compounds. Table 5.1 lists some of the actual values for log K_{tw} that were measured by Chiou and the corresponding published log K_{ow}'s.

As demonstrated by Figure 5.1, a compound's K_{tw} can be closely approximated by its K_{ow}, a value that is well documented by the pharmaceutical industry because of its significance in toxicity studies. In addition, since K_{ow}'s are large for hydrophobic organic contaminants (see Table 5.1), the concentration capacity of triolein-containing SPMDs for these contaminants is also large.

5.1.3 Uptake Kinetics of SPMDs

In modeling the uptake kinetics of compounds from water into the SPMDs, Huckins *et al.* (1993) made the following assumptions: a) the chemical concentration in the water is constant and there is no significant resistance to diffusion in the lipid (i.e., rapid mixing occurs), b) the steady-state flux, F, of an analyte into the device is controlled by the sum of the resistances to mass transfer in the membrane and a water boundary layer, and c) the capacity of the membrane to dissolve chemicals is negligible.

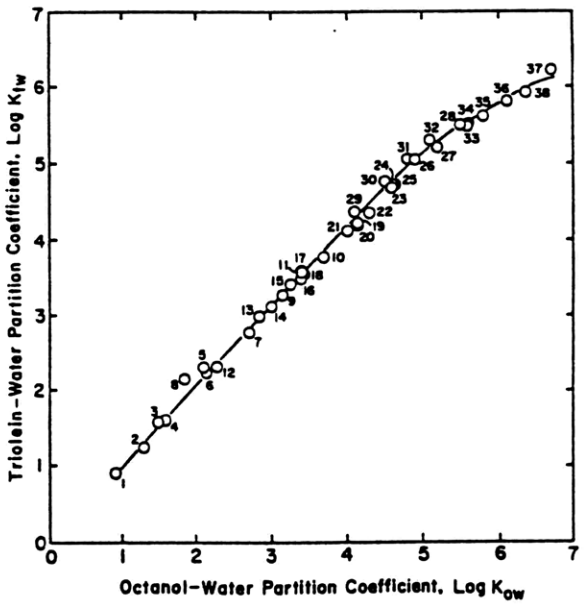

Figure 5.1 - Correlation of log K_{tw} with log K_{ow} for selected organic compounds (Chiou, 1985).

Table 5.1
A comparison of log K_{ow} values versus log K_{tw} values for a range of organic compounds (Chiou, 1985).

Compound	*log K_{ow}*	*log K_{tw}*
Aniline	0.90	0.91
Benzene	2.13	2.25
Hexachloroethane	4.14	4.21
1,2,4,5-	4.70	4.70
2-PCB	4.51	4.77
2,5,2',5'-PCB	5.81	5.62
p,p'-DDT	6.36	5.90

Figure 5.2 shows an exploded view of a membrane bounded by water on one side and solvent on the other. In the case of Huckins' SPMD, the membrane is polyethylene and the solvent is triolein. (Huckins *et al.*, 1993).

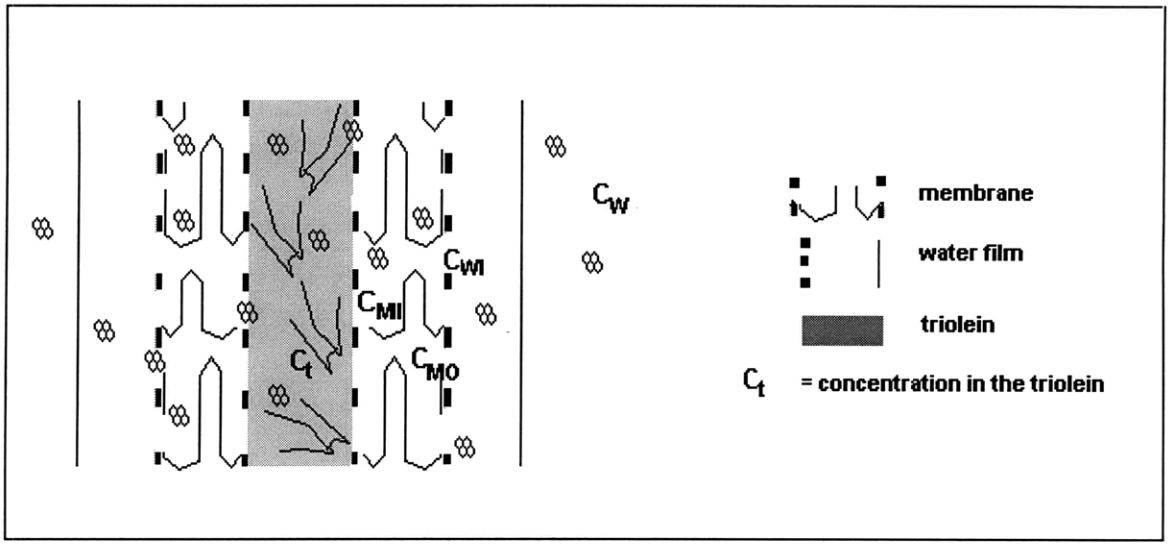

Figure 5.2 - An exploded view of the triolein-membrane-water film model. The diagram shows the tortuous pathways created by the membrane polymer which allow for retention of the triolein and transport of smaller compounds through the membrane. Drawing courtesy of Ana Pinheiro.

At constant temperature, the flux F (g/h) is given by the mass-transfer equation:

$$F = V_s \frac{dC_s}{dt} = \frac{D}{Y} A(C_{MO} - C_{MI}) = k_p A(C_{MO} - C_{MI}) = k_w A(C_W - C_{WI}) \qquad \text{(Eq. 5.1)}$$

where D = diffusivity or permeability of the analyte in the membrane (m^2/h)

A = membrane surface area (m^2)

Y = membrane thickness (m)

k_p = membrane mass-transfer coefficient (MTC) = D/Y

k_w = water boundary layer MTC

V_s = volume of the lipid or solvent used for the sequestering media (m^3)

t = time of exposure (h)

C_{MO} = analyte concentration at the outer surface of the membrane (g/m^3)

C_{MI} = analyte concentration at the inner surface of the membrane (g/m^3)

C_W = analyte concentration in the bulk water (g/m^3)

C_{WI} = analyte concentration at the interface or in the water boundary layer (g/m^3)

C_S = analyte concentration in the lipid or solvent (g/m^3) = C_t

Defining equilibrium partition coefficients for the inner membrane and the solvent as $K_{MS} = C_{MI}/C_S$, for the outer membrane and water as $K_{MW} = C_{MO}/C_{WI}$, and for the solvent and water as $K_{SW} = C_S/C_W$, the interfacial concentrations can be eliminated and equation 5.1 can be simplified to

$$F = V_s \frac{dC_s}{dt} = k_0 A(C_W K_{MW} - C_S K_{MS}) \qquad \text{(Eq. 5.2)}$$

where k_o is the overall MTC and is a measure of the combined resistances of the water-boundary layer and the membrane to molecular transport:

$$\frac{1}{k_0} = \frac{1}{k_p} + \frac{K_{MW}}{k_w} \qquad \text{(Eq. 5.3)}$$

Implicit in this equation is the assumption that the resistances for the membrane, $1/k_p$, and the water layer, K_{MW}/k_w, are additive and independent of each other. It has been suggested that in the case of the solvent, triolein, and the membrane, polyethylene, the membrane resistance is typically the dominant term so k_o is approximately equal to k_p. In the case of a very large value for K_{MW}, the second term can become significant and the resistance may become dominated by the water boundary layer. (Huckins *et al.*, 1993) There is currently insufficient data on the transition from membrane-controlled diffusion to aqueous film-controlled diffusion for SPMDs. (Huckins, 1998)

Assuming that C_W is constant, integrating Equation 5.2 yields

$$C_s = C_W \frac{K_{MW}}{K_{MS}}(1 - \exp(-k_0 A K_{MS} t / V_s)) = C_W K_{SW}(1 - \exp(-k_u t)) \qquad \text{(Eq. 5.4)}$$

where k_u = overall uptake rate constant (hr^{-1}):

$$k_u = k_0 A \frac{K_{MS}}{V_S} \quad \text{(Eq. 5.5)}$$

and the response time, τ, for the analyte in the SPMD is given by the reciprocal of k_u. Huckins *et al*'s model is similar to those used by other investigators who have modeled other membrane systems.

The value of k_u can be determined by measuring the loss or dissipation of a compound from the device into pure water over time. This assumes that the uptake behavior of the system is identical to its dissipation behavior. The loss from the SPMD can then be described by the following equation where C_{SO} is the initial concentration of the compound:

$$C_S = C_{S0} \exp(-k_u t) \quad \text{(Eq. 5.6)}$$

Equation 5.4 can be modified to account for the lag time, t_o, required for the analyte to first penetrate the membrane resulting in a delay in the concentration increase in the solvent. In the early stages of uptake, t_o is the positive intercept of the model on the time axis.

$$C_S = \left[1 - \exp\left(\frac{-k_0 A K_{MS}}{V_S}(t - t_0)\right)\right] K_{SW} C_W \ , t > t_0 \quad \text{(Eq. 5.7)}$$

Three Regions of the SPMD uptake curve:

The SPMD analyte uptake curve (C_S vs t) described by Equation 5.3.4 or 5.3.7 can be divided into three regions: linear, curvilinear, and asymptotic. These scenarios differ depending upon the physicochemical properties of the analyte and the duration of the exposure.

Linear uptake region:

When the term $k_oAK_{MS}t/V_S$ is small (i.e., $k_ut<<1$) or when $C_S/C_W << K_{SW}$, Equation 5.4 reduces to a linear equation with a slope of R_{WS} as shown in Equation 5.8.

$$C_S = \frac{K_{MW} k_0 At}{V_S} C_W = R_{WS} C_W \qquad \text{(Eq. 5.8)}$$

In the linear uptake kinetics region, C_S is controlled by the amount of chemical encountered by the device in relation to the volume of the solvent. The term $K_{MW}k_oAt$ (m^3) represents the volume of water from which the chemical has been extracted, while $K_{MW}k_oA$ can be thought of as the SPMD sampling rate (m^3/h). R_{SW}, the ratio of the sampling rate to the volume of solvent, V_S, thus determines the accumulation of the chemical in the solvent. As long as $C_S/C_W << K_{SW}$ or $K_{SW}>>R_{WS}$, the value of K_{SW} is irrelevant. Controlled laboratory experiments can be used to measure R_{WS} for a particular compound (fixed partitioning coefficient) and a particular SPMD configuration (fixed V_S, A, and membrane properties) then C_S can be used to quantify C_W. According to Huckins *et al.* (1993), SPMD exposure times of $< 0.5\,\tau$ or $0.5/k_u$ can be expected to be in the linear uptake region.

Curvilinear uptake region:

In the curvilinear uptake region, the sampling rate and, equivalently, the slope of the curve decreases as the solvent approaches saturation or equilibration with the water. Because K_{SW} and R_{WS} are now similar in magnitude, neither term can be ignored and both would have to be known to relate the value of C_S to C_W at a given point in time. Given a known K_{SW}, C_W can be derived by fitting Equation 5.4 or 5.7 to measured values of C_S over time. Huckins *et al.* (1993) suggest that in using this method, the number of estimated parameters (e.g., C_W and k_u) be no more than half the number of C_S values.

Asymptotic uptake region:

When the group $k_oAK_{MS}t/V_S$ in Equation 5.4 is large or R_{WS}/K_{SW} is very close to 1 or $t >> \tau$, the exponential term becomes negligible and Equation 5.4 reduces to the familiar equation

$$C_S = K_{SW}C_W \qquad \text{(Eq. 5.9)}$$

In this region, equilibrium has been reached between the solvent and the water and R_{SW} is simply the K_{SW}. A compound's water concentration, C_W, can then be determined from C_S in a straightforward manner given the compound's K_{SW}.

In summary, the relationship of C_S to C_W for a given exposure time is determined by two terms, R_{WS} and K_{SW}. R_{WS} is design-specific, that is, it is determined by the type of sequestering media used, the membrane surface area, the membrane resistance, and the volume of the solvent. K_{SW} is purely a function of the solvent and the compound of interest. For large values of K_{SW}, the uptake rate constant k_u decreases, resulting in a longer equilibration time. This phenomenon has been observed in polymeric membrane permeability and bioconcentration studies and may be due to increased resistances ($1/k_o$) to diffusion in both the water layer and the membrane.

In general, C_S can be expected to respond proportionally to C_W regardless of the region; but in order to interpret the data properly and obtain an accurate value for C_W based on a measured value of C_S, it is necessary to determine the applicable uptake kinetics region for the specific compound and exposure time.

5.2 FIELD WORK

5.2.1 Construction of the SPMD cages

Wire cages were constructed to hold one SPMD each. A 46 cm x 61 cm piece of the wire screen was rolled into a 61 cm long cylinder with a radius of 7 cm. The two lengthwise ends were sealed together, and three 7-cm cuts were made at the tops and bottoms of the cylinders with approximately equal spacing between them. The three sections were folded over later to close the tops and bottoms of the cages. Copper wire was wrapped around the cylinder in an attempt to minimize biofouling. Two snap metal hooks were connected to the side of each SPMD using nylon cord woven through and around the wire screen. The SPMD was held in place by a wire running diametrically across the top and two pieces of wire on the bottom sides. See Figure 5.3 for an illustration of an SPMD-loaded wire cage.

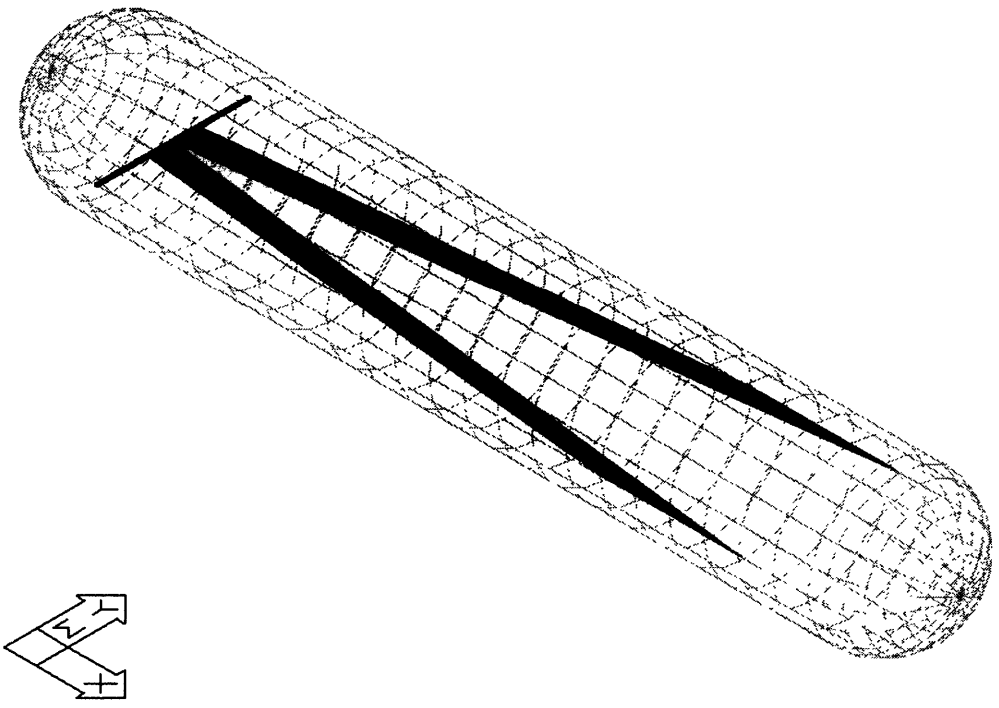

Figure 5.3 - SPMD-loaded wire cage.

5.2.2 Sampling Sites

The SPMDs were placed in four sites in the Boston Inner Harbor. Figure 5.4 shows a map of the Boston Inner Harbor indicating the location of the sampling sites.

One SPMD each was placed in 3 of the 4 sites: mouth of Chelsea River, across from the mouth of the Charles River, and Logan Airport, and two were placed at the near the north column of the Tobin Bridge. The sites were chosen for two main reasons. First, a good distribution of the sampling sites over the Boston Inner Harbor was necessary in order to see any spatial variation of the PAH concentrations. Besides revealing important information about their sources and fate, the results were also intended for comparison with a 3-D model of the PAH concentrations in the Boston Inner Harbor. Second, the site had to have a convenient and accessible point of attachment for the SPMDs. The initial plan included a sampling site at the confluence of the Mystic and Chelsea Rivers to incorporate PAH contributions from both sources, but obtaining a site there turned out to be difficult because of bureaucratic and navigational reasons. As a compromise, sampling sites were placed near the mouths of the Mystic and Chelsea Rivers. Two SPMDS at different depths were placed at the close to the north column of the Tobin Bridge to check for a vertical variation in PAH concentrations. This sampling site is located in one of the areas of the Inner Harbor that will be dredged so it is of particular interest. See Table 5.2 for the sampling depths at each site.

The SPMD cages were attached vertically to nylon ropes using the metal hooks. The ropes were marked to allow for measurement of the depths of the SPMD cages once they were lowered into the water. For the location under the Tobin Bridge, a buoy had to be constructed so that the SPMD cages could be placed farther away from the shore and some wood pilings in the area. There was some concern that the wood pilings could serve as a local source of PAHs because some pilings in the harbor are known to be coated with creosote to retard their decomposition. Table 5.3 shows the chemical composition of creosote (Supelco, 1996).

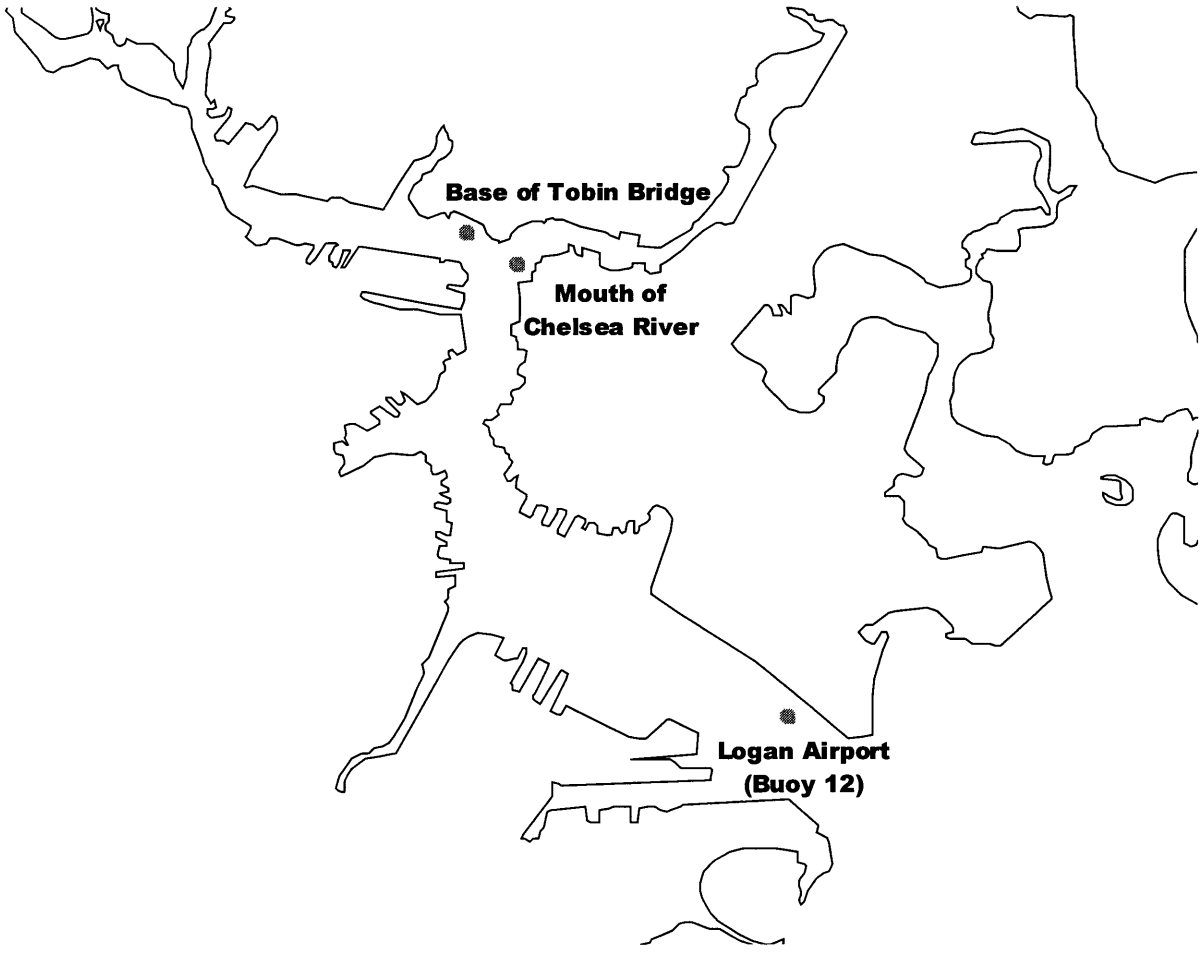

Figure 5.4 - Map of the Boston Inner Harbor showing the sampling locations.

Table 5.2
Sampling depths at the different sites

Location Name	Latitude & Longitude	Sampling Depth (m)
Base of Tobin Bridge - bottom (BTB-b)	N 42° 23.122 min W 071° 02.85 min	2.1 m[a]
Base of Tobin Bridge – surface (BTB-s)	N 42° 23.122 min W 071° 02.85 min	6.1 m[a]
Mouth of Chelsea River (MCR) (Buoy #16 – U.S. Coast Guard)	N 42°23.050 min W 071°02.534 min	4.3 m[b]
Across from the Mouth of the Charles River (AMCR)	N 42° 23.139 min W 071° 02.816 min	4.6m[b]
Logan Airport (LA) (Buoy #12 – U.S. Coast Guard)	N 42° 20.955 min W 071° 01.124 min	4.6 m[b]

[a]Measured from the bottom of the harbor. Note that the average depth of the harbor is approximately 10m.
[b]Measured from the water surface.

Table 5.3
Components of Creosote (Supelco, 1996)

Components of Creosote	
Naphthalene	Methyl fluorenes
2-Methylnaphthalene	Anthracene
1-Methylnaphthalene	Phenanthrene
Biphenyl	Carbazole
2,6-Dimethylnaphthalene	Fluoranthene
2,3-Dimethylnaphthalene	Pyrene
Acenaphthalene	Chrysene
Fluorene	Dibenzofuran

5.2.3 Deployment of the SPMDs: February 13th

The SPMDs were stored in a -75°C freezer until the day of deployment. They were then transported to the sites in a cooler with dry ice. The SPMDs were kept sealed in the cans to prevent contamination from the ambient air. The sites were accessed from a motor boat. During assembly of the SPMD apparatus, the motor of the boat was kept in a downwind position relative to the SPMDs to minimize their exposure to the exhaust from the motor. The motor could not be turned off because this would have made control of the boat difficult.

The SPMDs were quickly but carefully taken out of the cans, folded transversely and placed in the cages. The two free ends were attached to opposite sides of the cages with wire. The tops and bottoms of the cages were closed by folding over the three sections of the wire screen and were lowered into the water as quickly as possible.

In addition to the five SPMDs deployed, a blank was also brought to the field. At the same time the fifth SPMD was removed from its can, the blank can was also opened to expose the SPMD inside to the ambient air for the duration of the assembly. After the fifth SPMD was deployed into the water, the blank can was resealed and replaced in the cooler then stored back in the freezer.

5.2.4 SPMD collection: February 27th

The SPMD cages were retrieved after 14 days. The average temperature of the water over the exposure time was approximately 4°C. The SPMDs were removed from the cages as quickly as possible and directly returned to the cans. The resealed cans were kept in a cooler with dry ice until they could be placed in the freezer again. The blank SPMD was re-exposed to account for exposure during a collection procedure. As before, the boat motor was kept downwind. It should be noted that there was more exhaust from the motor of the boat used during the collection than the boat used during deployment.

Very little biofouling had occurred on the SPMDs, most likely due to the low temperature in the water. The cans were stored in the freezer at -75°C until later extraction and analysis.

5.3 LABORATORY METHODOLOGY

5.3.1 Reagents and Materials

5.3.1.1 Reagents and solvents

All solvents (methylene chloride (DCM), hexane, and methanol) used were JT Baker Ultra resi-analyzed grade. 2-methylnaphthalene, pyrene, and benzo(a)pyrene dissolved in DCM were ordered from Supelco, Bellafonte, PA in 200 μg/mL concentrations. The solutions came in sealed amber ampules. The recovery standards used were d_8-naphthalene, d_{12}-perylene, and *p*-terphenyl. The d_8-naphthalene and d_{12}-perylene dissolved in DCM were in 2000 μg/mL concentrations and were kept in sealed amber ampules. The *p*-terphenyl came in solid form and was dissolved in DCM per the procedure described below. *n*-C_{24} was used as the internal standard and was used for sample volume calculations. d_{10}-Acenaphthene (800 ng) and d_{10}-phenanthrene (400 ng) were spiked into all the SPMDs before they were heat-sealed by Environmental Sampling Technologies.

5.3.1.2 Materials

Ten SPMDs were purchased from Environmental Sampling Technologies (EST), a division of CIA Labs, St. Joseph, Missouri. The tubes were 32-36" x 1" and contained 1 mL high purity triolein. Upon request, each SPMD was spiked with 800 ng of d_{10}-acenaphthene and 400 ng of d_{10}-phenanthrene. EST is currently the only licensee of the government-owned SPMD patents (US Patents #5,098,573 and 5,395,426). The SPMDs came individually stored in sealed, argon-filled cans. Upon arrival at the lab, the cans were stored in a freezer at -75°C.

The metal cages for the SPMDs were constructed using a wire screen with 1 cm x 1 cm grid holes (61 cm wide), nylon cords, metal snap hooks, copper wire, and zinc alloy wire. For the deployment, cinder block and bricks were used as weights. The SPMD deployment also required the use of floats, nylon rope, and duct tape.

Kuderna-Danish concentrators (reservoirs, receiving flasks, and condensers with 50 mL and 500 mL capacities) were used to reduce sample volumes.

SiO_2 gel columns were prepared by making a slurry of SiO_2 and hexane: 3.8 grams of fully-activated SiO_2 in a small beaker were mixed with hexane until the SiO_2 was saturated. A small plug of glass wool was added to the bottom of each column. The slurry was poured into the column slowly using hexane to wash the solids out of the beaker and into the column. Approximately 0.5 grams of Na_2SO_4 was added to the top of each column to absorb any water in the sample. The column was then conditioned with 50 mL of hexane.

5.3.2 Methods

5.3.2.1 General glassware cleaning procedure

All glassware used was soaked for at least two days in a NaOH/trisodium nitrilotriacetate cleaning solution prior to use. They were then rinsed with water then air-dried and stored in a laminar flow clean hood. All water used in the laboratory was reverse osmosis pre-treated, cycled through ion-exchange resins and activated carbon filters until a resistance of 18-MΩ was achieved, then passed through a 0.2 μm filter pack just prior to dispensing. Immediately before use, glassware was rinsed three times each with DCM followed by hexane. If glassware was washed recently, it was rinsed first with methanol then followed by DCM and hexane, in order of decreasing polarity. All other materials (pipette, spatula, scissors, etc.) that were placed in direct or indirect contact with the samples were rinsed with DCM and/or hexane prior to use.

5.3.2.2 Analyte Discharge from the SPMDs

As was previously noted, it is important to determine the applicable kinetics region for the duration of the SPMD exposure. To accomplish this, a lab experiment was conducted in which 4 SPMDs containing 2-methynaphthalene, pyrene, and benzo(a)pyrene were exposed to water for varying time intervals to determine their discharge behavior over time

Spikes were prepared by taking the 1 mL 2-methylnaphthalene-, pyrene-, and benzo(a)pyrene-solutions and quantitatively transferring from the amber ampules into individual 10-mL volumetric flasks. Hexane was added to the 10 mL mark, then the solutions were transferred to 10 mL amber vials to protect them from photodegradation. The final spike solutions had concentrations of 20 μg/mL.

5.3.2.2.1 Analyte discharge from the SPMDs

An 8-L cylinder (approximately 15 centimeters in diameter and 46 centimeters in height) was filled to within 1 cm from the top with water. A pair of wooden sticks were crossed over, taped together, and placed on top of the cylinder.

Four cans containing SPMDs were removed from the freezer. Each SPMD was removed from the can and a pair of scissors was used to cut a 2-4 mm slit at one end of the polyethylene film. 25 μL of each spike solution (500 ng of analyte) were injected into these slits using a syringe. The film surface area exposed to the air was minimized as much as possible. Inevitably, some air (approximately 1 mL or less) was introduced into the SPMD during this procedure.

After spiking, the film was folded transversely so that the two ends met. One of the ends was then rotated 180°, so that the loop resembled a Mobius strip. This was done, as

suggested by Lebo *et al.* (1992), to prevent the two sides of the SPMD from clinging together, thereby assuring maximum surface area. The two ends were folded over twice then secured with a metal clip to ensure that the hole would not allow leakage of the triolein and the spike. A second metal clip was fastened to the bottom of the loop to act as a weight when the SPMD was suspended in water.

The four SPMDs were then lowered into the water-filled cylinder and were kept suspended from the sticks. The SPMDs were separated from each other as far as possible without allowing them to stick to the sides of the glass cylinder. The top and sides of the cylinder were kept covered with aluminum foil to prevent photodegradation of light-sensitive PAHs. The temperature in the laboratory was about $18^{o}C \pm 3^{o}C$ over the duration of the experiment.

To purge the water in the cylinder of any PAHs and other chemicals that diffused out of the SPMDs, water was flowed through the cylinder daily for a minimum of 30 minutes at a rate of 1 L/min. For the first two days, water was introduced at the top of the cylinder and the water was stirred with a spatula to induce mixing and water volume exchange. Realizing the inefficiency of this process, a 50-cm teflon tube was attached to the water nozzle and was then placed in the bottom of the cylinder to ensure better water exchange in the cylinder for the remaining fourteen days.

SPMDs were removed at 4-day intervals resulting in 4, 8, 12, 16-day exposures. The storage cans were prepared by blowing N_2 gas through them to purge them of any possibly-contaminated air. The SPMDs were then placed inside the can, and N_2 gas was blown through them again to induce partial drying. The SPMDs were not dried completely before the cans were resealed and replaced in the freezer at $-10^{o}C$ for later analysis.

5.3.2.3 Extraction and Analysis of the SPMDs

5.3.2.3.1 Dialysis

- **Lab samples**

The four SPMDs from the lab experiment were removed from the freezer and allowed to warm up to room temperature. Each SPMD was then spiked with 100 μL of a combined recovery standard solution (2.9 ug/mL *p*-terphenyl, 3.0 μg/mL d_8-naphthalene, 3.0 μg/mL d_{12}-perylene) through the original slits using micropipets. 600 mL beakers which served as the dialysis chambers were each filled with 485 mL DCM and 25 mL CH_3OH. The SPMDs were kept suspended in individual beakers with the clipped slits out of the solution to prevent leakage. An extra beaker containing only the solvent was included to serve as a blank. All beakers were covered with aluminum foil to minimize photodegradation and evaporation. All five beakers were placed in a N_2-filled glove bag to prevent possible contamination from the ambient air. The blank, day-4, day-8, day-12, and day-16 samples were dialyzed for 40, 46, 48, 69, and 71 hours, respectively.

- **Field samples**

In order to optimize the dialysis process and reproduce the methods utilized in previous studies by other investigators (Meadows *et al.*, 1993), a solution of 450 mL hexane and 50 mL DCM was used for the dialysis of the field samples. This was carried out in stoppered flasks that were used as dialysis chambers in order to minimize solvent evaporation and exposure to contaminants. The flasks were kept in a laminar flow-clean hood over the duration of the dialysis. The use of a N_2-filled glove bag was deemed unnecessary in light of the above-mentioned method improvements.

The SPMDs were allowed to warm up to room temperature before they were wiped down quickly with lint-free wipes and spiked with 100 μL of the combined recovery

standard solution. As previously mentioned, the SPMDs experienced very little biofouling and it was decided that attempting to clean the SPMDs (e.g., soaking in a KOH solution then isopropyl alcohol) might actually lead to more contamination, thus negating its potential benefit. After spiking, the SPMDs were lowered into the flasks and as much of the film as possible was exposed to the solvent (in some cases, adding approximately 50 mL solvent (9:1 hexane/DCM) was necessary). Again, a flask containing only solvent was included in the dialysis procedure. The field SPMDs were dialyzed for 80 hours.

5.3.2.3.2 Kuderna-Danish Concentration

A Kuderna-Danish (KD) concentrator was used to reduce the volume of the dialysates. It was noted that in the case of the field samples, some solvent had penetrated the SPMDs but their volumes were deemed insignificant relative to the total volume of the dialysates. The dialysates were transferred to the reservoir quantitatively. Kuderna-Danish concentration was also used after the silica gel column chromatography procedure described below. Concentrating proceeded until the sample volumes were reduced to approximately 4-8 mL.

5.3.2.3.3 N_2 blowdown and hexane exchange

A stream of dry nitrogen gas was used to further reduce volumes of samples. This step was performed to produce sample volumes of 1 mL for silica gel column chromatography and a few hundred microliters for the gas chromatographic analysis. The extracts were exchanged into hexane by reducing the volume to approximately 200 μL, filling up to the 1 mL mark with hexane, reducing the volume to a few hundred microliters, then repeating the process one more time until the sample volume is reduced to approximately 150 μL.

5.3.2.3.4 SiO_2 Gel Column Chromatography

The silica gel columns described previously were used to separate the samples into three fractions (F). The following eluants were collected:

F_1: 6 mL hexane
F_2: 44 mL hexane
F_3: 30 mL 10% DCM/hexane

F_3, the PAH-containing sample, was re-concentrated using Kuderna-Danish concentration and N_2 blowdown procedures in preparation for the gas chromatography.

It is worth mentioning that the lab SPMDs were expected to be relatively "clean", i.e. containing 8 compounds only (d_{10}-acenaphthene, d_{10}-phenathrene, three recovery standards, 2-methynaphthalene, pyrene, and benzo(a)pyrene) therefore it was assumed that fractionation would not be necessary. The pre-silica gel column chromatography samples turned out to be complex mixtures of various indeterminate groups so fractionation was also performed on them. The source(s) of the contamination have not been clearly identified. Contamination from brief exposures to the ambient air may be partially responsible.

5.3.2.3.5 Gas Chromatography

The gas chromatograph used in this experiment was equipped with a flame ionization detector (GC-FID). It is a Carlo Erba, HRGC 5160 mega series with an on-column injector, 30 m DB5 column, and hydrogen as the carrier gas. A Hewlett-Packard model 3396 series II integrator was used for data collection and peak area determinations.

The temperature program for the gas chromatograph was as follows: initial temperature of 70°C with a hold time of 1 min; increase temperature at 20°C/min until 180°C then increase temperature at 6°C/min until 300°C. For the lab samples, the temperature was

held at 300°C for 5 minutes. The hold time was increased to 15 minutes for the field samples to ensure complete elution of high-molecular weight compounds between runs.

F_3 sample volumes were reduced to approximately 150 μL then 50 μL of *n*-C_{24} was added as an internal standard for volume calculations. Each injection contained approximately 1 μL of each sample.

5.4 RESULTS AND DISCUSSION

5.4.1 Laboratory Experiment: Dissipation of Compounds from SPMDs

For half of the samples, the front and end regions of the gas chromatogram were difficult to analyze because of interfering peaks from contamination and a baseline drift. It has not been determined what the source(s) of contamination was (were). The sample recoveries for d_8-naphthalene were very low and ranged from 0-17%, most likely because of its loss through volatilization. Because of the poor recovery of its corresponding standard, 2-methylnaphthalene could not be quantified with confidence. On the other end, sample recoveries for d_{12}-perylene were erratic and unreasonable, ranging from 7% to 180% for the various samples. This may indicate that the d_{12}-perylene peak was not correctly identified or the integrator may not have been able to resolve it well. Chromatography runs through the silica column may have also been erratic. As a result, benzo(a)pyrene was also not quantified. The two compounds, d_{10}-acenaphthane and d_{10}-phenanthrene, which were spiked into the SPMDs by EST Technology, were also difficult to identify in the gas chromatograms.

Except for one of the samples (day 16), the recoveries for *p*-terphenyl were reasonably consistent, although somewhat low, and both *p*-terphenyl and pyrene were identifiable from the chromatograms. The sample recoveries ranged from 31% to 52% (42% ± 10%). Pyrene concentrations decreased smoothly over the 16-day test period (Figure 5.5).

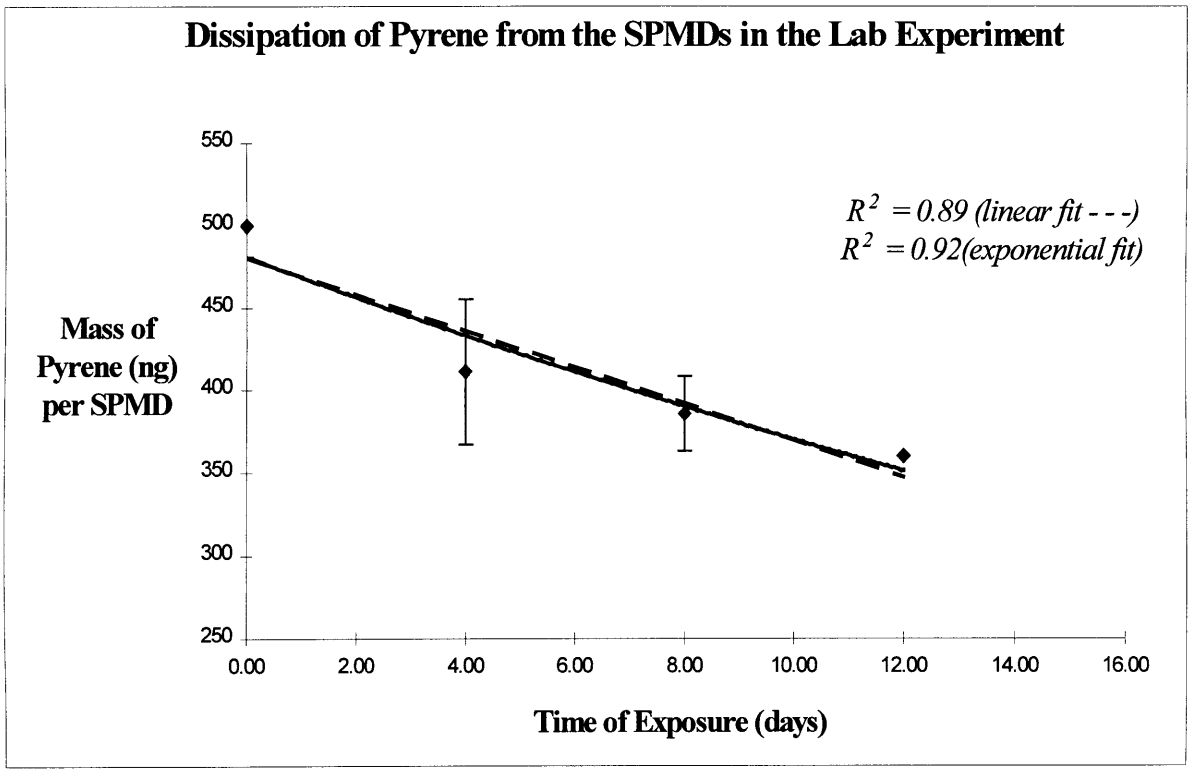

Figure 5.5 - Dissipation of pyrene from the SPMDs in the Laboratory Experiment. For the actual data, see Appendix A. Note that the SPMDs were originally spiked with 500 ng of pyrene prior to dissipation. Error bars on the two points are related to injection imprecision. Day 4 (n=4 injections), day 8 (n=2), day 12 (n=1). Day 16 was not quantified because the recovery was unreasonably high at an average of 160% for three injections.

The data for pyrene dissipation from SPMDs over time were fit into both exponential and linear models. As the graph demonstrates, the exponential dissipation kinetics of SPMDs for pyrene was closely approximated by a linear relationship over this time interval, in agreement with Huckins' model. Assuming that the uptake and dissipation behavior of the SPMDs were the same, the results suggested that, in the case of uptake, the following relationship could be used to relate pyrene concentration in the triolein, C_S, to its concentration in the water, C_W, over this time interval: $C_S = R_{WS}C_W$ (see Section 5.1.3, Eqn. 5.8), where R_{WS} is a function of time.

Recent work by Huckins *et al.* (1998) gave the equivalent relationship: $C_W = (C_{SPMD}V_{SPMD})/R_St$, where $C_{SPMD}V_{SPMD}$ is the mass of the analyte extracted from the membrane and the triolein in the dialysis procedure, and $R_S = k_eK_{SPMD}V_{SPMD}$ with K_{SPMD}

= C_{SPMD}/C_W. In this case, R_S is a variable that is independent of time but is a function of the membrane design and the compound of interest. The k_e can be derived from dissipation studies such as this one by using the following relationship between the initial concentration in the SPMDs, C_{SPMDo}, and concentrations over time, C_{SPMD}: $C_{SPMD} = C_{SPMDo}\exp(-k_e t)$. The k_e for pyrene in this controlled laboratory experiment was found to be 0.026/day at an average temperature of approximately 18°C. This value is slightly higher than what can be expected from the tabulated values in the Hucks Table (Huckins *et al.*, 1998) of 0.024/day at 26°C and 0.015/day at 18°C and 10°C, but it is in reasonable agreement (Table 7.1). Using pyrene's K_{SPMD} value of 62,100 tabulated in the same table and a total SPMD volume, V_{SPMD}, of 0.0057 L (volume of triolein = 1mL and volume of membrane = 4.7 mL), R_S was calculated to be 9.2 L/day. Huckins *et al.* calculated R_S to be 7.9 L/day at 26°C, 5.2 L/day at 18°C, and 5.1 L/day at 10°C.

Table 5.4
R_s or sampling rates (relative standard deviation in %) and k_e or dissipation rates at different temperatures.

TEMPERATURE		10°C		18°C		26°C	
Compound	K_{SPMD}	R_s (L/day)	k_e (day^{-1})	R_s (L/day)	k_e (day^{-1})	R_s (L/day)	k_e (day^{-1})
phenanthrene	29,600	3.9 (6)	0.024	3.4 (9)	0.021	4.6 (5)	0.029
fluoranthene	48,000	4.3[ab] (-)	0.016	4.6[ab] (-)	0.018	7.2[b] (8)	0.028
pyrene	62,100	5.1 (10)	0.015	5.2 (12)	0.015	7.9 (9)	0.024
benz(a)anthracene	210,800	3.6 (9)	0.003	3.6 (9)	0.003	5.5 (8)	0.005
chrysene	209,300	4 (11)	0.004	5.1 (7)	0.004	7.4 (9)	0.006

The relative standard deviation is the standard deviation divided by the mean multiplied by 100%. These values were taken from unpublished data in the Hucks Table. [a]$n \leq 2$, [b]Recovery from SPMDs based on average of anthracene and pyrene values because of interfering peaks (only in recovery studies). The R_S values in the Hucks Table were derived from 14-day controlled laboratory exposures of SPMDs to water containing 100 ng/L of the target compound (Huckins *et al.*, 1998).

The difference in R_s values may be a result of deviations in experimental procedure and associated errors and uncertainty. It is difficult to assess the errors and uncertainty associated with the measured values here because only one sample was available for each exposure time and only injection-associated errors could be quantified for two of the points.

5.4.2 Field Measurements

The hydrophobic, and generally nonpolar, structure of triolein makes it able to dissolve many organic compounds (e.g., PAHs, PCBs, etc.) found in the aquatic environment. Upon exposure in Boston Harbor, the triolein then became a complex "soup" of organic compounds. The extract from the field samples remained a complex mixture of compounds, even after clean-up with silica gel column chromatography. There appeared to be unresolved mixtures of compounds in the front ends of the chromatograms and interfering peaks at the back ends which obscured the PAH signal pattern (Figure 5.6). Lebo *et al.* (1992) speculated that, in addition to other contaminants in the water (e.g., chlorinated hydrocarbons), interferences may result from trace oligomers from the polyethylene that remained even after extraction of the tubings, co-dialyzed triolein, and various biogenic materials from the small amount of aufwuchs (biofilm) found on the membrane surface. As noted in Section 5.3.2.3, the outside surfaces of the SPMDs were wiped down with lint-free wipes but did not undergo any other extensive clean-up prior to dialysis. It is possible that the silica gel column became saturated with the various compounds and was not able to fractionate the various compounds effectively.

A second run through a silica gel column was performed on one of the samples, and it removed some of the signals at the back end, but it was unable to clean up the unresolved mixture at the front end. However, a combination of a second run through a silica gel column, attenuation of the integrator output, and a dilution of the sample to

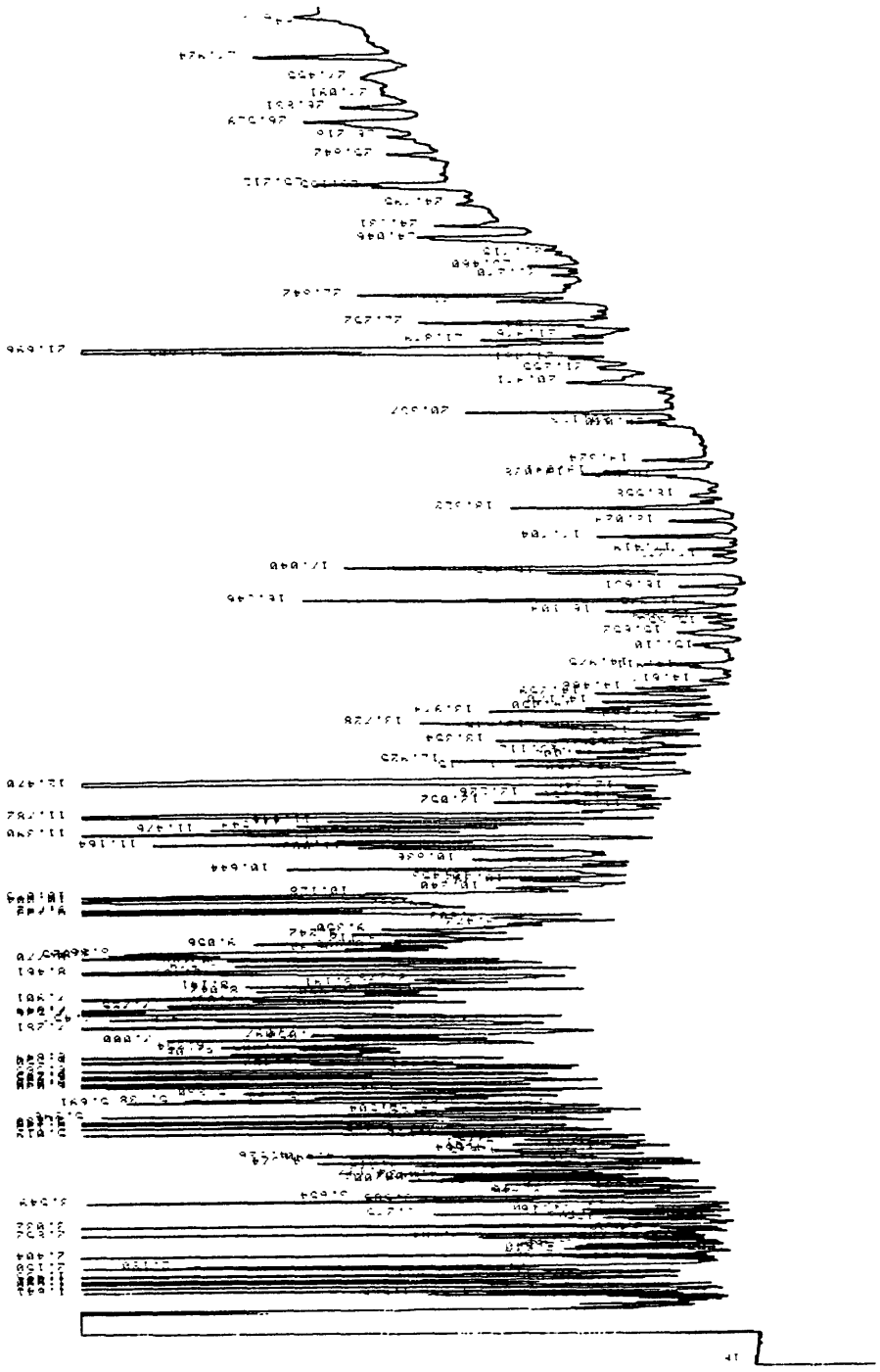

Figure 5.6 - PAH chromatogram of the Logan Airport - Buoy #12 (LA) sample after first run through the silica column.

approximately 340 μL (most samples were concentrated down to about 100 μL or less prior to injection into the GC) did yield a chromatogram that clearly showed a PAH pattern in the samples similar to that of a PAH chromatogram of Charles River sediment (Figure 5.7). The removal of some of the end peaks after a second run through a silica gel column indicated that the interferences in the back end were most likely not PAHs.

The use of a mass spectrometer in conjunction with a gas chromatogram (GC-MS) would have greatly simplified the process of compound identification since a GC-MS can be programmed to scan only certain pre-selected masses in the selected ion-monitoring mode (SIM). Unfortunately, a GC-MS was unavailable for use in this study. Further experiments should examine the improvements afforded by the use of this detection method.

A standard containing various PAHs commonly found in environmental samples was injected into the GC-FID in order to obtain a reference chromatogram. Under the same conditions (i.e., temperature settings, injection method, column length, etc.), compounds can be expected to travel through the column in the same manner. Therefore, this reference chromatogram can provide the expected retention times of the individual PAHs in the column and the means of identification of PAHs in the field samples (Figure 5.8). In addition, the reference chromatogram can be used to calculate relative retention times which are also useful tools for confirming the identity of a compound. For example, knowing that the retention time of pyrene in the column is usually 1.06 times greater than that of fluoranthene provides an alternative means of identifying fluoranthene when pyrene can be identified with confidence.

As with the laboratory samples, the two recovery standards d_8-naphthalene and d_{12}-perylene were difficult to identify from the gas chromatograms, and only *p*-terphenyl yielded recoveries that could be applied. The recovery for *p*-terphenyl was 63% ± 18%. The recoveries ranged from 26% to 99%, which is quite a big range. This suggests problems with the reproducibility of the data. This perhaps could improve as the person

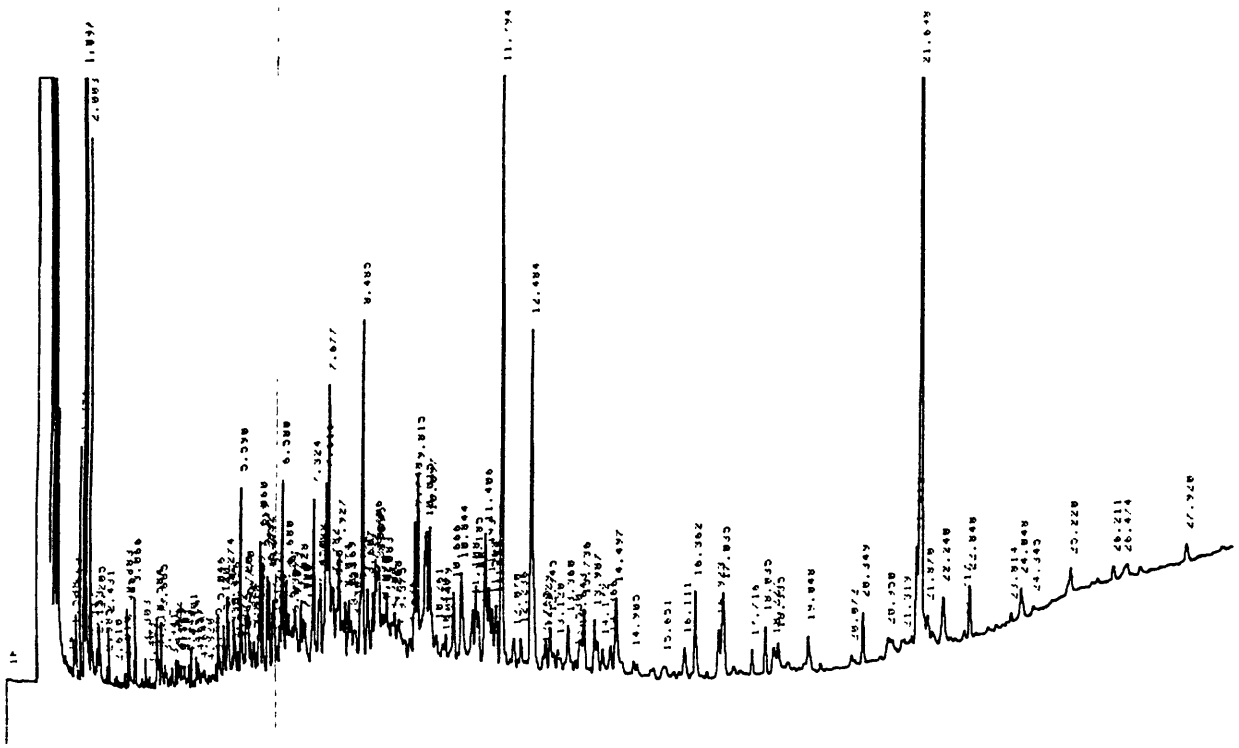

(a)

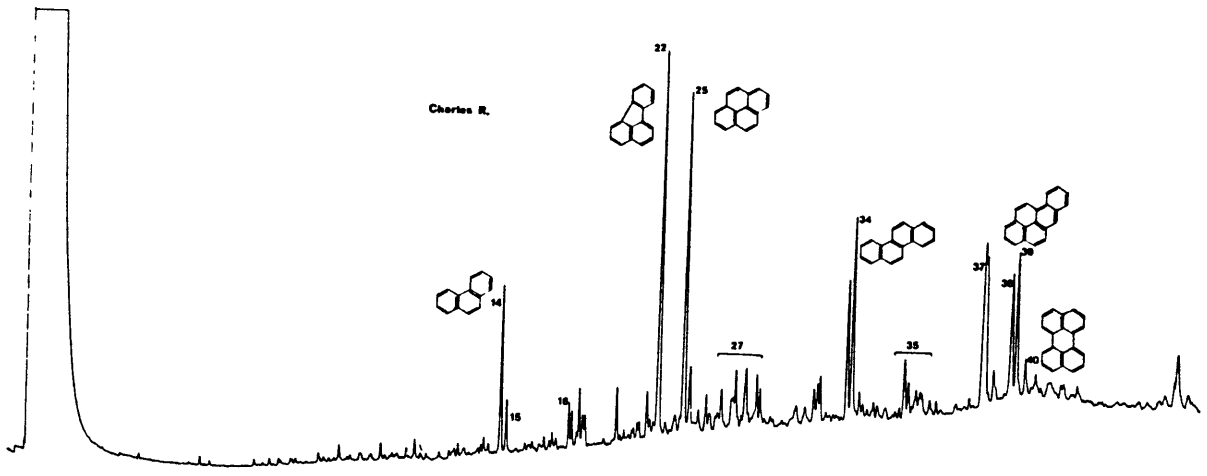

(b)

Figure 5.7 - (a) GC-FID chromatogram of the Tobin Bridge-surface PAH sample fraction and (b) High resolution gas chromatogram of PAH in Charles River sediment (Laflamme and Hites, 1978).

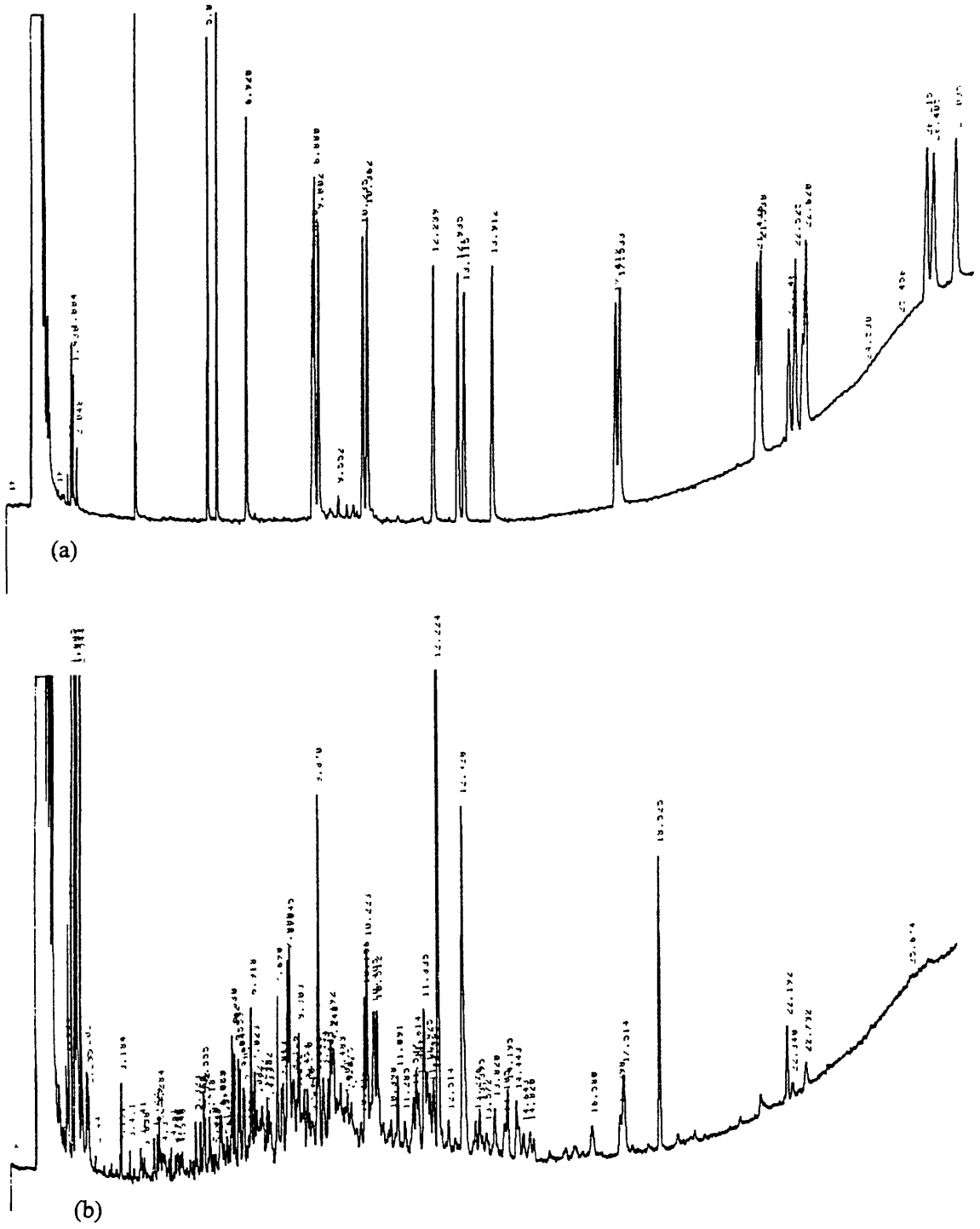

Figure 5.8 - (a) Gas chromatogram of a PAH standard and (b) gas chromatogram of the Tobin Bridge-bottom PAH fraction sample.

doing the analysis becomes more familiarized and experienced with the analytical procedure.

For most of the samples, the following compounds were identified: *p*-terphenyl, d_{10}-phenanthrene, phenanthrene, methyl-phenanthrene's (methyl groups in the 1, 2, 3, 4, and 9 positions; see Figure 3.1), fluoranthene, pyrene, benz(a)anthracene, and chrysene.

In deducing the water column concentrations of these compounds from their concentrations in the SPMDs, the following assumptions were made:

(1) the recovery of *p*-terphenyl is representative of the recoveries for the range of compounds identified and analyzed;
(2) the uptake kinetics for all compounds are in the linear region over 14 days;
(3) the sampling rates at 10°C tabulated in the Hucks Table are valid for this field sampling procedure; and
(4) biofouling did not significantly impede uptake into the SPMDs.

The use of *p*-terphenyl as the recovery standard for all compounds was obviously not ideal but was necessitated by the lack of data for any other recovery standards. However, *p*-terphenyl can be expected to be a reasonable representative for the bigger compounds (fluoranthene, benz(a)anthracene, chrysene, and pyrene). Previous experiments (data not shown) have demonstrated that the behavior of *p*-terphenyl throughout the analytical procedure used here mimics those of pyrene and structurally- and chemically-similar compounds (as exhibited by K_{OW}'s, column retention times, etc.) (MacFarlane, 1998). The greater vapor pressures of the smaller compounds relative to the heavier *p*-terphenyl possibly leads to greater loss through volatilization. In the past, experiments employing the same procedure used here have shown that *p*-terphenyl recoveries were usually greater by 10-20% compared to a smaller standard like d_8-naphthalene (MacFarlane, 1998).

The linearity of the uptake kinetics for all compounds identified is a justifiable assumption. Studies by Huckins *et al.* (1998) have shown that dissipation from the SPMDs is a linear function of time, or closely approximated by such, over 14 days for the range of compounds in this study (Huckins, 1998). In order to use data derived from homogeneous experimental procedures, all values used for R_S, including that of pyrene, were taken from the Hucks Table (Table 5.4). These values were derived from flow-through exposures of the SPMDs to 100 ng/L concentrations (kept constant over the duration of the experiment). Because only a value for phenanthrene was available in the Hucks Table, this R_S value was assumed to be a good approximation for d_{10}-phenanthrene and the methylated phenanthrene's.

The field sampling procedure deviated from the laboratory procedure of Huckins *et al.* (1998) in several important aspects. The fact that the R_S values used were derived for 10°C temperatures and the average water temperature in the harbor during the SPMD exposure was approximately 3°C may have resulted in an underestimation of the water column concentrations since sampling rates can be expected to decrease with lower temperatures. It should also be noted that the laboratory experiments were conducted under relatively quiescent flow conditions with velocities in the range of a few cm/s. Field velocities were greater, with velocities ranging from 0 to 30 cm/s. Uptake into the membrane can be expected to increase with increasing flow velocities because of the thinning of the water film layer, thus decreasing the water film resistance. An experiment by Huckins *et al.* (1993) showed that the amount of a PCB ([^{14}C]-2,2',5,5'-TCB) associated with the membrane under quiescent conditions versus turbulent conditions was greater by 26% .

The R_S values in the Hucks Table were derived from laboratory exposures, so biofouling was not taken into account. Assuming that biofouling did not significantly impede the uptake into the SPMDs over the 14-day field exposure may have resulted in an underestimation of extrapolated water concentrations since biofouling lowers sampling rates. According to a study by Huckins *et al.* (1998), biofouling impedance to PAH uptake increased with compound K_{OW} and ranged from a 20 to 70% decrease in uptake.

However, as was noted earlier, the biofouling on the membranes did not appear extensive (probably because of the low water temperatures) and was assumed to have had a negligible impact on uptake rates. It is possible that the temperature, velocity, and biofouling effects could have partially offset each other.

The field measurements ranged from 0.61 to 90 ng/L for the various PAHs (Table 5.5) Blank concentrations, which ranged from 0.0-0.64 ng/L, have been subtracted from the concentrations measured in each sample. The data appear reasonable in that the signal-to-noise ratio is good. On the average, the blank concentrations were only 2% of sample concentrations.

For all compounds measured, the highest concentrations were found in the Tobin Bridge–surface sample (Figure 5.9). There was a difference in the bottom (8 m from the surface) and surface (4 m from the surface) PAH concentrations in the Tobin Bridge site. The concentrations in the upper layer (BTB-s, MCR, and LA) versus the lower layer (BTB-b) were greater by approximately a factor of 10. All concentrations were found to be in the order of parts per trillion. For the three samples located in approximately the same depth (4 m below the surface), the magnitudes of the various PAH concentrations were quite comparable, varying within a factor of 3.

The ratios of methyphenanthrene's-to-phenanthrene and pyrene-to-fluoranthene were calculated as possible indicators of source and transport behavior. In all three sites, methylated phenanthrene levels were found to be about twice that of phenanthrene levels. This may indicate that one of the main sources of phenanthrene and related compounds into these sections of the harbor are of petrogenic origin.

However, the ratios of pyrene-to-fluoranthene suggest another origin. The ratios were found to be less than one for all sites, ranging from 0.61 to 0.96. Pyrene-to-fluoranthene ratios in the environment vary according to the primary sources (Table 5.6). These results suggest that the other potential major primary sources in the study areas are Boston air, street dust, and creosote.

Tables 5.5
Field Measurements Summary

	Phenanthrene	Methyl-Phenanthrene's	Methylphenan./ Phenanthrene
Blank	0.64	0.51	0.80
BTB-b	3.4	5.6	1.7
BTB-s	39	90	2.3
MCR	*N.I.*[a]	45	*N.I.*[a]
LA	25	55	2.2

	Fluoranthene	Pyrene	Pyrene/Fluoran
Blank	0.42	0.24	0.59
BTB-b	6.4	5.7	0.90
BTB-s	78	58	0.75
MCR	30	28	0.96
LA	48	29	0.61

	Chrysene	Benz(a)anthracene
Blank	0.00	0.00
BTB-b	1.3	0.7
BTB-s	15	8.7
MCR	5.0	2.6
LA	7.1	3.3

The extrapolated concentrations in the water column of the various PAHs identified in the gas chromatograms. [a] N.I.- could not be identified in the chromatograms. Base of Tobin Bridge - bottom (BTB-b), base of Tobin Bridge - surface (BTB-s), Mouth of Chelsea River (MCR), and Logan Airport (LA). See Figure 6.2 for the location of the sampling sites. For an explanation of the conversion from SPMD concentrations to water concentrations, see the text. All concentrations shown are in nanograms per liter. See Appendix B for the raw data and notes on uncertainties and assumptions.

Although creosote is expected to be present in areas of the harbor which have creosote-coated pilings, it seems unlikely that it was the major source. Combustion effluents have been found to be the major source of PAHs in diverse aquatic settings (Laflamme et al., 1977), suggesting that the Boston air is a likely source in this group. This does not

necessarily mean that the main mechanism of PAH input into the Inner Harbor is direct deposition from the atmosphere or diffusive air-water exchange. Other means of input (CSOs, runoffs, and river discharges) into the harbor could also carry with them previously-airborne PAHs.

Table 5.6
Pyrene-to-fluoranthene concentration ratios of common sources of PAHs in the environment.

Sample	Pyrene:Fluoranthene
Boston air[a]	0.77
Gasoline exhaust[b]	1.67
Street dust[c]	0.98
Creosote[d]	0.68
No.2 fuel oil[e]	1.11
SRC II coal liquid[f]	5.08
Coal synthoil C[g]	> 18.4

[a]Gschwend *et al.*, 1981. [b]Giger *et al.*, 1978. [c]Takada *et al.*, 1990. [d]Carey *et al.*, 1989. [e]Pancirov *et al.*, 1975. [f]Nishioka et al., 1988. [g]Guerin et al., 1978.

The pyrene-to-fluoranthene ratios found in this study agree well with those calculated for the rivers, CSOs, and stormwater drains that empty into the Inner Harbor (Table 5.7) (Menzie-Cura and Associates, 1995; Metcalf and Eddy, 1994; USGS, 1992). As illustrated in the table, the Charles River is a major source of pyrene and fluoranthene into the Inner Harbor.

Performing a rigorous error analysis on the use of SPMDs to deduce water concentrations was seriously hampered by the lack of sample duplicates. However, one can evaluate known errors associated with the calculations here in order estimate a minimum error. The errors (relative standard deviation = [standard deviation /mean] x 100%) associated with the injections and the p-terphenyl recoveries were 4% and 28%, respectively. The

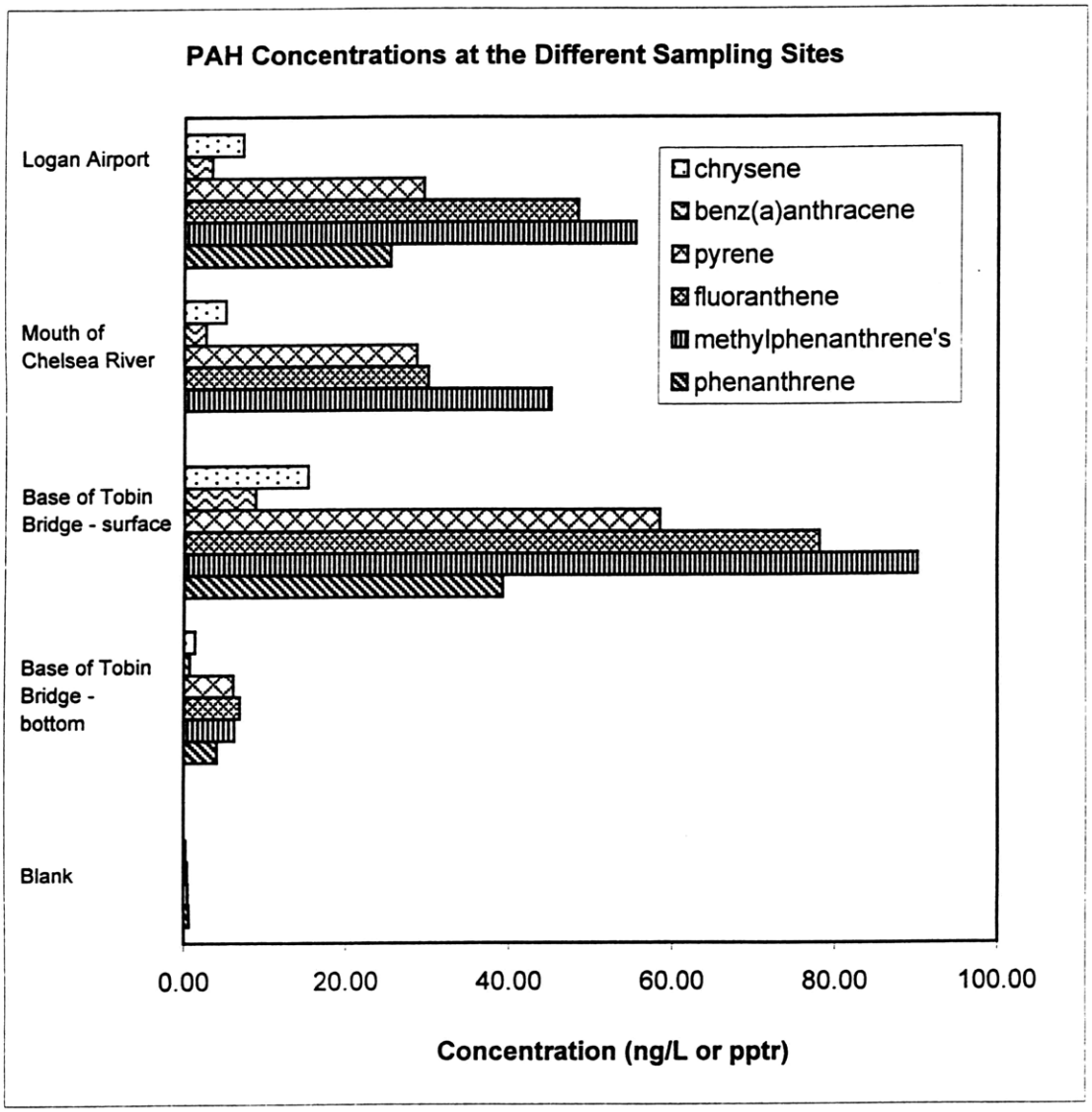

Figure 5.9 - Summary of PAH concentrations at the different sampling sites.

relative standard deviation associated with the Rs value of pyrene was 10%. The total error is given by the sum of these errors, which is 42%.

In the case of pyrene concentration at the base of Tobin Bridge–surface, for example, a total error of 42% yields a result of 58 ng/L ± 24 ng/L or, equivalently, 34-82 ng/L. Even with the associated errors, the concentration can still be expected to be well within an order of magnitude of the reported value of 58 ng/L.

One could also account for possible biofouling effects. Previous studies found a 20-70% impedance in uptake as a result of biofouling (Huckins et al., 1998). It is reasonable to assume that any impedance by biofouling in the measurements here would be in the low end of the range. Assuming a maximum impedance of 30%, which corresponds to a reduction in the sampling rate by 30%, the range then becomes 49-117 ng/L; again, this range is still in reasonable agreement with the reported value of 58 ng/L

It is therefore safe to assume that the values reported from the measurements have, at the least, the right order of magnitude .

Table 5.7
Pyrene to fluoranthene ratios in loadings

	Pyrene kg/yr	Fluoranthene Kg/yr	Ratios
Charles River	73	120	
Mystic River	7.6	11	
Chelsea River	0.4	0.6	
Total from Rivers	81	132	0.61
CSOs + stormwater	9	14	0.64

These loadings were calculated by multiplying averaged concentrations of pyrene and fluoranthene which were measured by Menzie-Cura and Associates in 3/25/92, 4/30/92, and 10/15/92 (1995) with average annual flow rates. The Charles River flow rates were taken from USGS measurements over the years 1931-1992 (USGS, 1992) and the Mystic and Chelsea River flow rates were scaled relative to those of the Charles River (Chan, 1993). The flow rates from the CSOs and stormwater drains were calculated from data collected by Metcalf and Eddy (1994).

6 THEORETICAL BASIS FOR MASS TRANSPORT

The purpose of the following chapter is to familiarize the reader with some of the basic theoretical concepts used in describing the fate and transport of PAHs in the environment. While there are many different ways to express each term in the overall system, the following is not intended to explore all possible options but rather the approaches used in the mass balance and 3D model presented in Chapters 7 and 8.

6.1 SEDIMENT-WATER EXCHANGE

It has been suggested that the most significant source of PAH loading to the Inner Harbor is the accumulated sediments in the bottom of the harbor (Stolzenbach *et al.*, 1998). The formulation of the theoretical model is therefore one of the most important components of the entire modeling effort. The transport of contaminants across the sediment-water interface is a complex physical process that can be modeled to varying degrees of physical and chemical precision.

There are a number of factors that influence transport of contaminants in a sediment environment. One general mechanism that often governs the transport of a contaminant in the environment is the process of molecular diffusion. This section will begin by introducing the process of molecular diffusion and then proceed to discuss this basic concept in the context of a more complex formulation of PAH transport from a sediment environment.

The process of molecular diffusion describes the migration of a chemical due to a concentration gradient. This flux is described by Fick's Law, as presented in Eq. 6.1.

$$F = -D_w \frac{\partial C}{\partial z} \qquad \text{(Eq. 6.1)}$$

where,

F	=	diffusive flux (kg/m^2s)
D_w	=	molecular diffusion coefficient (m^2/s)

$\partial c/\partial z$ = vertical concentration gradient (kg/m^4)

The concentration gradient which causes this flux exists between the sediment porewater and the overlying water column. One of the challenges in applying the concept of molecular diffusion is quantifying the distance over which this concentration gradient occurs. The conceptual layers which exist in the sediment water region and the transport within them will be discussed later in this section.

Within the sediment layer, PAHs can be freely dissolved in the porewater, sorbed to sediment material, or sorbed to colloidal material. However, only the dissolved and colloidal fractions of the PAHs can be considered mobile. In order to establish a concentration gradient, it is necessary to describe the porewater concentration within the sediment bed. To simplify the analysis, we will assume that the porewater is in equilibrium with the sediment, and that the dominant sorption mechanism is due to the organic content of the sediment. Porewater concentration of each PAH can be related to the amount of PAH sorbed to the organic content of the soil via the organic matter partitioning coefficient, K_{om}, defined as

$$K_{om} = \frac{C_{om}}{C_{pw}} \qquad \text{(Eq. 6.2)}$$

where,

C_{om} = concentration of PAHs sorbed to organic matter (g/kg)
C_{pw} = dissolved porewater concentration (kg/m^3)

Multiplying this constant by the fraction of organic carbon content of the sediment yields the distribution coefficient for the sediment water interface, which expresses the equilibrium distribution of the compound sorbed to the sediment to the porewater concentration.

$$K_d = \frac{C_s}{C_{pw}} \qquad \text{(Eq. 6.3)}$$

where,

C_s = concentration of PAHs sorbed to the sediments (g/kg)

In employing this distribution coefficient, K_d, to completely describe the partitioning process between the sediment and the porewater, two important assumptions have to be made. The first assumption is that the partitioning process can be described by a linear isotherm. It must also be assumed that only sorption to the organic matter of the sediment need be considered (i.e., other mechanisms such as mineral and ionized sorption are ignored). Because the PAHs of interest are all neutral, nonpolar compounds, both of these theoretical assumptions may be considered valid. Sorption isotherms for such compounds are linear, and provided there is a significant organic content in the sediment, organic matter sorption is the only process that need be considered (Schwarzenbach *et al.*, 1993). It should also be mentioned that recent research has suggested that a significant portion of PAHs measured in sediments may be permanently bound to soot particles and therefore unavailable for equilibium partitioning. This topic will be discussed further in Section 7.2.4.

There is a directly analogous equation which can be used to describe the partitioning of PAHs sorbed to colloidal material. The theoretical equilibrium between the colloidal distribution coefficient, K_{dcol}, is the ratio of concentration sorbed to colloidal material C_{col} to the concentration in the equilibrated porewater, C_{pw}. Fickian diffusion could also be employed in modeling the transport of these particles.

There are a number of other transport processes in a sediment bed environment which potentially affect the transport of PAHs into the overlying water column. In addition to diffusive processes, porewater advection can enhance the rate of transport. Advection, which can be defined as the transport of the organic contaminants by the movement of the carrier fluid, can be enhanced by processes such as groundwater discharge and biological (benthic) activity in the near bottom sediment layer. Biological sediment transport can generally be classified as either bioturbation (contaminant transport by the stirring of sediments by benthic organisms) or bioirrigation (the enhanced exchange of porewater through the burrowing of tube-dwelling organisms).

As previously mentioned, there are a number of processes which need to be incoporated into a model of sediment-water exchange. The following discussion outlines the model formulated by Hsiao-Wen Chen in her 1993 study of the fluxes of organic pollutants from Boston Harbor sediments. There are essentially four layers within the aquatic environment which are distinctly different in terms of transport mechanisms. These include the turbulent water layer, diffusive water boundary layer near the sediment-water interface, the biologically active sediment layer, and the buried sediment layer (Chen, 1993). These layers are depicted in Figure 6.1 in a conceptual way. In order to formulate a simplified yet accurate model of the net transport of contaminants across this interface, it is necessary to determine which layers limit the vertical flux of contaminants. The uppermost layer, which is dominated by turbulent diffusion in shallow waters such as the study area, can be considered flushed rapidly enough as to not limit the upward flux of chemicals (Chen, 1993). The next layer is the stagnant diffusive water-side boundary layer across which contaminants are transported primarily through molecular diffusion. This layer can limit the overall flux of contaminants, depending primarily on its thickness. The biologically active layer in the sediments exists immediately beneath the sediment-water interface and is dominated by bioturbation, bioirrigation, and molecular diffusion. Below the biologically active layer is the buried sediment layer in which there is very little benthic activity, which makes molecular diffusion the dominant transport process (Chen, 1993).

The mathematical formulation of the overall flux resulting from the combined effects of these transport processes can be expressed by Eq. 6.4

$$F = \frac{\frac{C_s}{K_d} - C_w}{\frac{t_{res}}{H} + \frac{\delta_w}{D_w} + \frac{1}{\phi r\left(\overline{D}_B + \overline{D}_m\right)(1+\varepsilon)} + \frac{L}{\phi D_B \rho K_d (1+\varepsilon)}} \qquad \text{(Eq. 6.4)}$$

where,

t_{res} = mean residence time (days)
H = depth of water column (m)

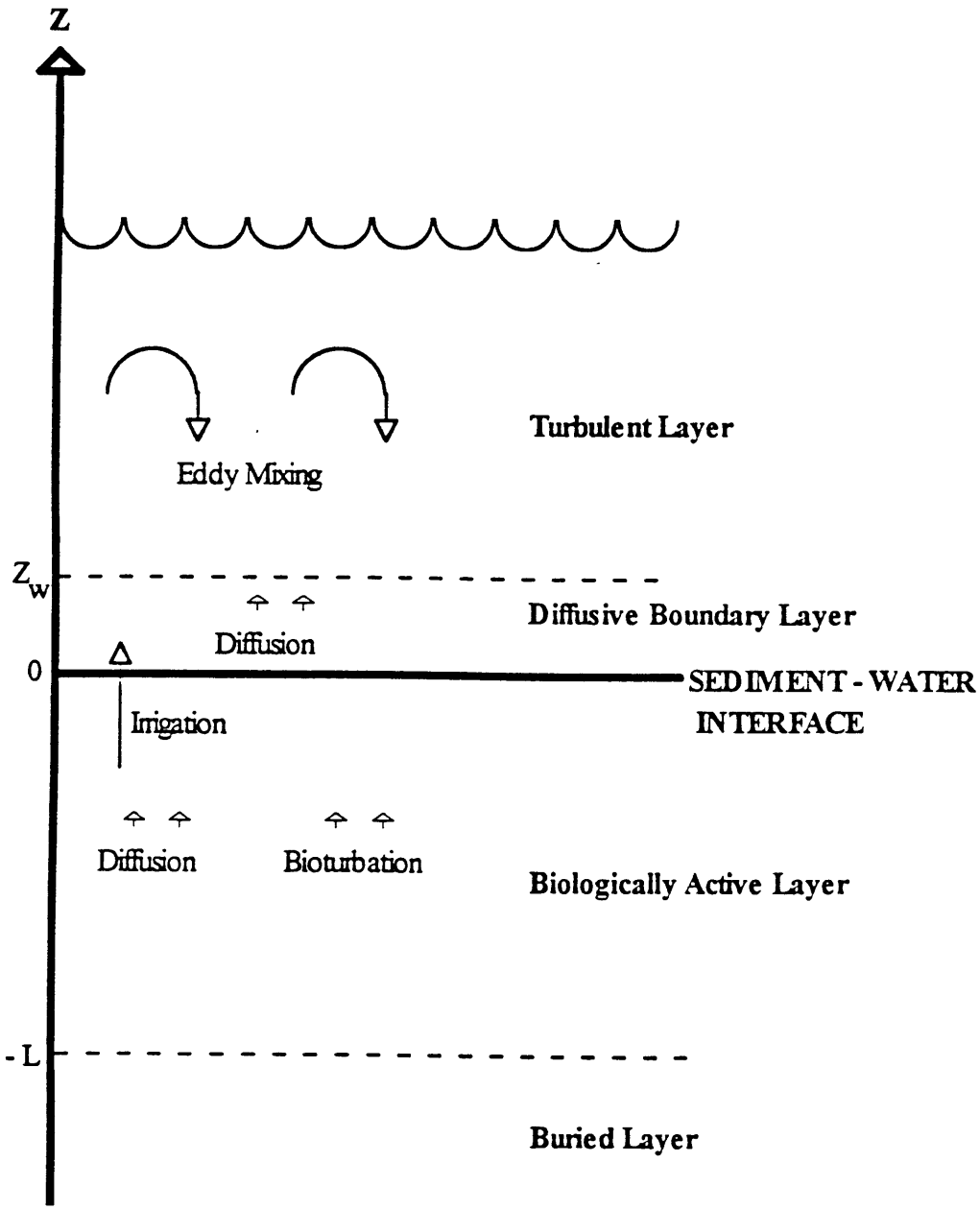

Figure 6.1 – Sediment-Water Exchange Model Layers (Chen, 1993)

δ_w = diffusive boundary layer thickness (m)
D_m = molecular diffusivity in aqueous solutions (m^2/s)
D_w = $D_m + D_c K_{dcol} C_{col}$ (m^2/s)
$\overline{D_m}$ = $D'_m + D'_c K_c m_{coc}$
D'_c = colloidal diffusivity in sediment porewater (m^2/s)
D'_m = molecular diffusivity in sediment porewater (m^2/s)
ϕ = porosity of sediment
r = reciprocal length scale (m^{-1})
D_B = bioturbation coefficient (m^2/s)
$\overline{D_B}$ = $D_B(1+K_c m_{coc})$ (m^2/s)
K_c = colloid-water distribution coefficient (m^3/kg)
m_{coc} = concentration of colloidal organic carbon (kg/m^3)
L = biologically active sediment layer depth (m)
ρ_s = bulk density of sediment (kg/m^3)
K_d = sediment-water distribution coefficient (m^3/kg)
ε = dimensionless constant defined by

$$\varepsilon = \frac{\overline{D_B} + \overline{D_m}}{D_B \rho K_d} \qquad \text{(Eq. 6.5)}$$

In Equation 6.4, the first term describes hydrodynamic flushing. The second term in the denominator represents the diffusive water boundary layer resistance. The third term in the denominator is the resistance associated with the sorption kinetics of a thin layer beneath the sediment across which the mobile and dissolved species are not in equilibrium. The final term in the denominator is the resistance due to bulk sediment diffusion over the biologically active sediment layer. The reader is referred to Chen, 1993 for a complete derivation of Eq. 6.4 and a full discussion of each of these processes.

In her study of the flux of organic contaminants across the sediment-water boundary layer, Chen determined that the actual flux could be expressed by a simplified formulation of Equation 6.4. Chen found that hydrophobic PAH compounds, especially in the case of benzo(a)pyrene, transport was limited primarily by water-side diffusion (Stolzenbach *et al.*, 1998). Using these assumptions, and neglecting colloidal PAHs, the basic model used to describe sediment water flux in the present study is Equation 6.6.

$$F = \frac{D_w}{\delta_w}\left(\frac{C_s}{K_d} - C_w\right) \qquad \text{(Eq. 6.6)}$$

Note that the above formulation neglects the effect of colloidal transport. Although colloids can enhance the transport of organic compounds across the sediment water interface, Chen found that the effect is not significant from the point of view of the bed-water fluxes even when colloidally sorbed concentrations are equal to dissolved concentrations (Chen, 1993). Also, two processes which have not been mentioned in the model presented above are the transport mechanisms associated with resuspension of the upper sediment layer and porewater advection due to groundwater inflow. A brief analysis of the impact of including some of the neglected terms will be addressed in the sensitivity analysis presented in Section 7.4.

6.2 ATMOSPHERIC EXCHANGE

As has been mentioned previously, one of the main ways in which PAHs are delivered to the environment is through the atmosphere. Once in the atmosphere, PAHs can exist either as vapor molecules dissolved in the air or sorbed to airborne particulate matter. The distribution between these two phases varies among different PAHs and is primarily dependent on the extent of the compound's hydrophobicity. The transport mechanisms for these two phases are distinctly different, and it is thus important to consider both in the mass balance. The exchange of vapor molecules across the water column boundary is referred to as *air – water exchange*, while the input of PAHs through the settling of particulate matter will be referred to as *atmospheric deposition.*

6.2.1 Atmospheric Deposition

One manner in which atmospheric PAH loadings will be considered is the deposition of particles to which PAHs are sorbed. These particles can either be washed out of the atmosphere by precipitation (*wet deposition*) or settled during dry weather (*dry*

deposition) conditions. Having entered the water column, sorbed PAHs may partition into the water column and thus influence the water column concentration. No theoretical model will be needed to quantify this phenomenon due to the availability of site-specific estimates of total annual atmospheric deposition of PAHs over the Boston Harbor region (see Section 7.2.6).

6.2.2 Air-Water Exchange

The concept of air-water exchange is analogous to the previous discussion of sediment-water exchange processes. Mass transport is accomplished by the molecular diffusion of compounds driven by a concentration gradient, as described by Fick's Law (Eq. 6.1). The direction of the resulting mass flux is entirely dependent upon the concentration of the compound in either phase. Thus air-water exchange can act as either a source or a sink of PAHs to an aquatic system.

The equilibrium distribution of a compound between water and air is described by a dimensionless Henry's Law constant, K'_H, which can be expressed as the ratio of the two equilibrium concentrations:

$$K'_H = \frac{C_a}{C_w} \qquad \text{(Eq. 6.7)}$$

It follows that if the concentration in the water column is higher than the theoretical equilibrium concentration dictated by the concentration in the air, calculated as C_a/K'_H, then the direction of mass flux will be from the aqueous phase to the vapor phase. Conversely if the water concentration is less than the theoretical concentration achieved by equilibration with the ambient air, the direction of the mass flux will be from the air to the water column.

A mathematical formulation of the air-water exchange process can be visualized as mass transport from one medium to the other across a series of two stagnant boundary layers

(Schwarzenbach *et al.*, 1993), the air-side and water-side diffusive layers. Because the layers are considered stagnant, the only transport process across them is molecular diffusion. Diffusive flux across each boundary layer occurs due to the concentration gradient generated by the concentration gradient between the ambient fluid and the concentration at the air-water interface, which is assumed to be at equilibrium. The flux across the water-side and air-side boundary layers is then expressed by Eqs. 6.8 and 6.9, respectively. This process is schematically represented in Figure 6.2.

$$F_a = -D_a \frac{C_a - C_{a/w}}{z_a} \qquad \text{(Eq. 6.8)} \qquad\qquad F_w = -D_w \frac{C_{w/a} - C_a}{z_w} \qquad \text{(Eq. 6.9)}$$

where,

F_a; F_w	= mass fluxes through the air and water layers (kg/m^2s)
C_a; C_w	= concentrations in the ambient air and water (kg/m^3)
$C_{a/w}$; $C_{w/a}$	= equilibrium concentrations at interface (kg/m^3)
z_a	= boundary layer thickness (m)
D_a	= molecular diffusion coefficient in air (m^2/s)
D_w	= molecular diffusion coefficient in water (m^2/s)

Recognizing that the flux through each of the two boundary layers must be the same under steady conditions, and that the interface concentrations are related by K'_H, the two equations can be combined to yield Eq. 6.10, which is the equation used in this study to represent the mass flux.

$$F = v_{tot} \cdot \left(C_w - \frac{C_a}{K'_H} \right) \qquad \text{(Eq. 6.10)}$$

where,

F	= total mass flux (kg/m^2s)
v_{tot}	= mass transfer coefficient or "piston velocity" (m/s)

The mass transfer coefficient, v_{tot}, represents the combination of the mass transfer velocities in air and in water, which are given by Eqs. 6.11 and 6.12.

$$v_w = \frac{D_w}{z_w} \qquad \text{(Eq. 6.11)} \qquad\qquad v_{a=} = \frac{D_a}{z_a} \qquad \text{(Eq. 6.12)}$$

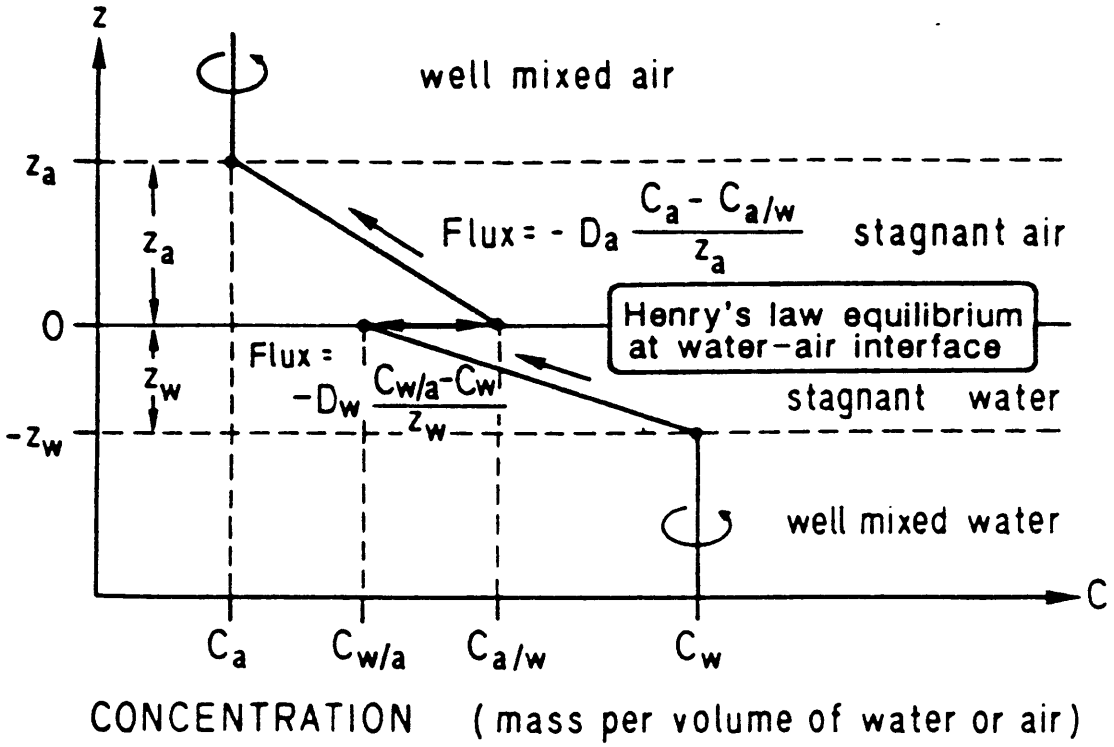

Figure 6.2 – Air-Water Exchange Stagnant Two-Film Model

(Schwarzenbach *et al.*, 1993)

v_{tot} is then calculated by Equation 6.13

$$\frac{1}{v_{tot}} = \frac{1}{v_w} + \frac{1}{v_a K_H'} \qquad \text{(Eq. 6.13)}$$

The direct quantification of the water and air-side diffusive boundary layers thickness is problematic but they are generally in the range of 5 x 10^{-3} to 5 x 10^{-2} cm and 0.1 to 1 cm, respectively (Schwarzenbach *et al.*, 1993). However, it is possible to estimate the transfer velocity of water vapor through air and of O_2 though water via a set of empirical formulas shown below as Eqs. 6.14. and 6.15 (Schwarzenbach *et al.*, 1993). It is obvious from these equations that the most important variable in determining the thickness of the boundary layers is the ambient wind speed.

$$v_a(H_2O) = 0.2u_{10} + 0.3 \qquad \text{(Eq. 6.14)}$$

$$v_w(O_2) \approx 4x10^{-4} - 4x10^{-5}u_{10}^2 \qquad \text{(Eq. 6.15)}$$

where,

u_{10}	=	wind speed measured at ten meters above the water (m/s)
v_a (H_20)	=	water vapor transfer coefficient (m/s)
v_w (O_2)	=	water vapor transfer coefficient (m/s)

Mass transfer coefficients for each PAH compound can then be related to the transfer velocities of oxygen and water vapor by the ratio of molecular diffusivities, as described in Eq. 6.16. An analogous relationship is used for the transfer velocity in water.

$$v_a(PAH) \approx v_a(H_2O)\left[\frac{D_a(PAH)}{D_a(O_2)}\right] \qquad \text{(Eq. 6.16)}$$

The use of this model relies on a number of assumptions which should be noted. Firstly, it requires that the air and water at the interface are at equilibrium with each other. Secondly, it relies on empirical relationships to estimate the transfer velocities. Finally, as explained in the beginning of this section, the direction of the mass flux F depends on the relative concentrations in the air and in the water. In order to quantify this flux in the mass balance, it will be necessary to assume that the diffusive flux is at steady-state conditions.

6.3 PHOTODEGRADATION

Photodegradation describes the process by which chemicals degrade due to the energy input associated with exposure to sunlight. This degradation can take place in two distinctly different ways, by either direct or indirect photolysis, and is only important in the upper layers of the water body through which light can penetrate.

6.3.1 Direct Photolysis

Direct photolysis is the process by which compounds are excited by direct absorption of energy from incoming radiation and consequently decay. The importance of this decay process varies between compounds because it is a direct function of a chemical's ability to absorb the available energy. One structural feature which enables this type of absorption is a delocalized π-electron system (Schwarzenbach *et al.* 1993), and since polycyclic aromatic compounds have multiple aromatic rings, they are susceptible to this type of degradation.

As incident radiation is absorbed by a compound, one of the compound's electrons will become excited and the compound will increase in energy level. Once excited, a chemical reaction that was not previously possible can take place (such as fragmentation, intermolecular rearrangement, etc.) and thus the concentration of that compound is decreased. It should be noted that chemical transformation does not necessarily occur, as the compound may lose its excess energy through various non-transforming processes (e.g., vibrational energy loss, luminescence, or transfer of energy to another compound). The ratio of molecules transformed to total number of photons (energy) absorbed is termed the *reaction quantum yield* (Φ_r) of the compound, and is dependent on the wavelengths, λ, of the incoming radiation.

The amount of light (energy) absorbed by a compound in a given environment is described by the *specific rate of light absorption*, $k_a(\lambda)$, which is calculated as

$$k_a(\lambda) = \frac{W(\lambda) \cdot \varepsilon(\lambda) \cdot [1 - 10^{-\alpha D(\lambda) z_{mix}}]}{z_{mix} \cdot \alpha(\lambda)} \qquad \text{(Eq. 6.17)}$$

where,

$W(\lambda)$	=	incident light intensity (einstein/cm^{2}s)
$\varepsilon(\lambda)$	=	decadic molar extinction coefficient (mol^{-1}cm^{-1})
$\alpha_D(\lambda)$	=	diffuse attenuation coeffiecient (cm^{-1})
z_{mix}	=	mean depth of water body (m)

Since the study area is about 10 m deep, all light is likely to be absorbed within the water column. The above equation can then be simplified ($1\text{-}10^{-\alpha D(\lambda) zmix} \approx 1$) to express the total light absorption rate, $k^t_a(\lambda)$ for each wavelength. This value is then summed over the entire spectrum of light (energy) available to yield the total absorption rate for the compound, k^t_a, as shown in Eq 6.18.

$$k_a^t = \frac{1}{z_{mix}} \sum \frac{W(\lambda)\varepsilon(\lambda)}{\alpha(\lambda)} \qquad \text{(Eq. 6.18)}$$

The first order decay rate of direct photolysis, k_p, can then be calculated by Eq. 6.19.

$$k_p = \Phi_r \cdot k_a^t \qquad \text{(Eq. 6.19)}$$

6.3.2 Indirect Photolysis

As mentioned above, compounds that are able to absorb incoming radiation sometimes lose their excited state because energy is transferred to another compound. This transfer can result in the breakdown of the compound to which the electron is transferred, a process termed *indirect photolysis*. The process is considered indirect because it is not

the process of photo-oxidation itself which degrades the chemical, rather it is the reaction with the photo-reactive species which breaks it down.

Most of the photo-reactive species which cause this type of degradation are unstable free radicals, such as the superoxide anion (O_2^-). This radical is produced by the photo-oxidation of dissolved organic carbon (DOC) as presented in Eq. 6.20.

$$DOC + O_2 \rightarrow oxidized\ DOC + O_2^- \qquad \text{(Eq. 6.20)}$$

This highly unstable radical can then react with another compound and cause indirect photolysis. Other common photo-reactive species include singlet oxygen ($^1O_2$), hydroxyl radical ($^\bullet OH$) and organic peroxy radicals ($ROO^\bullet$) (Schwarzenbach *et al.*, 1993).

Determining the overall degradation rate of PAHs due to indirect photolysis is a complicated matter. Many mechanisms for indirect photolysis are directly linked to the presence of dissolved organic matter in the system. The mechanisms themselves are also affected by the composition of the water body in question. For example, the presence of metals, such as iron, has been proven to significantly increase the rate at which indirect photolysis can occur. Since both metal and DOM chromophore speciation depend on pH, the rate of indirect photolysis will depend on pH as well (Ho, 1998 and Voelker, 1994). Thus, indirect photolysis is not only dependent on the amount of sunlight entering a system, but also on the nature of the water body itself.

Rates of indirect photolysis taken in one water body cannot be extrapolated to the Boston Harbor without first taking into consideration the differences in the two water systems. In addition, it is difficult to determine an overall rate constant for indirect photolysis, because different radicals will react with PAHs at different rates. Given these considerations, an attempt was made to give a rough estimate as to how fast indirect photolysis could occur. Three specific radicals were examined: singlet oxygen ($^1O_2$), hydroxyl radicals ($HO^\bullet$), and organic peroxy-radicals ($ROO^\bullet$).

Singlet oxygen is the energized form of molecular oxygen. It acts as an electrophile in chemical reactions. As such, electron-rich molecules may be susceptible to singlet oxygen reactions. For example, a back of the envelope calculation was made to determine the half life of phenolic compounds in a natural water body due to indirect photolysis. Phenols are noted for their high reaction rates with singlet oxygen due to the electron-withdrawing -OH groups in their structure. Even so, the half-life of these compounds was estimated to be on the order of 100 days, much longer than the flushing rate of the Boston Harbor. The PAHs in this study do not have such electron-withdrawing constituents, and may therefore take even longer than phenols to degrade via singlet oxygen (Schwarzenbach *et al.*, 1993).

A similar analysis was performed for contaminant reactions with hydroxyl radicals, which are extremely reactive and can react with many compounds at nearly diffusion-controlled rates. However, because they react in such a rapid manner, steady state concentrations are also very low. For most organic contaminants in a water system, the reaction rate constant is approximately $6x10^{-9}$ $M^{-1}s^{-1}$. This translates to a half-life of about 450 days.

Reactions involving organic peroxy-radicals ($^{\bullet}OOR$) can be even more complicated than other indirect photolysis mechanisms. It is suspected that peroxy-radicals degrade organic compounds by extracting a hydrogen atom from an electron rich group such as a hydroxide or amine group. Since these functional groups are not present in the compounds examined in this study, this reaction was not considered.

Investigating the role of indirect photolysis in the Boston Harbor is an extremely complicated matter. The initial analysis performed in this section suggests that it is unlikely to be significant in the Inner Harbor compared to other PAH removal mechanisms such as flushing. A more in depth treatment of this mechanism is beyond the scope of the present study.

6.4 CHEMICAL TRANSFORMATIONS

Chemical transformation refers to the set of reactions which occur in natural systems in the absence of light and without the aid of microbial transformation. This encompasses several different types of reactions. As a general rule, chemical transformation reactions will be very slow for PAHs. These compounds are very stable due to their aromatic structure. In addition, there are no good leaving groups on the compounds in question.

Substitution reactions occur when an outside constituent replaces part of the compound in question, as shown in Equation 6.21

$$R\text{-}L + :X \rightarrow R\text{-}X + :L \qquad \text{(Eq. 6.21)}$$

Of all the possible chemical transformation reactions that could take place, a number of literature sources agree that electrophilic substitution of PAHs by chlorine atoms is the only likely reaction which can occur (Kennish, 1997 and Neff, 1979). As a general rule, however, reactive electrophiles have very short life spans in the environment, and reactions with these species generally only occur in light induced (see Section 6.3.2 – indirect photolysis) and biologically mediated (see Section 6.5) processes (Schwarzenbach *et al.*, 1993). For this reason, chemical transformation reactions were considered negligible in this study.

6.5 BIODEGRADATION

Biodegradation describes the process in which microbes take in chemicals and then break them down into simpler forms. PAHs are noted to be more resistant to microbial degradation than other compounds, especially those PAHs with higher molecular weights (Pitter and Chudoba, 1990). Two specific studies cited in Pitter and Chudoba measure

the rate at which specific PAHs degrade in the water column. One lists a rate constant of $3.2x10^{-3}$ hr^{-1} for naphthalene and approximately 0 hr^{-1} for benzo[a]pyrene. The other lists half-lives of 17 to 31 days for napthalene, 238 to 630 days for pyrene, and 1400 to 2100 for benzo[a]pyrene (Pitter and Chudoba, 1990 and references cited therein).

Although these values represent average degradation rates in a natural system, this study is concerned with winter conditions only, when the temperatures in Boston are very low ($T \approx 3°C$). Several studies examining the biodegradation of petroleum products in natural environments state that biodegradation rates of PAHs are much slower in lower temperatures (Siron *et. al.,* 1993; Minas and Gunkel, 1995). As a result, the rate of biodegradation was assumed to be negligible during the modeled conditions. It should be noted that this assumption is unlikely to be valid if the model is applied to summer conditions, especially in the case of naphthalene.

6.6 FLUSHING

Flushing is one of the most important variables in the implementation of the box model because it represents the advective transport of the system. This transport is induced by the tides, supplemented by the residual currents of the system generated by the discharge of rivers, CSOs, stormwater drains, etc. Flushing is included as an explicit loss term in the box model, but is implicit in the 3D model, however, because this model actually calculates the residual currents solving the hydrodynamic and mass transport equations. In order to obtain the rate of flushing of a system the residence time of the system should be defined first.

The residence time of a contaminant in an estuarine environment can be related to the residence time of freshwater. The volume of freshwater in an estuary between the mouth (x=0) and some distance (x=L) can be calculated as (Chan, 1995).

$$V = \int_0^L \int_A f \, dA \, dx \qquad \text{(Eq. 6.21)}$$

where,

A	=	cross-sectional area (m^2)
f	=	freshness

The freshness is defined by the relationship given by Equation 6.22.

$$f = \frac{S_o - S}{S_o} \qquad \text{(Eq. 6.22)}$$

where,

S_o	=	salinity of ocean water (ppt)
S	=	salinity at specified location (x=L) (ppt)

The residence time of freshwater can then be calculated by Eq. 6.23.

$$t_{res,f} = \frac{V}{Q_f} \qquad \text{(Eq. 6.23)}$$

The flushing rate, k_f, is defined as the inverse of the residence time, as shown in Eq. 6.24.

$$k_f = \frac{1}{t_{res}} \qquad \text{(Eq. 6.24)}$$

This representation of flushing rate was applied to the box model presented in Chapter 7. The reader is referred to Section 7.2.8 for a discussion of the values used. Multiple studies of the residence time in Boston Inner Harbor have been performed in the past. For further discussion of this issue, the reader is referred to Chan *et al.*, 1998.

7 MASS BALANCE CALCULATIONS

Up to this point the reader has been introduced to the basic theory used to model the various components which are the subject of this study. The following section will focus on applying the theory to the available data and estimate a steady state concentration of each compound using a simplified "box" model. While this model has severe limitations in that it treats the study area as a well-mixed box, it does provide an effective tool to understand the relative influence of each term in the mass balance equation. Furthermore, the "box" model provides an effective way of performing sensitivity analysis and initial verification of the 3D model without having to go through a computationally intensive numerical simulation. This chapter will first present the base case conditions used to model each process and the resulting mass balance. Sensitivity analysis will then be performed to determine the implications of using alternative data, coefficient values, and theoretical models. Finally, a discussion of the results will follow.

7.1 CONCEPTUAL MASS BALANCE MODEL

The simplified model presented herein is a steady-state, zero-dimensional "box" model which allows order-of-magnitude estimates to be made with relative ease. The most important assumption in applying this model is that the study area is completely well-mixed, and thus contaminant concentrations can be described by a single value which does not vary in space or time.

The mass balance is calculated by combining all of the source terms with the sink terms and calculating the resulting steady-state concentration. Most of the theoretical framework for the sources and sinks was discussed in Chapter 6. The actual application to the box model will be addressed in this chapter. A summary of the sources and sinks considered and neglected in the model is presented in Table 7.1, and depicted conceptually in Figure 7.1

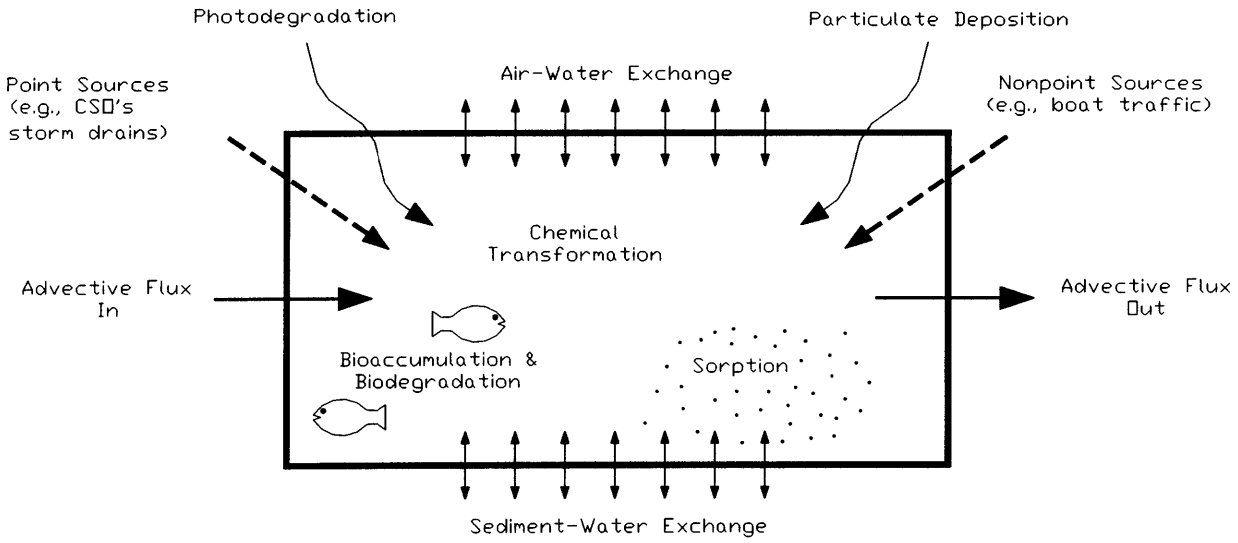

Figure 7.1 – Conceptual Box Model

Table 7.1
Sources and Sinks in the Mass Balance

Sources		*Sinks*	
Included	*Neglected*	*Included*	*Neglected*
Sediment-water exchange[1]	Nonpoint sources (e.g., boat traffic, pilings)	Air-water exchange[1]	Chemical transformations
River loadings		Direct photodegradation	Biological transformations
CSO loadings			Indirect photodegradation
Stormwater loading			
Atmospheric deposition			

[1]Can act as source or sink depending on the concentration gradient.

The mathematical representation of the system is give by Equation 7.1 below:

$$\frac{\partial C_w V}{\partial t} = \Sigma Q_{in} C_{in} + F_{atm} A + v_{tot} A\left(\frac{C_a}{K_H} - C_w\right) + \frac{D_w}{\delta_w} A\left(\frac{C_s}{K_d} - C_w\right) - C_w V(k_f + k_p) \quad \text{(Eq. 7.1)}$$

where,

ΣQ_{in}, C_{in}	=	Sum of loadings from rivers, CSOs and stormwater (m^3/s; kg/m^3)
v_{tot}	=	Total mass transfer velocity (air + water) m/s
A	=	Area of study area (m^2)
C_w	=	Dissolved concentration in water (kg/m^3)
C_a	=	Dissolved concentration in air (kg/m^3)
K_H	=	Henry's Law coefficient (m^3_{water}/m^3_{air})
D_w	=	Molecular diffusion coefficient in water (m^2/s)
δ_w	=	Water-side diffusive boundary layer thickness (m)
K_d	=	Sediment-water distribution coefficient ($m^3_{water}/kg_{sediment}$)
k_f	=	Flushing rate (s^{-1})
k_p	=	Direct photolysis decay rate (s^{-1})
V	=	Volume of study area (m^3)

The first terms in the RHS of Eq. 7.1 refer to the loadings from rivers, combined sewer overflows (CSOs), and stormwater. The second term is the contribution of the atmospheric deposition of particulate matter. The third term represents the air-water exchange process, and may thus act as either a source or a sink of PAHs. The fourth term describes the sediment flux, assumed to be limited by water side diffusion (as discussed in Section 6.1). The fifth and sixth term represent the mass losses due to hydrodynamic flushing and direct photolysis.

One characteristic of the equation presented above is that it neglects the presence of suspended solids within the water column. Other terms which have been considered negligible, include biodegradation, indirect photolysis, and chemical transformations.

7.2 PARAMETER ESTIMATION

As discussed in Section 7.1 and shown in Figure 7.1, the main sources which will be considered include river inputs, CSO and stormwater inputs, sediment-water exchange, air-water exchange, and atmospheric deposition. All remaining sources (e.g., boat traffic, pilings) presented in conceptual box model were neglected mainly because of the lack of data available for obtaining a useful estimate. Appendix A contains a summary of the calculations performed for the estimation of each of the following mass balance parameters

7.2.1 River Inputs

The Boston Inner Harbor receives freshwater inflow from three rivers. They include the Charles River, the Mystic River, and the Chelsea River, as shown in Figure 2.1. The Charles and Mystic Rivers, which account for about 99% of the total flow (Chan, 1995), are controlled by sluice gates and therefore only discharge intermittently. The Chelsea River discharge is continuous. River inputs are important not only because of the associated PAH advective flux, but also because they represent the main forcings of the flow regime, which will be discussed in more detail in Section 7.2.8.

7.2.1.1 Flow Estimation

The Charles River is by far the largest contributor of freshwater inflow to the Boston Inner Harbor. The flow is continually monitored by the United States Geological Survey (USGS) in Waltham. Flow data were obtained for the period 1992 to 1996, and averaged over the winter portion of the water year (November through April) months because the simulations are concerned with winter conditions. Given that Waltham is a considerable distance upstream of the Inner Harbor, a scaling factor was used to account for the extra flow received from the additional drainage area that exists between the gage (588 km^2)

and the Charles River Dam (744 km^2). The scaling factor used was 1.27 (Chan, 1995), and is calculated as the ratio of the two drainage areas. The resulting flow value used in the base case is 17.24 m^3/s.

In contrast to the Charles, flow data for the Mystic and Chelsea River was not as readily available. As a result, it was assumed that the relative contributions of the rivers to the Inner Harbor were 82%, 17%, and 1% for the Charles, Mystic, and Chelsea Rivers, respectively (Chan, 1995). Thus, flows from the Mystic and Chelsea Rivers were simply modeled as the Charles River flow multiplied by an appropriate weighting factor. The resulting winter average flows for the Mystic and Chelsea Rivers are 3.57 m^3/s and 0.21 m^3/s, respectively.

7.2.1.2 PAH Concentrations

PAH concentrations were measured in 1992 by Menzie-Cura & Associates in attempt to quantify PAH loadings to the Boston Inner and Outer Harbors (Menzie-Cura, 1995). The study included sampling stations at the Charles River dam and the Mystic River dam. Although there was no sampling station at the Chelsea River, it was assumed that the concentration here was similar to the Mystic River (the error associated with this assumption is likely to be minimal because of the small flow of the Chelsea River). Because the study included three sampling events (March, April, and October, 1992), results were averaged for each station. The available concentration data (Menzie-Cura, 1995) are presented in Appendix A, and summarized in Tables 7.2, 7.3 and 7.4. Also included in the table are the estimated annual loads for each compound, which is simply calculated as the product of the river flow and concentration of the contaminant.

Table 7.2
Charles River Loadings

Compound	Average Concentration (ng/l)	Flow (m3/s)	Annual Load (kg/year)
Naphthalene	83.8	17.24	45.6
Pyrene	268.4		145.9
Benzo(a)pyrene	14.3		7.8

Table 7.3
Mystic River Loadings

Compound	Average Concentration (ng/l)	Flow (m3/s)	Annual Load (kg/year)
Naphthalene	38	3.57	4.3
Pyrene	67.8		7.6
Benzo(a)pyrene	9.5		1.1

Table 7.4
Chelsea River Loadings

Compound	Average Concentration (ng/l)	Flow (m3/s)	Annual Load (kg/year)
Naphthalene	38	0.21	0.3
Pyrene	67.8		0.4
Benzo(a)pyrene	9.5		0.1

The total annual load (assuming that load does not vary over year) from all the rivers to the Inner Harbor is about 9 kg, 154 kg, and 50 kg for benzo(a)pyrene, pyrene, and naphthalene, respectively.

7.2.2 Combined Sewer Overflows

Although remediation measurements are being planned to eliminate much of the combined sewer overflows (CSO) of the Boston sewer system has been reevaluated and curtailed, there is still a considerable amount of flow which is discharged from these

sources on an annual basis. Because these systems are for the most part only active during storm events, an exact determination of the flow is problematic. Metcalf and Eddy conducted an extensive study in 1994 in which future usage of the system was predicted. These flow values were assumed to be representative of current usage. The exact locations of the active CSO drains were provided by the Massachusetts Water Resource Authority (MWRA), and are shown in Figure 7.2. The total average CSO flow to the study area is estimated to be about 0.07 m^3/s. The Metcalf & Eddy report divided up the study area into a series of regions which are also delineated in Figure 7.2. This nomenclature will be used in the following analysis.

Representative PAH concentration values were obtained from the Menzie-Cura 1992 sampling events (Menzie-Cura, 1995). Of the CSOs sampled in the report, two of them (CSO 012 and CSO 080) were located within the study area. Samples were collected on two occasions (November, 1992) and averaged for each value. PAH concentrations from the CSO 080 were applied to all CSO's within the *Mystic Chelsea Confluence* and *Upper Inner Harbor* regions (as defined by Metcalf & Eddy, 1994), whereas CSO 012 concentrations were applied to the CSO's in the remaining three regions (*Lower Inner Harbor, Fort Point Channel,* and *Reserved Channel* areas).

Total PAH load from each CSO was calculated as the product of the average flow and the average concentration. CSO flow, concentration and annual load values are presented in Table 7.2.4. The total annual CSO load to the system was estimated to be 0.17 kg, 0.49 kg, and 0.21 kg for naphthalene, pyrene, and benzo(a)pyrene, respectively.

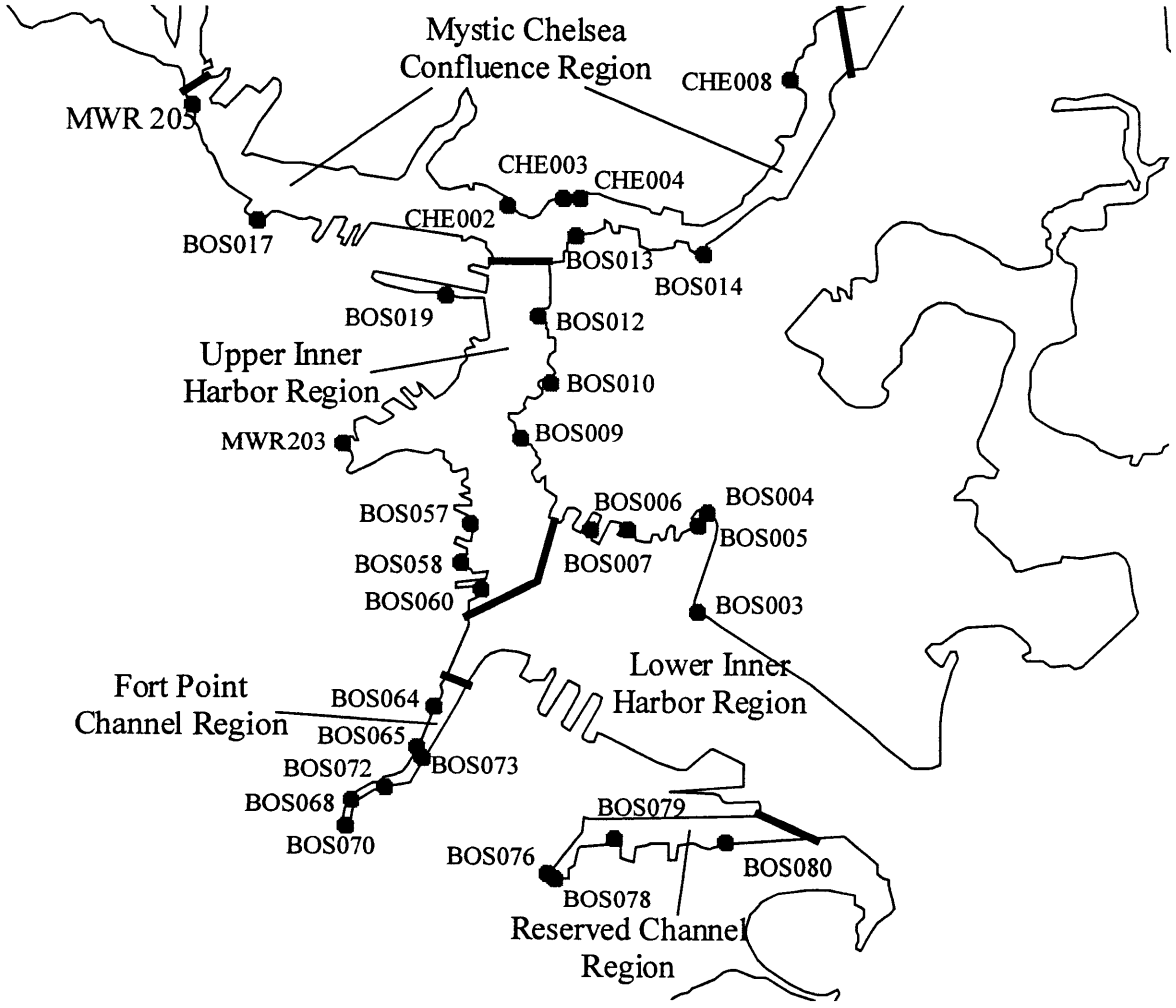

Figure 7.2 – Location of CSOs and Stormwater regions

Table 7.5
Estimated Annual CSO PAH Loads

Area Name	*CSO Name & Predicted Flow**	*PAH Concentrations*			*Annual PAH Loads*		
		Naph. (ng/l)	*Pyrene (ng/l)*	*BAP (ng/l)*	*Naph. (kg/yr)*	*Pyrene (kg/yr)*	*BAP (kg/yr)*
MC Conf.	CHE002 0.04 MG/yr	84	207	82.5	1.27E-05	3.13E-05	1.25E-05
MC Conf.	CHE003 0.35 MG/yr	84	207	82.5	1.11E-04	2.74E-04	1.09E-04
MC Conf.	CHE004 0.27 MG/yr	84	207	82.5	8.58E-05	2.12E-04	8.43E-05
MC Conf.	CHE008 8.32 MG/yr	84	207	82.5	2.65E-03	6.52E-03	2.60E-03
MC Conf.	BOS014 1.47 MG/yr	84	207	82.5	4.67E-04	1.15E-03	4.59E-04
MC Conf.	BOS013 4.38 MG/yr	84	207	82.5	1.39E-03	3.43E-03	1.37E-03
MC Conf.	BOS017 2.53 MG/yr	84	207	82.5	8.04E-04	1.98E-03	7.90E-04
MC Conf.	MWR205 99.95 MG/yr	84	207	82.5	3.18E-02	7.83E-02	3.12E-02
UI Harbor	BOS019 3.61 MG/yr	84	207	82.5	1.15E-03	2.83E-03	1.13E-03
UI Harbor	BOS012 6.65 MG/yr	84	207	82.5	2.11E-03	5.21E-03	2.08E-03
UI Harbor	BOS010 8.34 MG/yr	84	207	82.5	2.65E-03	6.53E-03	2.60E-03
UI Harbor	BOS009 3.94 MG/yr	84	207	82.5	1.25E-03	3.09E-03	1.23E-03
UI Harbor	MWR203 196.68 MG/yr	84	207	82.5	6.25E-02	1.54E-01	6.14E-02
UI Harbor	BOS057 0.38 MG/yr	84	207	82.5	1.21E-04	2.98E-04	1.19E-04
UI Harbor	BOS060 2.53 MG/yr	84	207	82.5	8.04E-04	1.98E-03	7.90E-04
FPC	BOS064 0.04 MG/yr	66	235	107.5	9.99E-06	3.56E-05	1.63E-05
FPC	BOS065 0.15 MG/yr	66	235	107.5	3.75E-05	1.33E-04	6.10E-05
FPC	BOS073 4.48 MG/yr	66	235	107.5	1.12E-03	3.98E-03	1.82E-03

FPC	BOS072 2.96 MG/yr	66	235	107.5	7.39E-04	2.63E-03	1.20E-03
FPC	BOS070 160.05 MG/yr	66	235	107.5	4.00E-02	1.42E-01	6.51E-02
LI Harbor	BOS007 4.26 MG/yr	66	235	107.5	1.06E-03	3.79E-03	1.73E-03
LI Harbor	BOS006 1.18 MG/yr	66	235	107.5	2.95E-04	1.05E-03	4.80E-04
LI Harbor	BOS005 0.06 MG/yr	66	235	107.5	1.50E-05	5.34E-05	2.44E-05
LI Harbor	BOS004 4.17 MG/yr	66	235	107.5	1.04E-03	3.71E-03	1.70E-03
LI Harbor	BOS003 3.2 MG/yr	66	235	107.5	7.99E-04	2.85E-03	1.30E-03
RC	BOS080 4.76 MG/yr	66	235	107.5	1.19E-03	4.23E-03	1.94E-03
RC	BOS079 2.09 MG/yr	66	235	107.5	5.22E-04	1.86E-03	8.50E-04
RC	BOS076 47.99 MG/yr	66	235	107.5	1.20E-02	4.27E-02	1.95E-02
RC	BOS078 11.69 MG/yr	66	235	107.5	2.92E-03	1.04E-02	4.76E-03

MC Conf. = Mystic – Chelsea Confluence
UI Harbor = Upper Inner Harbor
FPC = Fort Point Channel
LI Harbor = Lower Inner Harbor
RC = Reserved Channel

7.2.3 Stormwater

Because PAHS can more or less be considered ubiquitous in an urban environment, stormwater loading from an urban area such as Boston Harbor could have a significant impact on water quality. Unfortunately, there is little actual data collected on the flow values in each of the storm water drains located around Boston. However, average annual stormwater flows to each of the "CSO regions" defined in Section 7.2.2, were estimated by Metcalf & Eddy for a typical year (Metcalf & Eddy,1994). These estimates were used in the mass balance of the Inner Harbor.

Stormwater concentrations were obtained from 1992 PAH sampling performed by Menzie-Cura & Associates (Menzie-Cura, 1995). Samples were collected from five

"urban" stormwater drains in Dorchester, Hyde Park, Roxbury, Allston/Brighton, and Charlestown over three sampling events in May and June of 1992. Because PAH concentrations in stormwater are largely dependent on the nature and intensity of the storm event, it is difficult to generalize about them. Therefore, even though the Charlestown drain, which is located within the study area, appeared to have lower concentrations than the other urban drains, an "urban average" of the data for all the urban stormwater drains was applied.

Stormwater load was simply calculated as the product of the average flow and the average concentration for each region (see Table 7.6). The total annual load for naphthalene, pyrene, and benzo(a)pyrene are estimated to be 2.92 kg, 8.55 kg, and 1.73 kg, respectively.

Table 7.6
Annual Stormwater PAH Loads

Region	Average Annual Stormwater Flow (MG/yr)	PAH Concentration (kg/yr)			PAH Annual Load (kg/yr)		
		Naph. (ng/l)	Pyrene (ng/l)	BAP (ng/l)	Naph. (kg/yr)	Pyrene (kg/yr)	BAP (kg/yr)
MC Conf.	1680.27	98.3	816	161.9	0.62	5.19	1.03
UI Harbor	393.8	98.3	816	161.9	0.15	1.22	0.24
FPC	114.04	98.3	816	161.9	0.04	0.35	0.07
LI Harbor	485.36	98.3	816	161.9	0.18	1.50	0.30
RC	95.01	98.3	816	161.9	0.04	0.29	0.06

7.2.4 Sediment-Water Exchange

As discussed in Section 6.1, the sediment water exchange process is driven by a concentration gradient. The required inputs include concentration sorbed to sediment, diffusive boundary layer thickness, molecular diffusion coefficient, and sediment-water distribution coefficient.

Sediment quality data was obtained from a 1986 survey of sediment at several locations within the harbor (Shiaris and Jambard-Sweet, 1986). Although more recent data sets do exist, the Shiaris data set was used because of the geographic distribution of the sampling stations. Six sampling stations exist within the project area, and results are provided for all three of the compounds being studied. Figure 7.3 shows the geographic distribution of the sampling stations used in this study. Each sediment quality data point was taken as representative of a portion of the Inner Harbor, thus dividing the harbor into "six sediment quality regions" (also shown on Figure 7.3). The regions were delineated by taking into consideration the amount of industrial/urban activity in each area, primarily from a visual inspection of the study area. The reported sediment concentrations are listed in Table 7.7 together with the fraction of the total study area represented by each sediment quality region.

It should be noted that the data consistently show that the areas in the vicinity of the Fort Point Channel and the Mystic - Chelsea confluence have higher concentrations of PAH in the sediment. Substantially lower concentrations were observed in the other sampling areas, including the sampling station in the upper Chelsea River. In the interest of being conservative, the Mystic - Chelsea confluence data point was applied to all of the Mystic River as well as a large portion of the Chelsea River. This assumption was made based on the heavy amount of industrial and navigation activity in this area.

Since the box model allows no spatial variations in concentration, one representative sediment concentration for each compound was applied to the entire study area. These values were calculated as a weighted average, obtained by Eq. 7.1

$$C_s^{avg} = \sum_i C_s^i \cdot f_i \qquad \text{(Eq. 7.1)}$$

Where, C^i_s = concentration at region i (ng/g)

f = fraction of area occupied by region i

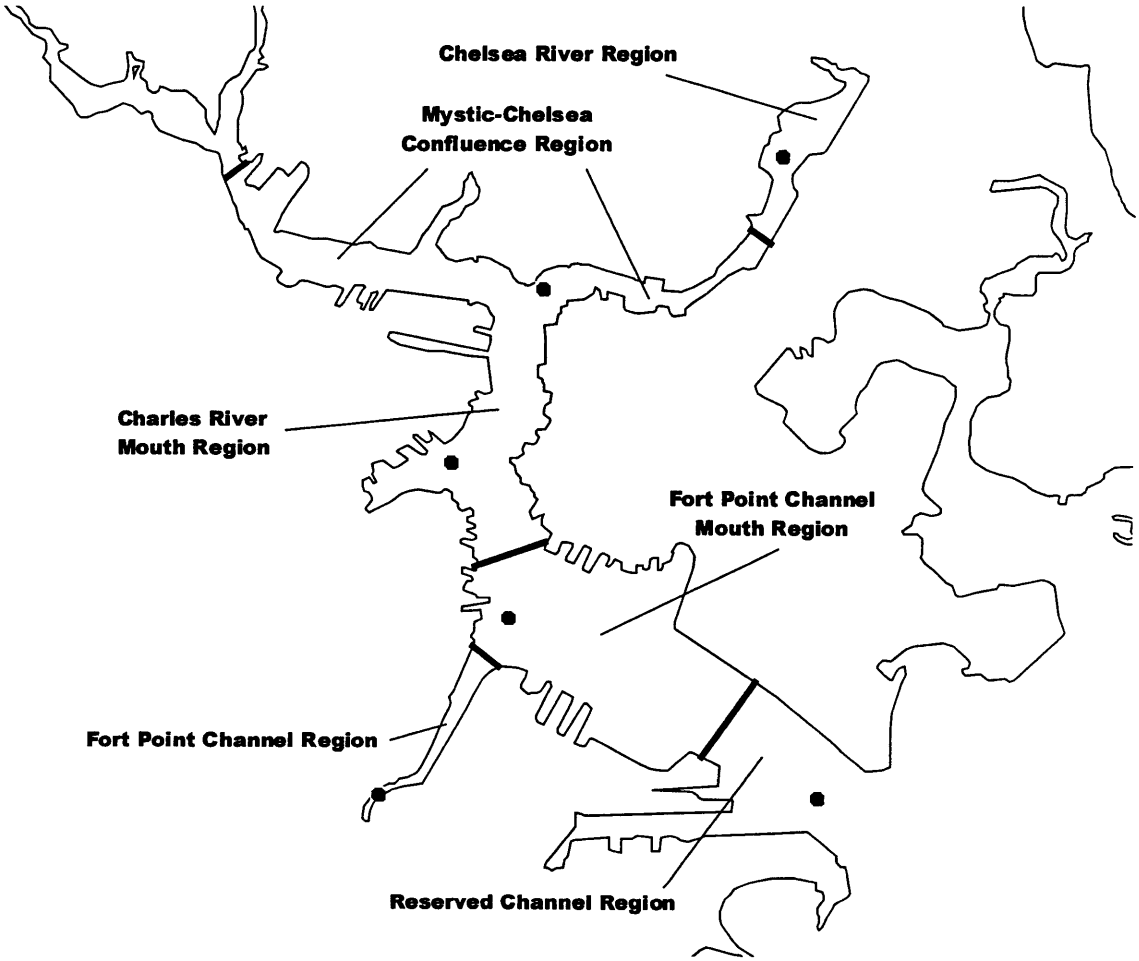

Figure 7.3 – Location of Core Samples (Shiaris and Jambard-Sweet, 1986) and Delineation of "Sediment Quality Regions"

The weighted averages values of sediment quality for each compound are summarized in Table 7.7.

Table 7.7
Weighted Sediment PAH Concentrations

Sediment Region	Fraction Area	Naphthalene (ng/g)	Pyrene (ng/g)	Benzo[a]pyrene (ng/g)
1) Chelsea River	0.03	10^{1}	8917	2950
2) Mystic-Chelsea Confluence	0.25	5082	50127	30277
3) Charles River Mouth	0.14	10^{1}	4419	7159
4) Fort Point Channel Mouth	0.35	10^{1}	3195	1949
5) Fort Point Channel	0.02	43628	66831	94984
6) Reserved Channel	0.21	10^{1}	1559	1418
Weighted Average Used:	1.00	2.29×10^{3}	1.66×10^{4}	1.19×10^{4}

[1]The detection limit value was assumed in the cases when no concentration was detected

The distribution coefficient, K_d, for each compound determines the magnitude of the concentration gradient between the equilibrated porewater and the overlying water column. A 1993 study by McGroddy suggested that a significant portion of the PAHs released into the environment are permanently bound to soot particles and therefore unavailable for desorption into the equilibrated sediment porewater (see also McGroddy and Farrington, 1995; McGroddy et al., 1996). McGroddy measured *in-situ* K_d values for a number of compounds including benzo[a]pyrene and pyrene. In the interest of accounting for the fact that a portion of the the total concentrations of these compounds measured by Shiaris may be bound to soot particles, the reported K_d values were applied to the model. In the case of naphthalene, a K_{om} was estimated from a literature value of the saturated aqueous solubility, C^{sat}_w, using the experimental linear free energy relationship (LFER) presented below as Equation 7.2 (Schwarzenbach *et al*, 1993).

$$\log K_{om} = -0.93 \cdot \log C_w^{sat} - 0.17 \qquad \text{(Eq. 7.2)}$$

where,

K_{om} = organic matter – water partition coefficient (l/kg_{om})

C^{sat}_{w} = saturated aqueous solubility (M)

This value of was C^{sat}_{w} adjusted for salinity using the Equation 7.3.

$$\log C^{sat}_{w,salt} = \log C^{sat}_{w} + K^{s}[salt] \qquad \text{(Eq. 7.3)}$$

where,

$C^{sat}_{w,salt}$ = saturated aqueous (saline) solubility (kg/m^3)

C^{sat}_{w} = saturated aqueous solubility (kg/m^3)

K^{s} = salting constant (M^{-1})

[salt] = total concentration of salt (M)

The K_d was calculated as the product of the K_{om} and the fraction organic matter reported by McGroddy for sediment samples taken in the vicinity of the Fort Point Channel mouth (0.05).

All three values were adjusted to account for the assumed ambient temperature of 3°C. This was accomplished using Eq. 7.4.

$$K_d^{276.15} = K_d^{298.15} \exp\left[\frac{\Delta H_s^e}{R}\left(\frac{1}{276.15K} - \frac{1}{298.15K}\right)\right] \qquad \text{(Eq. 7.4)}$$

Where ΔH^{e}_{s} = Excess enthalpy of solution (kJ/mol)

R = Universal gas constant (8.314×10^{-3} kJ/mol)

Excess enthalpy of solution literature values were available (Schwarzenbach *et al.*, 1993) for naphthalene and pyrene, but not for benzo[a]pyrene. However, it was possible to estimate the value for benzo[a]pyrene by extrapolating a linear relationship between known values of ΔH^{e}_{s} and molecular weight. The K_d values used in the model

formulation are presented in Table 7.8. In the case of naphthalene $K_d=K_{om}f_{om}$, where f_{om} is the fraction of organic matter. This value is, in general, about two times f_{oc} (Schwarzenbach *et al*, 1993) depending on the characteristics of the organic matter. In this study, with the purpose of being conservative in the calculations of the concentrations of naphthalene, f_{om} was considered to be equal to the value of f_{oc} reported by McGroddy. Appendix A contains a summary of the calculations performed.

Table 7.8
K_d Estimation

Compound	Calculated using	K_d, 25°C (m^3_{water}/kg_{sed})	ΔH^e_s (kJ/mol)	K_d, 3°C (m^3_{water}/kg_{sed})
Napthalene[1]	$LogC^{sat}_w + K^s[salt]$	3.02×10^{-2}	9.9	3.02×10^{-2}
Pyrene[2]	*In-situ* K_{oc}	16.2	26.4	27.3
Benzo[a]pyrene[2]	*In-situ* K_{oc}	50	32.6	250

[1]Log C^{sat}_w = -3.06, K^s[salt] = 0.1128.

[2]McGroddy values used with *in-situ* f_{oc} = 0.05.

The molecular diffusion coefficient for each compound was estimated using Eq. 7.5. The calculation of the molecular diffusion coefficient for each compound is presented in Appendix A. Note that the values were calculated for the model water temperature, 3°C.

$$D_w = \frac{13.26x10^{-5}}{\mu^{1.14} V_m^{0.589}} \qquad \text{(Eq. 7.5)}$$

where,

μ = water viscosity (cp)

V_m = molar volume (cm^3/mol)

The diffusive boundary layer thickness used for the base case was 5 x 10^{-4} m (Schwarzenbach *et al.*, 1993). Literature values for this parameter range from 10^{-4} to 10^{-2} meters (Chen, 1993). Sensitivity analysis (Section 7.4) will be performed to address the influence of varying this value.

The calculation of the sediment water exchange terms are presented in Table 7.9. In order to facilitate the inputs to the 3D model (see Section 8.2.2.1), sediment-water exchange has been divided into a source term and a sink term. The source term represents the input of PAH to the system from the concentration gradient between the equilibrated porewater and the overlying water column (assuming $C_w = 0$). The sink term is the loss of PAHs from the water column to the sediments (assuming $C_{pw} = 0$). Combining the two terms results in the net flux, the direction of which is dependent on the relative magnitude of the two terms. The mathematical formulation of each term is shown in Eq. 7.6 and 7.7.

$$Source\ Term = \frac{D_w \cdot C_s}{\delta_w \cdot K_d} \cdot A \qquad \text{(Eq. 7.6)} \qquad Sink\ Term = \frac{D_w \cdot C_w}{\delta_w} \cdot A \qquad \text{(Eq. 7.7)}$$

Table 7.9
Summary of Sediment-Water Exchange

Compound	Cs (ng/g)	Dw (m^2/s)	K_d[1] (m^3/g)	Source Term (kg/s)	Sink Term/C_w (m^3/s)
Naphthalene	2289	4.16 x 10^{-10}	3.02 x10^{-5}	5.33 x 10^{-4}	7.0
Pyrene	16586	3.13 x 10^{-10}	2.7 x 10^{-2}	3.25 x 10^{-6}	5.3
Benzo[a]pyrene	11894	2.94 x 10^{-10}	2.5 x 10^{-1}	2.37 x 10^{-7}	5.0

[1]Calculated using δ_w = 5 x 10^{-5}m

Because the magnitude of the sink term depends upon the concentration in the water, the above sink term value does not have much physical meaning. The reader is referred to Section 7.3 for the implementation of these terms to calculate the steady state

concentration. Also included in this section is a discussion of each compound and the relative contributions of each source and sink.

7.2.5 Air-Water Exchange

As has been discussed in previous sections, air-water exchange has the potential to be a sink or a source of PAHs depending on the relative magnitude of the air and water concentrations. In addition to these two variables, the mass transfer velocity for each compound must also be estimated.

Air quality measurements for all three compounds being studied were available from a study conducted for the United States Environmental Protection Agency (Lewis *et al.*). Data were collected from a sampling location in downtown Boston, described as an industrial site heavily impacted by automobile traffic and "general urban sources" (Lewis *et al.*). The sampler was located 12 m above the ground. Total concentration was measured (vapor and particulate) along with an estimate of the percentage contribution of each phase. Average concentrations were reported for each of the four seasons.

The study included measurements of naphthalene, pyrene, and benzo[a]pyrene. Since particlate bound atmospheric deposition is being estimated using another data set (see Section 7.2.6), only the vapor phase portion of each contaminant was incorporated into the mass balance. Also, only the winter portion of the data are used because of the scope of this modeling exercise. The data used are presented below in Table 7.10

Table 7.10
PAH Ambient Air Concentrations

Compound	Total Concentration (ng/m^3)	Percent Vapor Phase[1]	Vapor Phase Concentration (ng/m^3)
Naphthalene	453	80[2]	362
Pyrene	8.3	55	4.6
Benzo[a]pyrene	1.5	0	0

[1]Estimated from Figure 1, Lewis *et al.*, 1992
[2]Assumed to be same as Flourene

The next task is estimating the mass transfer velocity between the water and the air. The methodology employs the use of empirical formulas (Eq 6.14 and Eq. 6.15), as was discussed in some detail in Section 6.2.2. The mass transfer velocity is assumed to be dominated by the ambient wind speed. Daily averaged wind data were available from Boston Logan Airport, measured at an elevation of 10m. These data were averaged over the winter months obtaining a value of $u_{10} = 6.12$ m/s. Wind data are included in Appendix C.

The molecular diffusivities of each compound in the air and the water are necessary for the calculation of the mass transfer velocity. This is because the air-side and water-side piston velocities are calculated as the water and oxygen transfer velocities multiplied by the ratio of the molecular diffusivities (Section 6.2.2, Eq. 6.16). Assuming that the molecular diffusion coefficients vary similarly with temperature, then the resulting calculated values of v_a and v_w are in effect independent of temperature. Obviously, this is a result of the empirical equation being used to estimate the mass transfer velocities. Mass transfer velocities were therefore calculated using the ratio of the molecular diffusivities of the PAH compound and the fluid medium at 25°C (since the diffusivity of oxygen and water were readily available at this temperature).

Finally, air-water exchange requires the estimation of the equilibrium partitioning coefficient (dimensionless Henry's Law coefficient), K'_H. Literature values were used and corrected for temperature and salinity effects. Both temperature and salinity adjustments were performed by assuming that K'_H is approximately equal to K'^{sat}_H (Schwarzenbach *et al.*, 1993). Temperature adjustments are made using Eq 7.8.

$$K_H(276.15) = K_H(298.15)\exp\left[-\frac{\Delta H_{vap} - \Delta H_s^e}{R}\left(\frac{1}{276.15K} - \frac{1}{298.15K}\right)\right] \qquad \text{(Eq. 7.8)}$$

where,

ΔH_{vap}	=	heat of vaporization (kJ/mol)
ΔH_s^e	=	excess heat of solution (kJ/mol)
R	=	Universal gas constant (8.314×10^{-3} kJ/mol)

Salinity adjustments are made using the same methodology used for correcting the sediment water exchange. Therefore Equation 7.3 was used to calculate C_w^{sat}. The values of $C^{sat}_{w,salt}$ obtained is related to K^{sat}_H by Eq 7.9

$$K_H^{sat} \equiv \frac{P^0}{C_w^{sat}} \qquad \text{(Eq. 7.9)}$$

where,

P° = vapor pressure of pure compound (atm)

Thus, assuming K'_H varies in the same manner as K^{sat}_H, K'_H is inversely proportional to C^{sat}_w. Calculations of each of these values is presented in Appendix A, and summarized below in Table 7.11.

Table 7.11
Henry's Law Constant Estimation

Compound	ΔH_{vap} (kJ/mol)	ΔH_s^e (kJ/mol)	K_s (M^{-1})	K'_H (l_{water}/l_{air})
Naphthalene	43	9.9	0.26	8.80×10^{-3}
Pyrene	62	26.4	0.3[1]	1.92×10^{-4}
Benzo[a]pyrene	74.5	32.6	0.3[1]	1.76×10^{-5}

[1]Assumed based on similar compounds (Schwarzenbach *et al.*, 1993).

The calculation of the air water exchange terms are presented in Table 7.12. As in the sediment water exchange, air-water exchange has been divided into a source term and a sink term in order to facilitate the inputs to the 3D model. The source term represents the input of PAH to the system due to ambient air concentrations, while the sink term

represents loss to the atmosphere due to volatilization. The direction of this flux is determined by the relative magnitudes of the two terms. The mathematical formulation of each term is represented by Eqs. 7.10 and 7.11.

$$Source\ Term = \frac{v_{tot} \cdot A \cdot C_a}{K_H'} \qquad \text{(Eq. 7.10)} \qquad Sink\ Term = v_{tot} \cdot A \cdot C_w \qquad \text{(Eq. 7.11)}$$

Table 7.12
Air-Water Exchange Summary

Compound	C_a (ng/m^3)	v_{tot} (cm/s)	Source term[1] (kg/s)	Sink term/C_w[2] (m^3/s)
Napthalene	362	1.01×10^{-3}	3.53×10^{-6}	85.8
Pyrene	4.6	1.16×10^{-4}	2.33×10^{-7}	9.8
Benzo[a]pyrene	0	1.09×10^{-5}	0	0.9

Because the magnitude of the sink term depends upon the concentration in the water, the above sink term value does not have much physical meaning. The reader is referred to Section 7.3 for the implementation of these terms to calculate a steady state concentration. Also included in this section is a discussion of each compound and the relative contributions of each source and sink.

7.2.6 Atmospheric Deposition

The data available for the atmospheric deposition of PAHs was very useful because of its direct applicability to the study area. Annual wet and dry deposition rates were estimated specifically for the Boston and Massachusetts Bay area in a 1997 (Golomb, 1997). The two sampling stations used in this report were located in Nahant and Truro, MA. The Nahant data is the most applicable to the mass balance because of its proximity to Boston Logan International Airport. This station is thus assumed to be representative of the atmospheric loadings in the study area.

Total depositional loading was simply calculated as the sum of the dry and wet deposition multiplied by the area of the Inner Harbor. The data presented in the study for the three compounds of interest are presented below along with the estimated total annual load to the study area.

Table 7.13
Atmospheric Deposition Rates

Compound	Dry deposition[1] $ng/m^2/year$	Wet deposition[1] $Ng/m^2/year$	Total deposition kg /year
Naphthalene	2.2×10^4	2.4×10^4	0.39
Pyrene	7.8×10^4	1.9×10^4	0.82
Benzo(a)pyrene	2.6×10^4	4.8×10^3	0.26

[1]Golomb, *et al.*, 1995

It should be noted that the data presented in the study were intended to represent total atmospheric loading. In the mass balance and 3D model, the data are assumed to represent only the fraction associated with the particulate deposition. This is due to the fact that air-water exchange is expected to act as a sink rather than a source of PAHs (see Section 7.2.5). The result may be that atmospheric sources could be slightly over-estimated in the model.

7.2.7 Photodegradation

In modeling naphthalene, pyrene, and benzo[a]pyrene, only direct photolysis was considered. The primary motivation for this was that PAHs contain enough double bonds to allow direct photolysis to occur. Thus indirect photolysis was considered negligible. The validity of this assumption was addressed in Section 6.3.2.

Incident light intensity values for a clear mid-winter day at 40^o N latitude were used for the purposes of photolysis calculations. These light intensity values were adjusted for

cloud cover by using data from the National Climatic Data Center's database. Daily sunlight values in Boston were recorded as percentage of the maximum total sunlight possible. These percentages were averaged for the winter months resulting in a correction factor of 0.66. Sunlight intensities were adjusted by this percentage in the base case. Light attenuation coefficients were also not available for the study area. Literature values were taken from Schwarzenbach *et al.*, 1993.

Molar extinction coefficients proved to be the most cumbersome of the constants to estimate. There is a lack of data available due to the fact that it is difficult to measure the extinction coefficients of PAHs in aqueous solutions (Leifer, 1988). Molar extinction coefficients were available for some compounds in organic solutions. While there is obvious error associated with using this data, the approximation is best for compounds which do not exhibit acid-base functionalities, which none of the three compounds of interest do (Schwarzenbach *et al.*, 1993). Data were available for naphthalene in hexane and these were applied to the model. For pyrene and benzo[a]pyrene, the molar extinction coefficients for benz(a)anthracene (in heptane) was applied This compound has four aromatic rings like pyrene, but differs from it in that benz(a)anthracene as a straight chain of three rings. Because the manner in which the rings are fused together appears to have a significant impact on absorbance, the values are assumed to be a slight over-estimation for pyrene. However, since the compound has one ring less than benzo[a]pyrene, the use of these values is almost certainly an underestimation for benzo[a]pyrene.

Reaction quantum yields (Φ_r) for each compound were also taken from literature values. The sources include Schwarzenbach *et al.*, 1993, and Lyman *et al.,* 1982. Because the value is lower for benzo[a]pyrene than for pyrene, the overall rate of direct photolysis is lower for benzo[a]pyrene. This is an artifact of using the same molar extinction coefficients for the two compounds as discussed above. In reality, benzo[a]pyrene would be expected to be more susceptible to direct photolysis because of its chemical structure. Variations in the value of the overall decay rate will be addressed in the sensitivity analysis presented in Section 7.4.

Table 7.14 summarizes the calculations of the direct photolysis decay rate coefficients applied to the base case formulation. See Appendix A for more details on calculation procedure.

Table 7.14
Photodegradation Decay Rates

Compound	k_a^t einstein/mol/day	Φ_r (mol/einstein)	k_p (s^{-1})
Naphthalene	3.01×10^{-2}	1.50×10^{-2}	5.23×10^{-9}
Pyrene	1.56×10^{1}	2.00×10^{-3}	3.6×10^{-7}
Benzo[a]pyrene	1.56×10^{1}	8.90×10^{-4}	1.6×10^{-7}

7.2.8 Flushing

As discussed in Section 6.5, the flushing rate is the inverse of the mean residence time of the system. The flushing rate was estimated based on some analysis of available literature data. One of the difficulties in estimating this parameter for the entire Inner Harbor is that the residence time depends on where the contaminant is introduced. Thus the residence times of a particle entering at a CSO in the Reserved Channel and one entering through the Mystic River are considerably different. The only major studies of the residence time of the Inner Harbor have been focused on Charles River water. The results from a freshwater study by Bumpus *et al.*, 1953, estimated residence times between 2 days and 10 days for the Inner Harbor, corresponding to total freshwater inflows (Q_f) of 34 m^3/s and 2 m^3/s, respectively. A dye study in 1993 by Adams *et al.* found a mean residence time of 3.75 days for summertime ($Q_f = 5$ m^3/s). Both studies were analyzed by Chan-Hilton *et al.* (1998), and compared with the results of a numerical model of the area implemented by Chan (1995). Chan-Hilton derived an inverse relationship between the freshwater inflow and the mean residence time based on the data collected by Bumpus *et al.*, 1953., which is presented in Equation 7.12

$$t_{res} = 1.158 + \frac{12.88}{Q_f} \qquad \text{(Eq. 7.12)}$$

Using this relationship with the freshwater inflow estimate in the present study ($Q_f = 21$ m^3/s), a mean residence time of about 1.77 days is predicted. This corresponds to a flushing rate, k_f, of about 0.56 day^{-1}.

Because of the aforementioned difference between the residence time of the total system and the studied ones that only involve the Charles River, the 3D model was used to estimate the residence time and therefore the flushing coefficient. The methodology used is described in more detail in Section 8.3.1.2. In summary, the average concentration over the entire harbor was obtained using the 3D model results. Then, using the box model, the required residence time to obtain the integrated average concentration was "back-calculated".

Using this methodology for pyrene, a residence time of about 2.7 days ($k_f = 0.37$ day^{-1}) was obtained. This value is considerably higher than the one predicted by Equation 7.12 ($t_{res} = 1.77$ days). Because the flushing constant has a strong influence on the results of the box model, it will be revisited in the sensitvity analysis presented in Section 7.4.

7.3 STEADY STATE CONCENTRATIONS

Calculation of the steady state concentration for each compound can be accomplished by revisiting Equation 7.1.

$$\frac{\partial(C_w V)}{\partial t} = \Sigma Q_{in} C_{in} + F_{atm} A + v_{tot} A\left(\frac{C_a}{K_H} - C_w\right) + \frac{D_w}{\delta_w} A\left(\frac{C_w}{K_d} - C_w\right) - C_w V(k_f + k_p)$$

By definition, steady state requires that the total mass of PAH in the system does not vary with respect to time ($\partial M_w/\partial t = 0$). In other words, there is no additional mass accumulation/withdrawal in the system and thus the sum of the sources and sinks equals 0. Eq 7.1 can then be arranged such that all of the sink terms are equated with the source terms, as shown in Eq 7.13.

$$\Sigma Q_{in} C_{in} + F_{atm} A + \frac{C_a v_{tot}}{K_H'} A + \frac{C_s D_w}{\delta_w K_d} A = v_{tot} A C_w + \frac{D_w}{\delta_w} A C_w + k_f V C_w + k_p V C_w \quad \text{(Eq. 7.13)}$$

Solving for the steady state concentration yields Eq. 7.14

$$C_w^{ss} = \frac{\Sigma Q_{in} C_{in} + F_{atm} A + \frac{C_a v_{tot}}{K_H'} A + \frac{C_s D_w}{\delta_w K_d} A}{v_{tot} A + \frac{D_w}{\delta_w} A + k_f V + k_p V} \quad \text{(Eq. 7.14)}$$

Each of the terms listed above have been estimated in the preceding sections. Table 7.15 summarizes the base case value of each source term, whereas Table 7.16 shows the base case values of each sink term. Finally, Table 7.17 shows the predicted steady state concentrations, calculated by simply dividing the sum of the source terms by the sum of the sink terms.

Table 7.15
Source Term Summary

Source Term	Naphthalene (kg/s)	Pyrene (kg/s)	Benzo[a]pyrene (kg/s)
$\Sigma Q_{rivers} C_{rivers}$	1.59×10^{-6}	4.88×10^{-6}	2.82×10^{-7}
$\Sigma Q_{cso} C_{cso}$	5.38×10^{-9}	1.54×10^{-8}	6.55×10^{-9}
$\Sigma Q_{storm} C_{storm}$	3.26×10^{-8}	2.71×10^{-7}	5.65×10^{-8}
$F_{atm} A$	1.23×10^{-8}	2.60×10^{-8}	8.26×10^{-9}
$C_a v_{tot} A / K'_H$	3.53×10^{-6}	2.33×10^{-7}	0
$C_s D_w A / \delta_w K_d$	5.33×10^{-4}	3.25×10^{-6}	2.37×10^{-7}

Table 7.16
Sink Term Summary

Sink Term/C_w	Naphthalene (m^3/s)	Pyrene (m^3/s)	Benzo[a]pyrene (m^3/s)
$V_{tot}A$	85.8	9.8	0.9
D_wA/δ_w	7.0	5.3	5.0
K_fV	362.7	362.7	362.7
K_pV	0.4	30.5	13.6

Table 7.17
Estimated Steady-State Concentrations

Compound	Steady-state concentration (ng/l)
Naphthalene	1.2×10^3
Pyrene	21
Benzo[a]pyrene	1.5

These values are the predicted steady state concentrations for the modeled winter conditions. Given all of the uncertainties involved in much of the parameter estimation and the simplifying assumptions of the box model, the values calculated above should be viewed with an appropriate level of uncertainty. Based on the sensitivity analysis which follows in Section 7.4, it is estimated that the uncertainty for pyrene and benzo[a]pyrene is on the order of 50%. Naphthalene, however, may be substantially overestimated due to the assumptions made in the sediment-water exchange model. The reader is referred to Section 7.4.3 for further discussion on this topic.

The relative importance of each of the source and sink terms is perhaps best viewed graphically. Figures 7.4, 7.5, and 7.6 illustrate the relative contributions of each mass balance term for naphthalene, pyrene, and benzo[a]pyrene, respectively. It should be noted that in these figures, the source and sink terms for sediment-water exchange and air-water exchange have been combined to show the net fluxes. Sink terms were converted to mass per time using the predicted steady state concentration.

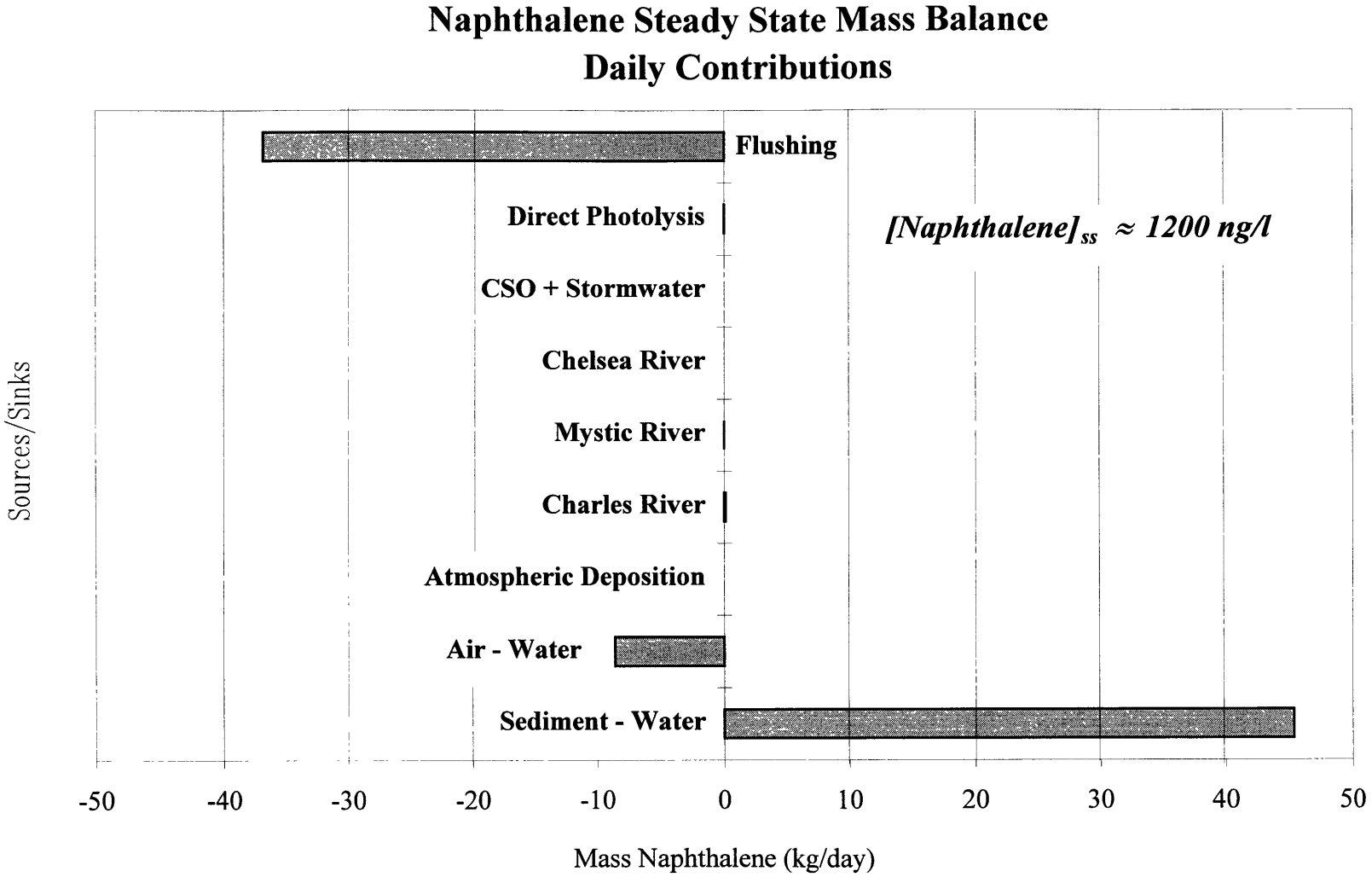

Figure 7.4 Relative Influence of Naphthalene Sources and Sinks

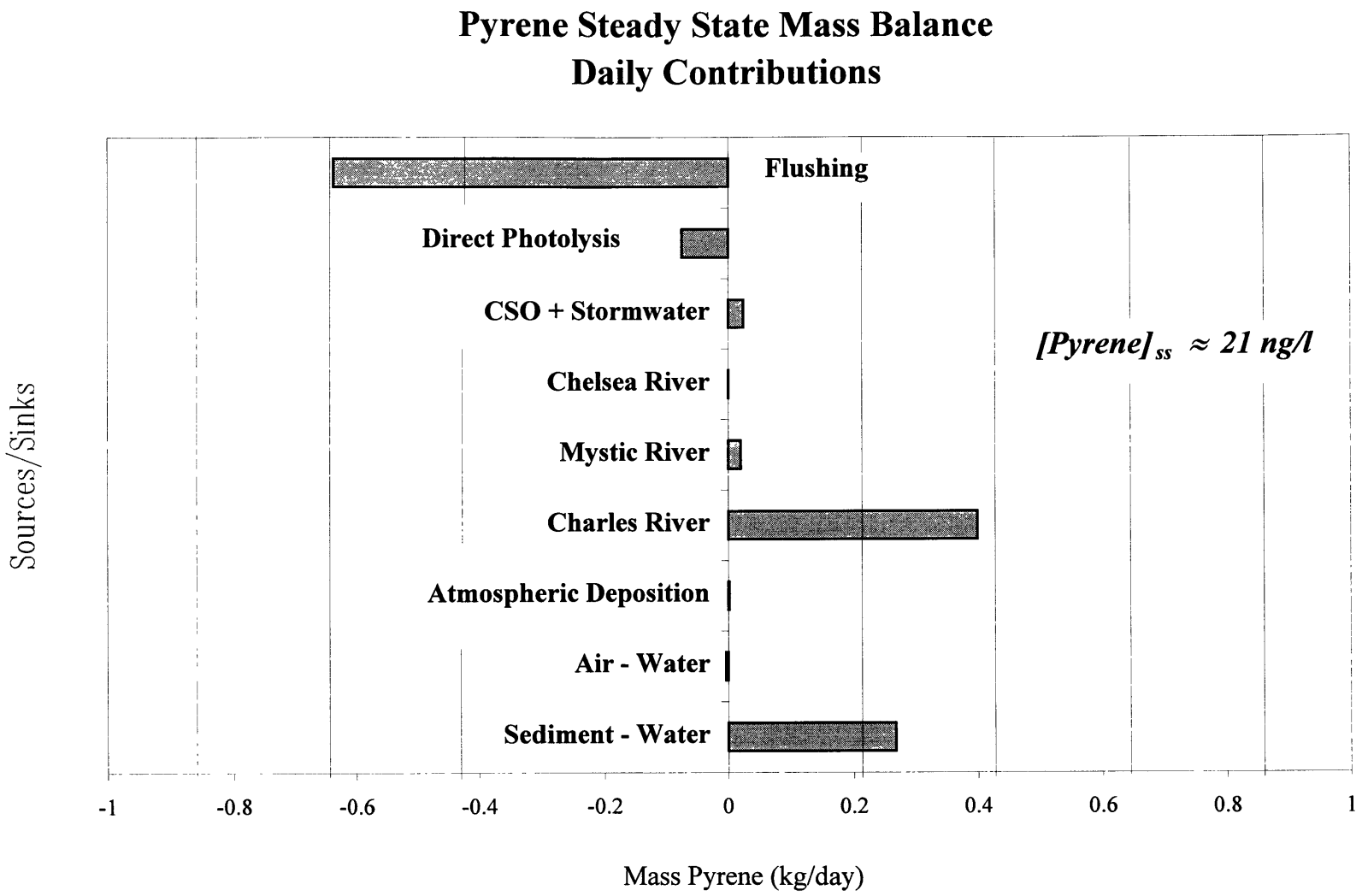

7.5 Relative Influence of Pyrene Sources and Sinks

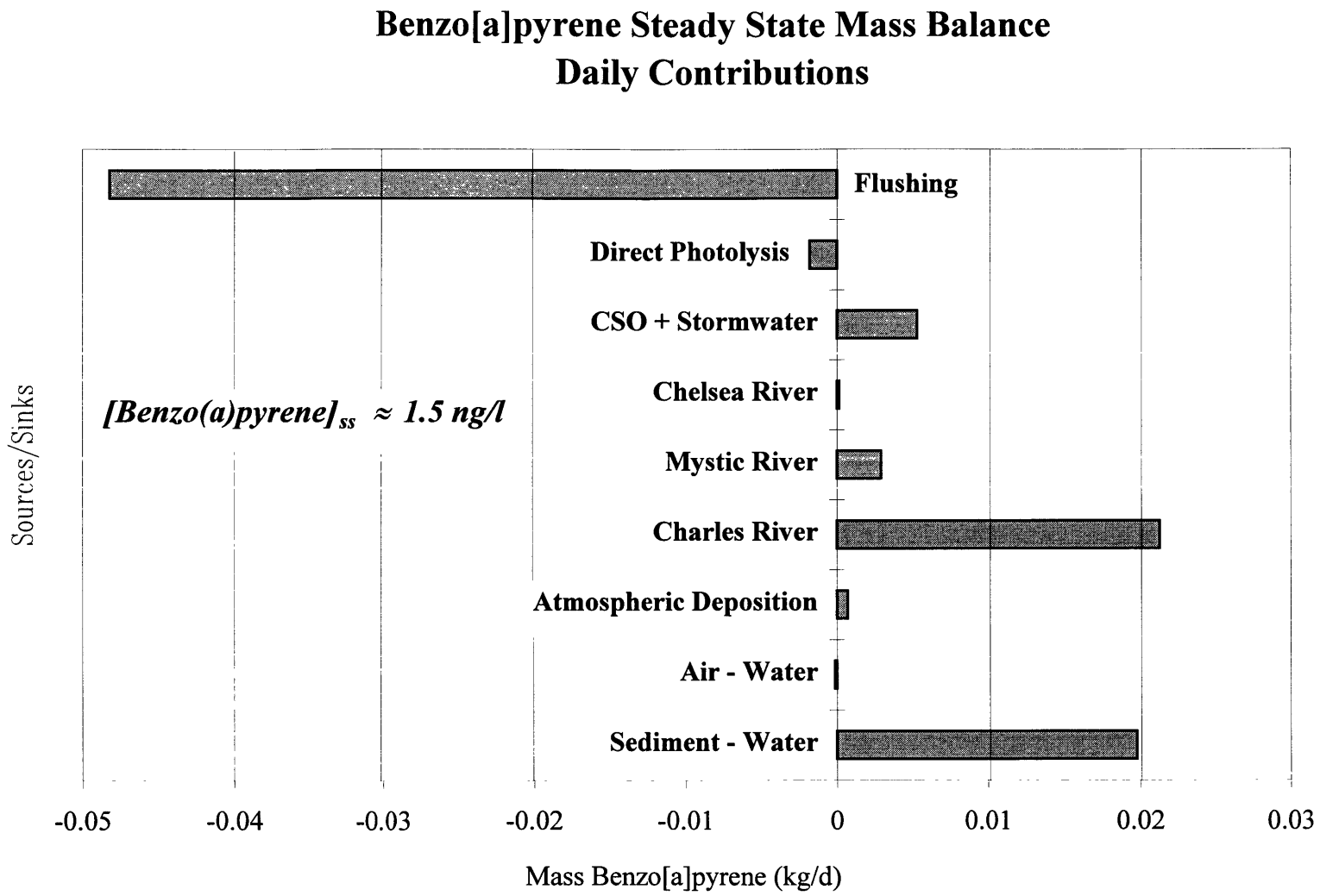

Figure 7.6 Relative Influence of Benzo[a]pyrene Sources and Sinks

7.4 SENSITIVITY ANALYSIS

The purpose of the sensitivity analysis is to address the impact of varying some of the most important variables as well as to assess the magnitude of error associated with neglecting certain terms in the conceptual mass balance (see Section 7.1, Figure 7.1)

7.4.1 Flushing

Flushing is the primary sink for each of the PAHs presented in the base case analysis. It is therefore prudent to understand the dependence of the steady state concentration to this variable. As discussed in Section 7.2.7, the flushing rate is calculated from the mean residence time. The following sensitivity analysis will investigate the impact of uncertainty in the flushing rate. The steady state concentrations presented in Section 7.3 used a flushing rate based on a residence time of 2.7 days. This value will be compared to the concentration predicted using a mean residence time of 1.75 days, as predicted by Equation 7.12 with a freshwater inflow of 21 m^3/s.

Table 7.18
Flushing Rate Sensitivity Analysis

Residence Time, t_{res} (days)	Flushing Rate, k_f[1] ($days^{-1}$)	Steady State Concentration, C_w		
		Naphthalene (ng/l)	Pyrene (ng/l)	Benzo[a]pyrene (ng/l)
2.7 (Base Case)	0.56	1.2×10^3	21	1.5
1.77 (Predicted from Eq. 7.12)	0.37	8.3×10^2	14	1.0

[1] k_f calculated as $1/t_{res}$

The impact of the uncertainty in the mean residence time is about a 33% change in steady state concentration.

The preceding uncertainty analysis was concerned only with the uncertainty in mean residence time given a constant freshwater inflow. The following analysis will vary the freshwater inflow to investigate the resulting impact on mean residence time and thus the predicted steady state concentration. In order to relate freshwater inflow to mean residence time, Equation 7.12 will be adjusted to fit the base case residence time of 2.7 days. The result of this reformulation is Equation 7.15.

$$t_{res} = 2.088 + \frac{12.88}{Q_f} \qquad \text{(Eq. 7.15)}$$

The sensitivity analysis will use the freshwater inflow range of 2 m3/s to 34 m^3/s, as reported by Bumpus *et al.*, 1953 (Chan-Hilton *et al.*, 1998). It should be noted that the PAH loadings from the Charles, Mystic, and Chelsea Rivers will be assumed constant in each case (i.e., the concentrations are assumed to vary with flow rate). Table 7.19 presents the result of the freshwater inflow sensitivity analysis.

Table 7.19
Freshwater Inflow Sensitivity Analysis

Total Freshwater Flow	Residence Time[1] (days)	Steady State Concentration, C_w		
		Naphthalene (ng/l)	Pyrene (ng/l)	Benzo[a]pyrene (ng/l)
2 m^3/s (Lower Limit)	8.5	2.6×10^3	54	4.4
21 m^3/s (Base Case)	2.7	1.2×10^3	21	1.5
34 $m^3/2$ (Upper Limit)	2.5	1.1×10^3	20	1.4

[1]Flushing rate calculated as $1/t_{res}$

Table 7.18 shows that a 91% decrease in freshwater flow results in a 315% increase in residence time, which causes increases in concentration of 117%, 154% , and 193% for naphthalene, pyrene, and benzo[a]pyrene, respectively. A 51% increase in total

freshwater flow (7% decrease in mean residence time) results in a concentration drops of 8%, 5%, and 7% for naphthalene, pyrene and benzo[a]pyrene, respectively. The three compounds exhibit similar responses to variations in freshwater inflow and mean residence time. This can be attribtuted to the fact that flushing is the primary removal mechanism for each compound.

7.4.2 River PAH Loads

The Charles River is a primary source of contaminants in the case of pyrene and benzo[a]pyrene. Sensitivity analysis was performed on the concentration of PAH in each of the rivers. This is important since the average values used in the base case formulation are based on a small number of data points for each compound. A variation of ± 50% was applied. The results of the sensitivity analysis are presented in Table 7.20

Table 7.20
River Load Sensitivity Analysis

Naphthalene		Pyrene		Benzo[a]pyrene	
Daily Load (kg/d)	C_w (ng/l)	Daily Load (kg/d)	C_w (ng/l)	Daily Load (kg/d)	C_w (ng/l)
0.275 (Upper Limit)	1.2×10^3	0.844 (Upper Limit)	33	0.0487 (Upper Limit)	2.3
0.137 (Base Case)	1.2×10^3	0.422 (Base Case)	21	0.0244 (Base Case)	1.5
0.0687 (Lower Limit)	1.2×10^3	0.211 (Lower Limit)	15	0.0122 (Lower Limit)	1.2

Doubling the concentration values for each river results in a 57% and 53% increase in pyrene and benxo[a]pyrene harbor concentrations, respectively, while the change in naphthalene is negligible. A factor of two decrease in river load causes a 29% and 20% drops in pyrene and benzo[a]pyrene concentrations. Napththalene is not sensitive to this parameter because river loads are only a small contribution to the total load. Pyrene and benzo[a] pyrene are much more sensitive since river loads comprise a significant portion of the total daily load for these compounds.

7.4.3 Sediment-Water Exchange

The main parameters of concern in modeling the sediment water exchange are C_s, K_d, D_w, and δ_w. The latter two coefficients affect the source and sink terms through their ratio, and thus the following analysis will focus on δ_w (since it is much more uncertain). Recalling Equation 6.6, we see that sediment flux is inversely proportional to δ_w. The base case formulation used a value of 5×10^{-4} m. Since published values of δ_w range from about 10^{-2} to 10^{-4} m, this value may be on the low side. Chen, 1993, used a lower limit of 10^{-5} m in her analysis of sediment flux. Therefore, a range of 10^{-2} to 10^{-5} m will be used in this analysis. All other values will remain the same as in the base case formulation. The results of the sensitivity analysis are presented in Table 7.21.

Table 7.21
Diffusive Boundary Layer Sensitivity Analysis

δ_w (m)	Steady State Concentration, C_w		
	Naphthalene (ng/l)	Pyrene (ng/l)	Benzo[a]pyrene (ng/l)
10^{-2} (upper limit)	7.7×10^{2}	14	1.0
5×10^{-4} (base case)	1.2×10^{3}	21	1.5
10^{-5} (lower limit)	3.5×10^{4}	2.5×10^{2}	20

A 98 % decrease in δ_w results in 2817%, 1090%, and 1233% increases in the concentrations of naphthalene, pyrene, and benzo[a]pyrene, respectively. A 1900% increase in δ_w results in a 36%, 33%, and 33% decrease in the concentrations of naphthalene, pyrene, and benzo[a]pyrene, respectively. All three compounds exhibit strong dependence on this parameter. Decreases in δ_w have a stronger effect than

increases for pyrene and benzo[a]pyrene because decreases allow sediment-water exchange to dominate the total loading to the system.

Sensitivity analysis of K_d for naphthalene is especially important since this value was calculated from a literature value of the aqueous solubility. The K_d's for benzo[a]pyrene and pyrene were obtained from McGroddy's *in-situ* measured values (see Section 7.2.4). In the sensitivity analysis, the naphthalene value of K_d was calculated using a K_{om} which is 280% larger than the literature value. This is equal to the percent difference between the measured *in-situ* value and the calculated literature value for pyrene. In the sensitivity analysis for pyrene and benzo[a]pyrene, alternate literature *in-situ* values were used. K_d values were calculated from the K_{oc} values reported by Chin and Gschwend, 1992 (referenced in Chen, 1993). The results of the sensitity analysis are presented in Table 7.22.

Table 7.22
Partition Coefficient Sensitivity Analysis

Naphthalene		Pyrene		Benzo[a]pyrene	
K_d (m^3/g)	C_w (ng/l)	K_d (m^3/g)	C_w (ng/l)	K_d (m^3/g)	C_w (ng/l)
3.02×10^{-5} (Base Case)	1.2×10^{3}	2.72×10^{-2} (Base Case)	21	2.49×10^{-1} (Base Case)	1.5
1.15×10^{-4} (Adj. Value)[2]	3.2×10^{2}	1.03×10^{-2} (Obs. Value)[1]	34	70.5 (Obs. Value)[1]	0.9

[1]Based on K_{oc} reported by Chin and Gschwend, 1992
[2]Value increased by factor of 3.8 (based on difference between McGroddy's reported value and calculated theoretical K_{om} value for pyrene)

For naphthalene, a 280% increase in K_d results in a 73% decrease in steady state concentration. The alternate *in-situ* K_d for benzo[a]pyrene is 283 times higher than the value used in the base case. The resulting change in steady state concentration is a 40% decrease. For pyrene, the alternate *in-situ* K_d is 62% lower than the base case value. The resulting change in pyrene steady-state concentration is a 62% increase.

The final sediment water exchange term to be considered is the PAH concentration in the sorbed sediments. A range of ± 50% was applied for the purposes of this analysis. The results are presented in Table 7.23.

Table 7.23
Sediment Concentration Sensitivity Analysis

Naphthalene		Pyrene		Benzo[a]pyrene	
C_s (ng/g)	C_w (ng/l)	C_s (ng/g)	C_w (ng/l)	C_s (ng/g)	C_w (ng/l)
4576.8 (Upper Limit)	2.4×10^3	33172 (Upper Limit)	29	23788 (Upper Limit)	2.2
2288.4 (Base Case)	1.2×10^3	16586 (Base Case)	21	11894 (Base Case)	1.5
1144.2 (Lower Limit)	5.9×10^2	8293 (Lower Limit)	17	5947 (Lower Limit)	1.2

Doubling the sediment concentrations results in harbor concentration increases of 100%, 38%, and 47% for naphthalene, pyrene, and benzo[a]pyrene, respectively. A 50% decrease in sediment concentrations results in 51%, 19%, and 20% harbor concentration decreases for naphthalene, pyrene, and benzo[a]pyrene, respectively. Note that the sensitivity of naphthalene water concentration to changes in the sediment concentration is essentially 1:1.

One other consideration in modeling the sediment water exchange is the choice of models for the base case. As discussed in Chapter 6.1, sediment water exchange was assumed to be limited by water-side diffusion in Boston Harbor. The following analysis will utilize the sediment flux described by a simplified version of Eq. 6.4, in which only the water side diffusion and bioturbation terms are considered (i.e. the second and fourth terms of the denominator.) The additional terms included in this formulation are L, ϕ, ρ_s, and D_B. Values for these terms were obtained from Chen, 1993. The values used are L = 1cm, ϕ = 0.84, ρ_s =2.5 g/cm^3, and $D_B = 1.7 \times 10^{-7}$ cm^2/s.

Table 7.24
Bioturbation Sensivity Analysis

Compound	C_w (ng/l) as predicted by Equation 6.6 (Base Case Formulation)	C_w (ng/l) as predicted by Simplified Equation 6.4 (Alternate Formulation)
Naphthalene	1.2×10^3	38
Pyrene	21	21
Benzo[a]pyrene	1.5	1.5

While the resulting change in the steady state concentration for pyrene and benzo[a]pyrene is negligible, the effect on naphthalene is dramatic. The sediment water exchange process becomes completely dominated by the rate of bioturbation and thus the sediment-water flux is virtually eliminated. The result strongly suggests that the simplification made in Eq. 6.6 does not apply for less hydrophobic PAHs. The concentration predicted by Eq. 6.5 is very dependent on the magnitude of D_B, which has been observed to vary between about 10^{-5} and 10^{-11} cm^2/s. If the lower value in this range is used, the predicted concentration is 6.8×10^2 ng/l. Given this result, it would appear that the model presented for naphthalene is an over-estimation of the steady-state concentration. Future model formulations for naphthalene should incorporate one or more of the other transport mechanisms described in Section 6.1.

7.4.4 Photodegradation

Because difficulty was encountered in obtaining some of the required input to calculate direct photolysis, it is prudent to include some analysis of how this value may affect the overall concentration in the water column. This parameter was believed to be underestimated for benzo[a]pyrene especially. Because direct photolysis rates increase

dramatically as higher wavelengths of light can be absorbed by a compound, a factor of ten was used in the sensitivity analysis. The results are presented in Table 7.25.

Table 7.25
Direct Photolysis Sensitivity Analysis

Naphthalene		Pyrene		Benzo[a]pyrene	
k_p (ng/g)	C_w (ng/l)	k_p (ng/g)	C_w (ng/l)	k_p (ng/g)	C_w (ng/l)
2.99×10^{-3} (Upper Limit)	1.2×10^{3}	3.112×10^{-1} (Upper Limit)	13	1.385×10^{-1} (Upper Limit)	1.2
2.99×10^{-4} (Base Case)	1.2×10^{3}	3.112×10^{-2} (Base Case)	21	1.385×10^{-1} (Base Case)	1.5
2.99×10^{-5} (Lower Limit)	1.2×10^{3}	3.112×10^{-3} (Lower Limit)	23	1.385×10^{-1} (Lower Limit)	1.6

Changes to the direct photolysis decay rate for napththalene had a negligible effect on calculated concentrations. Increasing the decay rate by a factor of 10 resulted in decreases of 38% and 20% in the steady state concentrations of pyrene and benzo[a]pyrene, respectively. Decreasing the rate by a factor of 10 resulted in concentration increases of 10% and 7% for pyrene and benzo[a]pyrene, respectively. Since the main concern is that the decay of benzo[a]pyrene is greatly underestimated, additional analysis was performed on benzo[a]pyrene. Increases of 2 and 3 orders of magnitude result in steady state concentrations of 0.3 ng/l (80% decrease) and 0.04 ng/l (97% decrease), respectively.

7.5 PREDICTED POST DREDGING CONCENTRATIONS

The navigation improvement project, as was introduced in Chapter 4, involves dredging a portion of the Inner Harbor. The proposed plan involves disposing of the contaminants in sub-aqueous disposal cells. Although it is unknown whether these cells will completely hinder the flux of contaminants to the overlying water column, the following analysis will

assume that the project will remove and cap the contaminated sediments from the proposed areas with 100% success. In other words, all contaminated sediments from the proposed areas will be removed and will no longer contribute PAHs. While this is a simplification, it is not unreasonable and is the only feasible scenario given the present uncertainty concerning capping effectiveness.

The proposed dredge areas are shown in Figure 2.1. Using these area delineations, the average sediment concentration for each compound was recalculated by reducing the fraction of the total Inner Harbor area covered by contaminated sediments. It is assumed that the sediment concentrations in the undredged areas remain the same as before. The post-dredge contributing areas and resulting average concentrations are presented in Table 7.26.

Table 7.26
Post Dredging Sediment Concentrations

Sediment Region	Fraction Area	Naphthalene (ng/g)	Pyrene (ng/g)	Benzo[a]pyrene (ng/g)
1) Chelsea River	0.00	10	8917	2950
2) Mystic-Chelsea Confluence	0.03	5082	50127	30277
3) Charles River Mouth	0.13	10	4419	7159
3) Fort Point Channel Mouth	0.35	10	3195	1949
5) Fort Point Channel	0.02	43628	66831	94984
6) Reserved Channel	0.18	10	1559	1418
Weighted Average Used:	**0.71**	**1.14×10^3**	**4.81×10^3**	**4.90×10^3**

It should be noted that approximately 71% of the Inner Harbor remains unaffected by the Navigation Improvement Project.

Using the same parameters as presented in the base case, steady state concentrations for each compound were calculated. The results are included in Table 7.27 along with the percent decrease in steady state concentration resulting from the dredging operations.

Table 7.27
Post Dredging Concentration Analysis

Compound	Pre Dredging (ng/l)	Post Dredging (ng/l)	Percent Improvement
Naphthalene	1.2×10^3	5.9×10^2	51%
Pyrene	21	16	24%
Benzo[a]pyrene	1.5	1.2	20%

Based on this analysis, it is clear that potential improvements can be effected by the navigation improvement analysis. While the effect is most noticeable for naphthalene, there is a significant decrease in each of the compounds. Since this analysis assumes perfect dredging and capping, it is an optimistic prediction. If a 50% efficiency is assumed, the resulting steady state concentrations are 8.9×10^2 ng/l (25% decrease), 19 ng/l, (10% decrease) and 1.4 ng/l (7% decrease) for naphthalene, pyrene, benzo[a]pyrene, respectively. Future investigations as to the feasibility of effectively sequestering contaminated sediments using subaqueous disposal cells will provide the information required for a more thorough analysis of the long term impacts of the navigation improvement project.

8 3-D MODEL

8.1 BRIEF DESCRIPTION OF THE 3-D MODEL

ECOMsi is a three-dimensional circulation model developed and coded by Blumberg and Mellor in Fortran. The model has undergone numerous modifications since it was first released. The version used in this study is the August 1991 revision that has been previously used by Chan (1995).

The model solves the momentum and mass conservation equations in time using a finite difference scheme. As a result, the model outputs the water surface elevation, the velocity components in the three dimensions, temperature and salinity in each of the levels of each of the horizontal grid cells. These grid cells can have variable spacing in the horizontal dimension. For the vertical dimension, however, the model works with a constant number of levels that vary in size according to the total depth in each cell (i.e., it uses a sigma-coordinate system).

The model allows the user to specify the elevations, temperature and salinity at each open boundary of the grid layout. The elevation values can be calculated using up to 6 harmonics of the astronomic tide or can be introduced as a time series. The values for salinity and temperature can be constant in time or variable with a specified time series.

In addition to the open boundary conditions, point discharges may be specified. These inputs may be located at any place on the grid and may have any vertical distribution. Each point source needs to have specified values for discharge, temperature, salinity and the concentration of a tracer of interest. These values can also vary with time.

The model also accepts other forcings such as Coriolis force, surface wind stress, salinity flux, heat flux and atmospheric pressure gradients.

This version of the model assumes that the tracer transported is conservative. As PAHs are not conservative, it was necessary to modify the source code to account for losses. The main processes that affect PAHs are discussed in Chapters 6 and 7 in more detail. Among them, sediment water exchange, air water exchange and photodegradation involve a first order decay process as shown in Sections 6.1, 6.2, and 6.3. In order to model these phenomena, a new loop was introduced to the source code. This loop multiplies the concentration at each time step by $exp(-k\Delta t)$, where k is the sum of the first order decay coefficient of the processes that takes places in that grid cell and Δt is the time step.

A more detailed description of the mathematical formulation of the equations is given in Blumberg and Mellor (1987). In addition, the model and its capabilities are described in the manual written by HydroQual (1993).

8.2 MODEL FORMULATION

The grid layout is a very important step in any modeling effort. This is due to the fact that, in general, the more features represented of the actual system, the more complex the grid is. Therefore, previous to the definition of the grid layout, the objectives of the model need to be clear. In this study, the interest is to study possible impacts of the dredging project over Boston's Inner Harbor. In particular, the objective is to analyze in a conceptual way the distribution of PAH inside the Inner Harbor before and after the dredging and capping takes place.

With this objective in mind, it is important that the grid be fine enough to resolve the area that will be dredged, but not too fine because that would make the simulation time very long and the formulation of the grid more complex. The selected horizontal layout is shown in Figure 8.1, and a brief description of the main characteristics of the grid is presented below.

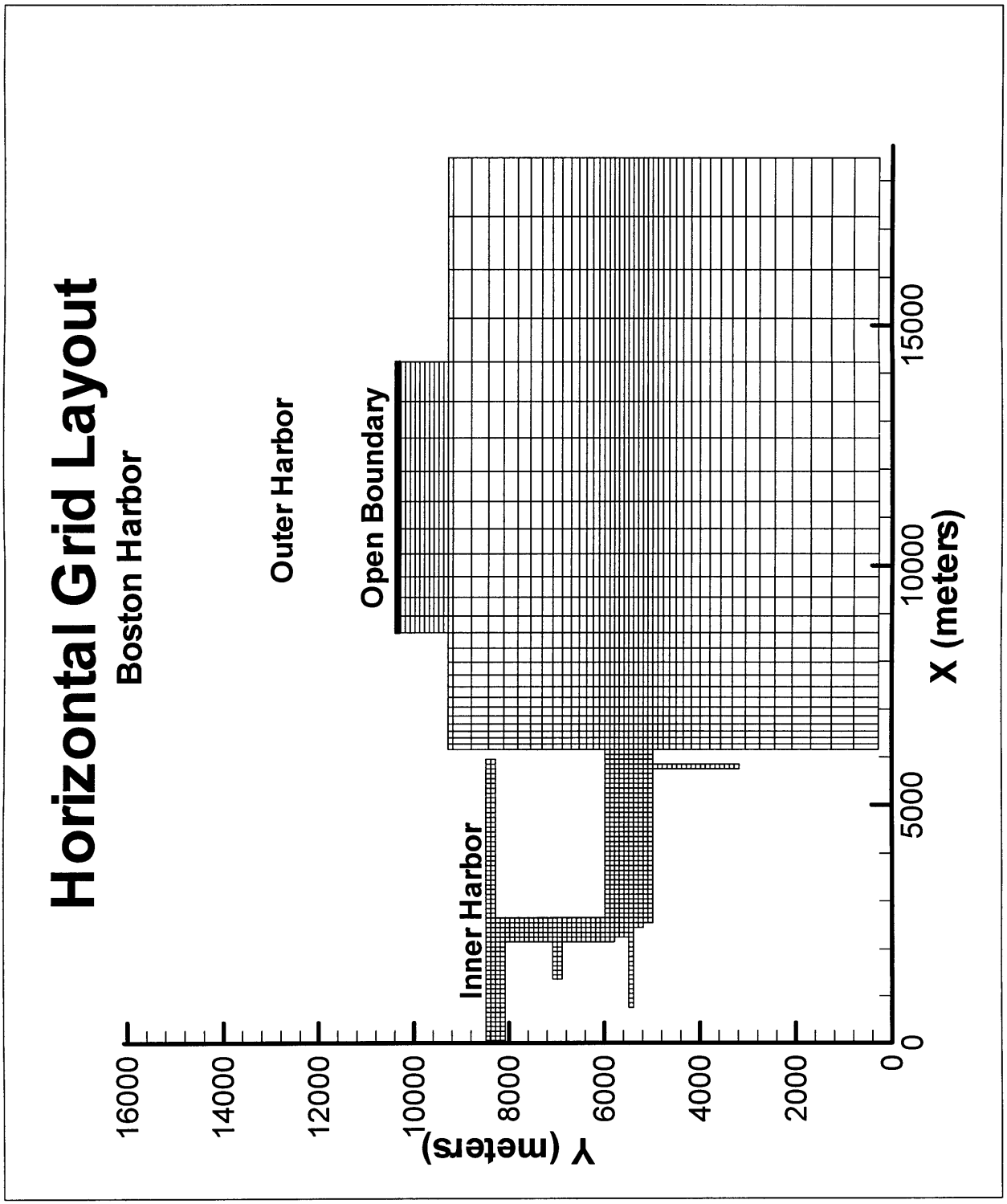

Figure 8.1 – Horizontal Grid Layout

8.2.1 Grid Layout

The grid represents Boston's Inner and Outer Harbor. The Inner Harbor is represented in more detail because it is the area of interest of this project. In contrast, the Outer Harbor is only represented with the purpose of placing the boundary conditions as far as possible away from the Inner Harbor.

In particular, the dredging zone needs to be represented in the Inner Harbor grid. This zone, as defined by the navigation improvement project, includes portions of the Mystic and Chelsea Rivers and part of their confluence. The exact location of this zone is shown in Figure 2.1.

To fulfill this objective, all the grid cells inside the Inner Harbor have the dimension of 100 x 100 meters. As the Mystic River averages about 400 meters wide and the Chelsea River about 200 meters wide, the grid size selected allows the resolution of the Mystic, Chelsea and Charles Rivers. Furthermore, the Reserved and Fort Point Channels can also be resolved.

The Outer Harbor, as previously mentioned, is included to attenuate the impacts of the boundary conditions into the Inner Harbor area. Therefore, it does not include any physical features and is represented as a large rectangular box. Because of the large surface area of the Outer Harbor, a variable horizontal grid size was implemented in order to minimize the calculation time. The growth increment between grids is 10% moving in an "easterly" direction.

The vertical dimension is divided into 10 levels each one having one tenth of the total depth at that point. This number of levels was used in previous studies and seems to be appropriate to represent the vertical mixing.

The Inner Harbor grid has a constant depth of 10 meters. This is representative of the entire main channel, the Mystic and Chelsea rivers and the Reserved Channel. This

simplification does not apply to the Charles River and the Fort Point Channel. However, this is not a major problem because this river and channel are not located in the area of main interest and the total volume of the Inner Harbor is maintained, thus ensuring that the momentum transport is correct.

The Outer Harbor grid has a constant depth of 5 meters representing the average depth. As mentioned before is does not include any geographical features, so the islands are not depicted. The only feature represented is President Roads Channel that connects the mouth of the Inner Harbor to Massachusetts Bay and has a depth of 10 meters. Again, the total approximate volume of the Outer Harbor is represented by the grid.

8.2.2 Initial and Boundary conditions

ECOMsi is a 3D model that calculates the circulation of the water due to hydrodynamic (tide, discharges), salinity and temperature forcings. In this version, it also calculates the transport of a substance that may be conservative or degradable by a first order process. To represent the hydrodynamic and the transport processes it is necessary to define the boundary and initial conditions appropriately. The initial and open boundary conditions are presented first, followed by the chemical sources and sinks.

8.2.2.1 Initial and Open Boundary

Before calculations begin the entire area has initial values of elevation, temperature and salinity. The elevation is considered constant and equal to the mean sea level in the entire domain. The salinity is also considered constant and equal to 30 psu. During the winter the Inner Harbor is not stratified, thus this value can be applied to all the harbor without any major simplification. The temperature has a value of 3 degrees Celsius over the entire area which is representative of the winter condition.

There is only one open boundary in the model representation as can be seen in Figure 8.1. This boundary represents the mouth of the Outer Harbor defined as a straight line between Deer Island and Hull. Temperature and salinity are considered constant along this boundary and steady in time, having values equal to the initial conditions. Although this is a simplification it is unlikely to affect the circulation inside the Inner Harbor (i.e. the area of interest of this project).

The main hydrodynamic forcing is given by the elevations at the boundary conditions. Only the M2 component of the astronomic tide is considered in the model. The period of this tide is, therefore, 12.42 hours. The amplitude selected is 1.5 meters (i.e. the boundary oscillates between 1.5 meters below mean sea level and 1.5 meters above mean sea level). No phase lag was introduced, so at the beginning of the model the boundary is at high tide. This tidal forcing is consistent with the tides in the Boston Harbor area and was previously used by Chan (1995).

8.2.2.2 Sources and Sinks

As there are many sources and sinks that affect PAHs, this section will be subdivided to explain each one separately. The main focus will be to address how the actual input of the values to the model was implemented.

8.2.2.2.1 River inputs

The Inner Harbor receives water from three rivers: The Mystic, Charles and Chelsea. The Mystic and Charles have a dam controlling the discharge to the harbor. The Chelsea River does not have any flow restrictions. All rivers have a considerable amount of PAH diluted in their waters, so they are all considered in the model.

Although the dams allow water to flow during low tide periods only, the input is simplified and considered constant in time. This is a good approximation as demonstrated

by Chan (1995). The river discharges for winter conditions are calculated in Section 7.2.1, giving values of 17.2, 3.6 and 0.2 m^3/s for the Charles, Mystic, and Chelsea Rivers, respectively. The concentration of each compound is also given in Section 7.2.1. In the 3D model the base case loadings were used.

8.2.2.2.2 CSOs (Combined Sewer Overflow) and Stormwater

There are multiple CSO discharges to the Inner Harbor. They are identified by the MWRA and Figure 7.2 shows their location in the Harbor. The discharges and PAH loadings contributed by the CSOs were discussed previously in Section 7.2.2.

The information regarding stormwater discharges is not as detailed as the information about CSOs. The data available is the sum of the average discharges in certain regions inside the Inner Harbor. These regions are also shown in Figure 7.2, and the discharge and loadings of each one is tabulated in Table 7.5.

The exact location of the stormwater discharges is also not known. For this reason, the average discharge in each area was distributed among the CSOs present in the same area. As the size of these areas is small, and because the model is intended to analyze the global distribution of contaminants along the Inner Harbor, this simplification is acceptable.

8.2.2.2.3 Bottom Flux

The bottom flux is one of the most important contributions to the PAH concentration in the water column (Stolzenbach *et al.*, 1998). The theory behind this transport and the values obtained was explained in Section 6.1.

As the sediment concentration of PAHs varies substantially along the Inner Harbor, the bottom flux also does. To represent this in the model the Inner Harbor was divided into six sub-areas (see Section 7.2.4). Each of the cells belonging to each of these areas was

assigned a constant bottom flux that depends on the sediment concentration of the modeled compound at that location. The values of the sediment concentration were obtained by core measurements as described in Section 7.2.4.

As previously described in Section 6.1 the sediment-water exchange is a diffusive process. The expression that summarizes the process is:

$$\frac{\partial C_w}{\partial t} = \frac{D_w}{h\delta_w}\left(\frac{C_s}{K_d} - C_w\right) \qquad \text{(Eq. 8.1)}$$

where:

C_w = the concentration of the compound in the water (ng/l)

t = time (s)

D_w = the diffusivity of the compound of interest in water, (m^2/s)

h = the well-mixed depth, which is represented in the model by the height of the bottom layer cell, (m)

δ_w = the diffusive boundary layer thickness, (m)

C_s = the concentration of the compound in the sediments. (ng/g)

K_d = the sediment-water partition coefficient. (l/g)

This expression describes a first order process involving the differences between sediment and water concentration. However, as C_s is constant for the time interval considered in the simulation, the expression can be rewritten as:

$$\frac{\partial C_w}{\partial t} = K_1 - K_2 C_w \qquad \text{(Eq. 8.2)}$$

where:

$$K_1 = \frac{C_s D_w}{h K_d \delta_w} \qquad \text{(Eq. 8.3)}$$

and

$$K_2 = \frac{D_w}{h\delta_w} \qquad \text{(Eq. 8.4)}$$

Eqn. 8.2 shows a process that is a combination of a constant source and a first order sink. Therefore, in the model the sediment-water exchange can be represented as a constant source dependent on the concentration of the sediments and a first order sink that is a function of the (variable in time) concentration in the water.

The ECOMsi model has no capabilities to simulate diffusion-driven sources. To overcome this problem, the constant source portion of the sediment-water exchange process was represented as a virtual diffuser discharge in the bottom layer. Therefore, the mass flux of contaminant is represented by discharge and concentration values. These values should be selected appropriately so that they represent the physical system.

The bottom flux does not introduce water to the system because it is a diffusive process. Therefore, to accurately represent the inflow to the system, the virtual diffuser discharge should be selected as small as possible. The selected discharge is $1x10^{-9}$ m^3/s in each cell.

The virtual concentration should be selected so that the virtual discharge times this virtual concentration is equal to the mass flux of pollutant as calculated by theory. Therefore, the concentration introduced to the virtual diffusers is calculated as C = flux/Q. The calculated values of C and Q for each sediment quality region are applied to the bottom cells within that region.

The first order decay process is represented using the modification to the code previously explained in Section 8.1. The value of the decay coefficient is equal to K_2, which is calculated as described above.

8.2.2.2.4 Atmospheric deposition

The atmospheric deposition can be considered constant in time and over the entire Inner Harbor. Therefore, the estimated value as shown in Section 7.2.6 is added to the top layer of each cell.

8.2.2.2.5 Air-water exchange

The air-water exchange is similar in theory to the bottom-water exchange. Therefore, it can also be represented as the sum of a constant source and a first order sink. In this case, however, the concentration in the air will determine the value of the constant source portion of the process.

8.2.2.2.6 Photodegradation

PAHs are, in general, susceptible to photodegradation. This process takes place in the top layer, where the sunlight penetrates in the water. The theoretical explanation of how to calculate the photodegradation is presented in detail in Section 6.3. It is important to note that the theory shows that the process is of first order in time with a constant decay coefficient.

As described previously, the ECOMsi model was modified to accept a first order decay. Photodegradation was considered to act in the top layer representing an average depth of 1 meter. Therefore, the decay coefficients of the sink portion of the air-water exchange process were simply added to the decay coefficient of photodegradation in this top layer. This is possible because they are both linear processes.

8.2.2.3 Other conditions

As previously mentioned in the model description, ECOMsi has the capability to deal with Coriolis force, heat flux, salinity flux, and wind stresses. All these processes are neglected in this study because of their small influence in the behavior of the Inner Harbor (Chan, 1995).

The non-dimensional bottom friction coefficient selected was 0.0025; the bottom roughness was 0.003 meters. A constant horizontal diffusion coefficient of 2.0 m^2/s was used. The momentum mixing was considered equal to the dispersive mixing; i.e. a Prandtl number of 1.0 was used for both the horizontal and the vertical dimensions. All these values were taken from Chan's thesis (1995).

ECOMsi includes a level 2.5 turbulence closure model to calculate spatially and temporally varying values of vertical diffusion. The model also allowse specification of a background vertical diffusivity which is added to the closure derived value. Chan (1995) noted that the turbulence closure model does not represent accurately the vertical mixing if the tracer is introduced at the top level of the grid, where the greatest density stratification occurs. To overcome this situation she adjusted the value of the molecular diffusivity and found that the optimal one is approximately $5x10^{-5}$ m/s^2. Therefore, this value was used in the model.

8.2.3 Modeling Scenarios

In this section the different scenarios represented are described. The grid utilized is the same for all the cases modeled. The boundary conditions are modified according to the compound and the situation modeled, except for the open boundary condition that remains the same.

Because the main objective of this modeling is to analyze the quasi-steady state distribution of pollutants inside the Inner Harbor, it is important that the simulation runs long enough to reach such state. The length of the simulation is, therefore, related to the characteristic residence time of the Inner Harbor. Previous studies (Bumpus *et al.*, 1953; Adams *et al.*, 1993; Chan-Hilton *et al.*, 1998) show that the residence time varies between 2 and 10 days for inputs located in the Charles River. Chan-Hilton *et al.* (1998) provide a regression that relates the total freshwater inflow to the residence time. This regression is given by Eqn. 7.12 and, for the total freshwater discharge of 21 m^3/s and gives a residence time of 1.77 days. Since this residence time is based on freshwater flow (which is mainly from the Charles River), the residence time is expected toincrease somewhat if more of the inputs are from the Mystic or Chelsea river areas, because of the increased distance to the mouth of the Harbor.

Taking these considerations about residence time into account, all the simulations were run for seven days (168 hours). This time has demonstrated to be long enough to reach a quasi-steady state situation without making the computational time too long. First, the time step of the simulations was 30 seconds, giving a total of 20,160 time steps. After verifying that the hydrodynamic conditions were not affected by using 45 seconds, the time step was changed for the next simulations in order to shorten the simulation time.

For benzo[a]pyrene, an output file with the velocities in each direction and the tracer concentration for each cell of the domain was generated every three hours (360 time steps). In the case of the other two compounds, the output was generated every fourth of the tidal cycle (248 time steps).This time between outputs allows analyzing the tidal effect over the concentration distribution. This is important to determine if the steady state situation is reached. This issue will be further discussed in following points.

The model varies the values for the elevations at the open boundary and the discharges in the sources linearly from zero to the final desired value using a ramp function. This is done to minimize the numerical problems associated with large gradients. The number of time steps during which this linear variation takes place can be specified. A value of 1.5

hours (180 time steps for benzo[a]pyrene and 120 for pyrene and naphthalene) was selected based on previous studies (Chan, 1995).

Two situations were modeled for each of the three compounds. These correspond to a base case and a post-dredge case. The source and sink values for the base case are the same that were utilized for the box model, with the exception of the flushing which is replaced with the tidal condition defined on the open boundary in the 3D model.

In this study only long term post-dredging conditions were modeled. That is to say that impacts during the actual dredging and capping process were not taken into consideration. In addition, due to time limitations and the fact that capping efficiency is not well known yet, the removal of contaminated sediments and subsequent capping was considered perfect. In other words, all the sediments located in the proposed dredge area were considered removed and capped and are therefore assumed to no longer contribute to the mass balance.

As mentioned in previous sections, the Inner Harbor was divided into six areas of constant bottom flux according to the location of the available core samples. These areas are depicted in Figure 7.3. In Figure 2.1 the projected dredging areas are shown. For the post-dredging case, the bottom flux was considered to be zero in the cells located where the dredging and capping would take place according to the project. In all remaining cells the bottom flux was the same as in the base case situation.

An additional run was made for benzo[a]pyrene. The situation modeled corresponds to a higher sediment water exchange than the base case. This was done to observe the impact on the distribution generated by the uncertainties in the values of the parameters involved in the sediment water exchange. One of the most uncertain values is the thickness of the diffusive layer. Therefore, for this simulation the value of the thickness of the diffusive layer was reduced by a factor of 5 in order to simulate a high sediment water flux. For a more detailed explanation of the theory behind the sediment water exchange, please refer to Section 6.1. Furthermore, the actual calculation of the sediment

water exchange values used in this model is discussed in Section 7.2.4. All the other sources and sinks for this simulation (rivers, air-water exchange, photodegradation, etc.) are the same as in the base case.

8.3 RESULTS

The results obtained from the model are discussed in this section. Results were first evaluated to determine if steady state was reached in each case. Afterwards, the distribution of each the compounds inside the Inner Harbor was also evaluated.

The hydrodynamic conditions are the same for all the runs. Therefore, it is only necessary to analyze one case. Once the open boundary condition has reached its maximum (dictated by the ramp function), the elevation follows a cycle with constant period and amplitude. This behavior of the boundary, coupled with the fact that there are no wind stresses and that the length of the harbor is small compared to the length of the tidal wave, allows the system to reach hydrodynamic steady state in a very short time.

Figures 8.2a to 8.2e show the horizontal flow distribution in the surface layer of the Inner Harbor for five consecutive tidal situations of one entire tidal cycle. These situations correspond to high tide, mean water level descending, low tide, mean water level ascending, and the next high tide. Figures 8.3a to 8.3e show the same than the previous figures but in the bottom layer. Analyzing the figures it can be seen that the ones corresponding to high tide are practically equal, which is consistent with the conclusion derived in the previous paragraph. It can also be seen that there is a strong influence on the surface layer flow by the river discharges, and therefore a less important flow reversing effect due to the tides.

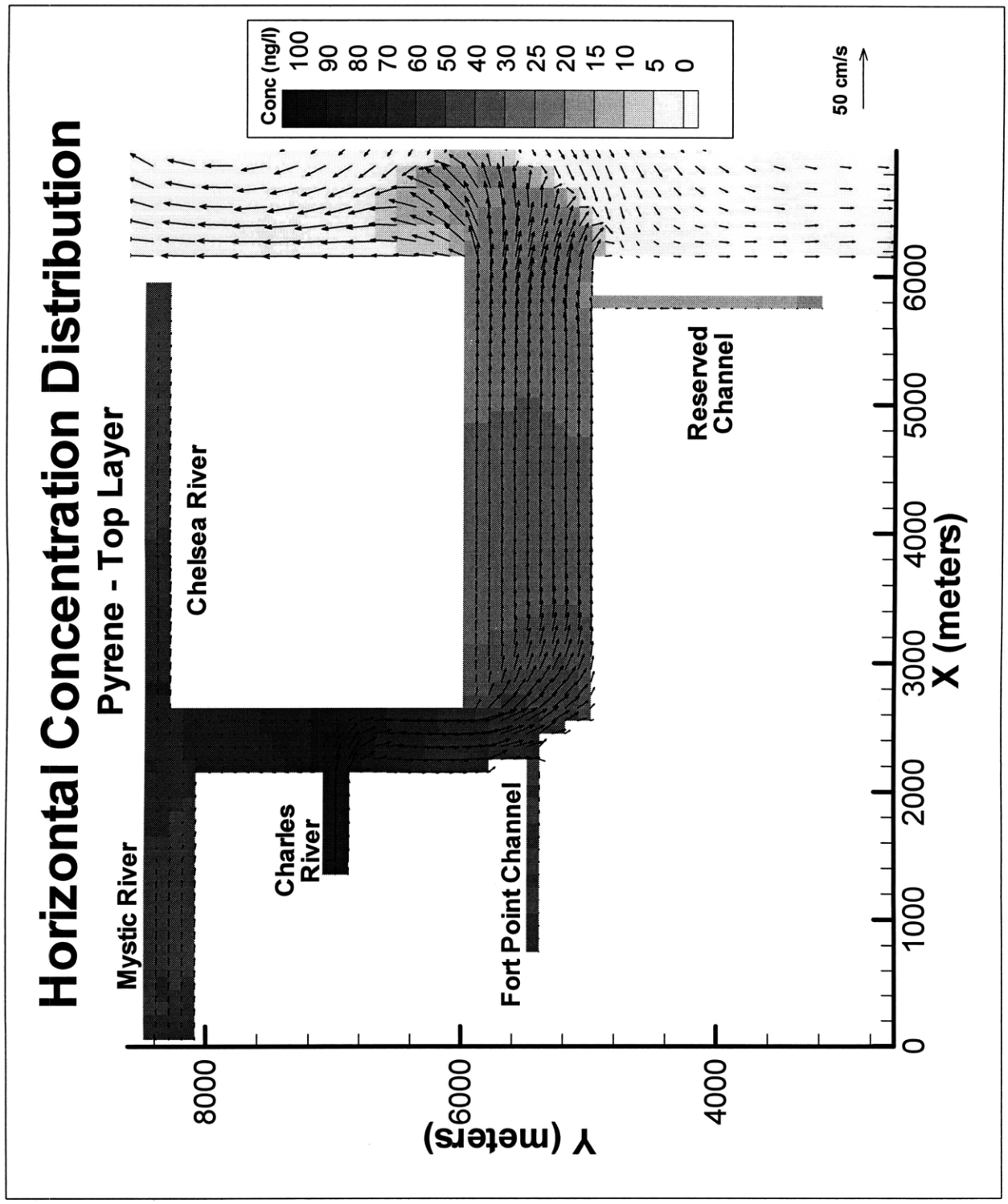

Figure 8.2a – Flow and Concentration Distribution for Pyrene at the Surface High Tide

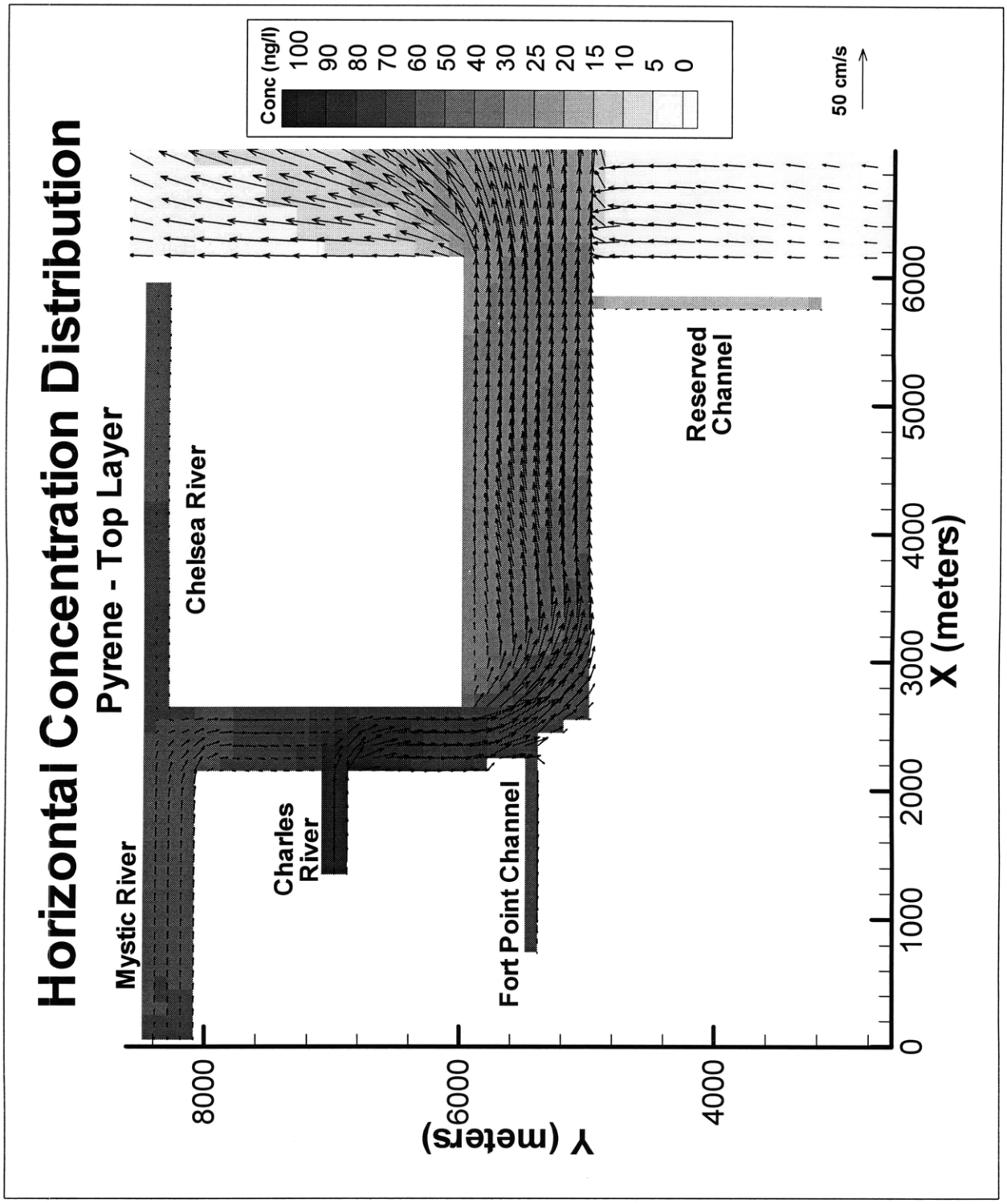

Figure 8.2b – Flow and Concentration Distribution for Pyrene at the Surface Mean Water Level Descending

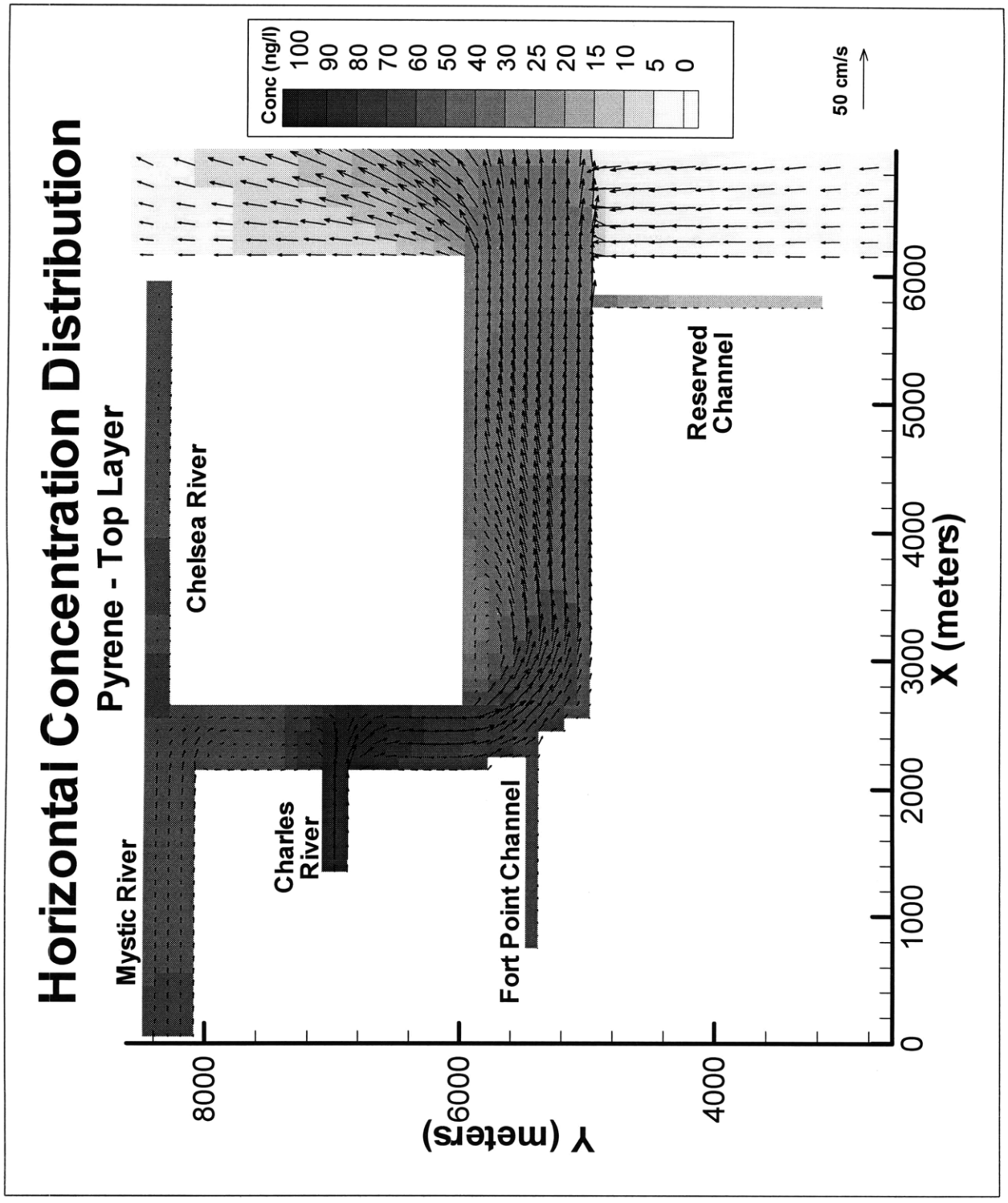

Figure 8.2c – Flow and Concentration Distrbution for Pyrene at the Surface. Low Tide

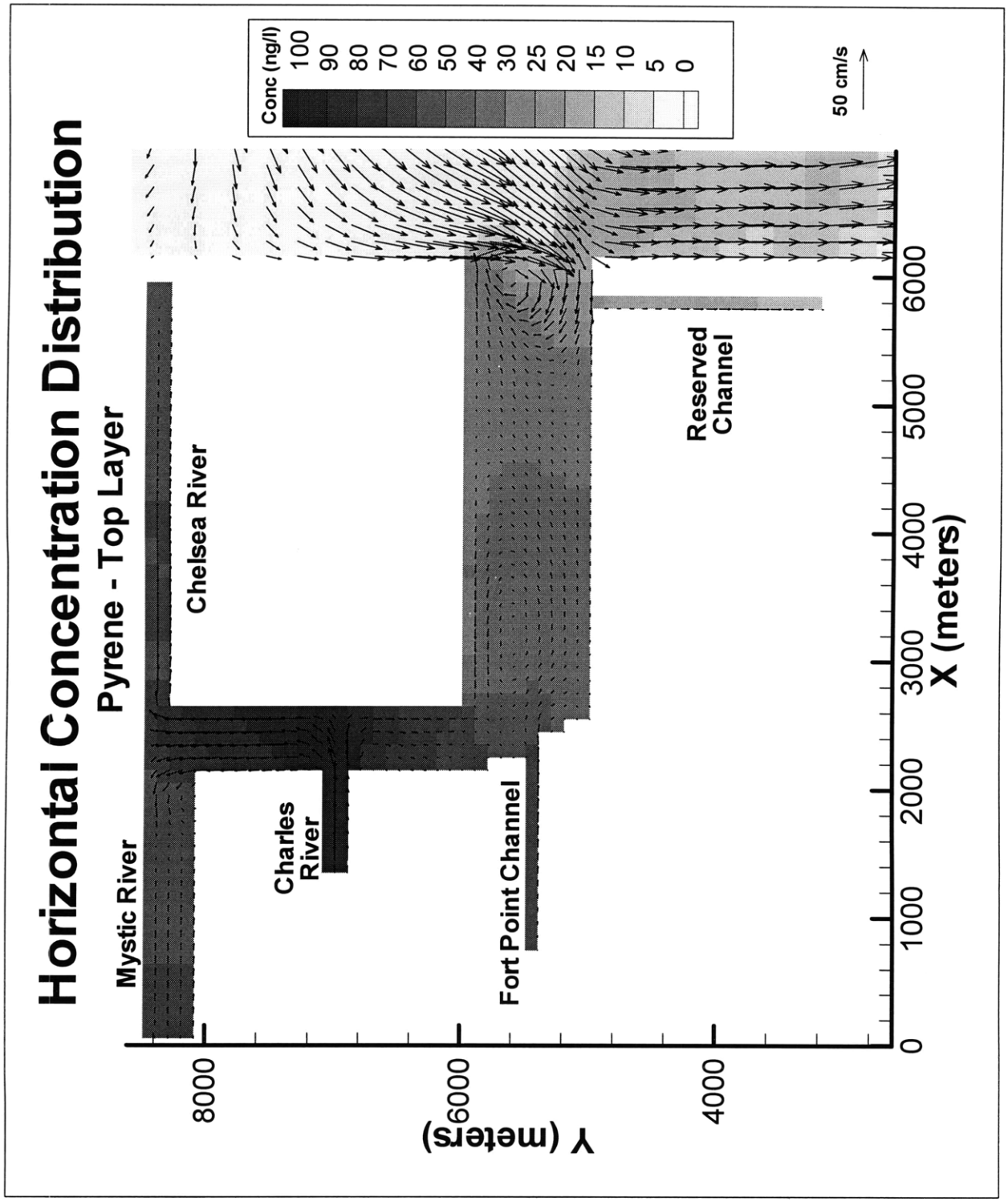

Figure 8.2d – Flow and Concentration Distrbution for Pyrene at the Surface. Mean Water Level Ascending

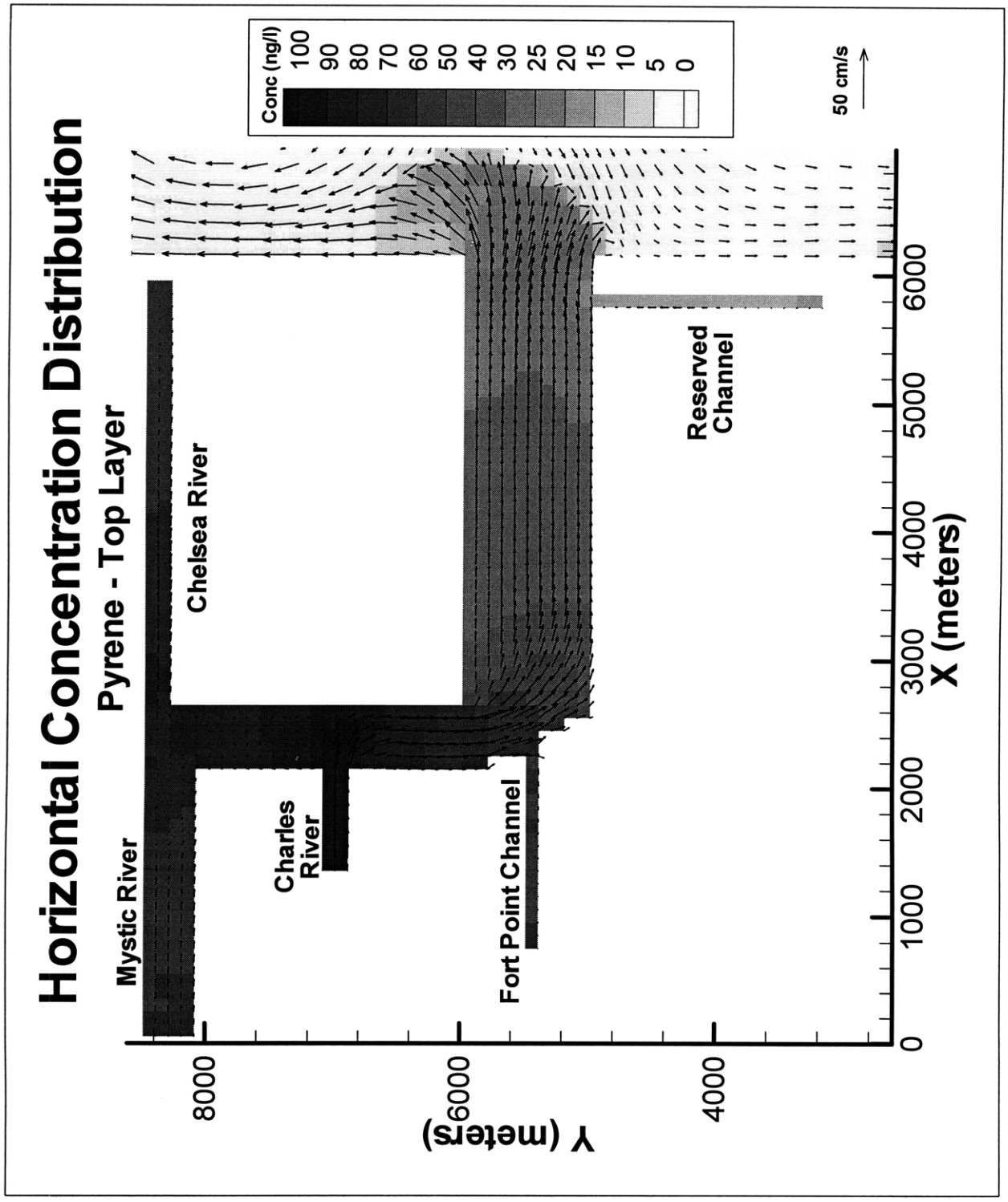

Figure 8.2e – Flow and Concentration Distrbution for Pyrene at the Surface. Next High Tide

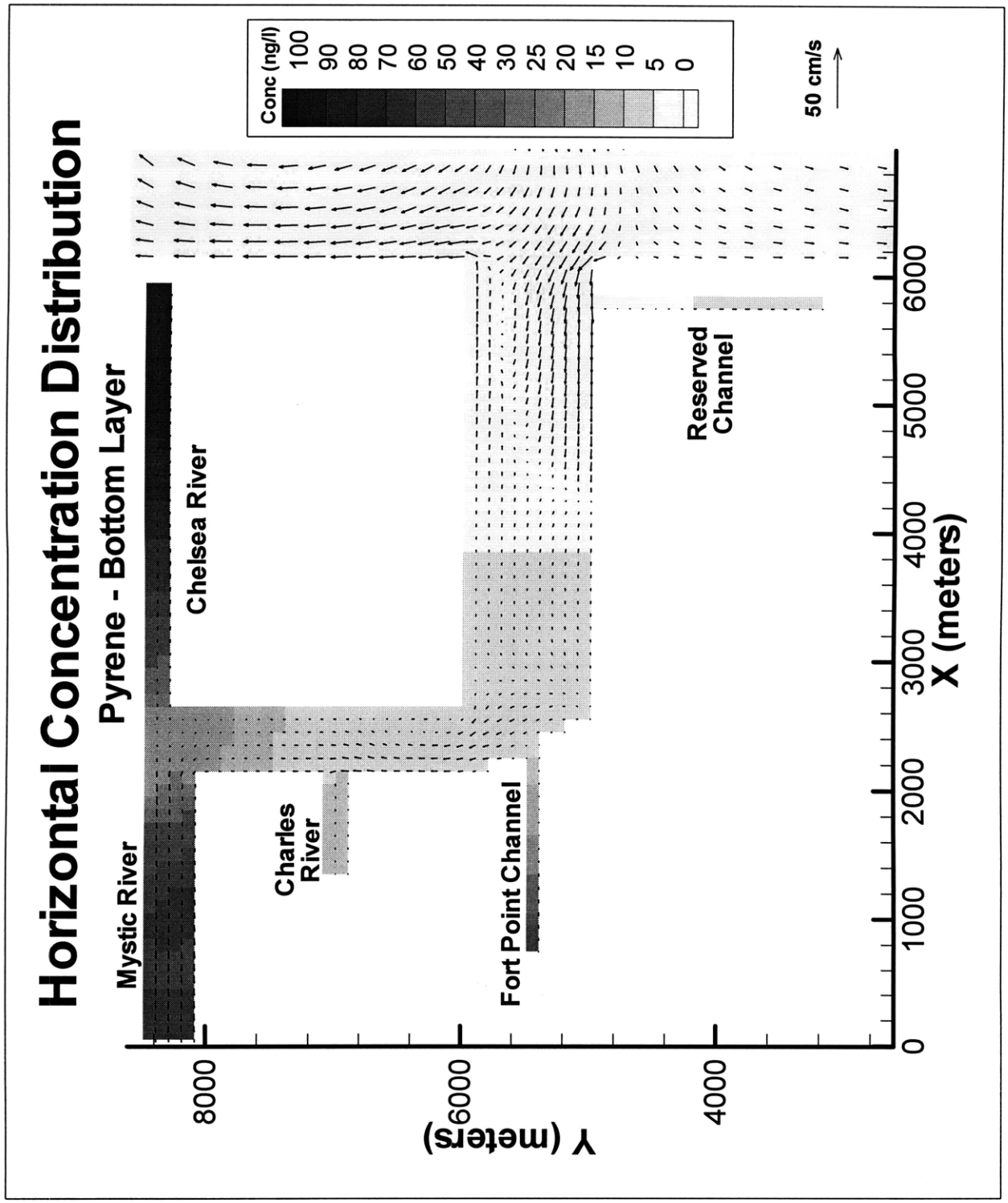

Figure 8.3a – Flow and Concentration Distrbution for Pyrene at about 1.5 m from the Bottom - High Tide

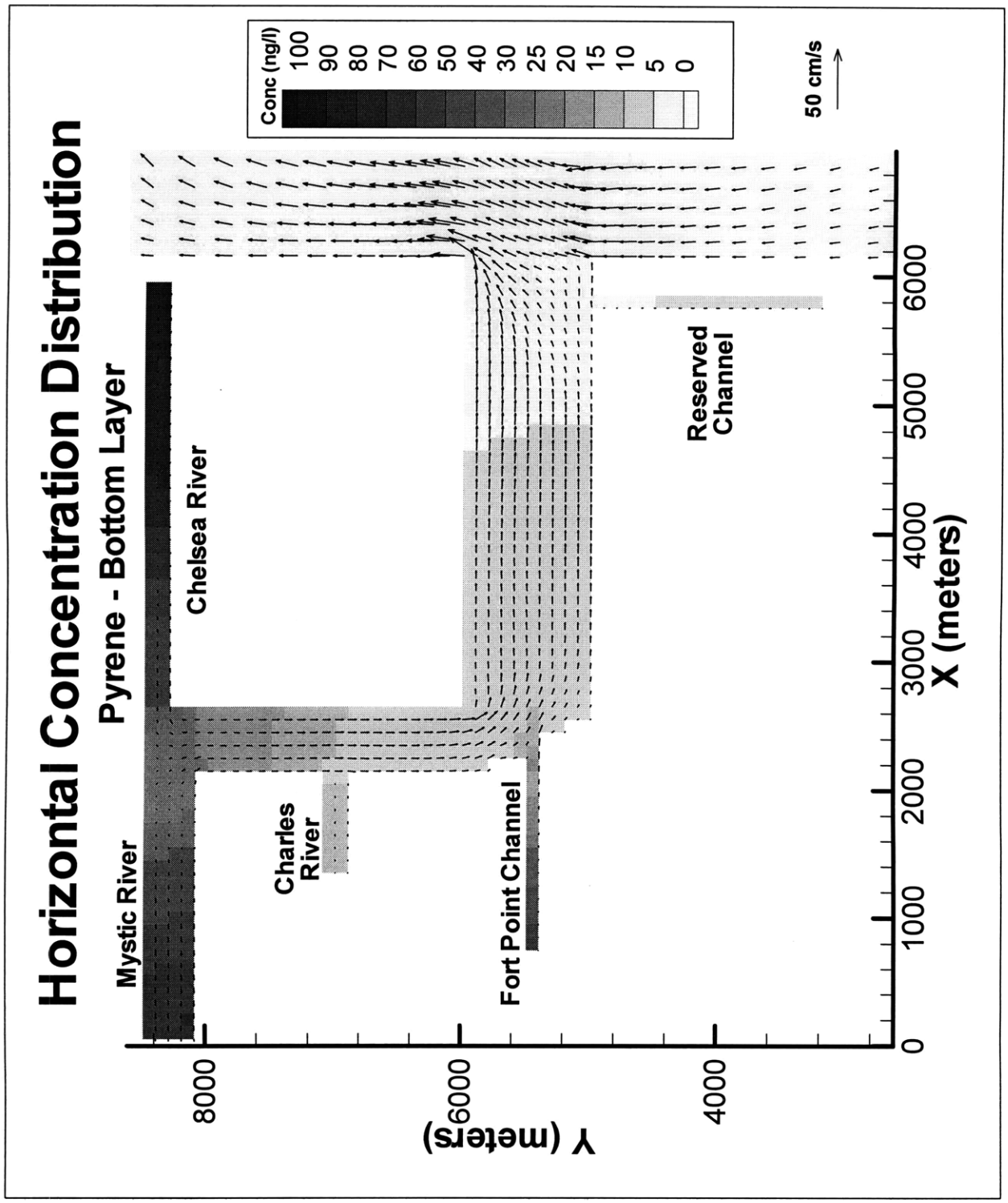

Figure 8.3b – Flow and Concentration Distrbution for Pyrene at about 1.5 m from the Bottom – Mean Water Level Descending

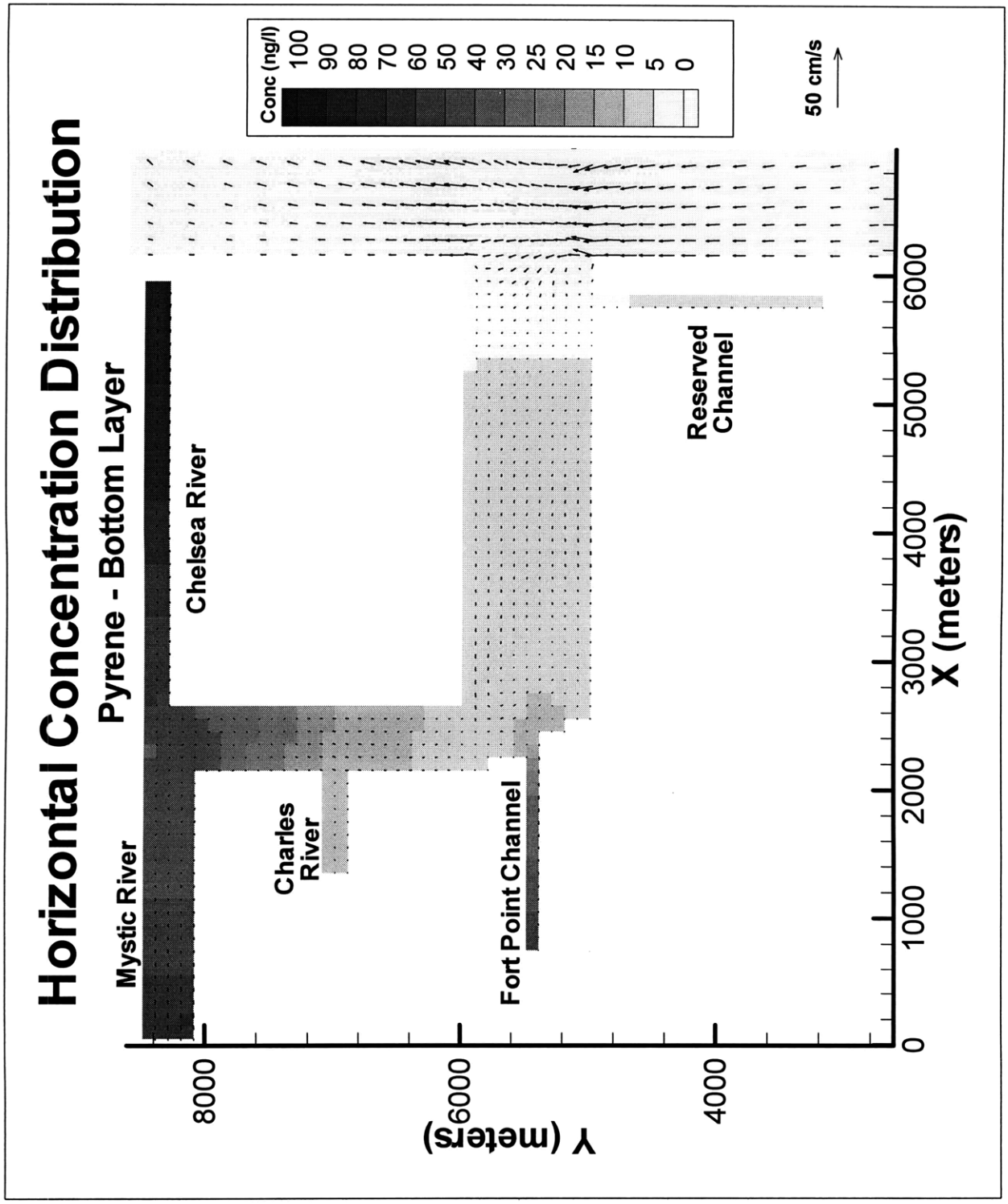

Figure 8.3c – Flow and Concentration Distrbution for Pyrene at about 1.5 m from the Bottom - Low Tide

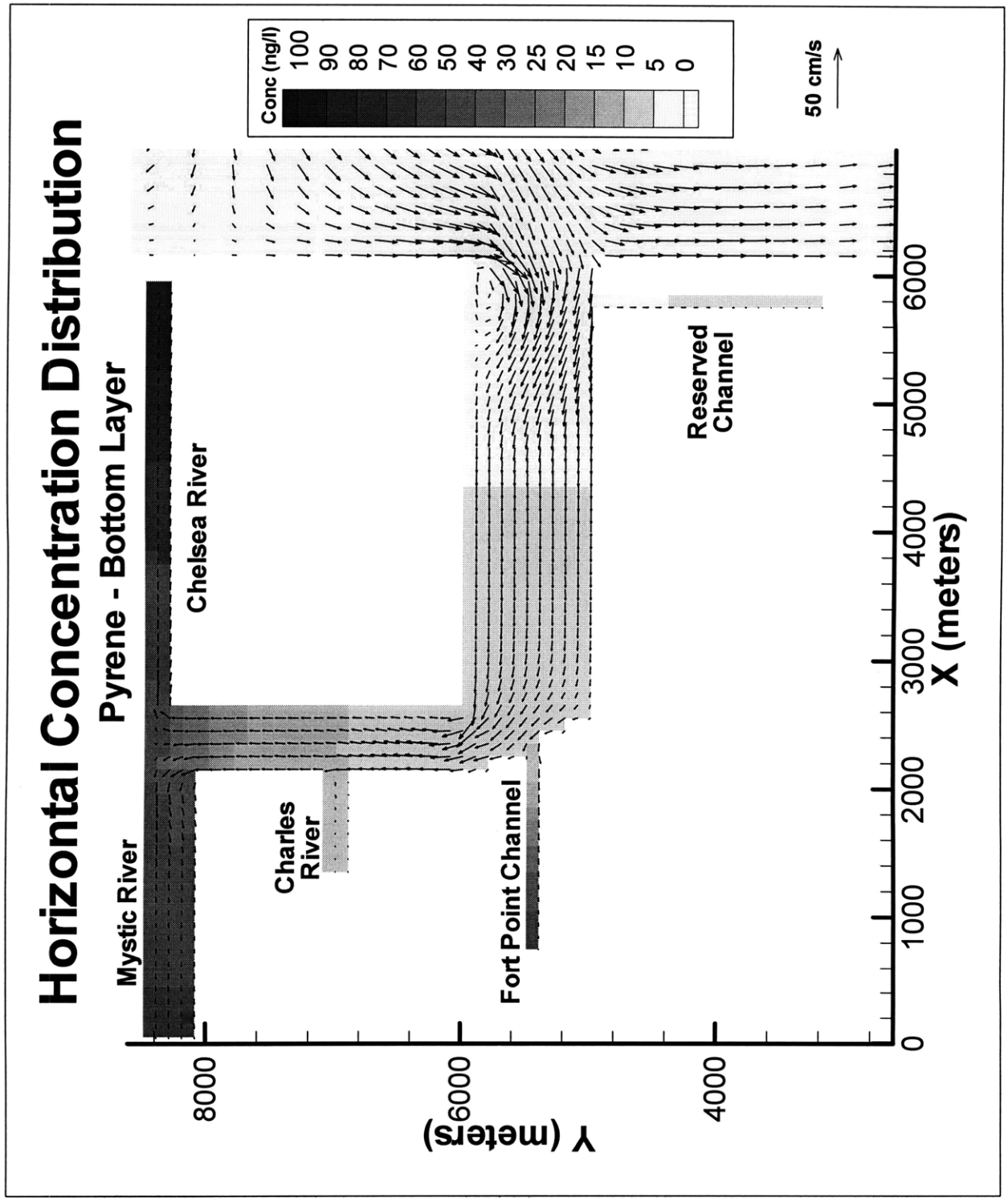

Figure 8.3d – Flow and Concentration Distrbution for Pyrene at about 1.5 m from the Bottom – Mean Water Level Ascending

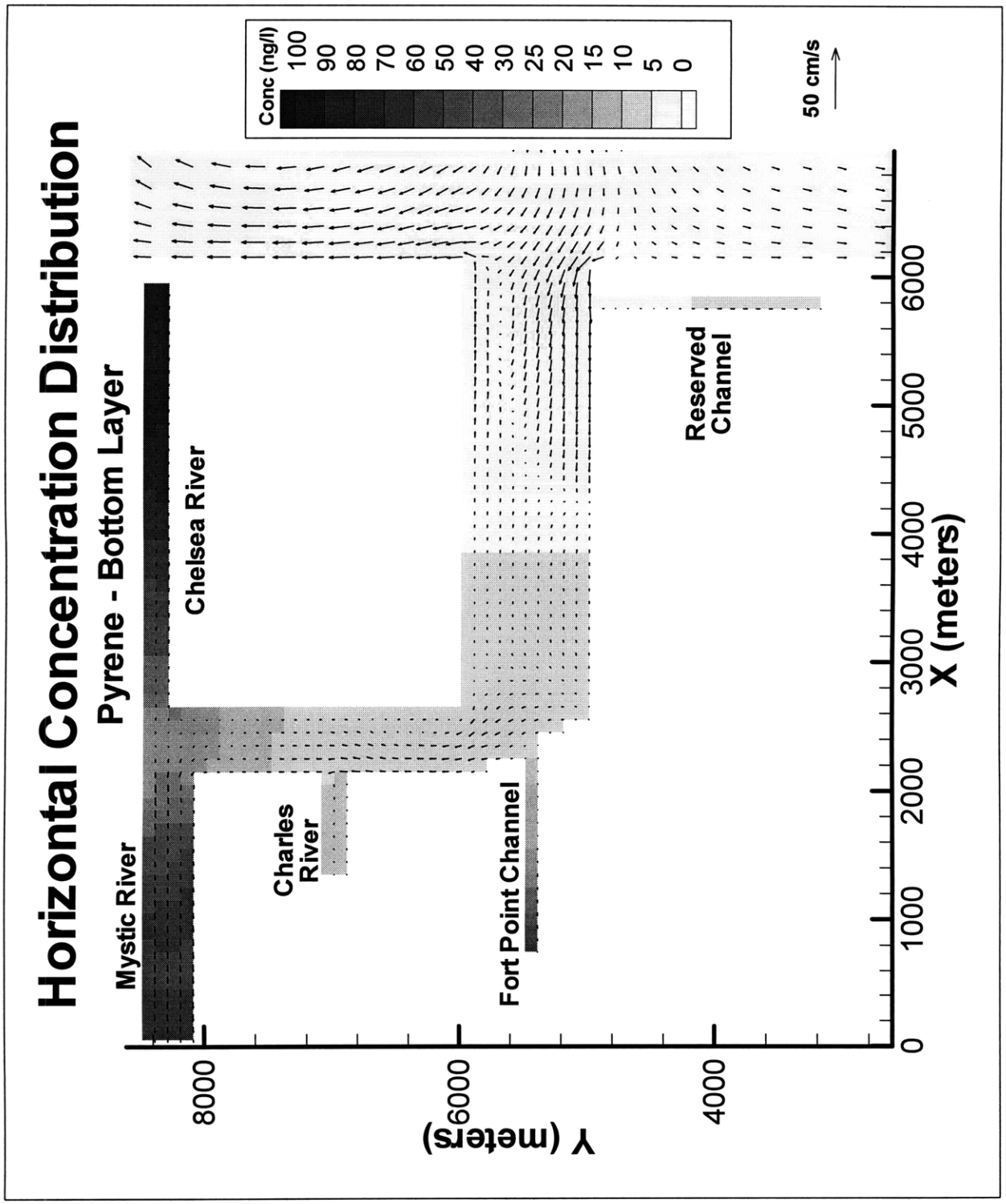

Figure 8.3e – Flow and Concentration Distrbution for Pyrene at about 1.5 m from the Bottom – Next High Tide

The steady state situation for the tracer takes much longer. In the case of the hydrodynamics the time to reach steady state depends on the model configuration and size. On the other hand, the time to reach steady state for the tracer depends on the residence time.

As explained in Section 8.2.3, each simulation was run for 7 days, and then the results were analyzed to find if steady state concentrations were reached. Figure 8.4 shows the time series of surface and bottom concentrations of benzo[a]pyrene obtained with the model for the base case at a point located at the confluence of the Mystic and Chelsea Rivers. The concentrations in the bottom increase during the first 2 days and oscillate around a mean value after that. The top concentration, on the other hand, takes more time to stabilize, but it can be considered stable by the end of the simulation.

Given these results, it can be considered that steady state was reached for benzo[a]pyrene. Although, the situation changes among compounds and situations, a practical steady state situation is reached in each run. This point will be demonstrated in the following sections where each compound and run is analyzed separately.

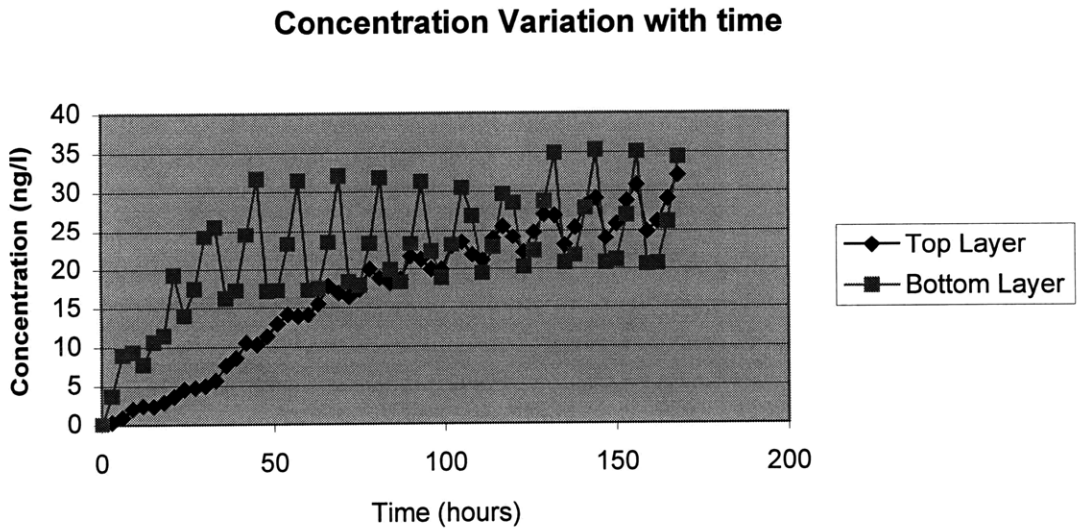

Figure 8.4 – Concentration variation with time in the Inner Confluence

The distribution along the Inner Harbor depends on the relative importance of the sources and sinks for each compound. This relative importance is very similar for benzo[a]pyrene and pyrene as shown in Section 7.3. However, for naphthalene, the situation is completely different. For these reasons, the results for benzo[a]pyrene and pyrene are discussed in the same section, leaving naphthalene for the follwing section.

8.3.1 Benzo[a]Pyrene and Pyrene

As the distribution of these two compounds is very similar along the Inner Harbor, only the results for pyrene are shown in this section. The results for benzo[a]pyrene are included in Appendix D. First, the results for the base case are shown and analyzed. The base case is then analyzed to obtain the total steady state mass of pyrene inside the Inner Harbor. This analysis has the objective of giving feedback to the box model as to the actual residence time of the total system. Finally the post dredge results are shown.

8.3.1.1 Base Case Results

Figures 8.2a to 8.2e show the horizontal concentration distribution of pyrene in the top layer for five different tidal conditions. The figures represent high tide, mean water level descending, low tide, mean water level ascending and the next high tide of the last tidal cycle of the base case simulation. It can be seen that the distribution of the two high tides is practically the same implying that a steady state was reached.

Figures 8.3a to 8.3e show the same situation but for the bottom layer. Comparing these figures with the previous ones it can be seen that the concentrations in the bottom are in general lower than on the surface. Another important aspect is that the Charles River has a significant impact on the top layers of the harbor showing the highest concentrations of the entire harbor.

The differences between the results in the top and bottom layer suggest a non-uniform vertical distribution. To illustrate further this situation, vertical profiles were extracted from four different locations: the Inner Confluence, Charles River mouth, Fort Point Channel mouth and Buoy 12 near the Inner Harbor mouth (See Figure 8.5.) The first and the last of these locations coincide with the places where water quality measurements were made. (See Chapter 5.)

Figures 8.6a to 8.6d show the actual vertical profiles for each location. The vertical axis shows the ten vertical layers of the model. Each layer represents a depth of one tenth of the total depth in that location at that time (i.e. about 1 meter.) In each location five profiles are depicted, corresponding to different tidal conditions. These conditions are high tide, mean water level descending, low tide, mean water level ascending, and the next high tide. It is important to note that, as the depth for each situation changes, each layer's height also changes. The figures, however, represent the profile normalized to the depth.

Analyzing the profiles for each location, it can be seen that both profiles representing high tide conditions are very similar. This is implying again that the model has reached the mass balance steady state situation. In addition, as we move downstream in the locations the profiles get even more similar.

Another aspect to observe is that for every location the profile with higher concentration corresponds to the low tide situation and, conversely, the profile with lower concentrations corresponds to the high tide situation. These variations are expected because at high tide there is more water to dilute the pollutant and vice-versa.

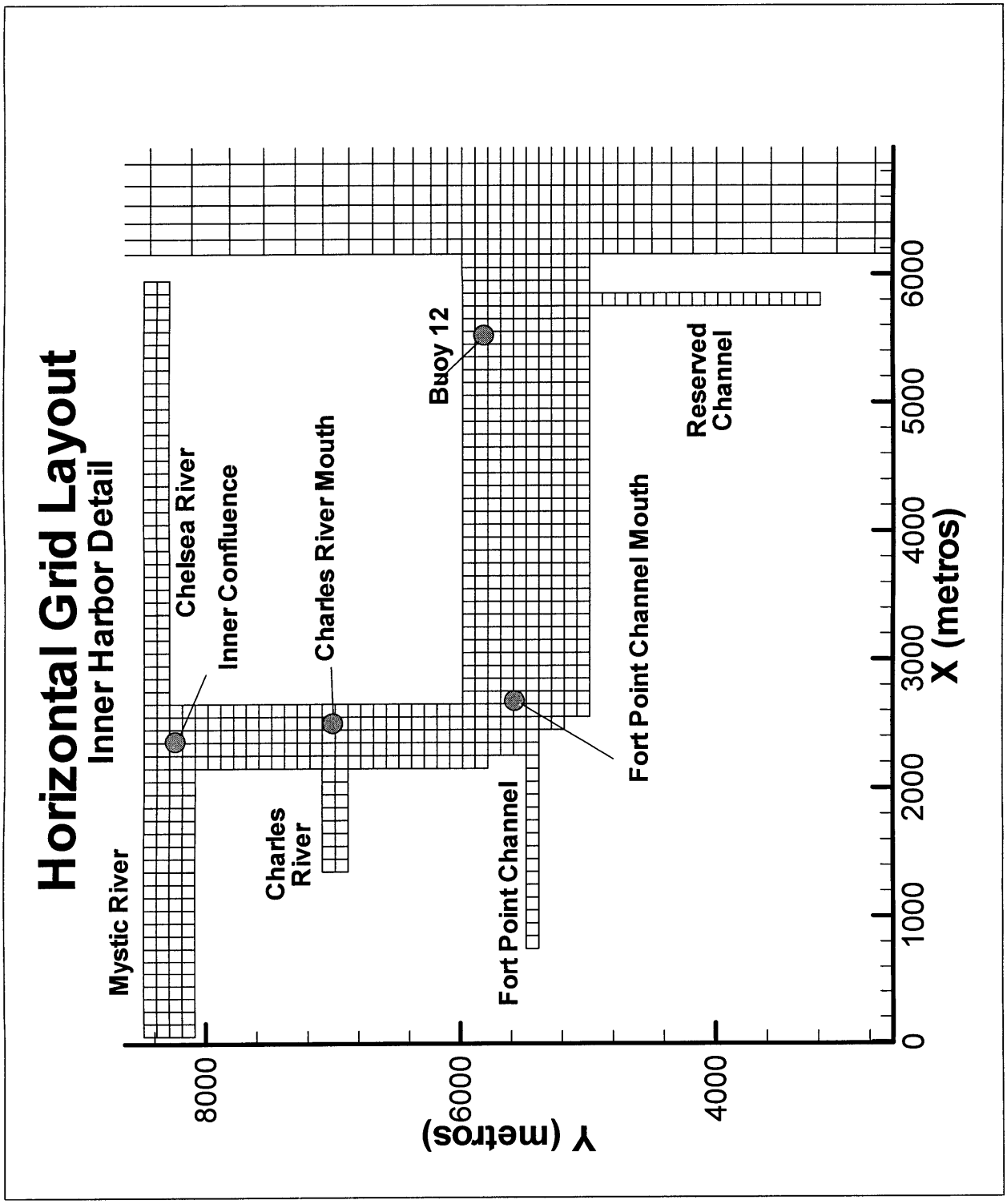

Figure 8.5 – Location of the Vertical Profiles for Pyrene on the Model Grid

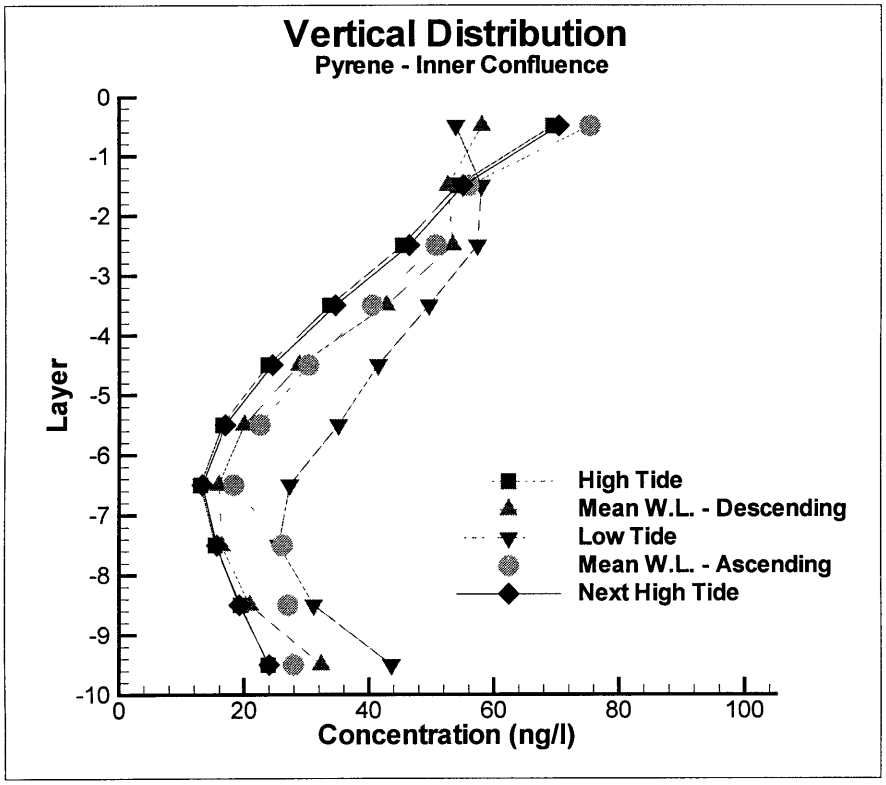

Figure 8.6a

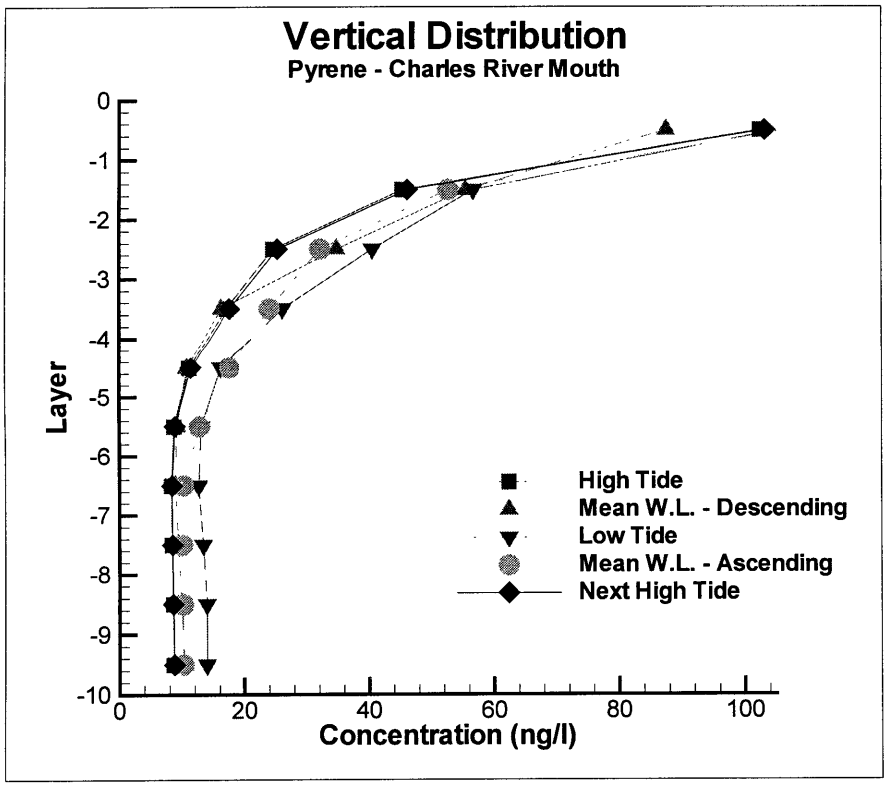

Figure 8.6b

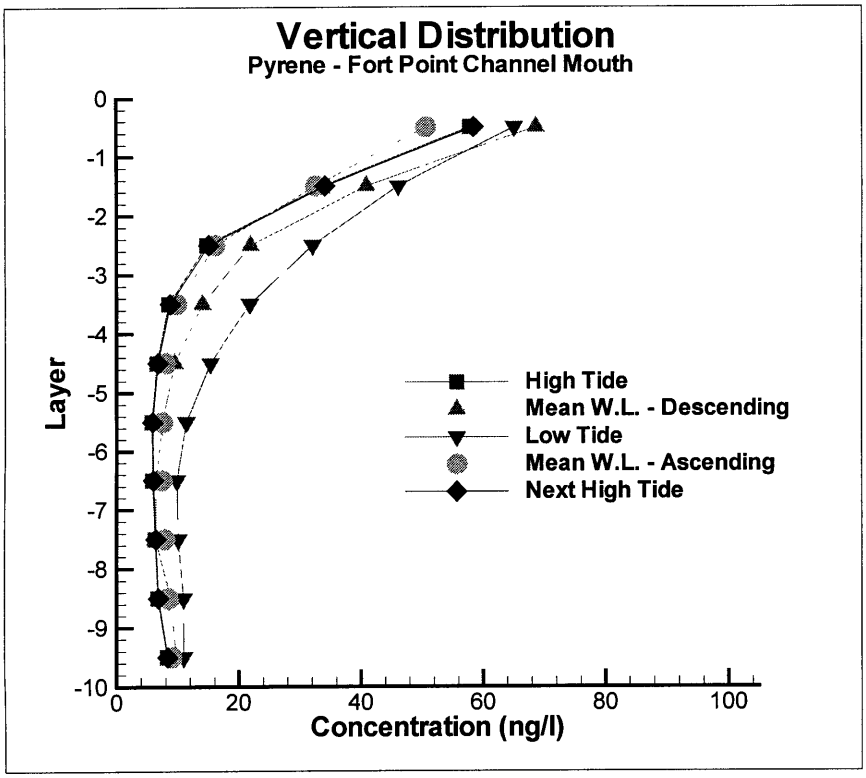

Figure 8.6c

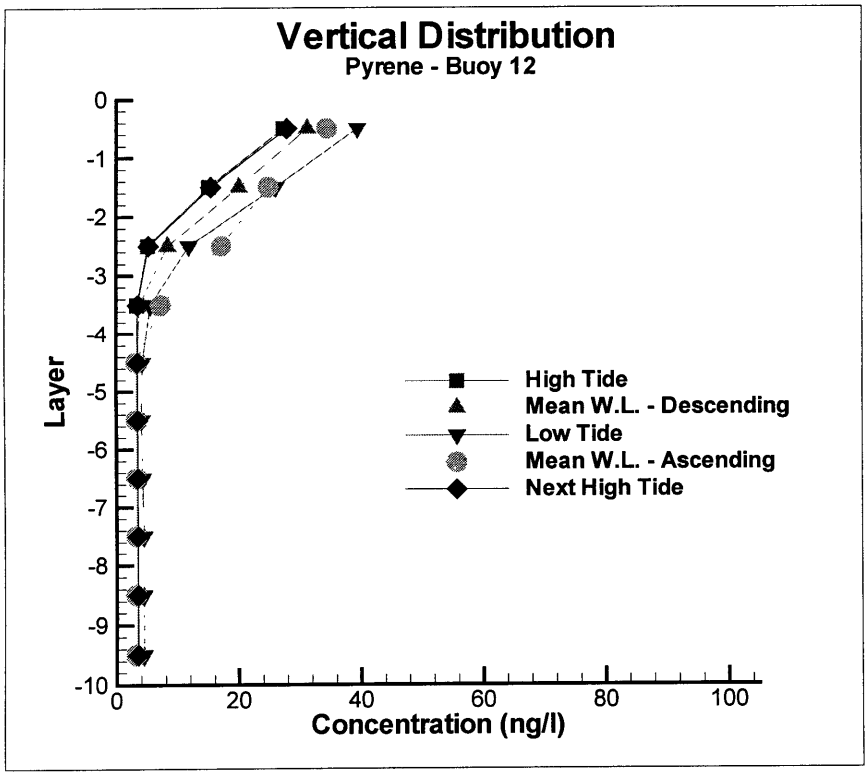

Figure 8.6d

The profiles located in the Inner Confluence show a relatively uniform concentration with a somewhat larger concentration near the surface than near the bottom. This seems a priori to be a contradiction because the bottom is a larger source than all the combined sewers and rivers that discharge on top of the Mystic and Chelsea Rivers. To explain this behavior it is important to remember that all the inputs of the rivers and CSO are freshwater, which is less dense than seawater and, therefore, tends to remain in the surface. This tendency depends on the vertical mixing generated by the tidal motion and the freshwater flow.

The profile in the mouth of the Charles River shows the significant impact that this river has on the quality of the water near the surface. The concentrations in this profile are much larger near the surface than near the bottom. This, again, is the effect of the discharge being less dense than the ambient water. In addition, the low concentrations shown in the bottom reflect the fact that the sediments are less contaminated in this area.

Moving further downstream this situation gets accentuated. That is to say that the concentrations in the bottom are even lower and the majority of the contaminant flux through a horizontal cross section takes place in the surface layers.

8.3.1.2 Mass Integration

The 3D model gives as a result the concentration of pyrene in each of the nodes of the Inner Harbor for the base case conditions. These concentrations were integrated over the total volume of the Inner Harbor to obtain the total steady state mass of pyrene inside the study area. As the concentrations vary along the tidal cycle the integration was performed for each of the four tidal situations shown in the previous section. The mass obtained can be divided by the total volume of the harbor to obtain a tidal average concentration over the entire domain. The mass values obtained for each situation and the corresponding average concentration are presented in Table 8.1.

Table 8.1
Mass integration for pyrene

Situation	Total Mass (μg)	Volume (m^3)	Av. Concentration (ng/l)
High Tide	$1.85x10^9$	$9.73x10^7$	19.0
M.w.l. descending	$1.75x10^9$	$8.46x10^7$	20.7
Low Tide	$1.7x10^9$	$7.19x10^7$	23.6
M.w.l ascending	$1.84x10^9$	$8.46x10^7$	21.7

Averaging the result for each situation, the steady state average concentration is obtained, resulting in 21.3 ng/l. This value can now be used with the box model to back-calculate the corresponding residence time that results in this average concentration value. The residence time calculated using this methodology is about 2.7 days.

8.3.1.3 Post Dredging Results

Figures 8.7a to 8.7d show a comparison between the pre and post-dredge simulations for high tide and for the same locations mentioned above. As explained in previous sections the post-dredge simulations assume that all the sediments located in the projected dredging area are perfectly removed and capped. Therefore, these new sediments act as a sink of PAHs rather than a source.

As expected all the profiles show lower concentrations for the post-dredging simulation. This reduction of the concentrations is proportionally most important for the Inner Confluence location. This is also expected because this location is inside the dredging area.

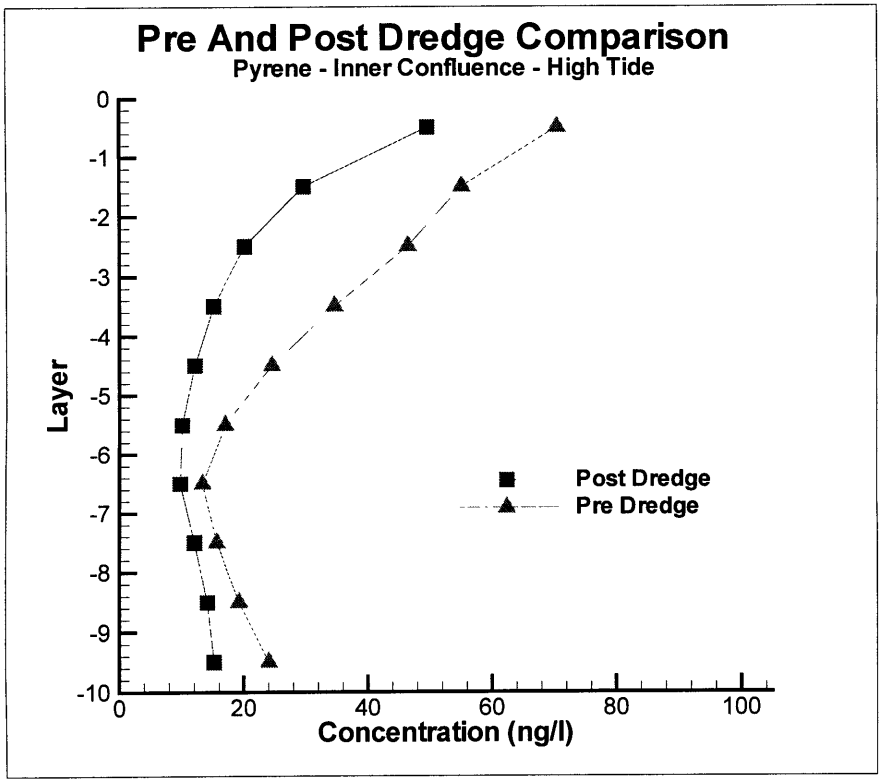

Figure 8.7a

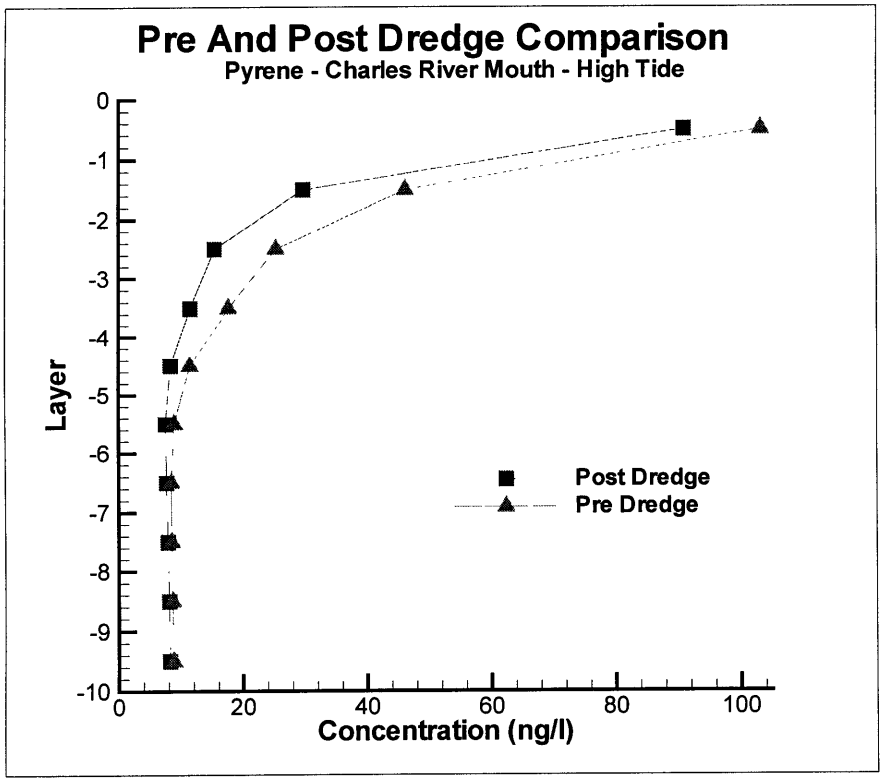

Figure 8.7b

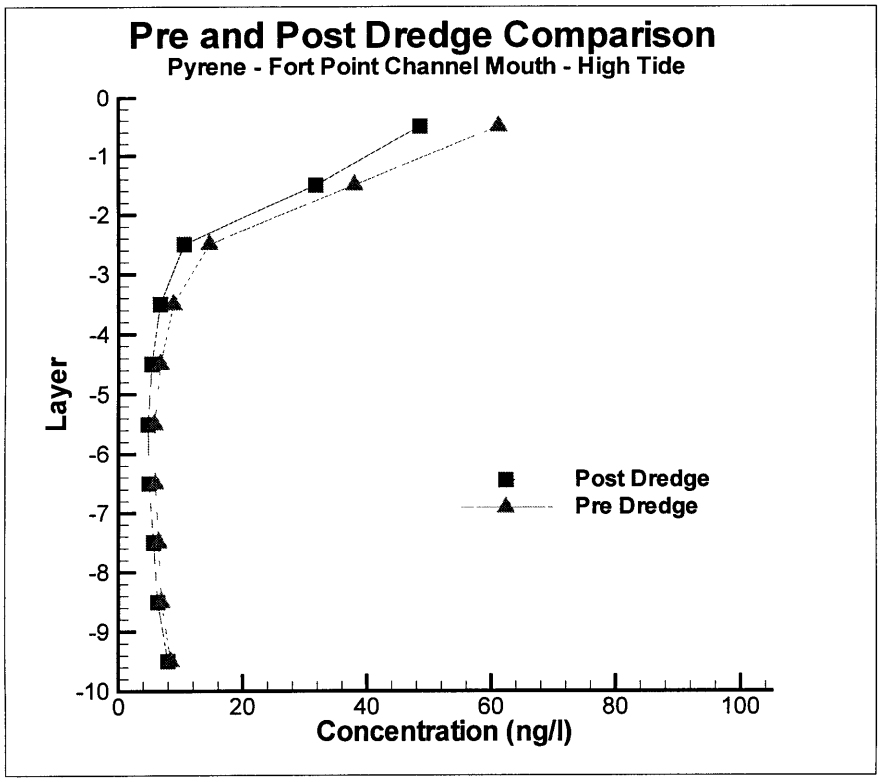

Figure 8.7c

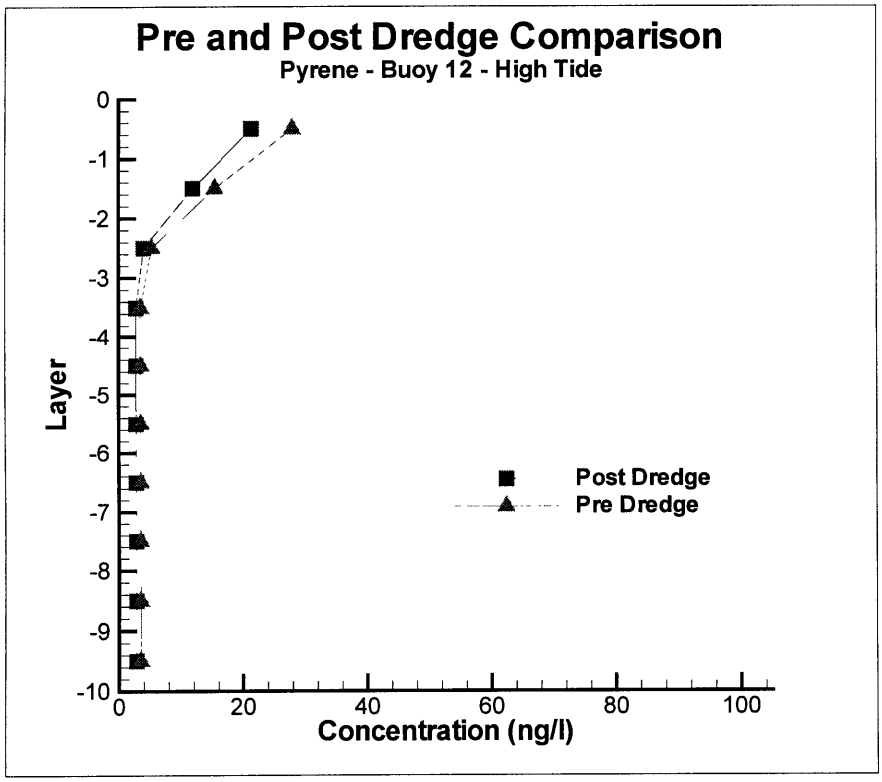

Figure 8.7d

8.3.2 Naphthalene

As in the previous section, the results for the simulation with naphthalene using the base case are presented first followed by the post-dredging results.

8.3.2.1 Base Case Results

The main source of naphthalene is the sediment-water exchange. In particular this process is more important in the Fort Point Channel and the Mystic and Chelsea Rivers confluence. The sediments in these areas have measured values that are much higher than the values encountered for any other portion of the Inner Harbor (Section 7.2.4).

Figures 8.8a to 8.8e show the horizontal distribution of naphthalene concentrations for the surface layer. As for the previous compounds, these plots represent five different tidal situations: high tide, mean water level descending, low tide, mean water level ascending and the next high tide. The distribution for both high tide situations are similar, thus implying that the simulation has reached a mass balance steady state.

The concentrations in this case are expressed in micrograms per liter as opposed to nanograms per liter used for the previous compounds. The horizontal distribution shows that the concentrations in the area of Mystic and Chelsea Rivers are quite uniform. The highest concentrations for the surface are located in Fort Point Channel. In addition, the Charles River seems to have a positive influence for naphthalene because it provides dilution.

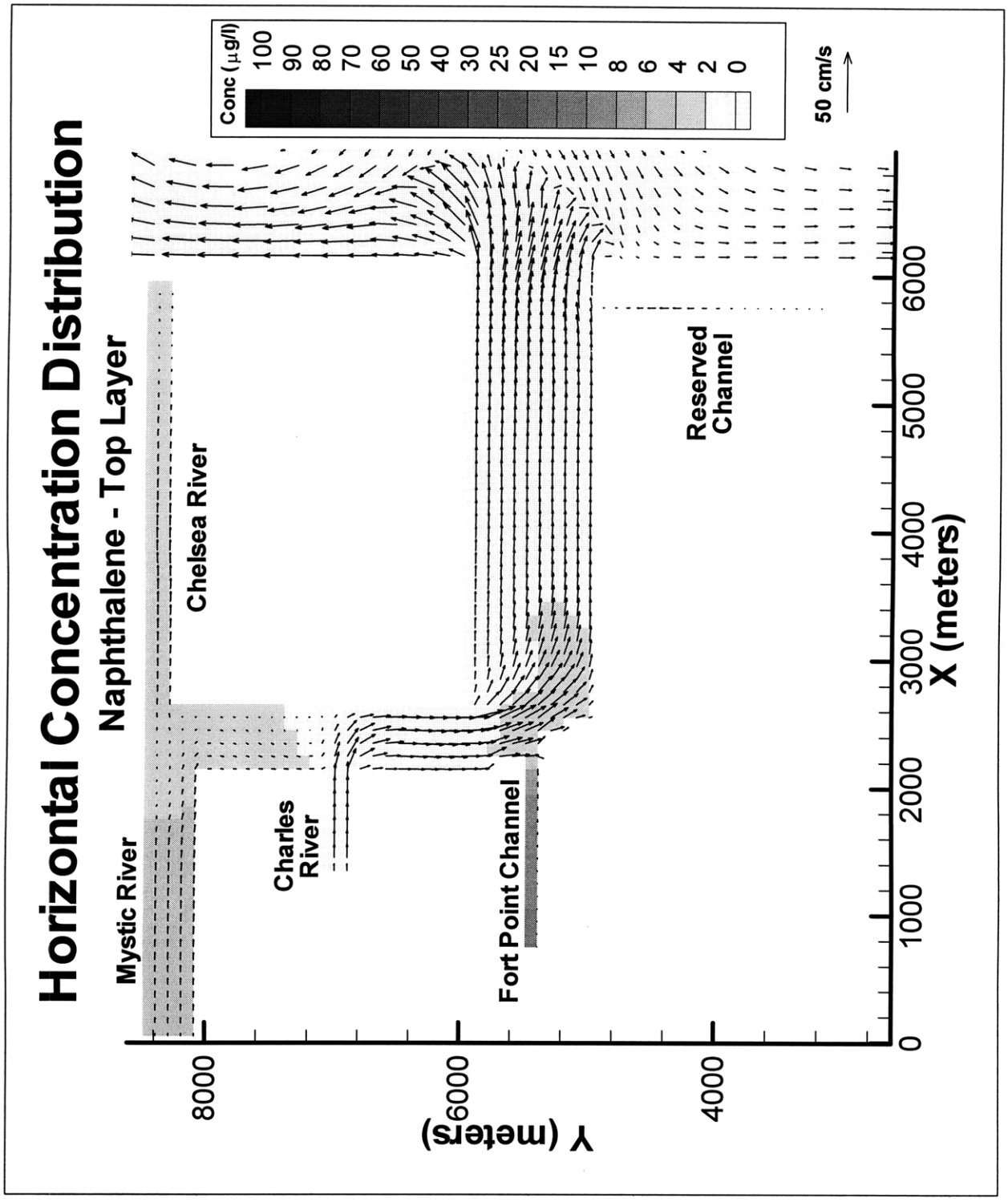

Figure 8.8a – Flow and Concentration Distribution for Naphthalene at the Surface High Tide

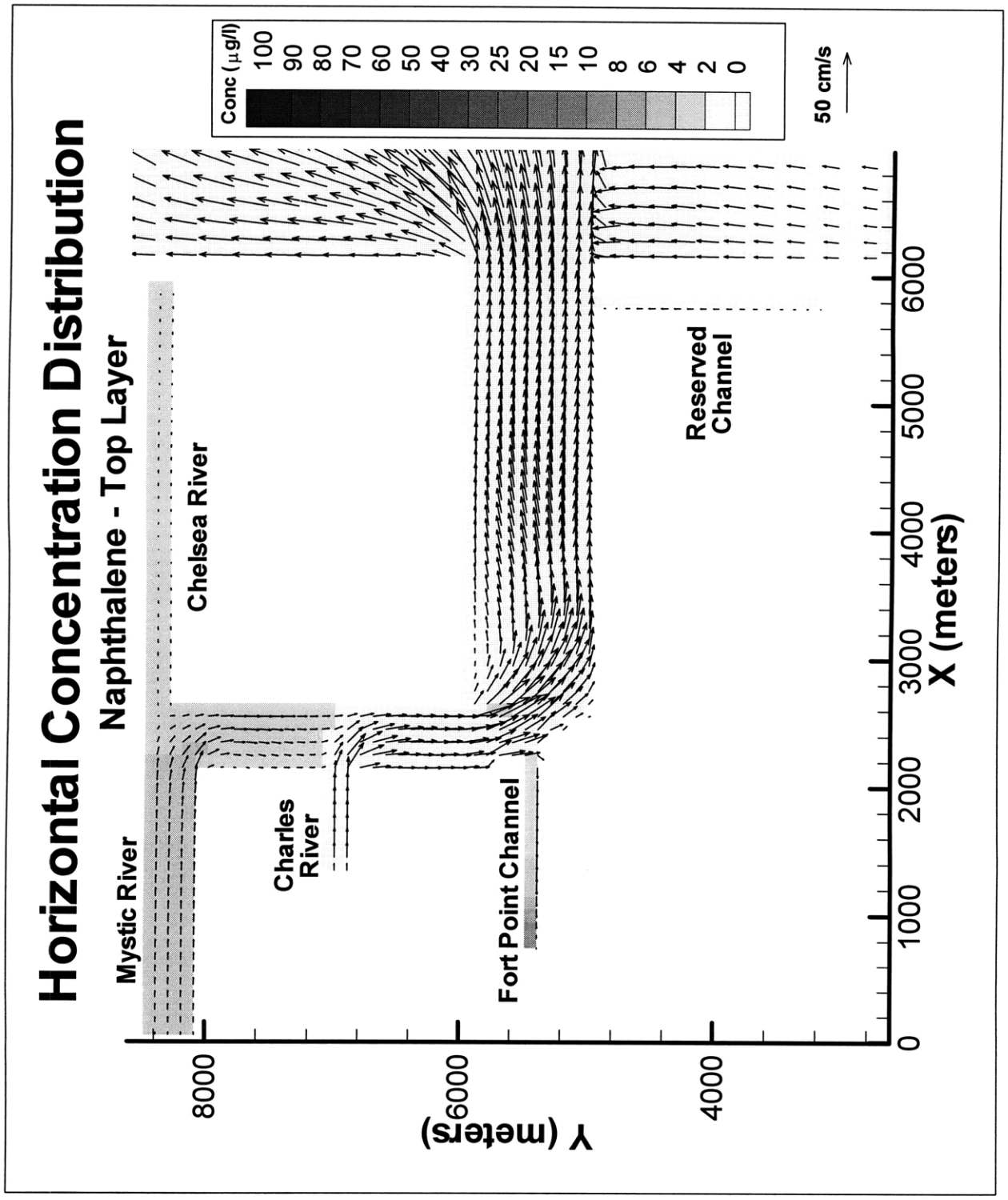

Figure 8.8b – Flow and Concentration Distribution for Naphthalene at the Surface Mean Water Level Descending

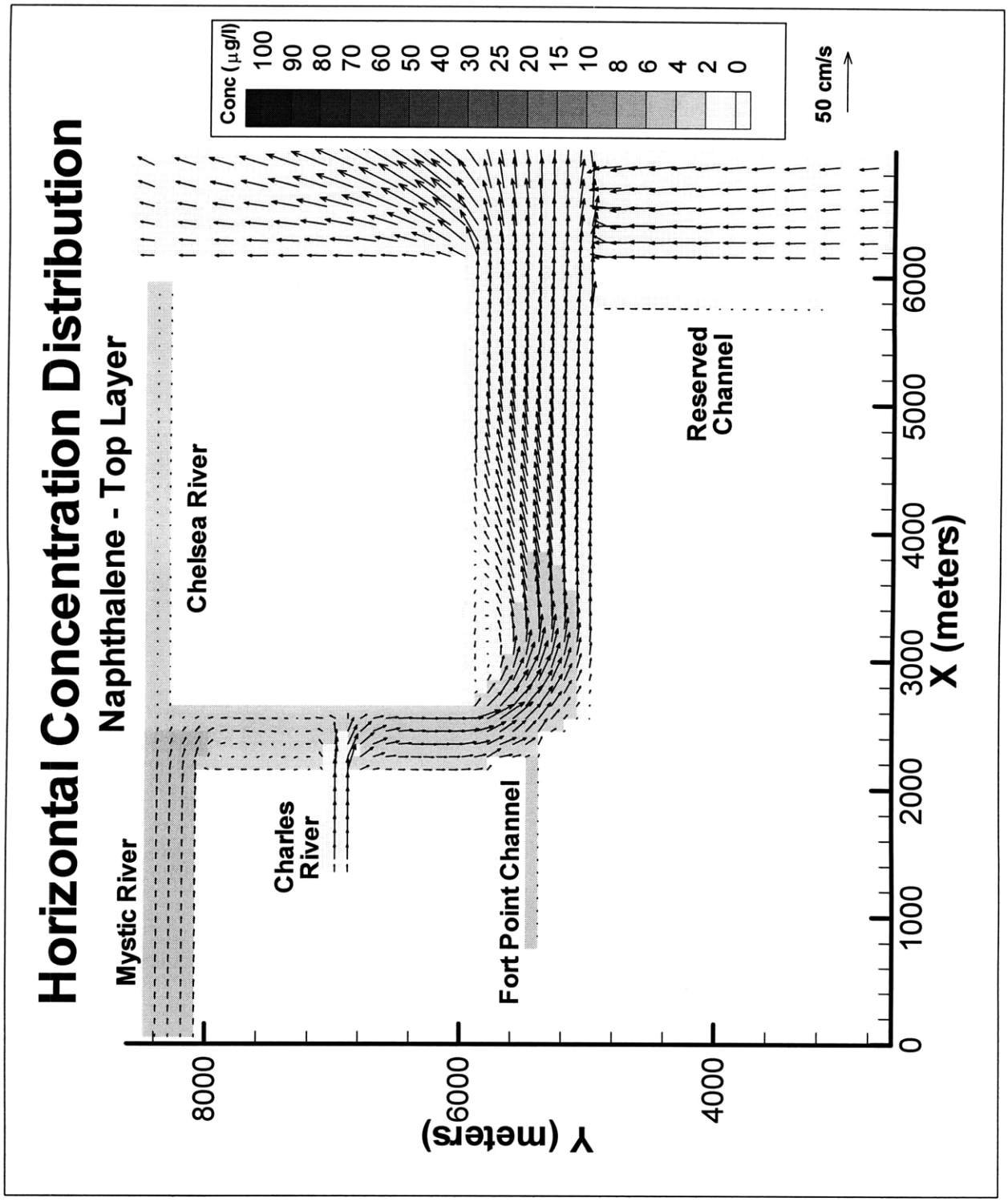

Figure 8.8c – Flow and Concentration Distribution for Naphthalene at the Surface Low Tide

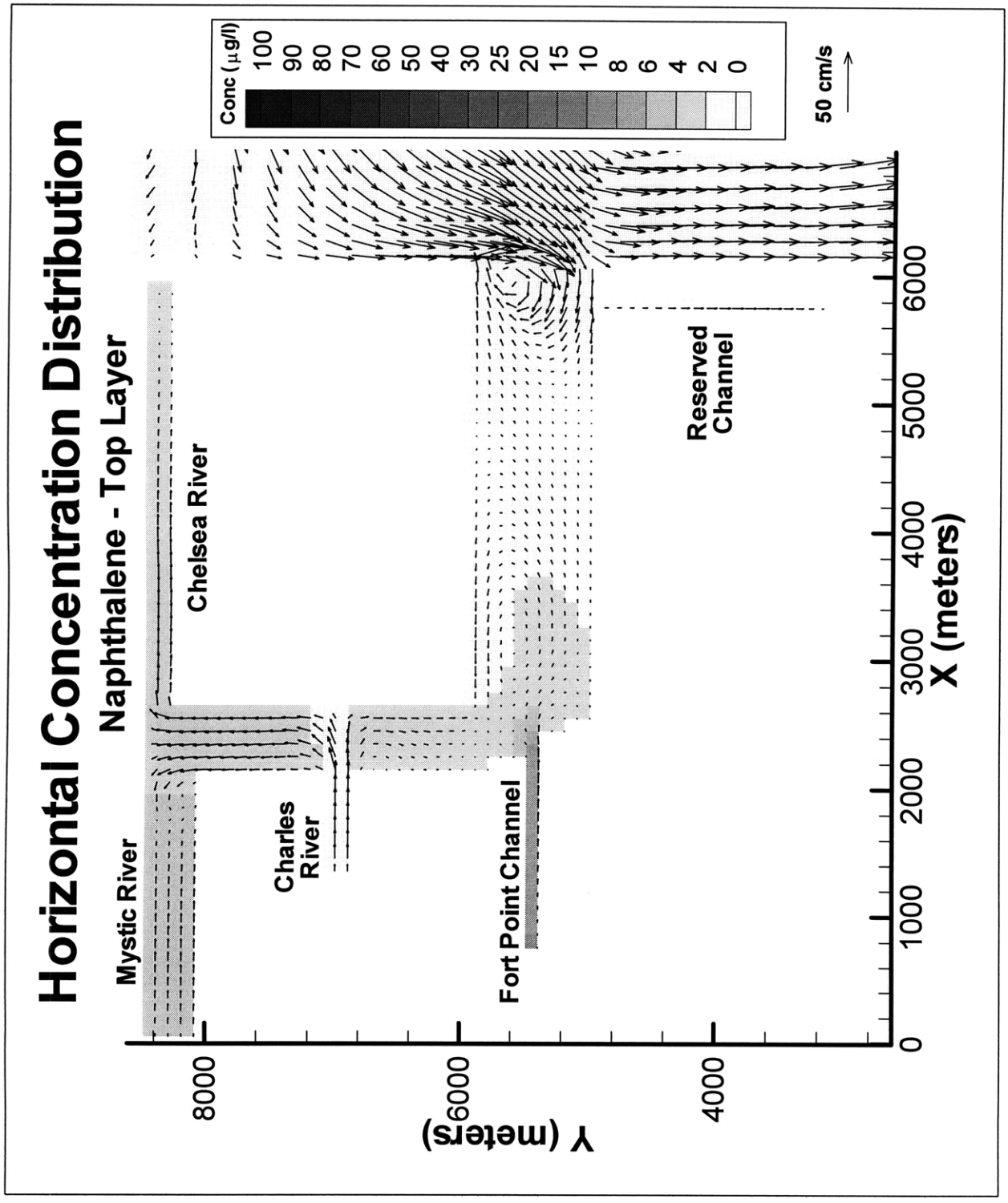

Figure 8.8d – Flow and Concentration Distribution for Naphthalene at the Surface Mean Water Level Ascending

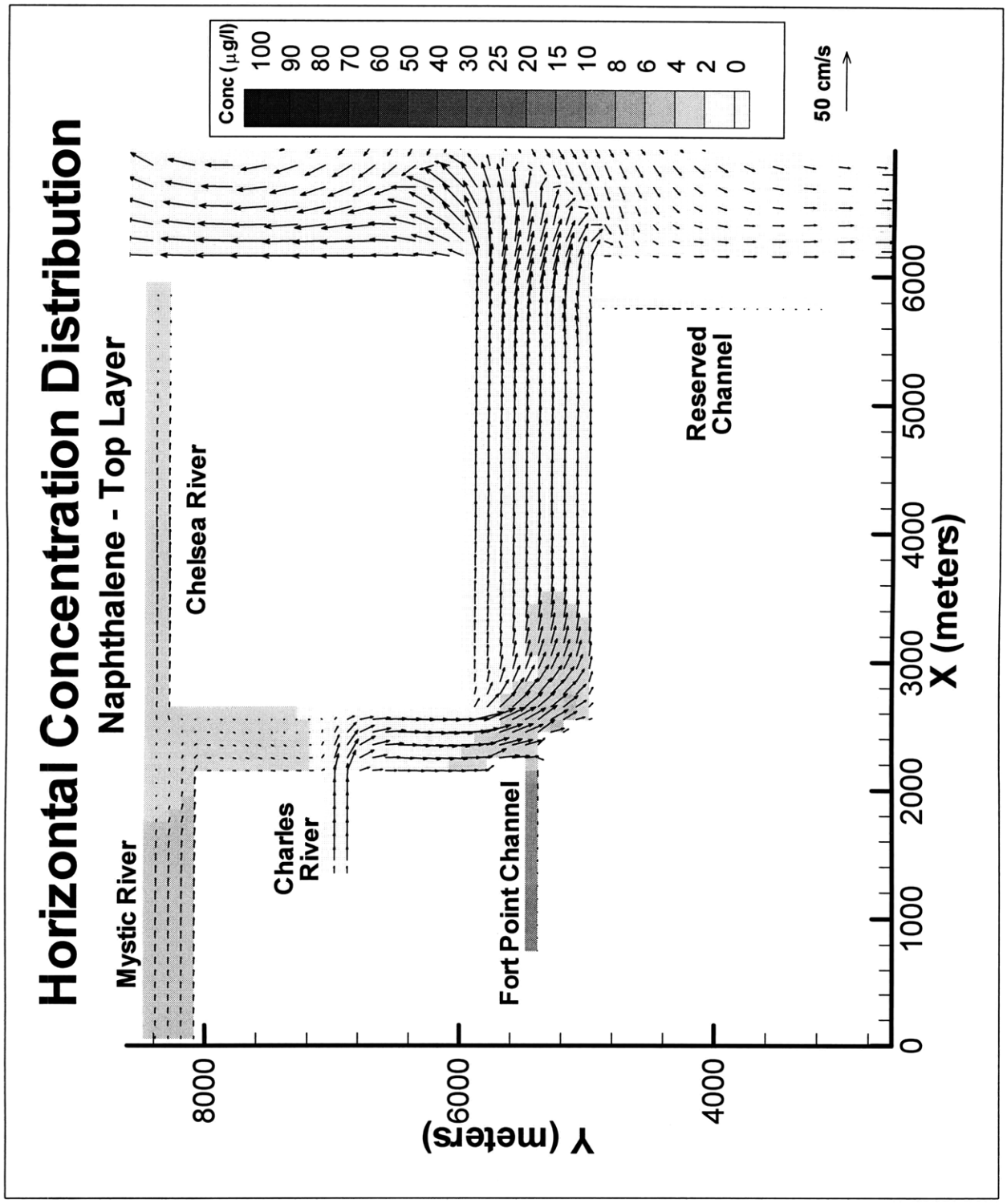

Figure 8.8e – Flow and Concentration Distribution for Naphthalene at the Surface Next High Tide

Figures 8.9a to 8.9e represent the horizontal distribution for the bottom layer. The higher concentrations are again located in the Fort Point Channel area. Moreover, the concentrations are much higher than on the surface layer. This is consistent with the high concentrations that the sediments have in this area. It can also be noted that the concentrations in the Inner Confluence are practically the same for the bottom layer as for the top layer. This, however, is not the case for the Mystic and Chelsea Rivers, where concentrations in the bottom are higher than in the surface layer.

Taking the previous analysis of the distribution into consideration, three locations were selected to extract vertical profiles. These locations are in the Mystic River, the Inner Confluence and the Fort Point Channel mouth, as shown in Figure 8.10. In addition, because the main source of naphthalene is the Fort Point Channel, a vertical cut along the longitudinal axis of the channel was extracted.

Figures 8.11a, 8.11b, and 8.11c show the vertical profiles at the Mystic River, Inner Confluence, and the Fort Point Channel Mouth, respectively, for the same five tidal situations represented before. The vertical distribution in the Mystic River shows higher concentrations at the bottom than at the surface. It can be seen that the vertical distribution in the Inner Confluence is uniform with almost no variation between the concentration in the top layer and the bottom layer. The vertical profiles at the Fort Point Channel mouth show that the concentrations are also rather uniform but still slightly higher near the bottom than at the surface layer.

Figures 8.12a – 8.12e show the concentration distribution in the vertical along the Fort Point Channel. According to these figures, the concentrations on the bottom of Fort Point Channel are much higher than on top, as previously demonstrated by the horizontal distributions. This plot also shows that as the flow moves downstream, the concentrations get more evenly distributed in the vertical. This is consistent with the vertical profile extracted at the mouth of the Fort Point Channel.

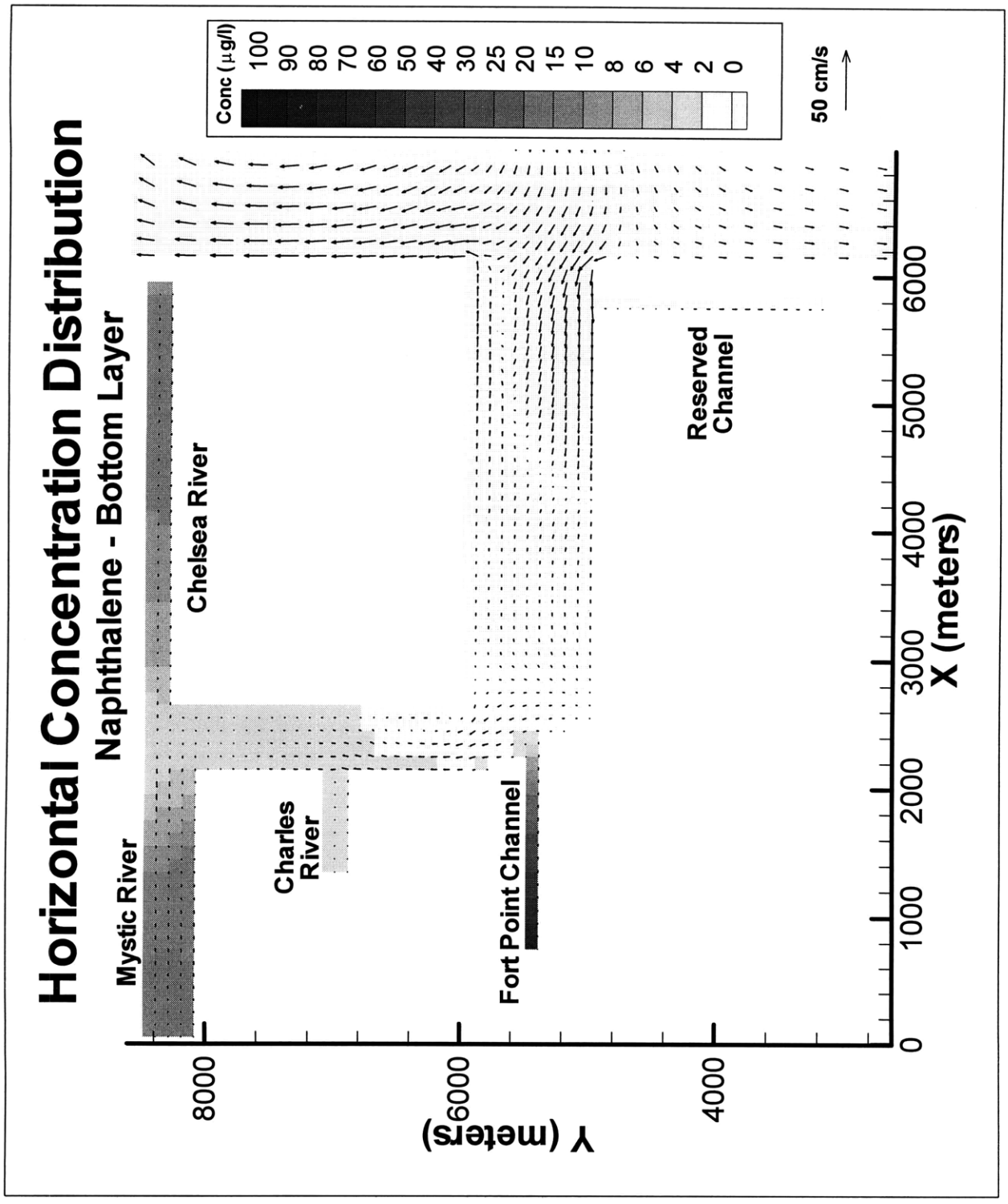

Figure 8.9a – Flow and Concentration Distrbution for Naphthalene at about 1.5 m from the Bottom – High Tide

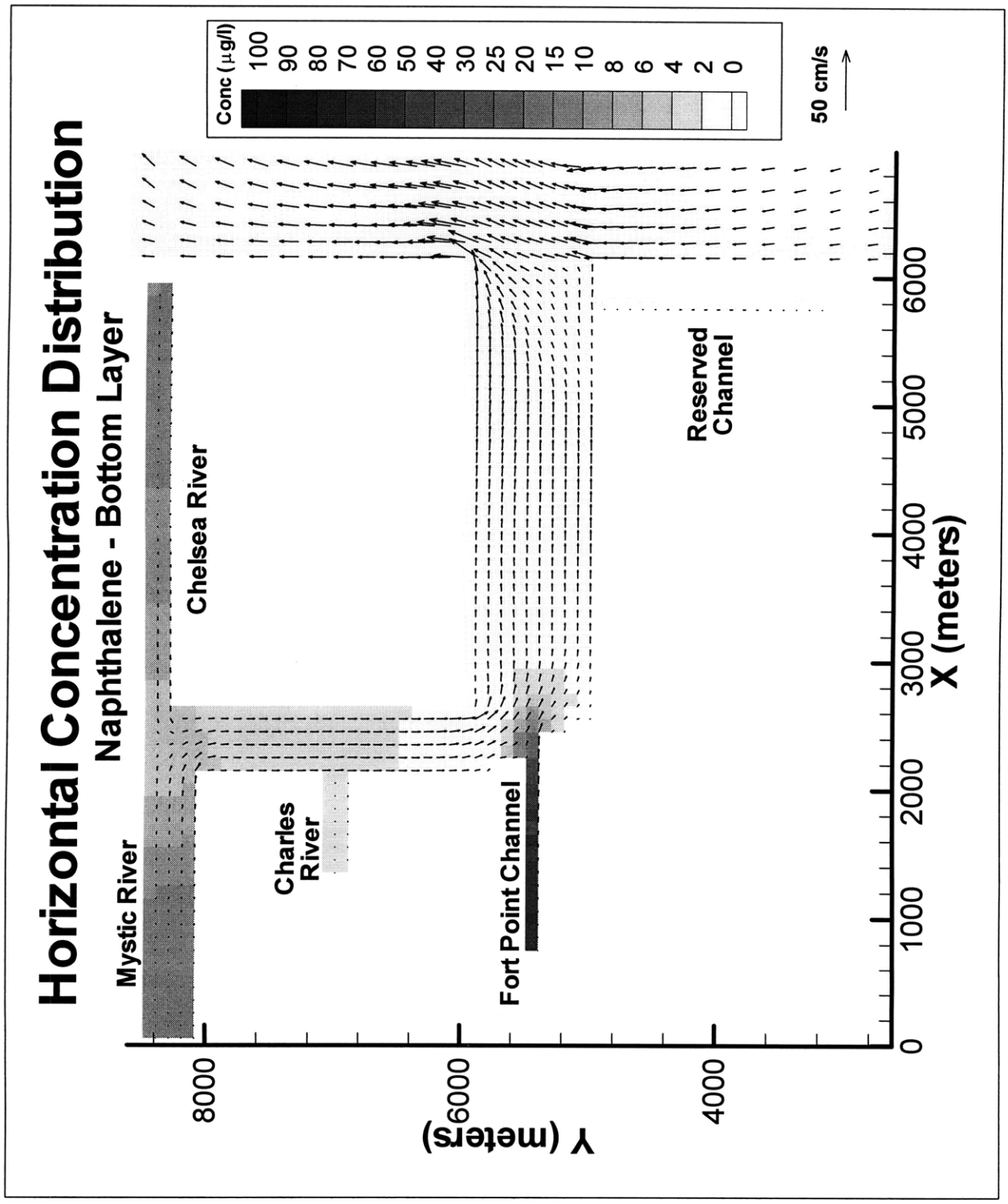

Figure 8.9b – Flow and Concentration Distrbution for Naphthalene at about 1.5 m from the Bottom – Mean Water Level Descending

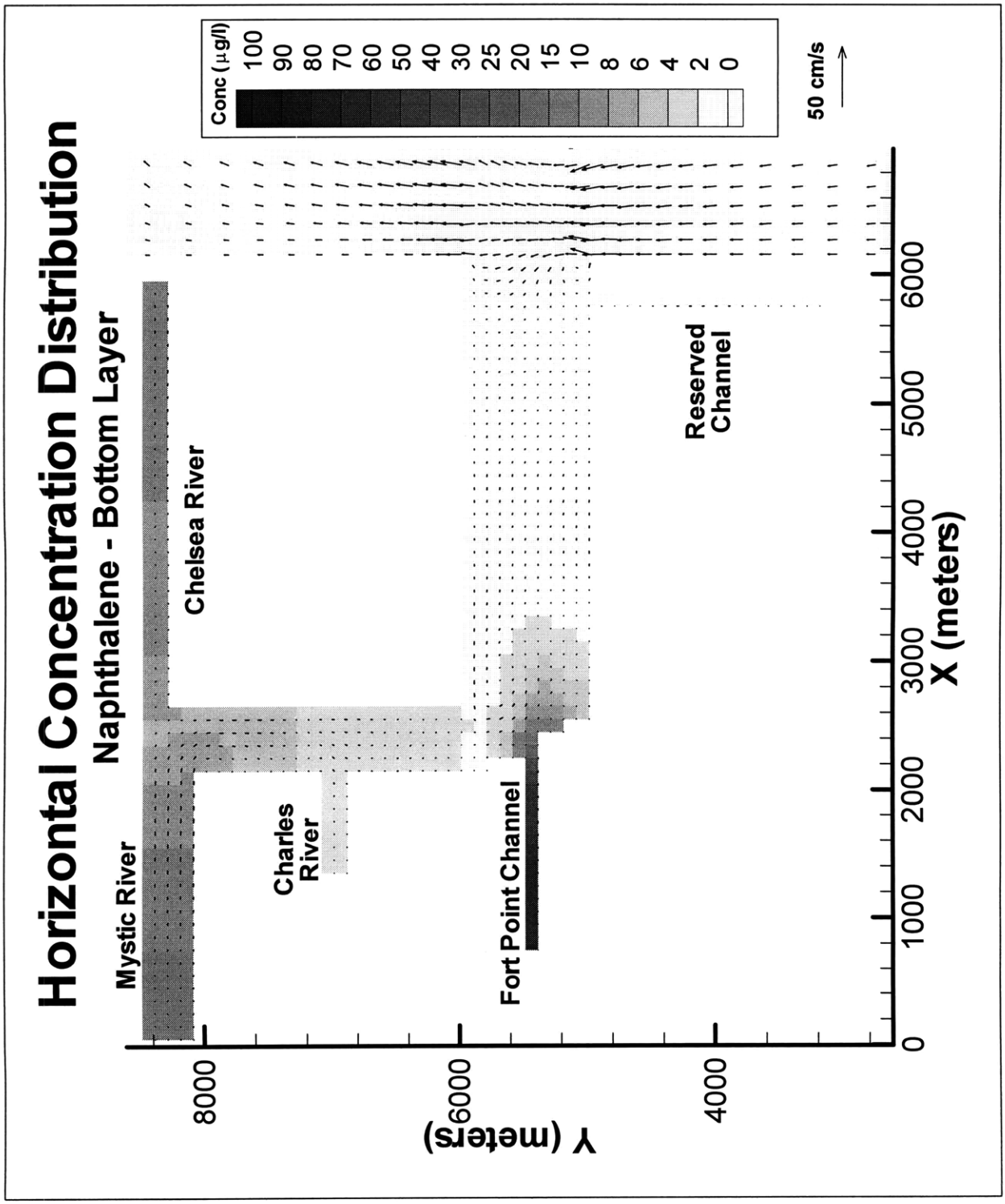

Figure 8.9c – Flow and Concentration Distrbution for Naphthalene at about 1.5 m from the Bottom – Low Tide

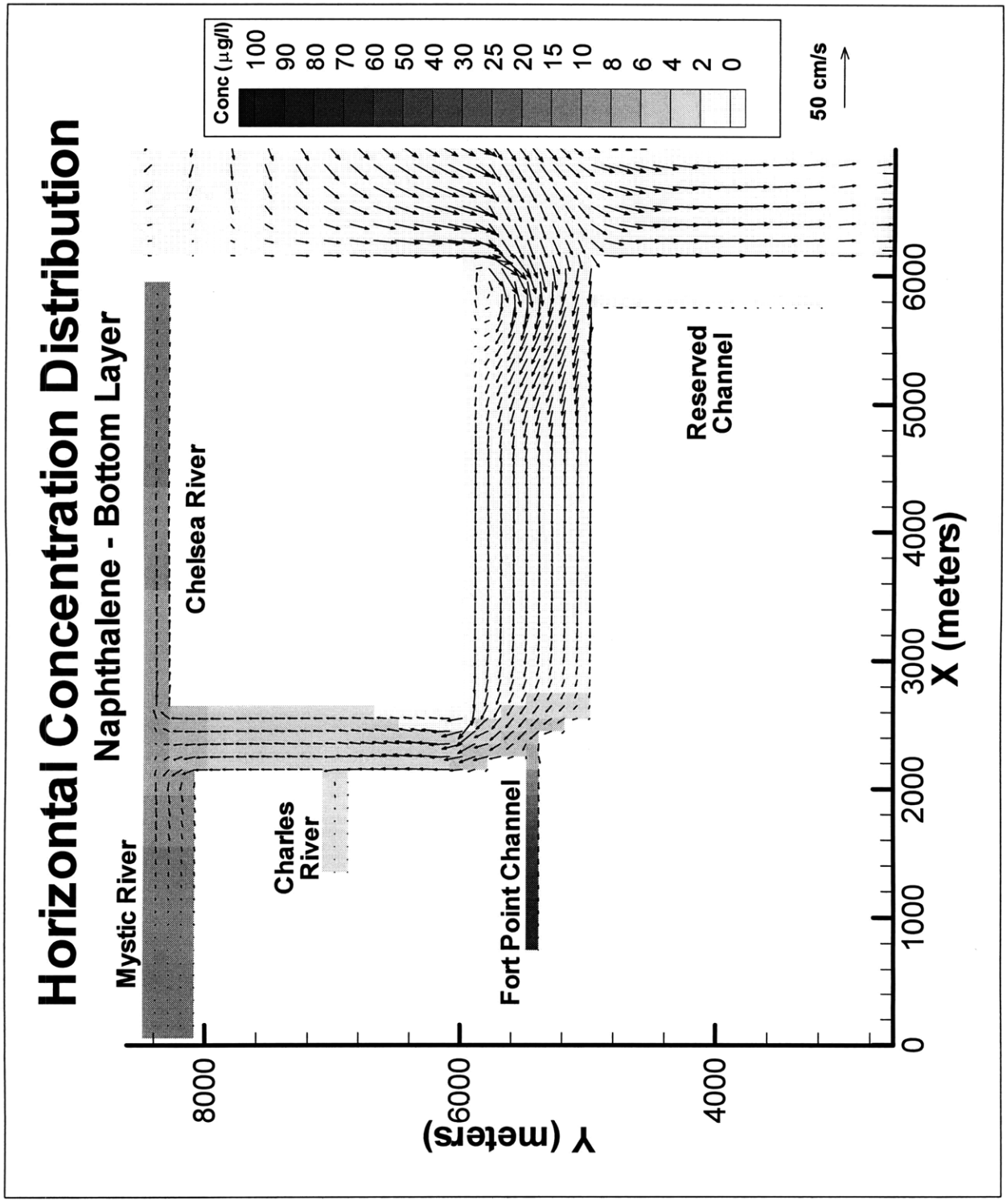

Figure 8.9d – Flow and Concentration Distrbution for Naphthalene at about 1.5 m from the Bottom – Mean Water Level Ascending

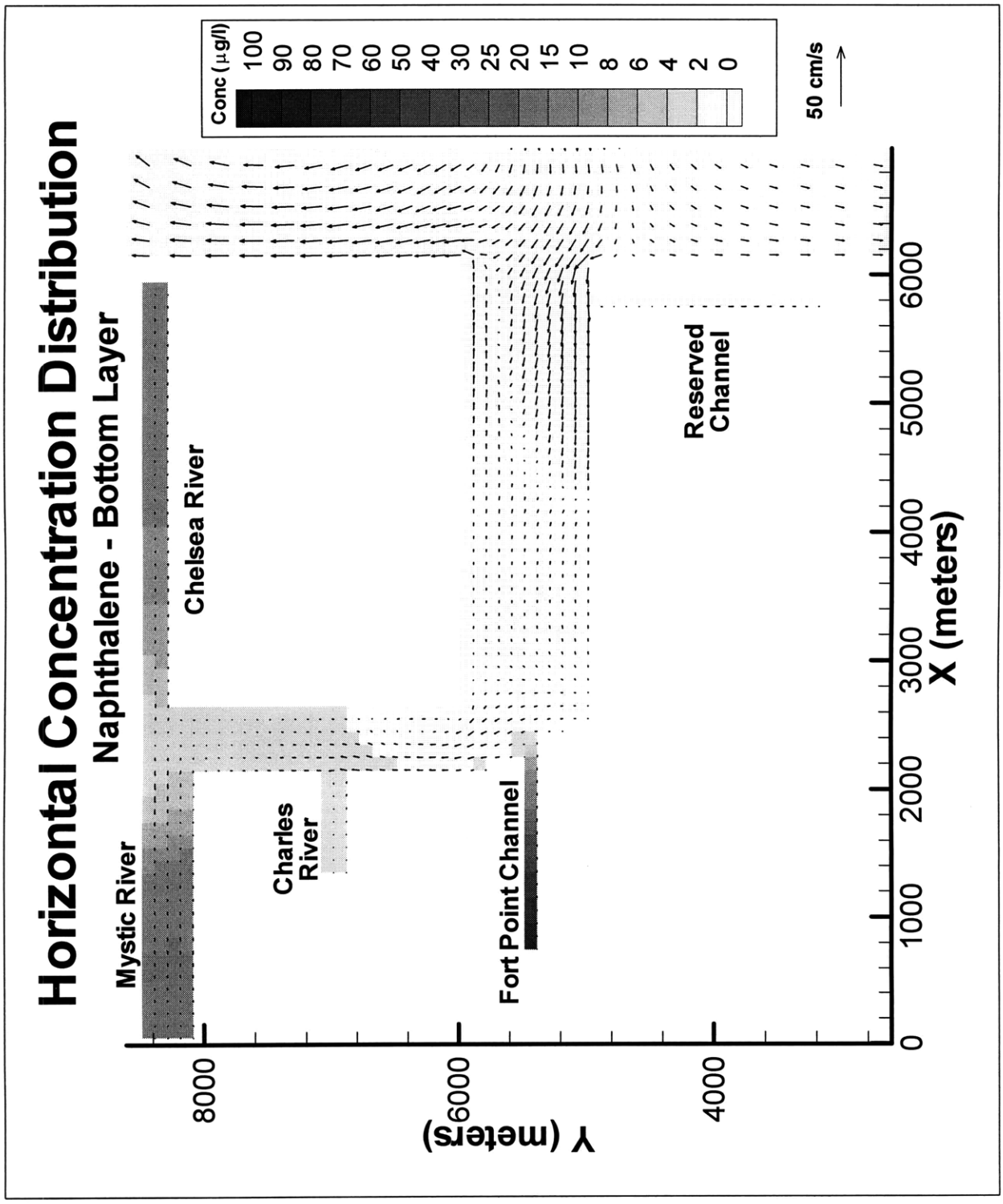

Figure 8.9e – Flow and Concentration Distrbution for Naphthalene at about 1.5 m from the Bottom – Next High Tide

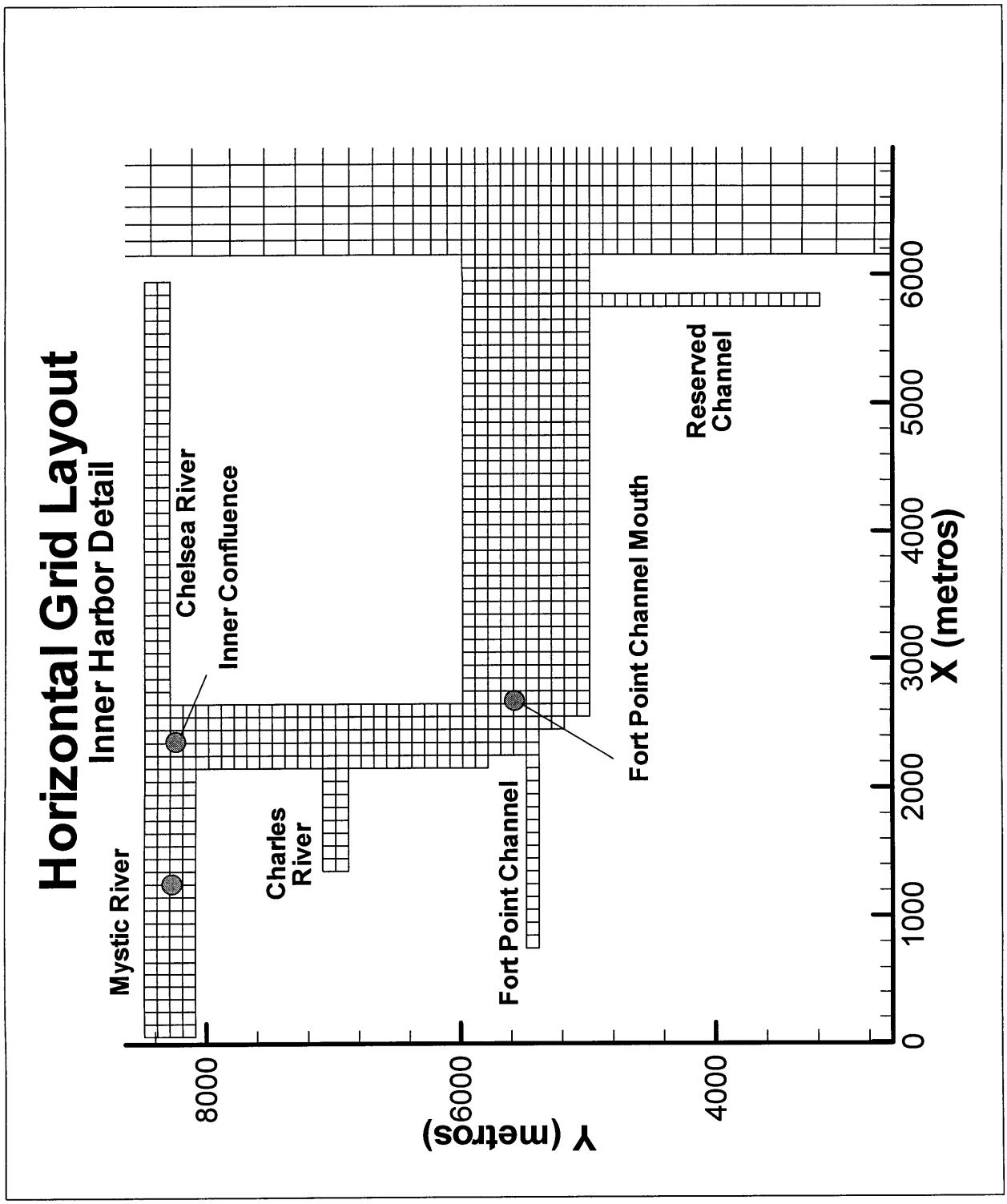

Figure 8.10 – Location of the Vertical Profiles for Naphthalene on the Model Grid

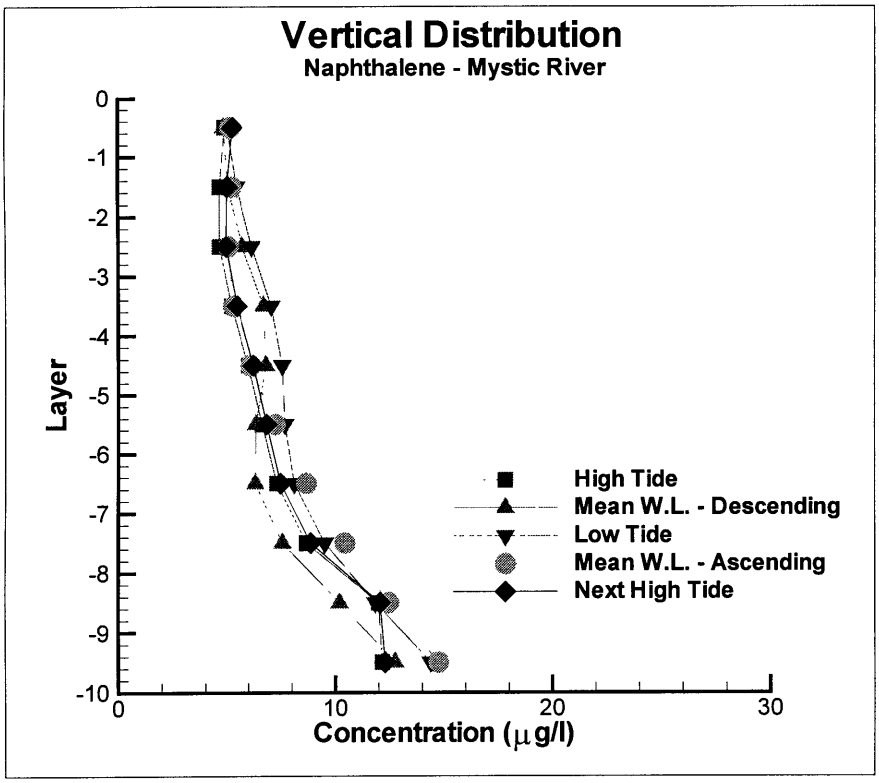

Figure 8.11a

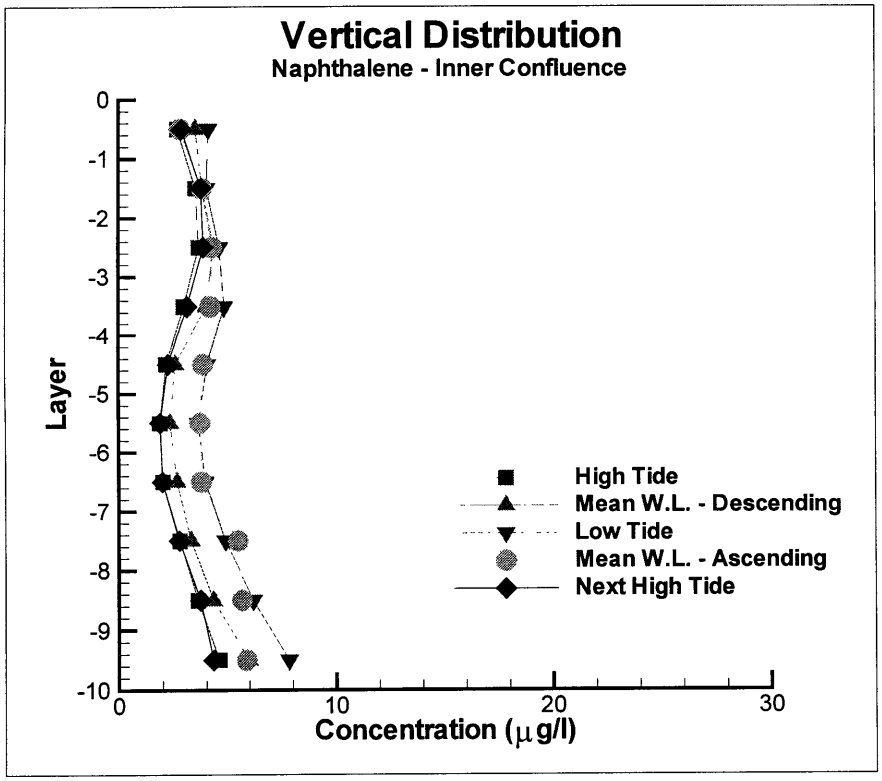

Figure 8.11b

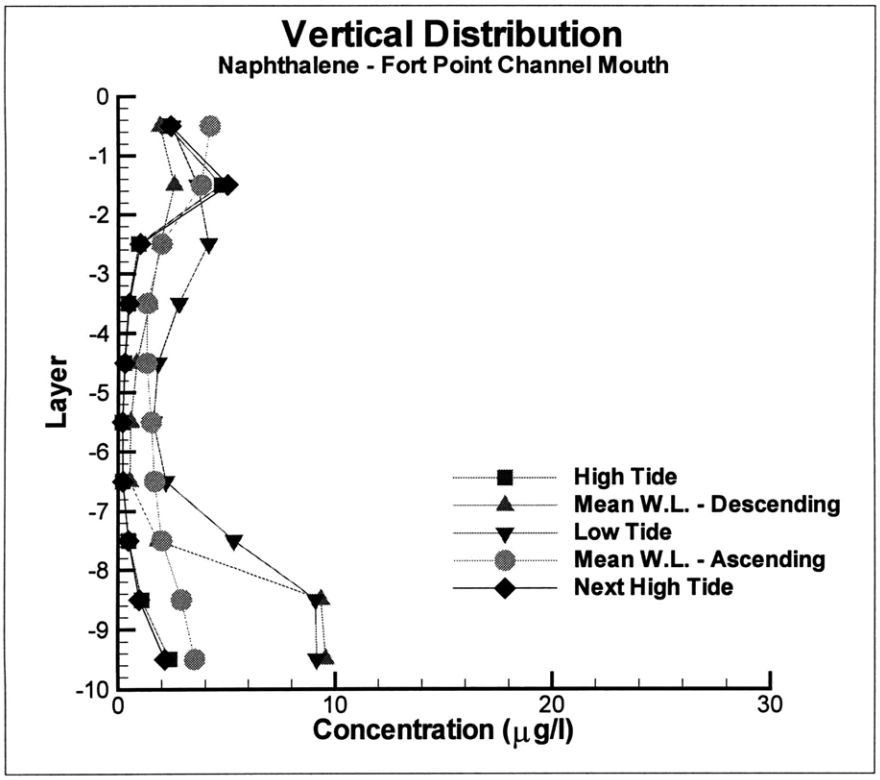

Figure 8.11c

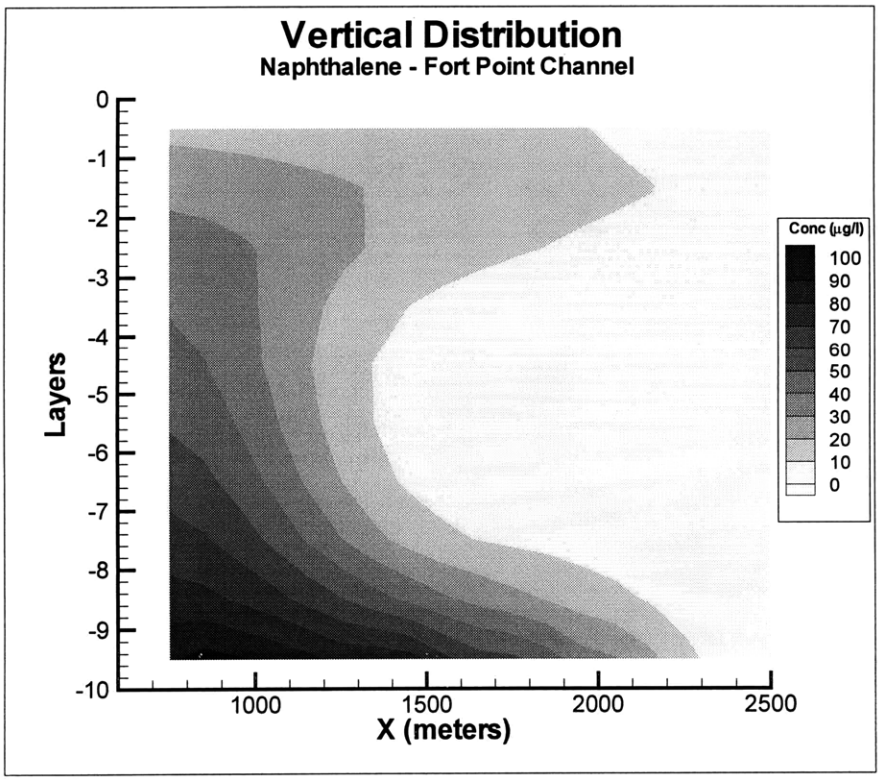

Figure 8.12a

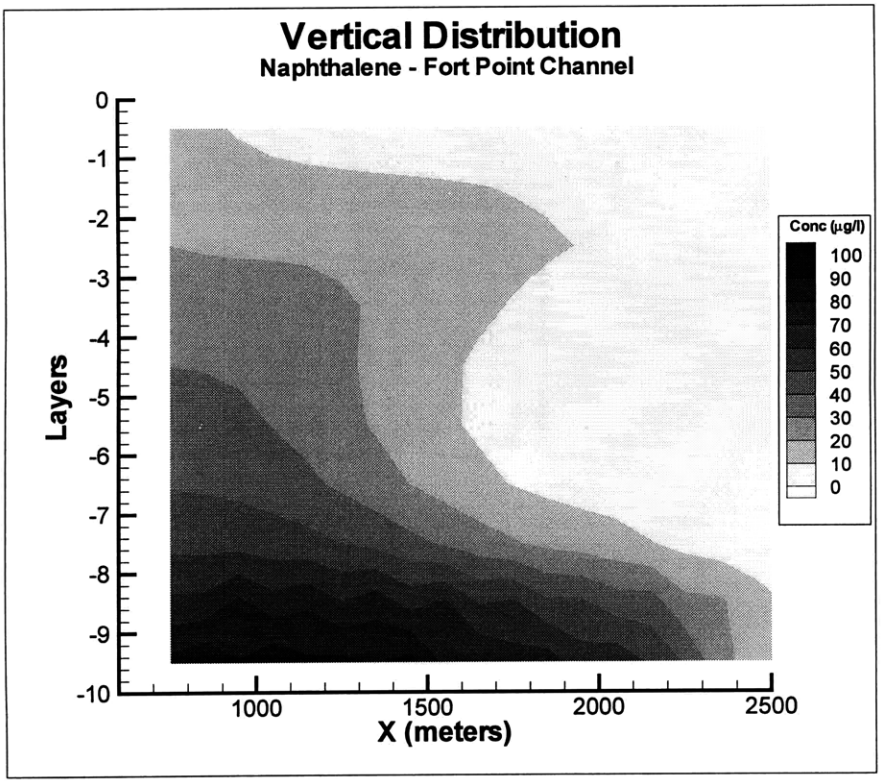

Figure 8.12b

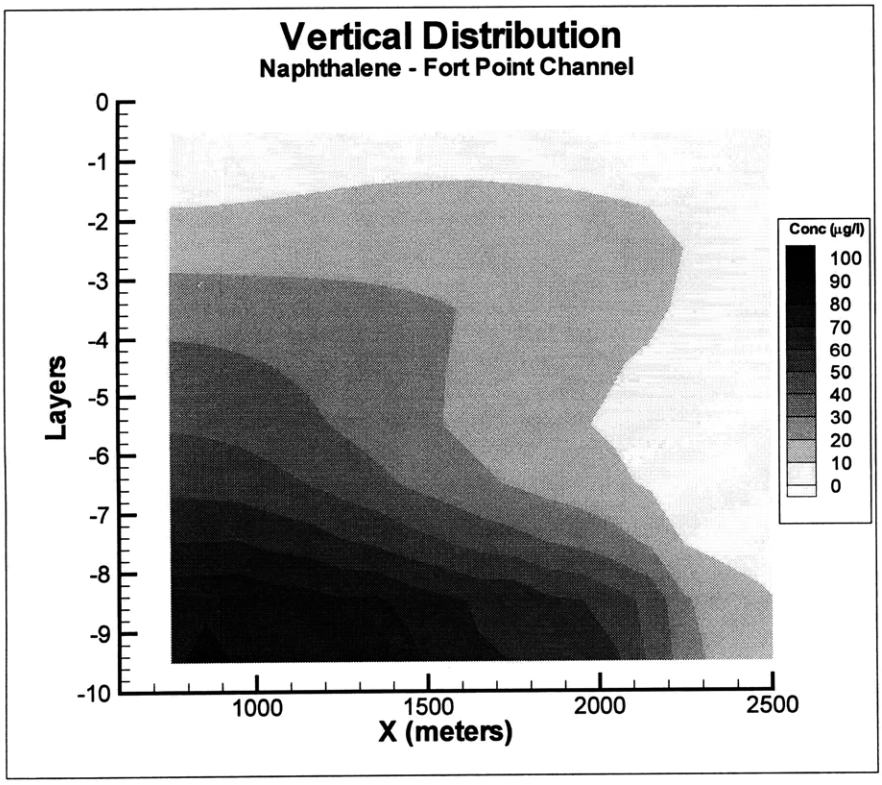

Figure 8.12c

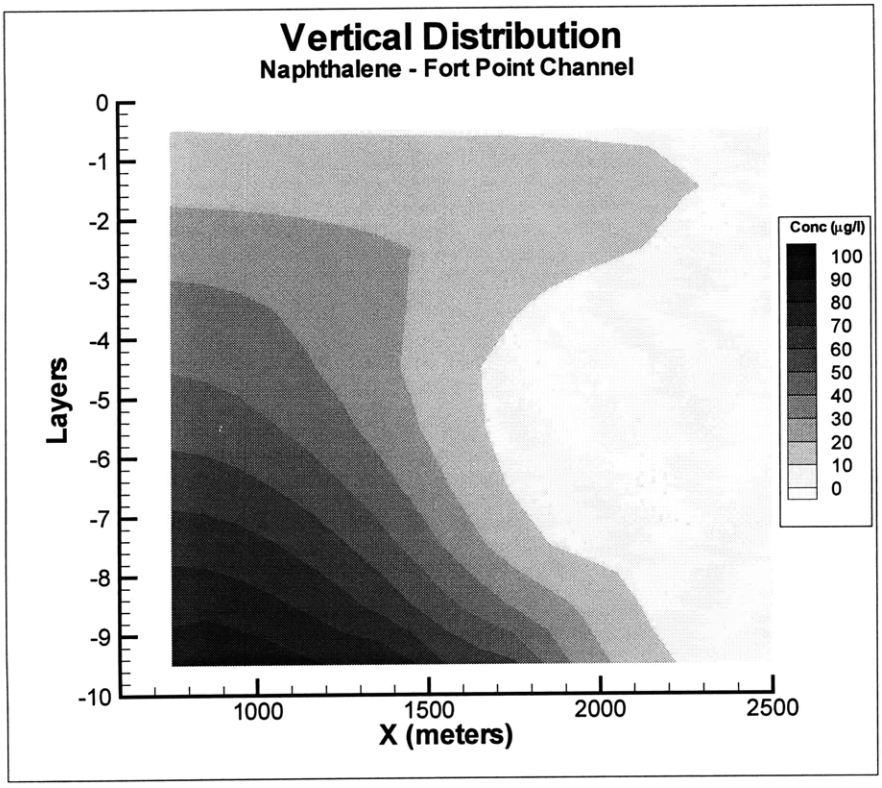

Figure 8.12d

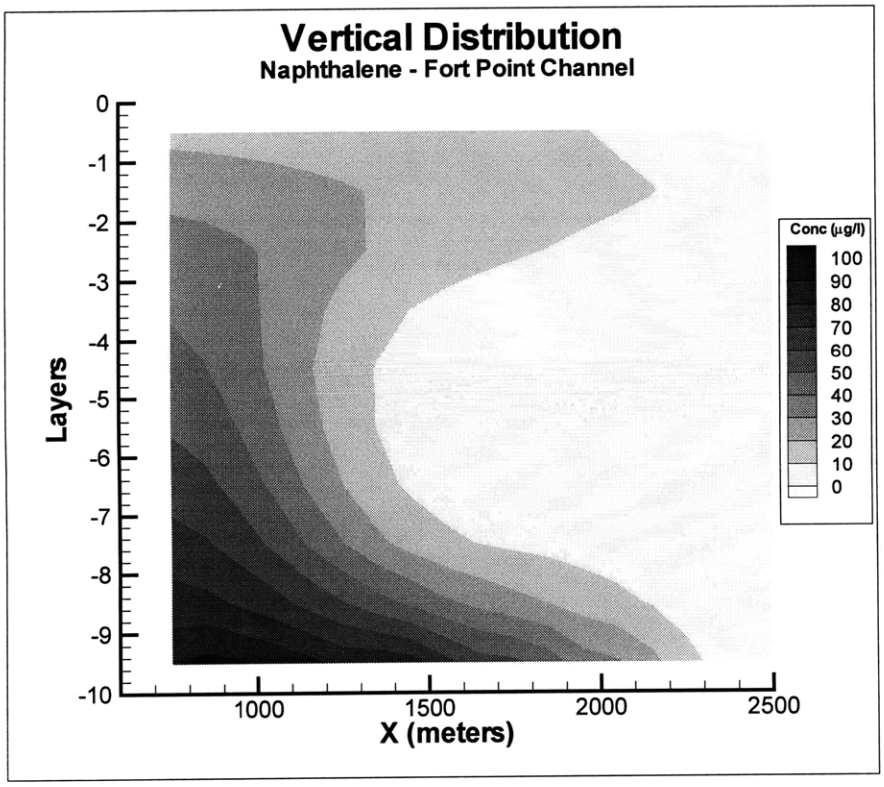

Figure 8.12e

8.3.2.2 Post-Dredging Results

The dredging project has an important impact over the concentrations around the Inner Confluence. This is expected because for naphthalene the most important source is the sediment-water exchange. In particular the sediments located in the Fort Point Channel and on the Inner Confluence are the more contaminated ones. As shown in previous sections (Figure 2.1), the dredging project plans to remove and cap the sediments located in the vicinity of the Inner Confluence. Therefore it is reasonable to expect that the simulation will predict an important reduction of the concentration in the water column in the Inner Confluence. At this point, it is important to remember that in this study the removal and capping are considered perfect.

Figure 8.13a shows a comparison of the pre and post-dredging vertical profile for high tide in the Mystic River. The dredging appears to cause a significant decrease in naphthalene concentrations in both the bottom and the top. Figure 8.13b shows a similar comparison for the Inner Confluence at high tide. Again, there is a significant reduction in the concentrations for the post-dredging situation. In contrast, as the Fort Point Channel is not included in the dredging project, the concentrations in it remain the same for both situations. This is presented in Figure 8.13c.

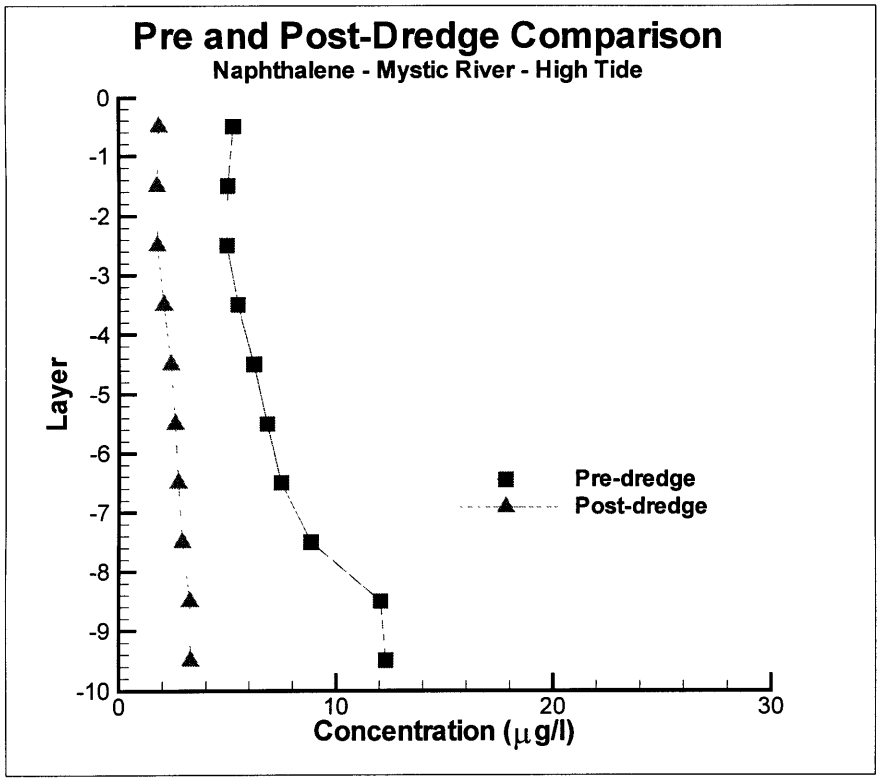

Figure 8.13a

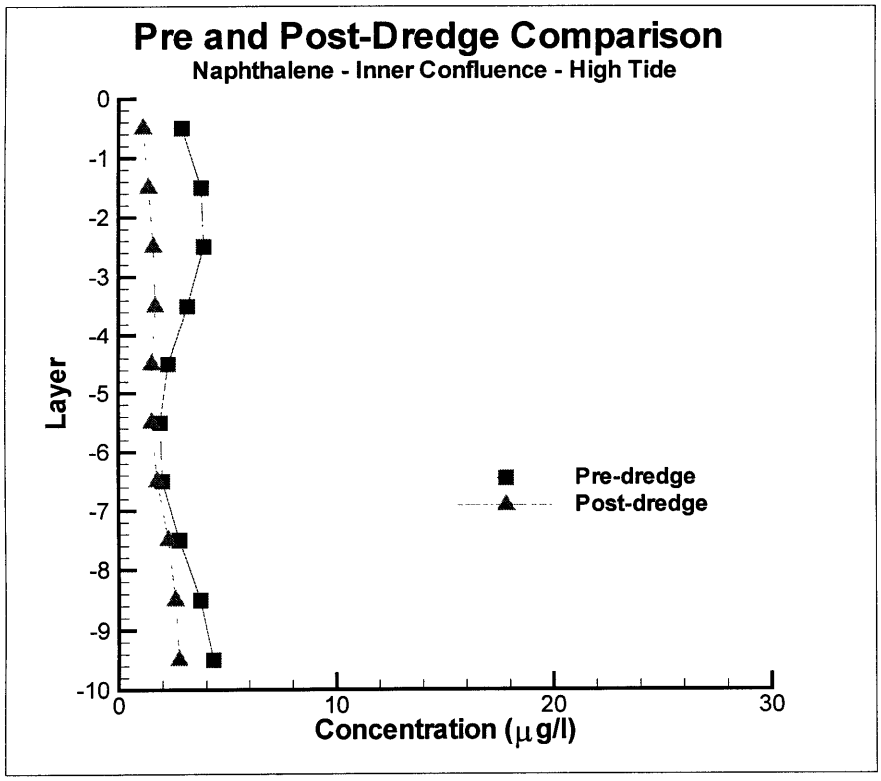

Figure 8.13b

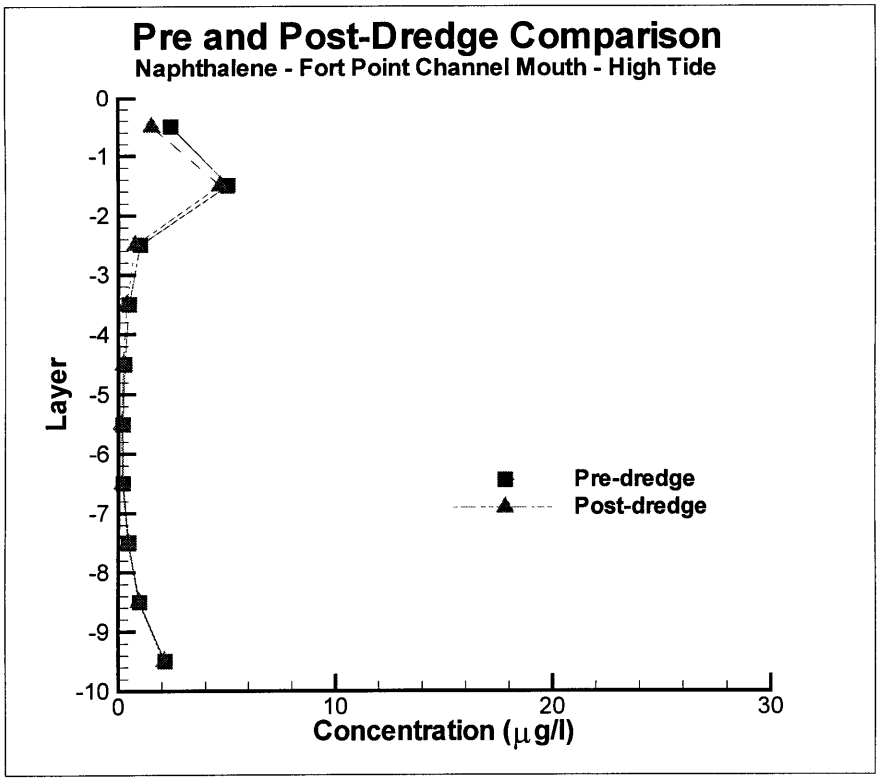
Pre and Post-Dredge Comparison
Naphthalene - Fort Point Channel Mouth - High Tide
Layer
0
-1
-2
-3
-4
-5
-6
-7
-8
-9
-10
0
10
20
30
Concentration (μg/l)
Pre-dredge
Post-dredge

Figure 8.13c

9 ANALYSIS OF RESULTS

Chapter 5 of this report deals with the PAH measurements of the water column of Boston's Inner Harbor. These measurements were conducted with a new device (SPMD) that gives a time-averaged value of the concentration in the water column. The results obtained will help to validate the two modeling approaches.

The first and more simplified modeling approach is the box model presented in Chapter 7. This model analyzes all the sources and sinks and gives as a result a constant steady state concentration over the entire Inner Harbor. It is was intended to give an idea of the order of magnitude of the pollution in the study area while being easy enough to allow the realization of a sensitivity analysis of the most important parameters.

The second modeling approach was intended to identify the actual distribution of the pollutants inside the Inner Harbor. The 3D model takes into account the same sources and sinks used by the box model, but provides a better representation of the flushing process given by actually solving the hydrodynamic situation in the area of interest.

The present chapter will compare the results of the three different approaches to PAH assessment and then provide conclusions and comments to the overall study.

9.1 COMPARISON OF RESULTS

The best way to compare the results is using vertical profiles in the locations where the measurements have been made. Of the three compound modeled, only pyrene was measured with an acceptable level of confidence. Therefore, Figures 9.1a and 9.1b show the vertical profiles of pyrene in the Inner Confluence and Buoy 12. These locations are shown in the model grid in Figure 8.5.

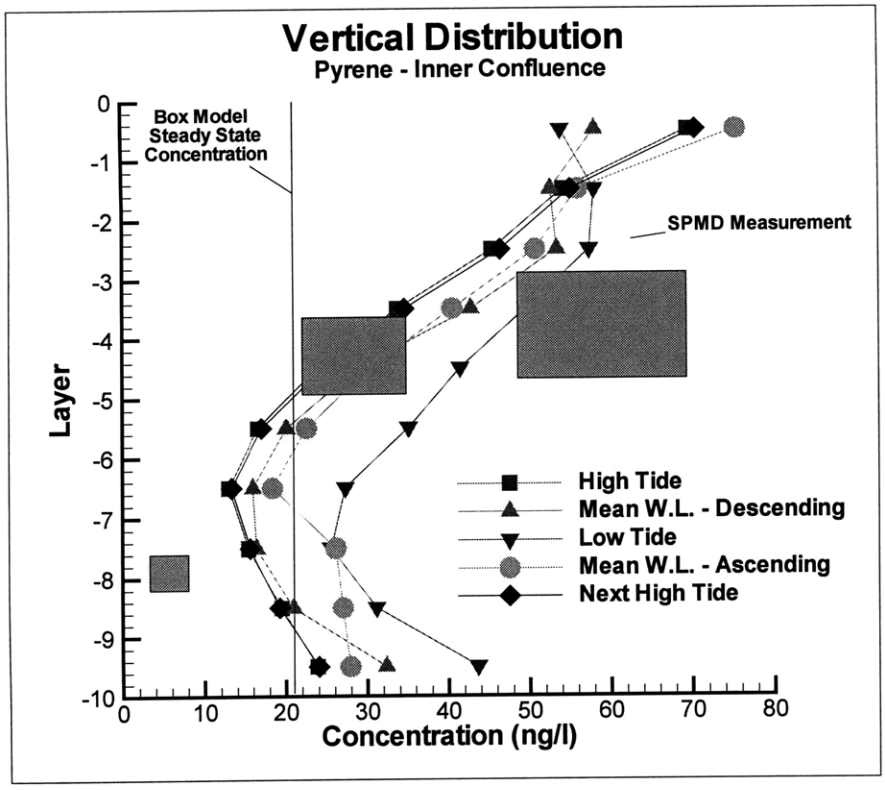

Figure 9.1a

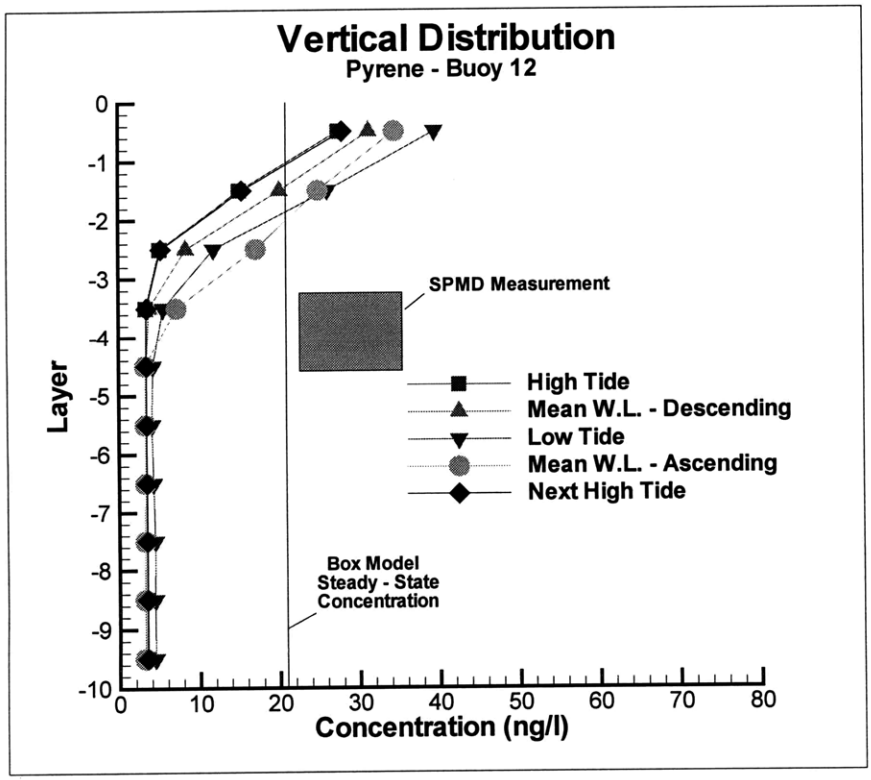

Figure 9.1b

The figures show the vertical profiles obtained with the model which were previously presented in Section 8.3.1. In addition, a constant concentration line representing the box model result and rectangles representing the SPMD measurements are also depicted. The size of each rectangle represents the uncertainty in both the depth and the concentration value. It can be seen that the concentration given by the box model seems to be underestimating the average concentration obtained with the 3D model in the Inner Confluence and vice versa in Buoy 12. More importantly, the values obtained with the SPMDs are in the same order of magnitude of the value obtained with both models. Furthermore, the vertical distribution obtained with the 3D modes in the Inner Confluence is analogous to that obtained with the SPMDs. This results suggest that the principal sources and sinks are accurately represented in the models.

9.2 CONCLUSIONS AND COMMENTS

The following conclusions will be divided into modeling conclusions and PAH distribution conclusions.

9.2.1 Modeling Conclusions

In this section the model representations of the real system are discussed.

- The box model is a very useful tool to verify more complex models because of the ease of implementation. In addition, sensitivity analysis of the different variables can be performed in a very fast way using the box model. This allows the user to concentrate on the most important variables with more complex and demanding models.
- One of the drawbacks of the box model is that, in a situation like Boston Harbor, it over or under-estimates the fluxes across surfaces. As an example, the vertical profile in the area of the Charles River for pyrene (Figure 8.6b) shows a very high concentration in the top layer and relatively low concentration in the bottom. For the

same location the box model assumes a constant concentration in the vertical. As the PAH flux across the surface and the bottom depends on the concentration in the water in contact with it, the box model will inaccurately represent these fluxes.

- Neither of the two models take into account for the fact that a fraction of the PAHs that are in the water column are bound to suspended solids. This will affect mostly the fluxes across the surfaces. In effect the mass of PAHs bounded to particles is unable to participate in certain processes, such as air water exchange. The particles can also settle and become unavailable for transport.
- The sediment-water exchange assumptions of the model formulation, which apply to hydrodynamic contaminants, appear to overestimate the sediment flux of the relatively hydrophilic naphthalene and thus over-predict the steady-state concentration of this compound.

9.2.2 Distribution Conclusions

In this section some observations about the distribution obtained with the 3D model are presented.

- In the horizontal distribution graphs and the vertical profiles for pyrene (Section 8.3.1) and for benzo[a]pyrene (Appendix D), it can be seen than the concentration in the top layers is, in general, higher than the concentration in the bottom layers. This is more noticeable in the area near the Charles River, and less obvious in the Chelsea and Mystic Rivers and the Inner Confluence. This situation is a result of the fact that the PAH contributed by rivers, CSOs and stormwater discharges are carried by freshwater. The freshwater tends to remain in the surface due to density differences, thereby concentrating the mass of pollutants released in these layers. In contrast, the bottom flux is a pure transport of mass without any associated discharge. Therefore, the mass of pollutants released from the bottom mixes faster in the vertical direction.
- The Charles River discharge has a strong influence on the top layer of the Inner Harbor for pyrene and benzo[a]pyrene. This influence is related to the fact that the discharge is freshwater and that the flow value used in the model is relatively high.

- For all three compounds, the Mystic and Chelsea Rivers can be considered well mixed.
- The system is in all cases well mixed in the transverse direction.
- The concentrations of all three compounds tend to decrease as the Inner Harbor mouth is approached.
- Naphthalene concentrations are higher in the Fort Point Channel and the Mystic and Chelsea Rivers, being higher in the former place due to the elevated loadings observed in these areas.
- Post dredge situations have, as expected, lower concentrations in the Chelsea and Mystic River area. The improvements are less significant going downstream.

9.2.3 Future work

This study describes the current concentration distribution of benzo[a]pyrene, pyrene and naphthalene and is intended to serve as a basis for future "what if" studies. In particular, it would be interesting to study the short term effect of the dredging and capping activities, i.e. to analyze the impact of the dredging and disposal procedures and the contaminated porewater flow due to the settling of the sand caps.

The distribution of pollutants suggests that it may be sufficient to develop a multiple box model that can resolve the different characteristics of the Inner Harbor without the inconvenience of a time consuming 3D model. There should be at least three boxes in vertical to represent accurately the air-water and sediment-water exchanges. Only one box in the transverse direction would be needed since the pollutants are well mixed in this direction. For the longitudinal direction, one box is enough to represent the Chelsea and Mystic Rivers. For the rest of the Inner Harbor the optimal number of boxes may be determined by performing some sensitivity analysis.

10 REFERENCES

Adams, E.E.; Gillivary, D.L.; Suh, S.-W.; Luxemberg R.R. 1993. *Analysis of Boston Inner Harbor Dye Study.* Submitted to the Massachusetts Water Resources Authority.

Alber M.; Chan A.B. 1994. *Sources of contaminants to Boston Harbor: revised loading estimates.* Tech. Report 94-1. Environmental Quality Dept., Massachusetts Water Resources Authority, Boston, MA. As quoted in Chan-Hilton *et al*, 1998.

Bjorseth A. (ed.). 1983. *Handbook of Polycyclic Aromatic Hydrocarbons.* New York.

Bjorseth A.; Ramdahl T.; Dekker M. (ed.). 1985. *Handbook of Polycyclic Aromatic Hydrocarbons Vol 2.* New York. Pp. 1-20.

Blumberg, A.F.; Mellor, G.L. 1987. *A Description of a Three Dimensional Coastal Ocean Circulation Model.* In Three-Dimensional Coastal Ocean Models, Coastal and Estuarine Sciences 4, N. Heaps, Editor. American Geophysical Union, Washington D.C. Pp. 1-16.

Borneff J.; Kunte H. 1965. *Carcinogenic substances in water and soil. Part XVI: Evidence of polycyclic aromatic hydrocarbons in water samples through direct extraction.* Arch. Hyg. (Berlin) 148, 585-597 (German). As cited in Neff, 1979.

Bray, R.N.; Bates, A.D.; and Land, J.M. 1997. *Dredging: A Handbook for Engineers (2nd ed.).* London. John Wiley & Sons.

Bridboard K.; Finklea J.F.; Wagoner J.K.; Moran J.B. and Caplan P. *Human exposure to polynuclear aromatic hydrocarbons.* 1976. Pp. 319-324. In: Freudenthal R.; Jones P.W. (editors). *Carcinogenesis – A comprehensive survey. Vol. I.* Polynuclear aromatic hydrocarbons. Chemistry, Metabolism, and carcinogenesis. New York. Raven Press. As cited in Neff, 1979.

Budavari S. (ed.). 1996. The Merck Index. Merck & CO., Inc. Whitehouse Station, NJ.

Bumpus D.F.; Butcher W.S.;Athern W.D., Day C.G. 1953. *Inshore survey project, Boston final harbor report.* Ref 53-20, Woods Hole Oceanographic Institution, Woods Hole, MA. As cited in Chan-Hilton *et al*, 1998.

Byrne, G.A.; Aylott, R.I. 1980. British Patent 1566253. *Concentrator for Removing Organic Materials from Aqueous Systems.* As cited in Huckins *et al*, 1990.

Chan-Hilton A.B.; McGillivary D.L.; Adams E.E. 1998. *The residence time of freshwater in Boston's Inner Harbor.* Journal of Waterway Port Coastal and Ocean Engineering ASCE. In press.

Chen, H.-W. 1993. *Fluxes of Organic Pollutants from the Sediments in Boston Harbor.* Master of Science Thesis. Department of Civil and Environmental Engineering. Massachusetts Institute of Technology.

Chen, H.-W.; Adams, E.E.; Gschwend, P.M. *Modeling the Fluxes of Organic Pollutants from Sediments.* R.M. Parsons Laboratory, Dept. Of Civil and Environmental Engineering, Massachusetts Institute of Technology. Unpublished as of 5/98.

Chiou, C.T. 1985. *Partition coefficients of organic compounds in lipid-water systems and correlations with fish bioconcentration factors.* Environmental Science and Technology. 19(1): 57-62.

Cleveland L.; Little E.E.; Petty J.D.; Johnson B.T.; Lebo J.A.; Orazio C.E.; Dionne J.; Crockett A. 1997. *Toxicological and chemical screening of Antarctica sediments: Use of whole sediment toxicity tests, Microtox, Mutatox and semipermeable membrane devices (SPMDs).* Marine Pollution Bulletin. 34(3), 194-202.

Crunkilton, R.L.; DeVita, W.M. 1997. *Determination of aqueous concentrations of polycyclic aromatic hydrocarbons (PAHs) in an Urban Stream.* Chemosphere. 35(7), 1447-1463.

Cura, J.; Studer, M. 1996. *Measurement of PAH loadings to Massachusetts Bay from various waterborne sources.* Proceedings of the Water Environment Federation. 69th Annual Conference and Exposition. Dallas, TX.

Downey, P.C. 1994. *Bioaccumulation of selected organic compounds and metals in mussels deployed near Deer Isalnd discharge and in Massachusetts Bay, 1993.* MWRA Enviro. Quality Dept. Tech. Rpt. Series No. 94-8. Massachusetts Water Resources Authority, Boston, MA

Ellis, G.S.; Huckins, J.N.; Rostad, C.E.; Schmitt, C.J.; Petty, J.D.; MacCarthy, P. 1995. *Evaluation of lipid-containing semipermeable membrane devices for monitoring organochlorine contaminants in the Upper Mississippi River.* Environmental Toxicology and Chemistry. 14(11), 1875-1884.

Flores, A. 1998. *Assesing the Fate of PAHs in the Boston Inner Harbor Using Semipermeable Membrane Devices (SPMDs).* Master of Engineering Thesis. Massachusetts Institute of Technology.

General Electric. 1998. *An Evaluation of the Feasibility of Environmental Dredging in the Upper Hudson River.* http://www.hudsonwatch.com/dredging1.html.

Golomb, D.; Ryan, D.; Underhill, J.; Wade, M.; Zemba, S. 1997. *Atmospheric Deposition of Toxics onto Massachusetts Bay – II. Polycyclic Aromatic Hydrocarbons.* Atmospheric Environment Vol. 31, No. 9, pp. 1361-1368.

Golomb, D.; Ryan, D.; Eby, N.; Underhill, J.; Wade, M.; Zemba, S. 1996. *Atmospheric deposition of contaminants onto Massachusetts and Cape Cod Bays.* MBP-95-07, Massachusetts Bays Program. Boston, MA.

Gray, M.A.; Spacie, A. 1991. 12th Meeting of the Society of Environmental Toxicology and Chemistry, EMAP session. Poster No. 272

Gustaffson, O.; Haghseta, F.; Chan, C.; MacFarlane, J.; Gschwend, P.M. 1997. *Quantification of the dilute sedimentary soot phase: Implications for PAH speciation and bioavailability.* Environmental Science and Technology. 31(1), 203-209.

Harvey, R.G. 1991. *Polycyclic Aromatic Hydrocarbons: Chemistry and Carcinogenicity.* Cambridge University Press: Cambridge, U.K. Chapter 4.

Harvey, R.G. 1997. *Polycyclic Aromatic Hydrocarbons.* Wiley-VCH, New York, NY.

Hellmann, von H. 1974. *Occurrence and origin of so-called carcinogens and other polycyclic hydrocarbons in water.* Deut. Gewasserkund. Mitteil. 18, 155-157 (German). As cited in Neff, 1979.

Herve, S.; Prest, H.F.; Heinonen, P.; Hyotylainen, T.; Koistinen, J.; Paasivirta, J. 1995. *Lipid-filled semipermeable membranes and mussels as samplers of organochlorine compounds in lake water.* Envi. Sci. Pollut. Res. Int. 2(1), 24-30. As cited in Prest, Huckins *et al*, 1995.

Ho, S.W. 1998. *The Effect of Iron on the Photo-oxidation of Humic Substances.* Masters of Engineering Thesis, Department of Civil and Environmental Engineering, Massachusetts Institute of Technology.

Hofelt, C.S.;Shea, D. 1997. *Accumulation of organochlorine pesticides and PCBs by semipermeable membrane devices and Mytilus edulis in New Bedford Harbor.* Environmental Science and Technology. 31(1), 154-159.

Huckins, J.N.; Manuweera, G.K.; Petty, J.D.; MacKay, D.; Lebo, J.A. 1993. *Lipid-containing semipermeable membrane devices for monitoring organic contaminants in water.* Environmental Science and Technology. 27(12), 2489-2496.

Huckins, J.N.; Petty, J.D.; Orazio, C.E.; Lebo, J.A.; Clark, R.C.; Gibson, V.L.; Gala, W.R.; and Kaiser, E.M. 1998. *Calibration of semipermeable membrane devices (SPMDs) for estimation of polycyclic aromatic hydrocarbon (PAH) concentrations in water.* (unpublished as of 2/98)

Huckins, J.N.; Petty, J.D.; Lebo, J.A.; Orazio, C.E.; Clark, R.C.; Gibson, V.L. 1997. *SPMD technology - a tutorial.* Midwest Science Center, Biological Resources Division, US Geological Survey. 573-875-5399.

Huckins, J.N.; Tubergen, M.W.; Lebo, J.A.; Gale, R.W.; Schwartz, T.R. 1990. *Polymeric film dialysis in organic solvent media for cleanup of organic contaminants.* Journal of the Association of Official Analytical Chemists. 73(2), 290-293.

Huckins, J.N. 1998. Personal Communication. Environmental Contaminants Researchg Center. Columbia, MO.

HydroQual, Inc. 1993. *A primer for ECOM-si*

International Agency for Research on Cancer. *Monograph on the evaluation of carcinogenic risk of the chemical to man: Certain polycyclic aromatic hydrocarbons and heterocyclic compounds.* 1973. Vol. 3. Geneva, Switzerland: World Health Organization. As cited in Neff, 1979.

Johnson, G.D. 1991. *Hexane-filled Dialysis Bags for Monitoring Organic Contaminants in Water.* Environmental Science and Technology. 25(11), 1897-1903.

Laflamme R.E., Hites R.A. 1977. The global distribution of polycyclic aromatic hydrocarbons in recent sediments. *Geochimica et Cosmochimica Acta.* 42, 289-303.

Lebo, J.A.; Zajicek, J.L.; Huckins, J.N.; Petty, J.D.; Peterman, P.H. 1992. *Use of semipermeable-membrane devices for in-situ monitoring of polycyclic aromatic-hydrocarbons in aquatic environments.* Chemosphere. 25(5), 697-718.

Leifer, A. 1988. *The Kinetics of Environmental Aquatic Photochemistry.* ACS Professional Reference Book, American Chemical Society, Washington DC.

Lewis, R.G.; Kelly, T.J.; Chuang, J.C.; Callahan, P.J. and Coutant, R.W. *Phase Distributions of Airborne Polycyclic Aromatic Hydrocarbons in Two U.S. Cities.* U.S. Environmental Protection Agency and BATELLE.

Lyman, W.J., Reehl, W.F., and Rosenblatt, D.H. (eds). 1982. Handbook of Chemical Property Estimation Methods. McGraw-Hill, New York, NY.

Kennish, M.J. 1997. *Chapter 4: Polycyclic Aromatic Hydrocarbons.* In Practical Handbook of Estuarine and Marine Pollution. New York. CRC Press. pp141-175.

Massachusetts Water Resources Authority (MWRA). 1991. *The State of Boston Harbor: 1991.* Technical Report No. 92-3. Boston, MA.

Massachusetts Water Resources Authority (MWRA). 1993. *The State of Boston Harbor.* Boston, MA.

Massachusetts Water Resources Authority (MWRA). 1996a. *The State of Boston Harbor.* Technical Report No. 97-5. Boston, MA.

Massachusetts Water Resources Authority (MWRA). 1994. *Sources of Contaminants to Boston Harbor: Revised Loading Estimates.* Boston, MA.

Massachusetts Water Resources Authority (MWRA). 1996b. *History: Boston Harbor.* Boston, MA.

MacFarlane, J. 1998. Personal Communication. Ralph M. Parsons Laboratory, MIT. Cambridge, MA.

McGroddy, S.E. 1993. *Sediment-porewater Partitioning of PAHs and PCBs in Boston Harbor, Mass.* Doctor of Philosophy Thesis, Environmental Sciences Program, University of Massachusetts at Boston.

McGroddy, S.E.; Farrington J.W. 1995. *Sediment Porewater Partitioning of Polycyclic Aromatic Hydrocarbons in Three Cores from Boston Harbor, Massachusetts.* Environmental Science and Technology, Vol. 29, No. 6, pp. 1542-1550.

McGroddy, S.E.; Farrington, J.W.; Gschwend, P.M. 1996. *Comparison of in situ and desorption sediment-water partitioning of polycyclic aromatic hydrocarbons and polychlorinated biphenyls.* Environmental Science and Technology. 30 (1), 172-177.

Meadows, J.; Tillitt, D.; Huckins, J.; Schroeder, D. 1993. *Large-scale dialysis of sample lipids using a semipermeable-membrane device.* Chemosphere. 26(11), 1993-2006.

Menzie-Cura & Associates, Inc. 1995. *Measurements and Loadings of Polycyclic Aromatic Hydrocarbons (PAH) in Storm Water, Combined Sewer Overflows, Rivers, and Publicly Owned Treatment Works (POTWs) Discharging to Massachusetts Bays.* Massachusetts Bays Program. U.S. Environmental Protection Agency – Water Management Division.

Metcalf & Eddy. 1994. *Master Planning and CSO Facility Planning: System Master Plan Baseline Assessment.*

Miere, J.P.; Mappes, G.W.; Tucker, E.S.; Dietrich, M.W.; Keith, L.H. (editor). 1977. *Identification and Analysis of Organic Pollutants in Water.* Ann Arbor Science Publishers, Inc. Ann Arbor, MI. Pp. 113-133. As cited in Huckins *et al*, 1990.

Minas, W and Gunkel, W. 1995. *Oil pollution in the North Sea - A microbiological point-of-view.* Helgolander Meeresuntersuchungen. 49(1-4), 142-158.

Moring, J.B.; Rose, D.R. 1997. *Occurrence and concentrations of polycyclic aromatic hydrocarbons in semipermeable membrane devices and clams in three urban streams of the Dallas-Fort Worth Metropolitan Area, Texas.* Chemosphere. 34(3), 551-566.

National Academy of Sciences, Committee on Biological Effects of Atmospheric Pollutants. *Particulate Polycyclic Organic Matter.* Washington, D.C. As cited in Neff, 1979.

Neff, J.M. 1979. *Polycyclic Aromatic Hydrocarbons in the Aquatic Environment: Sources, Fates and Biological Effects.* Applied Science Publishers, London, U.K.

Neff, J.M. 1985. *Fundamentals of Aquatic Toxicology.* Hemisphere Publishers Corporation.

Petty J.D.; Ituckins, J.N.; Zajicek, J.L. 1993. *Application of Semipermeable Membrane Devices (SPMDs) as Passive Air Samplers.* Chemosphere 27(9) pp. 1609-1624

Peven, C.S.; Uhler, A.D.; Querzoli, F.J. 1996. *Caged mussels and semipermeable membrane devices as indicators of organic contaminant uptake in Dorchester and Duxbury Bays, Massachusetts.* Environmental Toxicology and Chemistry. 15(2), 144-149.

Pitter, P.; Chudoba, J. 1990. *Chapter 5: Relationship between molecular structure and biological degradability. Section II: Hydrocarbons. Subsection E: Aromatic Hydrocarbons.* In Biodegradibility of Organic Substances in the Aquatic Environment. Boca Raton. CRC Press. pp 170-178.

Prest, H.F.; Huckins, J.N.; Petty, J.D.; Herve, S.; Paasivirta, J.; Heinonen, P. 1995. *A survey of recent results in passive sampling of water and air by semipermeable membrane devices.* Marine Pollution Bulletin. 31(4-12), 306-312.

Prest, H.F.; Jacobson, L.A.; Wilson, M. 1997. *Passive water sampling for polynuclear aromatic hydrocarbons using lipid-containing semipermeable membrane devices (SPMDs): Application to contaminant residence times.* Chemosphere. 35(12), 3047-3063.

Prest, H.F.; Jarman, W.M; Burns, S.A.; Weismiller, T.; Martin, M.; Huckins, J.N. 1992. Chemosphere 25, pp 1811-1823. As cited in Hofelt and Shea (1997).

Prest, H.F.; Richardson, B.; Jacobson, L.A., Vedder, J.; Martin, M. 1995. *Monitoring organochlorines w/SPMDs and mussels (Mytilus edulis) in Corio Bay, Victoria, Australia.* Marine Pollution Bulletin. 30(8), pp 543-554.

Sea Grant Program: www.whoi.edu/seagrant/Exhibits/Background.html

Schellbach, C.P.; Van Veen, W. March 1997. *Dredging Up Toxic Sediments.* Civil Engineering. 67(3), 55-57.

Schwarzenbach, R.P.; Gschwend, P.M. and Imboden, D.M. 1993. *Environmental Organic Chemistry.* John Wiley and Sons, Inc.

Shiaris, M.P. 1989. *Seasonal biotransformation of naphthalene, phenanthrene, and benzo(a)pyrene in surficial estuarine sediments.* Applied Environmental Microbiology. 1391-1399.

Shiaris, M.P.; Jambard-Sweet, D. 1986. *Polycyclic Aromatic Hydrocarbons in Surficial Sediments of Boston Harbour, Massachusetts, USA.* Marine Pollution Bulletin, Vol. 17, No. 10, pp. 469-472.

Signell, R.P.; Butman, B. 1992. *Modeling Tidal Exchange and Dispersion in Boston Harbor.* Journal of Geophysical Research, Vol. 97, No. C10, pp. 15,591-15,606

Siron, R.; Pelletier, E.; Delille, D.; and Roy, S. 1993. *Fate and effects of dispersed crude-oil under icy conditions simulated in mesocosms.* Marine Environmental Research. 35(3), 273-302.

Sodergren, A. 1987. *Solvent-filled dialysis membranes simulate uptake of pollutants by aquatic organisms.* Environmental Science and Technology. 21(9), 855-859.

Stivers, C.E; Sullivan, R. 1994. *Restoration and Capping of Contaminated Sediments.* In McNair, E.C. Jr. Vol. 2. Dredging '94: Proceedings of the Second International Conference on Dredging and Dredged Material Placement. New York, American Society of Civil Engineers.

Stolzenbach, K.D.; Adams E.E. 1998. (eds.) *Contaminated Sediments in Boston Harbor.* MIT Sea Grant College Program.

Strandberg, B.; Wagman, N.; Bergqvist, P-A.; Haglund, P.; Rappe, C. 1997. *Semipermeable membrane devices as passive samplers to determine organochlorine pollutants in compost.* Environmental Science and Technology. 31(10), 2960-2965.

Suess, M.J. 1976. *The environmental load and cycle of polycyclic aromatic hydrocarbons.* Sci. Total Environ. 6, 239-250. As cited in Neff, 1979.

Suffet, I.H.; Jafvert, C.T.; Kukkonen, J.; Servos, M.R.; Spacie, A.; Williams, L.; and Noblet, J.A. 1994. *Bioavailability: Physical, Chemical, and Biological Interactions - Influences of particulate and dissolved material on the bioavailability of organic compounds.* Pp. 93-108. As cited in Crunkilton *et al*, 1997.

Supelco Catalog: *Chromatography Products.* 1996.

Thibodeaux, L.J.; Valsaraj, K.T.; and Reible, D.D. 1994. *Capping Contaminated Sediments - The Theoretical basis and Laboratory Experimental Evidence for Chemical Containment.* In McNair, E.C. Jr. Vol. 2. Dredging '94: Proceedings of the Second

International Conference on Dredging and Dredged Material Placement. New York, American Society of Civil Engineers.

United States Army Corps of Engineers (USACOE), New England Division. Draft 1988. *Navigation Improvement Study: Feasibility Study and Environmental Assessment, Boston Harbor, Massachusetts: Mystic River, Chelsea River, and Reserved Channel.*

United States Army Corps of Engineers (USACOE), New England Division and Massachusetts Port Authority, Maritime Department. 1995. *Boston Harbor Massachusetts. Navigation Improvement Project and Berth Dredging Project: Final Environmental Impact Report and Final Environmental Impact Statement.*

United States Army Corps of Engineers (USACOE), New England Division. 1995. *Sediment Capping of Subaqueous Dredged Material Disposal Mounds. An overview of the New England Experience 1979-1993.*

United States Geological Survey (USGS). 1992. *Water Resources Data, Massachusetts and Rhode Island, Water Year 1992,* U.S. Geological Survey Water-Data Report MA-RI-92-1. As cited in Chan-Hilton *et al*, 1998.

Voelker, B.M. *Iron redox cycling in surface waters: effects of humic substances and light.* Doctoral thesis for Natural Sciences, Swiss Federal Institute of Technology Zurich.

Warshawsky, D.; Cody, T.; Radike, M.; Reilman, R.; Schumann, B.; LaDow, K.; Schneider, J. 1995. *Biotransformation of benzo(a)pyrene and other polycyclic aromatic hydrocarbons and heterocyclic analogs by several green algae and other algal species under gold and white light.* Chemico-Biological Interactions. 97: 131-148.

Yell, D.; Riddell, J. 1995. *ICE design and practice guides: Dredging.* New York. American Society of Civil Engineers.

APPENDIX A: TABLES FOR SOURCE AND SINK ESTIMATION

For further information on the nature of the data collected and the calculations of estimated loadings, the reader is referred to Section 7.2.

A1: RIVERS, CSOS, AND STORMWATER DRAINS

Measured river concentrations:

Naphthalene		
Date	*Charles (ng/l)*	*Mystic (ng/l)*
3/25/92	232.23	62.62
4/30/92	16.21	36.5
10/15/92	3.1	15
Average	83.9	38.0

Pyrene		
Date	*Charles (ng/l)*	*Mystic (ng/l)*
3/25/92	421.7	110.08
4/30/92	43.48	47.23
10/15/92	340	46
Average	268.4	67.8

Benzo[a]pyrene		
Date	*Charles (ng/l)*	*Mystic (ng/l)*
3/25/92	14.1	5.8
4/30/92	8.74	11.55
10/15/92	20	11
Average	14.3	9.5

Averaged measured CSO and stormwater drain concentrations:

Naphthalene		
Area	*CSOs (ng/l)*	*Stormwater (ng/l)*
MC conf.	84	98.3
UI Harbor	84	98.3
LI Harbor	66	98.3
FPC	66	98.3
RC	66	98.3

Pyrene		
Area	*CSOs (ng/l)*	*Stormwater (ng/l)*
MC conf.	207	815.7
UI Harbor	207	815.7
LI Harbor	235	815.7
FPC	235	815.7
RC	235	815.7

Benzo[a]pyrene		
Area	*CSOs (ng/l)*	*Stormwater (ng/l)*
MC conf.	82.5	161.9
UI Harbor	82.5	161.9
LI Harbor	107.5	161.9
FPC	107.5	161.9
RC	107.5	161.9

Estimated river loadings:

Naphthalene												
	Grid info		Flow	Conc	Flux river	flux atm	flux sed	Grid conc	Percent	Percent	Percent	Total
	I	J	(m^3/s)	(kg/m^3)	(kg/s)	(kg/s)	(kg/s)	(kg/m^3)	top	bottom	in between	Percent
Charles	16	42	8.62	8.39467E-08	7.23493E-07	5.01E-09	3.30E-09	8.49E-08	99.5	0.5	0.0	100.0
Charles	16	43	8.62	8.39467E-08	7.23493E-07	5.01E-09	3.30E-09	8.49E-08	99.5	0.5	0.0	100.0
Mystic	3	57	0.8925	3.804E-08	3.39507E-08	5.01E-09	1.67E-06	1.92E-06	2.3	97.7	0.0	100.0
Mystic	3	56	0.8925	3.804E-08	3.39507E-08	5.01E-09	1.67E-06	1.92E-06	2.3	97.7	0.0	100.0
Mystic	3	55	0.8925	3.804E-08	3.39507E-08	5.01E-09	1.67E-06	1.92E-06	2.3	97.7	0.0	100.0
Mystic	3	54	0.8925	3.804E-08	3.39507E-08	5.01E-09	1.67E-06	1.92E-06	2.3	97.7	0.0	100.0
Chelsea	61	57	0.105	3.804E-08	3.9942E-09	5.01E-09	3.30E-09	1.17E-07	44.4	26.8	3.6	100.0
Chelsea	61	56	0.105	3.804E-08	3.9942E-09	5.01E-09	3.30E-09	1.17E-07	44.4	26.8	3.6	100.0

Pyrene												
	Grid info		Flow	Conc	Flux river	flux atm	flux sed	Grid conc	Percent	Percent	Percent	Total
	I	J	(m^3/s)	(kg/m^3)	(kg/s)	(kg/s)	(kg/s)	(kg/m^3)	top	bottom	in between	Percent
Charles	16	42	8.62	2.68393E-07	2.31314E-06	3.67E-10	1.23E-09	2.69E-07	99.9	0.1	0.0	100.0
Charles	16	43	8.62	2.68393E-07	2.31314E-06	3.67E-10	1.23E-09	2.69E-07	99.9	0.1	0.0	100.0
Mystic	3	57	0.8925	6.777E-08	6.04847E-08	3.67E-10	1.39E-08	8.38E-08	81.4	18.6	0.0	100.0
Mystic	3	56	0.8925	6.777E-08	6.04847E-08	3.67E-10	1.39E-08	8.38E-08	81.4	18.6	0.0	100.0
Mystic	3	55	0.8925	6.777E-08	6.04847E-08	3.67E-10	1.39E-08	8.38E-08	81.4	18.6	0.0	100.0
Mystic	3	54	0.8925	6.777E-08	6.04847E-08	3.67E-10	1.39E-08	8.38E-08	81.4	18.6	0.0	100.0
Chelsea	61	57	0.105	6.777E-08	7.11585E-09	3.67E-10	1.39E-08	2.04E-07	5.0	68.3	3.3	100.0
Chelsea	61	56	0.105	6.777E-08	7.11585E-09	3.67E-10	1.39E-08	2.04E-07	5.0	68.3	3.3	100.0

Benzo[a]pyrene												
	Grid info		Flow	Conc	Flux river	flux atm	flux sed	Grid conc	Percent	Percent	Percent	Total
	I	J	(m^3/s)	(kg/m^3)	(kg/s)	(kg/s)	(kg/s)	(kg/m^3)	Top	bottom	in between	Percent
Charles	16	42	8.62	1.428E-08	1.23072E-07	1.17E-11	2.57E-10	1.43E-08	99.8	0.2	0.0	100.0
Charles	16	43	8.62	1.428E-08	1.23072E-07	1.17E-11	2.57E-10	1.43E-08	99.8	0.2	0.0	100.0
Mystic	3	57	0.8925	9.45E-09	8.43413E-09	1.17E-11	1.09E-09	1.07E-08	88.6	11.4	0.0	100.0
Mystic	3	56	0.8925	9.45E-09	8.43413E-09	1.17E-11	1.09E-09	1.07E-08	88.6	11.4	0.0	100.0
Mystic	3	55	0.8925	9.45E-09	8.43413E-09	1.17E-11	1.09E-09	1.07E-08	88.6	11.4	0.0	100.0
Mystic	3	54	0.8925	9.45E-09	8.43413E-09	1.17E-11	1.09E-09	1.07E-08	88.6	11.4	0.0	100.0
Chelsea	61	57	0.105	9.45E-09	9.9225E-10	1.17E-11	1.09E-09	1.06E-08	11.0	9.9	9.5	100.0
Chelsea	61	56	0.105	9.45E-09	9.9225E-10	1.17E-11	1.09E-09	1.06E-08	11.0	9.9	9.5	100.0

Estimated CSO and stormwater drain loadings:

Naphthalene																
Area Name	*CSO Name*	*I Location*	*J Location*	*Expected Flow (MG/year)*	*Additional Stormwater Flow (MG/year)*	*Total Flow (MG/year)*	*Total Flow (m^3/s)*	*Flow Weighted Conc. (ng/l)*	*Annual Total Load (kg)*	*CSO flux (kg/s)*	flux atm (kg/s)	flux sed (kg/s)	Grid Conc (kg/m^3)	Percent top	Percent Bottom	Percent in between
MC Conf.	CHE002	24	57	0.04	210.03	210.07	2.5E-02	98.3	7.8E-02	2.5E-09	5.01E-09	1 67E-06	1.36E-03	0.0	100.0	0.0
MC Conf.	CHE003	29	57	0.35	210.03	210.38	2.5E-02	98.3	7.8E-02	2.5E-09	5.01E-09	1.67E-06	1.36E-03	0.0	100.0	0.0
MC Conf.	CHE004	30	57	0.27	210.03	210.30	2.5E-02	98.3	7.8E-02	2.5E-09	5.01E-09	1.67E-06	1.42E-03	0.0	100.0	0.0
MC Conf.	CHE008	55	57	8.32	210.03	218.35	2.6E-02	97.8	8.1E-02	2.6E-09	5.01E-09	1.67E-06	1.40E-03	0.0	100.0	0.0
MC Conf.	BOS014	40	56	1.47	210.03	211.50	2.5E-02	98.2	7.9E-02	2.5E-09	5.01E-09	1.67E-06	3.59E-03	0.0	100.0	0.0
MC Conf.	BOS013	30	56	4.38	210.03	214.41	2.6E-02	98.0	8.0E-02	2.5E-09	5.01E-09	1.67E-06	6.32E-01	0.0	100.0	0.0
MC Conf.	BOS017	6	54	2.53	210.03	212.56	2.6E-02	98.1	7.9E-02	2.5E-09	5.01E-09	1.67E-06	5.61E-01	0.0	100.0	0.0
MC Conf.	MWR205	4	54	99.95	210.03	309.98	3.7E-02	93.7	1.1E-01	3.5E-09	5.01E-09	1.67E-06	5.36E-01	0.0	100.0	0.0
UI Harbor	BOS019	24	50	3.61	56.26	59.87	7.2E-03	97.4	2.2E-02	7.0E-10	5.01E-09	3.30E-09	1.25E-06	63.4	36.6	0.0
UI Harbor	BOS012	28	50	6.65	56.26	62.91	7.6E-03	96.8	2.3E-02	7.3E-10	5.01E-09	3.30E-09	1.20E-06	63.5	36.5	0.0
UI Harbor	BOS010	28	46	8.34	56.26	64.60	7.8E-03	96.5	2.4E-02	7.5E-10	5.01E-09	3.30E-09	1.17E-06	63.6	36.4	0.0
UI Harbor	BOS009	28	41	3.94	56.26	60.20	7.2E-03	97.4	2.2E-02	7.0E-10	5.01E-09	3.30E-09	1.25E-06	63.4	36.6	0.0
UI Harbor	MWR203	17	43	196.68	56.26	252.94	3.0E-02	87.2	8.3E-02	2.6E-09	5.01E-09	3.30E-09	3.61E-07	69.9	30.1	0.0
UI Harbor	BOS057	24	35	0.38	56.26	56.64	6.8E-03	98.2	2.1E-02	6.7E-10	5.01E-09	3.30E-09	1.32E-06	63.3	36.7	0.0
UI Harbor	BOS060	25	29	2.53	56.26	58.79	7.1E-03	97.7	2.2E-02	6.9E-10	5.01E-09	3.30E-09	1.28E-06	63.4	36.6	0.0
FPC	BOS064	22	27	0.04	97.07	97.11	1.2E-02	98.3	3.6E-02	1.1E-09	5.01E-09	1.44E-05	1.23E-03	0.0	100.0	0
FPC	BOS065	19	27	0.15	97.07	97.22	1.2E-02	98.3	3.6E-02	1.1E-09	5.01E-09	1.44E-05	1.23E-03	0.0	100.0	0
FPC	BOS073	18	27	4.48	97.07	101.55	1.2E-02	96.9	3.7E-02	1.2E-09	5.01E-09	1.44E-05	1.18E-03	0.0	100.0	0
FPC	BOS072	15	27	2.96	97.07	100.03	1.2E-02	97.3	3.7E-02	1.2E-09	5.01E-09	1.44E-05	1.20E-03	0.0	100.0	0
FPC	BOS070	10	27	160.05	97.07	257.12	3.1E-02	78.2	7.6E-02	2.4E-09	5.01E-09	1.44E-05	4.66E-04	0.1	99.9	0
LI Harbor	BOS007	31	32	4.26	22.81	27.07	3.2E-03	93.2	9.6E-03	3.0E-10	5.01E-09	3.30E-09	2.65E-06	61.7	38.3	0.0
LI Harbor	BOS006	34	32	1.18	22.81	23.99	2.9E-03	96.7	8.8E-03	2.8E-10	5.01E-09	3.30E-09	2.98E-06	61.6	38.4	0.0
LI Harbor	BOS005	39	32	0.06	22.81	22.87	2.7E-03	98.2	8.5E-03	2.7E-10	5.01E-09	3.30E-09	3.13E-06	61.6	38.4	0.0
LI Harbor	BOS004	40	32	4.17	22.81	26.98	3.2E-03	93.3	9.5E-03	3.0E-10	5.01E-09	3.30E-09	2.66E-06	61.7	38.3	0.0
LI Harbor	BOS003	42	32	3.2	22.81	26.01	3.1E-03	94.3	9.3E-03	2.9E-10	5.01E-09	3.30E-09	2.76E-06	61.7	38.3	0.0
RC	BOS080	60	16	4.76	23.75	28.51	3.4E-03	92.9	1.0E-02	3.2E-10	5.01E-09	3.30E-09	2.52E-06	61.8	38.2	0.0
RC	BOS079	60	8	2.09	23.75	25.84	3.1E-03	95.7	9.4E-03	3.0E-10	5.01E-09	3.30E-09	2.78E-06	61.7	38.3	0.0
RC	BOS076	60	5	47.99	23.75	71.74	8.6E-03	76.7	2.1E-02	6.6E-10	5.01E-09	3.30E-09	1.04E-06	63.3	36.7	0.0
RC	BOS078	60	6	11.69	23.75	35.44	4.3E-03	87.6	1.2E-02	3.7E-10	5.01E-09	3.30E-09	2.04E-06	62.0	38.0	0.0

Pyrene																
Area Area	*CSO Name*	*I Location*	*J Location*	*Expected Flow (MG/year)*	*Additional Stormwater Flow (MG/year)*	*Total Flow (MG/year)*	*Total Flow (m^3/s)*	*Flow Weighted Conc (ng/l)*	*Annual Total Load (kg)*	*CSO flux (kg/s)*	flux atm (kg/s)	flux sed (kg/s)	Grid Conc (kg/m^3)	Percent top	Percent Bottom	Percent in between
MC Conf.	CHE002	24	57	0.04	210.03	210.07	2.5E-02	815.6	6.5E-01	2.1E-08	3.67E-10	1.39E-08	1.38E-06	60.1	39.9	0.0
MC Conf.	CHE003	29	57	0.35	210.03	210.38	2.5E-02	814.7	6.5E-01	2.1E-08	3.67E-10	1.39E-08	1.38E-06	60.1	39.9	0.0
MC Conf.	CHE004	30	57	0.27	210.03	210.30	2.5E-02	814.9	6.5E-01	2.1E-08	3.67E-10	1.39E-08	1.38E-06	60.1	39.9	0.0
MC Conf.	CHE008	55	57	8.32	210.03	218.35	2.6E-02	792.5	6.5E-01	2.1E-08	3.67E-10	2.47E-09	9.01E-07	89.5	10.5	0.0
MC Conf.	BOS014	40	56	1.47	210.03	211.50	2.5E-02	811.5	6.5E-01	2.1E-08	3.67E-10	1.39E-08	1.37E-06	60.1	39.9	0.0
MC Conf.	BOS013	30	56	4.38	210.03	214.41	2.6E-02	803.3	6.5E-01	2.1E-08	3.67E-10	1.39E-08	1.36E-06	60.2	39.8	0.0
MC Conf.	BOS017	6	54	2.53	210.03	212.56	2.6E-02	808.5	6.5E-01	2.1E-08	3.67E-10	1.39E-08	1.37E-06	60.2	39.8	0.0
MC Conf.	MWR205	4	54	99.95	210.03	309.98	3.7E-02	619.4	7.3E-01	2.3E-08	3.67E-10	1.39E-08	1.00E-06	62.7	37.3	0.0
UI Harbor	BOS019	24	50	3.61	56.26	59.87	7.2E-03	779.0	1.8E-01	5.6E-09	3.67E-10	1.23E-09	1.00E-06	82.9	17.1	0.0
UI Harbor	BOS012	28	50	6.65	56.26	62.91	7.6E-03	751.4	1.8E-01	5.7E-09	3.67E-10	1.23E-09	9.62E-07	83.1	16.9	0.0
UI Harbor	BOS010	28	46	8.34	56.26	64.60	7.8E-03	737.1	1.8E-01	5.7E-09	3.67E-10	1.23E-09	9.43E-07	83.2	16.8	0.0
UI Harbor	BOS009	28	41	3.94	56.26	60.20	7.2E-03	775.9	1.8E-01	5.6E-09	3.67E-10	1.23E-09	9.96E-07	83.0	17.0	0.0
UI Harbor	MWR203	17	43	196.68	56.26	252.94	3.0E-02	342.4	3.3E-01	1.0E-08	3.67E-10	1.23E-09	3.95E-07	89.8	10.2	0.0
UI Harbor	BOS057	24	35	0.38	56.26	56.64	6.8E-03	811.6	1.7E-01	5.5E-09	3.67E-10	8.86E-10	9.96E-07	86.9	13.1	0.0
UI Harbor	BOS060	25	29	2.53	56.26	58.79	7.1E-03	789.5	1.8E-01	5.6E-09	3.67E-10	8.86E-10	9.67E-07	87.0	13.0	0.0
FPC	BOS064	22	27	0.04	97.07	97.11	1.2E-02	815.5	3.0E-01	9.5E-09	3.67E-10	1.85E-08	2.44E-06	34.7	65.3	0.0
FPC	BOS065	19	27	0.15	97.07	97.22	1.2E-02	814.8	3.0E-01	9.5E-09	3.67E-10	1.85E-08	2.44E-06	34.7	65.3	0.0
FPC	BOS073	18	27	4.48	97.07	101.55	1.2E-02	790.1	3.0E-01	9.6E-09	3.67E-10	1.85E-08	2.34E-06	35.0	65.0	0.0
FPC	BOS072	15	27	2.96	97.07	100.03	1.2E-02	798.5	3.0E-01	9.6E-09	3.67E-10	1.85E-08	2.37E-06	34.9	65.1	0.0
FPC	BOS070	10	27	160.05	97.07	257.12	3.1E-02	454.2	4.4E-01	1.4E-08	3.67E-10	1.85E-08	1.07E-06	43.7	56.3	0.0
LI Harbor	BOS007	31	32	4.26	22.81	27.07	3.2E-03	724.3	7.4E-02	2.4E-09	3.67E-10	8.86E-10	1.11E-06	75.4	24.6	0.0
LI Harbor	BOS006	34	32	1.18	22.81	23.99	2.9E-03	787.1	7.1E-02	2.3E-09	3.67E-10	8.86E-10	1.22E-06	74.8	25.2	0.0
LI Harbor	BOS005	39	32	0.06	22.81	22.87	2.7E-03	814.2	7.0E-02	2.2E-09	3.67E-10	8.86E-10	1.27E-06	74.6	25.4	0.0
LI Harbor	BOS004	40	32	4.17	22.81	26.98	3.2E-03	725.9	7.4E-02	2.4E-09	3.67E-10	8.86E-10	1.11E-06	75.4	24.6	0.0
LI Harbor	BOS003	42	32	3.2	22.81	26.01	3.1E-03	744.3	7.3E-02	2.3E-09	3.67E-10	8.86E-10	1.15E-06	75.2	24.8	0.0
RC	BOS080	60	16	4.76	23.75	28.51	3.4E-03	718.7	7.8E-02	2.5E-09	3.67E-10	4.33E-10	9.52E-07	86.7	13.3	0.0
RC	BOS079	60	8	2.09	23.75	25.84	3.1E-03	768.7	7.5E-02	2.4E-09	3.67E-10	4.33E-10	1.03E-06	86.4	13.6	0.0
RC	BOS076	60	5	47.99	23.75	71.74	8.6E-03	427.2	1.2E-01	3.7E-09	3.67E-10	4.33E-10	5.20E-07	90.3	9.7	0.0
RC	BOS078	60	6	11.69	23.75	35.44	4.3E-03	624.2	8.4E-02	2.7E-09	3.67E-10	4.33E-10	8.12E-07	87.5	12.5	0.0

Benzo[a]pyrene																
Area Name	*CSO Name*	*I Location*	*J Location*	*Expected Flow (MG/year)*	*Additional Stormwater Flow (MG/year)*	*Total Flow (MG/year)*	*Total Flow (m^3/s)*	*Flow Weighted BAP conc (ng/l)*	*Annual Total Load (kg)*	*CSO* flux (kg/s)	flux atm (kg/s)	flux sed (kg/s)	*Grid* Conc (kg/m^3)	Percent top	Percent Bottom	*Percent in between*
MC Conf.	CHE002	24	57	0.04	210.03	210.07	2.5E-02	161.9	1.3E-01	4.1E-09	1.17E-11	1.09E-09	2.1E-07	79.0	21.0	0.0
MC Conf.	CHE003	29	57	0.35	210.03	210.38	2.5E-02	161.8	1.3E-01	4.1E-09	1.17E-11	1.09E-09	2.1E-07	79.0	21.0	0.0
MC Conf.	CHE004	30	57	0.27	210.03	210.30	2.5E-02	161.8	1.3E-01	4.1E-09	1.17E-11	1.09E-09	2.1E-07	79.0	21.0	0.0
MC Conf.	CHE008	55	57	8.32	210.03	218.35	2.6E-02	159.8	1.3E-01	4.2E-09	1.17E-11	1.06E-10	1.6E-07	97.5	2.5	0.0
MC Conf.	BOS014	40	56	1.47	210.03	211.50	2.5E-02	161.5	1.3E-01	4.1E-09	1.17E-11	1.09E-09	2.0E-07	79.1	20.9	0.0
MC Conf.	BOS013	30	56	4.38	210.03	214.41	2.6E-02	160.8	1.3E-01	4.1E-09	1.17E-11	1.09E-09	2.0E-07	79.2	20.8	0.0
MC Conf.	BOS017	6	54	2.53	210.03	212.56	2.6E-02	161.3	1.3E-01	4.1E-09	1.17E-11	1.09E-09	2.0E-07	79.1	20.9	0.0
MC Conf.	MWR205	4	54	99.95	210.03	309.98	3.7E-02	144.4	1.7E-01	5.4E-09	1.17E-11	1.09E-09	1.74E-07	83.2	16.8	0.0
UI Harbor	BOS019	24	50	3.61	56.26	59.87	7.2E-03	158.6	3.6E-02	1.1E-09	1.17E-11	2.57E-10	1.96E-07	81.8	18.2	0.0
UI Harbor	BOS012	28	50	6.65	56.26	62.91	7.6E-03	156.1	3.7E-02	1.2E-09	1.17E-11	2.57E-10	1.92E-07	82.2	17.8	0.0
UI Harbor	BOS010	28	46	8.34	56.26	64.60	7.8E-03	154.9	3.8E-02	1.2E-09	1.17E-11	2.57E-10	1.90E-07	82.5	17.5	0.0
UI Harbor	BOS009	28	41	3.94	56.26	60.20	7.2E-03	158.3	3.6E-02	1.1E-09	1.17E-11	2.57E-10	1.96E-07	81.8	18.2	0.0
UI Harbor	MWR203	17	43	196.68	56.26	252.94	3.0E-02	119.6	1.1E-01	3.6E-09	1.17E-11	2.57E-10	1.28E-07	93.4	6.6	0.0
UI Harbor	BOS057	24	35	0.38	56.26	56.64	6.8E-03	161.5	3.5E-02	1.1E-09	1.17E-11	7.00E-11	1.74E-07	94.1	5.9	0.0
UI Harbor	BOS060	25	29	2.53	56.26	58.79	7.1E-03	159.6	3.6E-02	1.1E-09	1.17E-11	7.00E-11	1.71E-07	94.2	5.8	0.0
FPC	BOS064	22	27	0.04	97.07	97.11	1.2E-02	161.9	5.9E-02	1.9E-09	1.17E-11	3.41E-09	4.55E-07	35.8	64.2	0.0
FPC	BOS065	19	27	0.15	97.07	97.22	1.2E-02	161.8	6.0E-02	1.9E-09	1.17E-11	3.41E-09	4.55E-07	35.8	64.2	0.0
FPC	BOS073	18	27	4.48	97.07	101.55	1.2E-02	159.5	6.1E-02	1.9E-09	1.17E-11	3.41E-09	4.40E-07	36.4	63.6	0.0
FPC	BOS072	15	27	2.96	97.07	100.03	1.2E-02	160.3	6.1E-02	1.9E-09	1.17E-11	3.41E-09	4.45E-07	36.2	63.8	0.0
FPC	BOS070	10	27	160.05	97.07	257.12	3.1E-02	128.0	1.2E-01	4.0E-09	1.17E-11	3.41E-09	2.39E-07	53.8	46.2	0.0
LI Harbor	BOS007	31	32	4.26	22.81	27.07	3.2E-03	153.3	1.6E-02	5.0E-10	1.17E-11	7.00E-11	1.78E-07	87.9	12.1	0.0
LI Harbor	BOS006	34	32	1.18	22.81	23.99	2.9E-03	159.2	1.4E-02	4.6E-10	1.17E-11	7.00E-11	1.88E-07	87.0	13.0	0.0
LI Harbor	BOS005	39	32	0.06	22.81	22.87	2.7E-03	161.8	1.4E-02	4.4E-10	1.17E-11	7.00E-11	1.92E-07	86.7	13.3	0.0
LI Harbor	BOS004	40	32	4.17	22.81	26.98	3.2E-03	153.5	1.6E-02	5.0E-10	1.17E-11	7.00E-11	1.79E-07	87.9	12.1	0.0
LI Harbor	BOS003	42	32	3.2	22.81	26.01	3.1E-03	155.2	1.5E-02	4.8E-10	1.17E-11	7.00E-11	1.81E-07	87.6	12.4	0.0
RC	BOS080	60	16	4.76	23.75	28.51	3.4E-03	152.8	1.6E-02	5.2E-10	1.17E-11	5.09E-11	1.71E-07	91.3	8.7	0.0
RC	BOS079	60	8	2.09	23.75	25.84	3.1E-03	157.5	1.5E-02	4.9E-10	1.17E-11	5.09E-11	1.78E-07	90.8	9.2	0.0
RC	BOS076	60	5	47.99	23.75	71.74	8.6E-03	125.5	3.4E-02	1.1E-09	1.17E-11	5.09E-11	1.33E-07	95.5	4.5	0.0
RC	BOS078	60	6	11.69	23.75	35.44	4.3E-03	144.0	1.9E-02	6.1E-10	1.17E-11	5.09E-11	1.59E-07	92.5	7.5	0.0

A2: SEDIMENT FLUX AND ATMOSPHERIC DEPOSITION

Naphthalene													
	Grids	fraction area	Cs (ng/g)	Ks (m^3/g)	delta (m)	Dtot (m^2/s)	J sed (ng/m^2s)	J sed grid (kg/s)	J Atmos (ng/m^2s)	J atmos grid (kg/s)	J grid total (kg/s)	Percent bottom	Percent top
Chelsea River	(I61,J56&57) to (I51,J56&57)	0.03	10	3.02E-05	0.0005	4.16E-10	0.275411991	3.29559E-09	0.419088343	5.01483E-09	8.31043E-09	39.7	60.3
Confluence	all of Mystic and rest of Chelsea, down to J=48	0.25	5082	3.02E-05	0.0005	4.16E-10	139.9643737	1.67482E-06	0.419088343	5.01483E-09	1.67984E-06	99.7	0.3
Charles	down to J=32	0.14	10	3.02E-05	0.0005	4.16E-10	0.275411991	3.29559E-09	0.419088343	5.01483E-09	8.31043E-09	39.7	60.3
FPC area	all down, goto I=50	0.35	10	3.02E-05	0.0005	4.16E-10	0.275411991	3.29559E-09	0.419088343	5.01483E-09	8.31043E-09	39.7	60.3
FPC data	fpc only	0.02	43628	3.02E-05	0.0005	4.16E-10	1201.567433	1.4378E-05	0.419088343	5.01483E-09	1.4383E-05	100.0	0.0
RC	rest	0.21	10	3.02E-05	0.0005	4.16E-10	0.275411991	3.29559E-09	0.419088343	5.01483E-09	8.31043E-09	39.7	60.3

Pyrene													
	Grids	fraction area	Cs (ng/g)	Ks (m^3/g)	delta (m)	Dtot (m^2/s)	J sed (ng/m^2s)	J sed grid (kg/s)	J Atmos (ng/m^2s)	J atmos grid (kg/s)	J grid total (kg/s)	Percent bottom	Percent top
Chelsea River	(I61,J56&57) to (I51,J56&57)	0.03	8917	2.70E-02	0.0005	3.13E-10	0.206742296	2.47389E-09	0.030655881	3.6683E-10	2.84072E-09	87.1	12.9
Confluence	all of Mystic and rest of Chelsea, down to J=48	0.25	50127	2.70E-02	0.0005	3.13E-10	1.162203778	1.3907E-08	0.030655881	3.6683E-10	1.42738E-08	97.4	2.6
Charles	down to J=32	0.14	4419	2.70E-02	0.0005	3.13E-10	0.102455333	1.22599E-09	0.030655881	3.6683E-10	1.59282E-09	77.0	23.0
FPC area	all down, goto I=50	0.35	3195	2.70E-02	0.0005	3.13E-10	0.074076667	8.86405E-10	0.030655881	3.6683E-10	1.25324E-09	70.7	29.3
FPC data	fpc only	0.02	66831	2.70E-02	0.0005	3.13E-10	1.549489111	1.85413E-08	0.030655881	3.6683E-10	1.89081E-08	98.1	1.9
RC	rest	0.21	1559	2.70E-02	0.0005	3.13E-10	0.036145704	4.32521E-10	0.030655881	3.6683E-10	7.99351E-10	54.1	45.9

Benzo[a]pyrene													
	Grids	fraction area	Cs (ng/g)	Ks (m^3/g)	delta (m)	Dtot (m^2/s)	J sed (ng/m^2s)	J sed grid (kg/s)	J Atmos (ng/m^2s)	J atmos grid (kg/s)	J grid total (kg/s)	Percent bottom	Percent top
Chelsea River	(I61,J56&57) to (I51,J56&57)	0.03	2950	2.50E-01	0.001	7.50E-10	0.00885	1.059E-10	0.000976662	1.16868E-11	1.17586E-10	90.1	9.9
Confluence	all of Mystic and rest of Chelsea, down to J=48	0.25	30277	2.50E-01	0.001	7.50E-10	0.090831	1.08689E-09	0.000976662	1.16868E-11	1.09858E-09	98.9	1.1
Charles	down to J=32	0.14	7159	2.50E-01	0.001	7.50E-10	0.021477	2.56995E-10	0.000976662	1.16868E-11	2.68682E-10	95.7	4.3
FPC area	all down, goto I=50	0.35	1949	2.50E-01	0.001	7.50E-10	0.005847	6.99655E-11	0.000976662	1.16868E-11	8.16523E-11	85.7	14.3
FPC data	fpc only	0.02	94984	2.50E-01	0.001	7.50E-10	0.284952	3.40975E-09	0.000976662	1.16868E-11	3.42144E-09	99.7	0.3
RC	Rest	0.21	1418	2.50E-01	0.001	7.50E-10	0.004254	5.09036E-11	0.000976662	1.16868E-11	6.25904E-11	81.3	18.7

A3: AIR-WATER EXCHANGE

u_{10} (m/s)	6.12

Water			
Va	1.524	Da	0.26

Air			
Vw	0.0018982	Dw	0.000021

	Naphthalene	Pyrene	Benzo[a]pyrene	
K_H'	1.97E-02	4.44E-04	5.00E-05	
	6.78E-03	1.41E-04	1.30E-05	Adjusted for temperature*
	8.80E-03	1.92E-04	1.76E-05	Adjusted for salinity*
Dw(cm2/s)	8.22E-06	6.62E-06	5.84E-06	
Da(cm2/s)	9.70E-02	7.76E-02	6.90E-02	
Va (cm/s)	7.87E-01	6.78E-01	6.27E-01	
Vw (cm/s)	1.19E-03	1.07E-03	1.00E-03	
$1/V_{tot}$	9.86E+02	8.63E+03	9.15E+04	
V_{tot} (cm/s)	1.01E-03	1.16E-04	1.09E-05	
V_{tot} (m/day)	8.76E-01	1.00E-01	9.44E-03	
kaw (day^{-1})	8.76E-02	1.00E-02	9.44E-04	

* For details on the nature of adjustments made for salinity and temperature, see Appendix B.

A4: PHOTODEGRADATION:

					napthalene		pyrene/benzo[a]pyrene	
λ nm	λ range nm	W(noon, λ) (millieinstein/cm^2/s	W(cloudy)	α(λ) cm^{-1}	ε(λ) cm^{-1}M^{-1}	k(λ) **	ε(λ) cm^{-1}M^{-1}	k(λ) **
297.5	2.5	0.00E+00	0.00E+00	4.30E-02	1259	0.00E+00	10000	0.00E+00
300	2.5	1.00E-10	2.28E-06	4.15E-02	398	2.18E-05	7943	4.36E-04
302.5	2.5	4.98E-10	1.13E-05	3.95E-02	316	9.08E-05	3981	1.14E-03
305	2.5	2.31E-09	5.26E-05	3.75E-02	251	3.52E-04	3981	5.59E-03
307.5	2.5	6.12E-09	1.39E-04	3.55E-02	158	6.21E-04	3981	1.56E-02
310	2.5	1.16E-08	2.64E-04	3.35E-02	158	1.25E-03	3981	3.14E-02
312.5	2.5	2.41E-08	5.49E-04	3.20E-02	158	2.71E-03	3981	6.83E-02
315	2.5	3.69E-08	8.41E-04	3.05E-02	126	3.47E-03	3981	1.10E-01
317.5	2.5	4.92E-08	1.12E-03	2.90E-02	100	3.87E-03	3981	1.54E-01
320	2.5	6.78E-08	1.54E-03	2.75E-02	79	4.44E-03	3981	2.24E-01
323.1	3.75	1.23E-07	2.80E-03	2.60E-02	79	8.51E-03	3981	4.29E-01
330	10	4.63E-07	1.05E-02	2.20E-02	10	4.79E-03	3981	1.91E+00
340	10	5.66E-07	1.29E-02	1.85E-02	0	0.00E+00	6309	4.40E+00
350	10	6.03E-07	1.37E-02	1.50E-02	0	0.00E+00	3162	2.90E+00
360	10	6.36E-07	1.45E-02	1.25E-02	0	0.00E+00	2511	2.91E+00
370	10	6.94E-07	1.58E-02	1.00E-02	0	0.00E+00	1000	1.58E+00
380	10	7.48E-07	1.70E-02	8.30E-03	0	0.00E+00	316	6.49E-01
390	10	1.07E-06	2.44E-02	6.90E-03	0	0.00E+00	32	1.13E-01
400	10	1.55E-06	3.53E-02	5.50E-03	0	0.00E+00	10	6.42E-02
420	10	6.19E-06	1.41E-01	4.20E-03	0	0.00E+00	0	0.00E+00
450	10	7.92E-06	1.80E-01	2.80E-03	0	0.00E+00	0	0.00E+00
					k_a=	3.01E-02	k_a=	1.56E+01

** Units are in einstein(mol compound)$^{-1}$d^{-1}

Compound	Φ_r	k_p (s^{-1})
Naphthalene	1.50E-02	4.5E-04
Pyrene	2.00E-03	3.6E-07
Benzo[a]pyrene	8.90E-04	1.6E-07

APPENDIX B: TEMPERATURE AND SALINITY ADJUSTMENTS

As explained in Section 7.2, the flux of chemical contaminants is highly dependent on the ambient conditions in the environment. Factors such as temperature and salinity must be taken into account to accurately model the distribution of chemical compounds in a natural system. This appendix describes the changes made to the K_d and K_H partitioning coefficients used in the chemical flux calculations.

The solid-water partitioning coefficient was adjusted for temperature using equation 7.4 in section 7.2.4 of this report. The enthalpies of solution (ΔH_s^e) for both naphthalene and pyrene were given in Wauchope and Getzen (1972) as quoted by Schwarzenbach et. al. (1993). However, no information was given on benzo[a]pyrene. However, Schwarzenbach et. al. notes that several properties of a chemical compound are roughly correlated to its molecular weight. Graphing the known ΔH_s^e values for various PAHs as a function of molecular weight produces the graph shown in figure B.1.

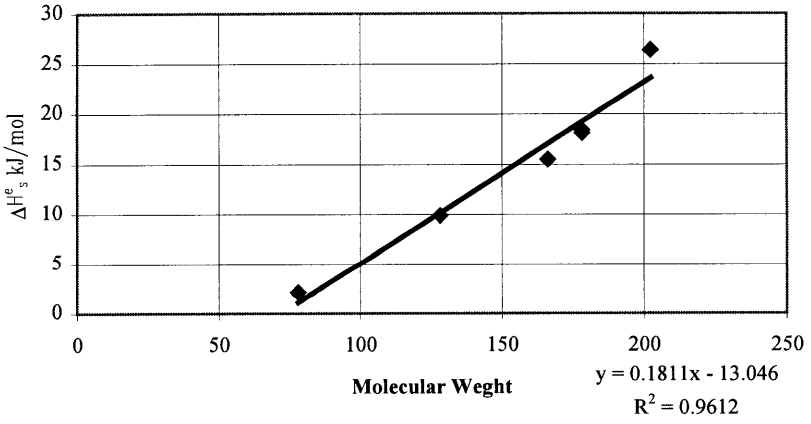

Figure B.1 - Enthalpy of solutions as a function of molecular weight in PAHs.

ΔH_s^e for benzo[a]pyrene was estimated using the relationship derived above. These values were then used to calculate the change in K_d which would occur if the temperature

was about 3° Celsius, which is typical of winter conditions. The resulting partition coefficients are given in Table B.1.

Table B.1
K_d values for naphthalene, pyrene, and benzo[a]pyrene adjusted for a temperature of 3° Celsius.

	temp (K)	naphthalene	pyrene	benzo[a]pyrene
Kd (25 deg)	2.98E+02	3.02E-02	1.62E+01	5.00E+01
ΔH_s^e (kJ/mol)		9.90E+00	2.64E+01	*3.26E+01
K(25)/K(3)		9.99E-01	5.95E-01	2.00E-01
Kd (3 deg)	2.76E+02	3.02E-02	2.72E+01	2.49E+02

(*) denotes data estimated from molecular weight.

Similarly, dimensionless Henry's law constants were adjusted for temperature using equation 7.8 given in the same section of text. In addition to the ΔH_s^e values calculated above, adjusting $K_H^{'}$ for temperature also requires heat of vaporization (ΔH_{vap}) values for each of the compounds. ΔH_{vap} data was given for naphthalene in Schwarzenbach et. al.'s text. However, data was lacking for both pyrene and benzo[a]pyrene. A relationship was derived expressing ΔH_{vap} as a function of molecular weight. The results are given in figure B.2.

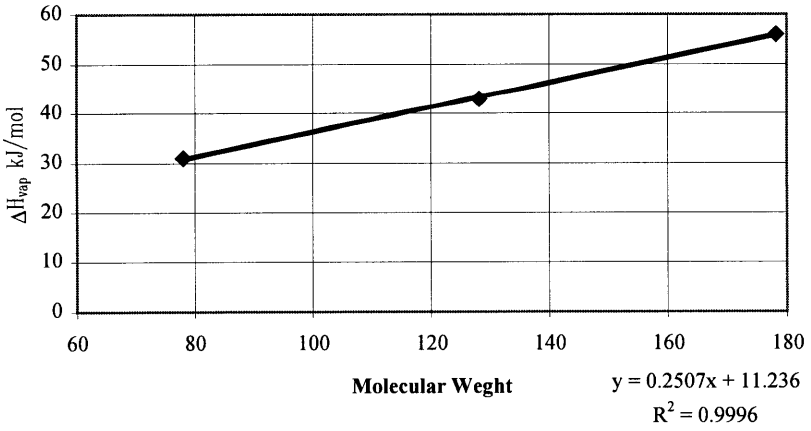

Figure B.2 - Heat of vaporization as a function of molecular weight in PAHs.

This relationship was used to estimate ΔH_{vap} for both pyrene and benzo[a]pyrene. The ΔH_{vap} and ΔH_s^e values were used to estimate the value of $K_H^{'}$ at 3° Celsius. The resulting $K_H^{'}$ values, along with the estimated ΔH_{vap} and ΔH_s^e values, are summarized in table B.2.

Table B.2

$K_H^{'}$ values for naphthalene, pyrene, and benzo[a]pyrene adjusted for a temperature of 3° Celsius.

	temp (K)	naphthalene	Pyrene	benzo[a]pyrene
K_H' (25)	2.98E+02	1.97E-02	4.44E-04	5.00E-05
ΔH_{vap} (kJ/mol)		4.30E+01	*6.20E+01	*7.45E+01
ΔH_s^e (kJ/mol)		9.90E+00	2.64E+01	*3.26E+01
K_H' (3)	2.76E+02	6.78E-03	1.41E-04	1.30E-05

(*) denotes data estimated from molecular weight.

The dimensionless Henry's law constants were also adjusted to take into account salinity conditions near the surface of the Inner Harbor. This was done by adjusting the saturation concentration (C_w^{sat}) of each compound with the Setschenow, or "salting out", constant (K^s) using equation B.1 as explained in Schwarzenbach et. al. (1993).

$$\log[\frac{C_w^{sat}}{C_{w,salt}^{sat}}] = K^s[salt]_t \qquad \text{B.1}$$

The value of K^s changes depending on which compound and which salt is examined. In natural systems, water contains many different types of salts. In this case, the K^s used in equation B.1 is a weighted average of the K^s values for the different salts in the system. In mathematical terms:

$$K^s = \sum_i K_i^s x_i \qquad \text{B.2}$$

where x_i is the mole fraction and K_i^s is the salting constant for salt i in a system.

Salting constants were taken from Schwarzenbach's text. These values were used to estimate the salting constant for naphthalene in Boston Harbor (salinity = 30 psu). The results are shown in table B.3.

Table B.3

Estimation of K^s for naphthalene.

	$[salt]_i$	K_s	x_i	$K_s * x_i$
NaCl	3.52E-01	2.20E-01	8.00E-01	1.76E-01
KCl	8.02E-03	1.90E-01	1.82E-02	3.46E-03
CaCl2	8.83E-03	3.20E-01	2.01E-02	6.42E-03
MgCl2	4.53E-02	3.00E-01	1.03E-01	3.09E-02
Na2SO4	2.42E-02	7.00E-01	5.50E-02	3.85E-02
NaHCO3	1.59E-03	3.20E-01	3.61E-03	1.16E-03
			$\Sigma K_s * x_i$	0.256463

Setschenow constants for individual salts were not available for pyrene or benzo[a]pyrene. Instead, Schwarzenbach gives 0.3 as a typical salting constant for compounds similar to pyrene in natural conditions. Due to lack of data, this value was used as an estimate for K^s for both pyrene and benzo[a]pyrene.

Salinity adjustments were not made for sediment-water partitioning coefficients, since McGroddy measured K_d values *in-situ*. Thus, the partitioning coefficients already account for salinity in the harbor.

APPENDIX C: WEATHER CONDITIONS IN BOSTON HARBOR

Boston Logan International Airport
Average Daily Wind Speed in MPH
Jan 1990- June 1996

Wind	Average	Std. Dev.	# pts
December	13.80	4.46	186
January	13.27	3.97	217
February	14.13	3.95	169
Winter	13.70	4.14	572
June	11.44	2.88	210
July	11.06	2.37	186
August	11.41	2.65	186
Summer	11.31	2.65	582

Boston
Ave. Monthly Temperature in Fahrenheit
January 1915 - March 1997

Temp	Average	Std. Dev.	# pts
December	33.40	4.03	82
January	29.37	4.18	83
February	30.30	3.72	83
Winter	31.01	4.32	248
June	67.56	2.66	82
July	73.19	2.32	82
August	71.66	2.46	82
Summer	70.80	2.34	246

Boston Logan International Airport
Ave. Tot. Monthly Precipitation in Meters
January 1990 - March 1996

Rain	Average	Std. Dev.	# pts
December	4.87	2.26	6
January	4.18	1.73	7
February	3.02	1.07	7
Winter	4.11	1.80	20
June	2.06	1.47	6
July	2.38	0.89	6
August	0.14	2.63	6
Summer	2.88	1.96	18

Boston Logan International Airport
Average Daily Sunshine in Minutes
January 1990 - March 1995

Sun	Average	Std. Dev.	# pts
December	264.16	217.06	186
January	285.44	220.92	217
February	355.22	236.89	197
Winter	301.76	228.01	600
June	604.74	307.37	180
July	576.98	267.43	186
August	557.40	266.02	186
Summer	579.44	280.78	552

Boston Logan International Airport
Daily Percent of Total Sunshine
January 1990 - February 1996

Sun	Average	Std. Dev.	# pts
December	48.12	39.55	186
January	49.96	38.57	217
February	56.39	37.53	198
Winter	51.51	38.62	600
June	66.22	33.64	180
July	64.38	29.71	186
August	67.18	32.15	186
Summer	65.93	31.82	552

Data from:
National Climatic Data Center: www.ncdc.noaa.gov/onlineprod/drought/xmgr.html
National Weather Service: www.nws.noaa.gov/er/box/climate.html

APPENDIX D: HORIZONTAL DISTRIBUTION OF BENZO[A]PYRENE

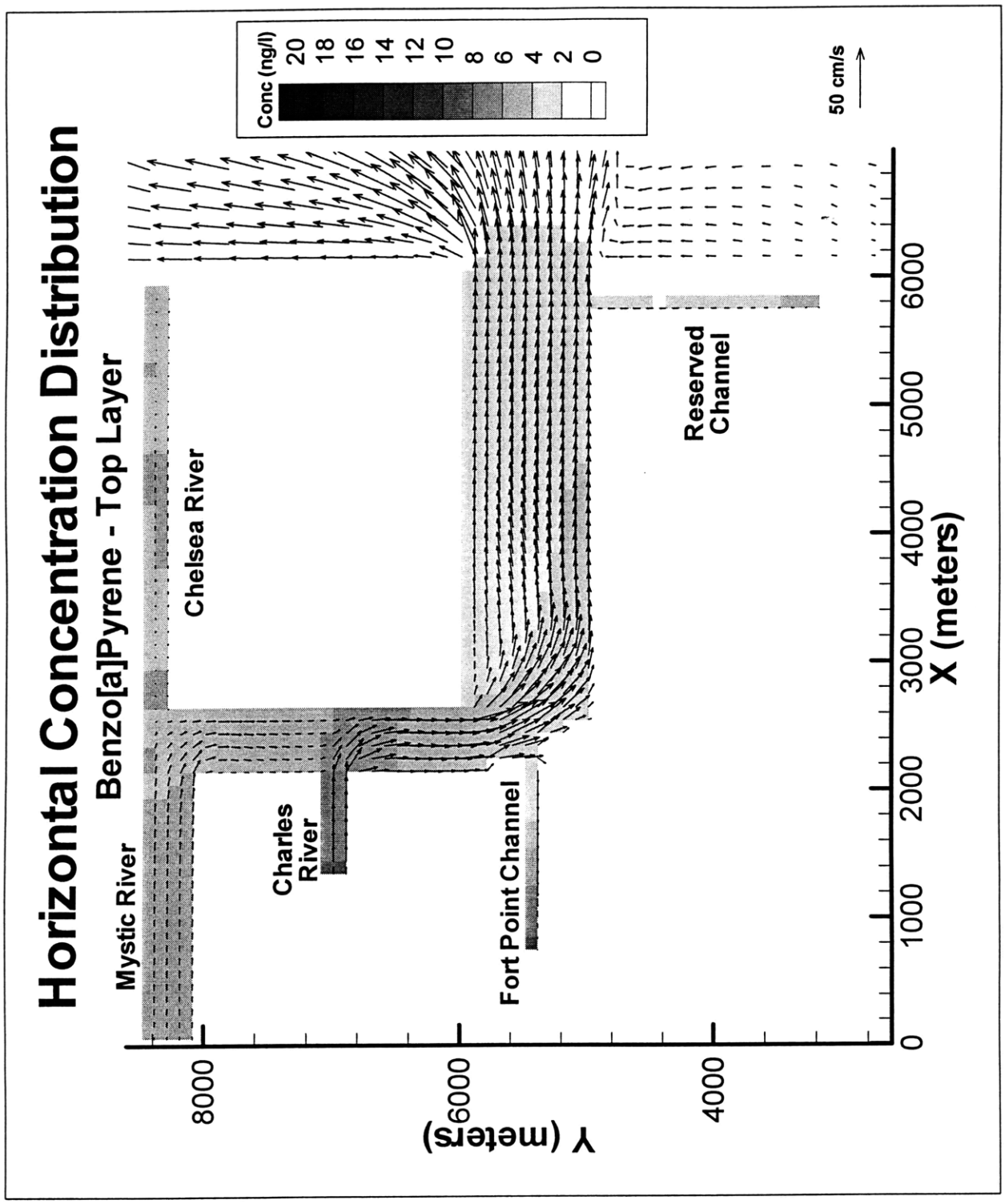

Figure D.1 – Flow and Concentration Distribution for Benzo[a]pyrene at the Surface at t = 114 hs (descending)

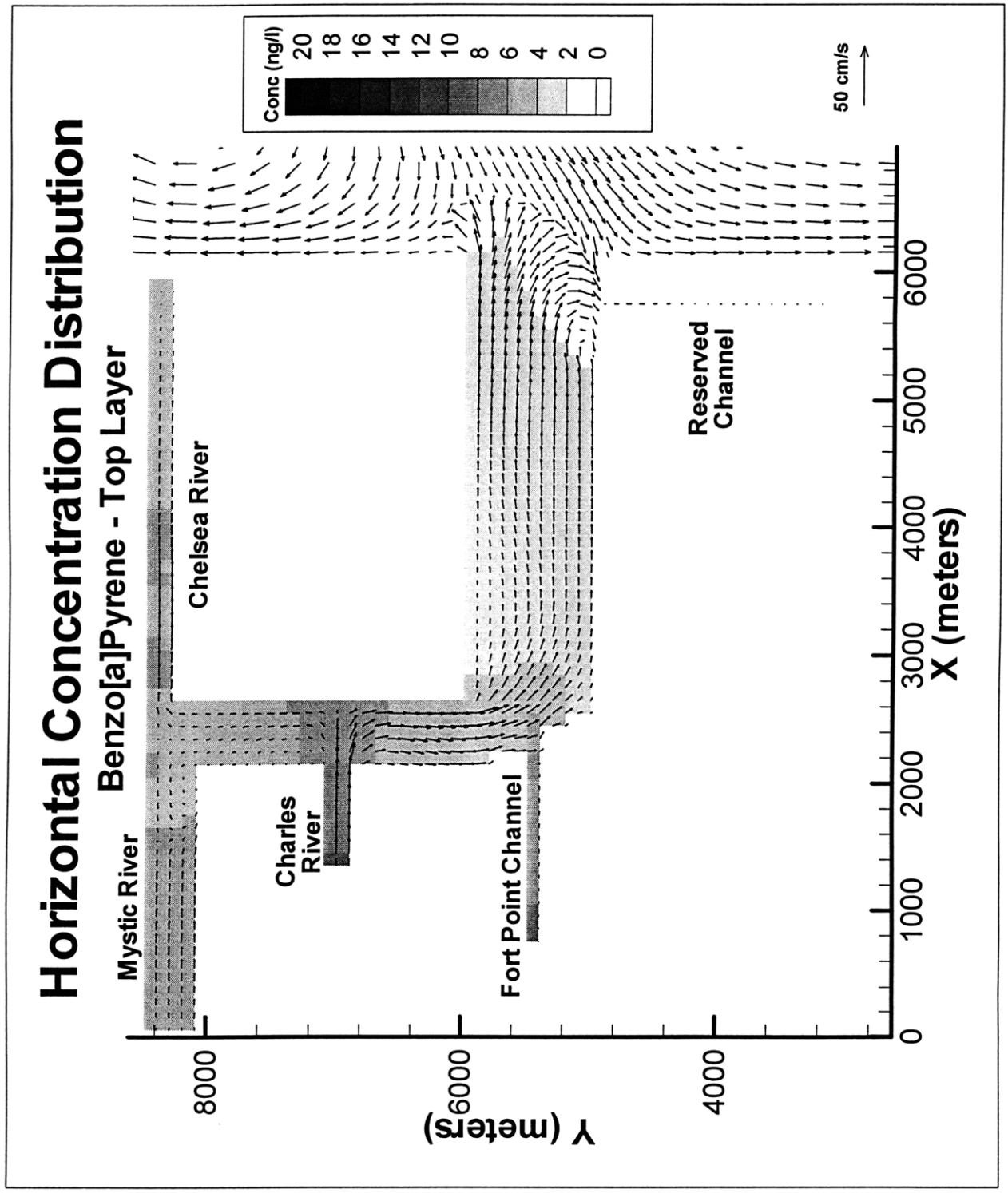

Figure D.2 – Flow and Concentration Distribution for Benzo[a]pyrene at the Surface at t = 147 hs (low tide)

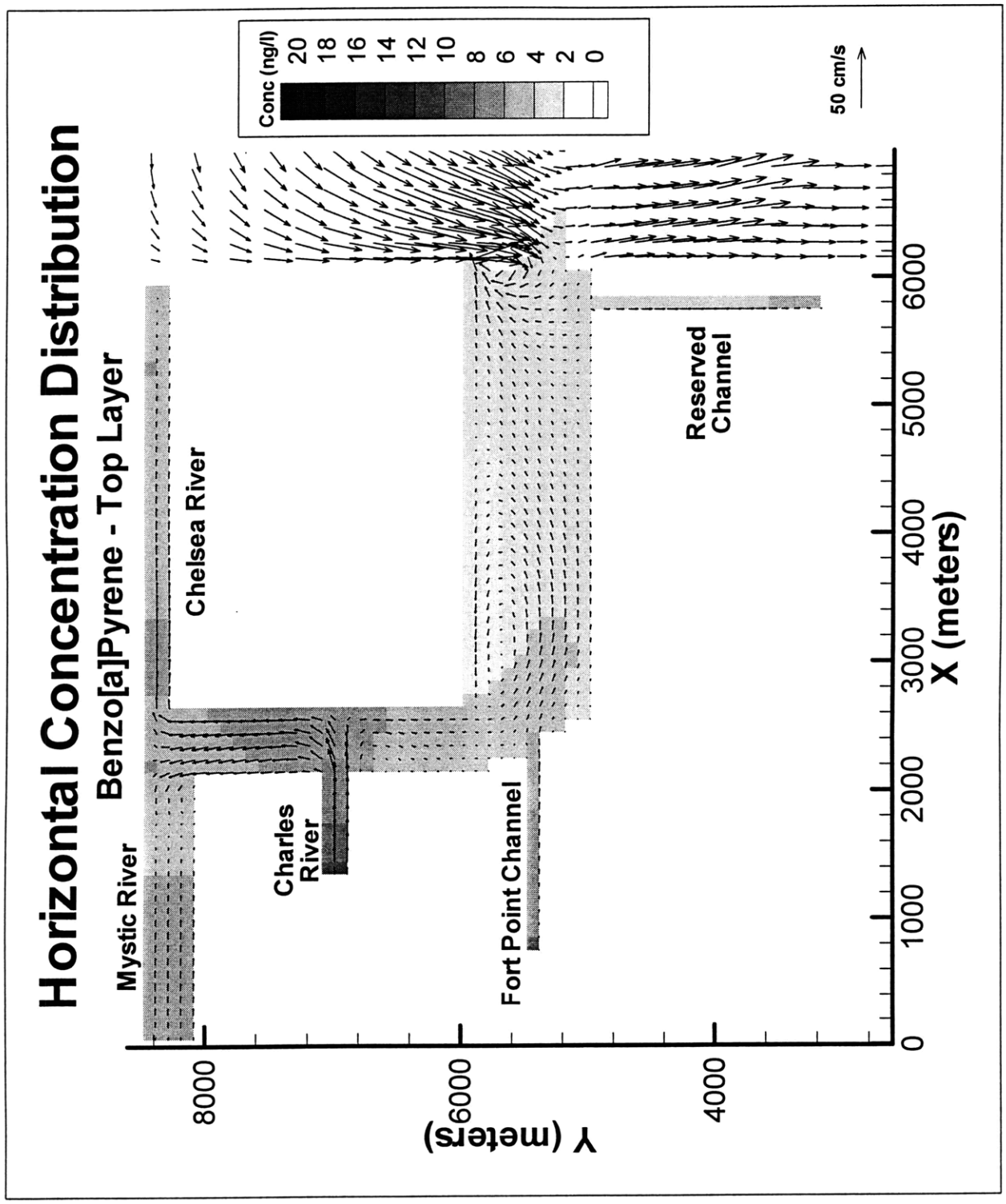

Figure D.3 – Flow and Concentration Distribution for Benzo[a]pyrene at the Surface at t = 150 hs (ascending)

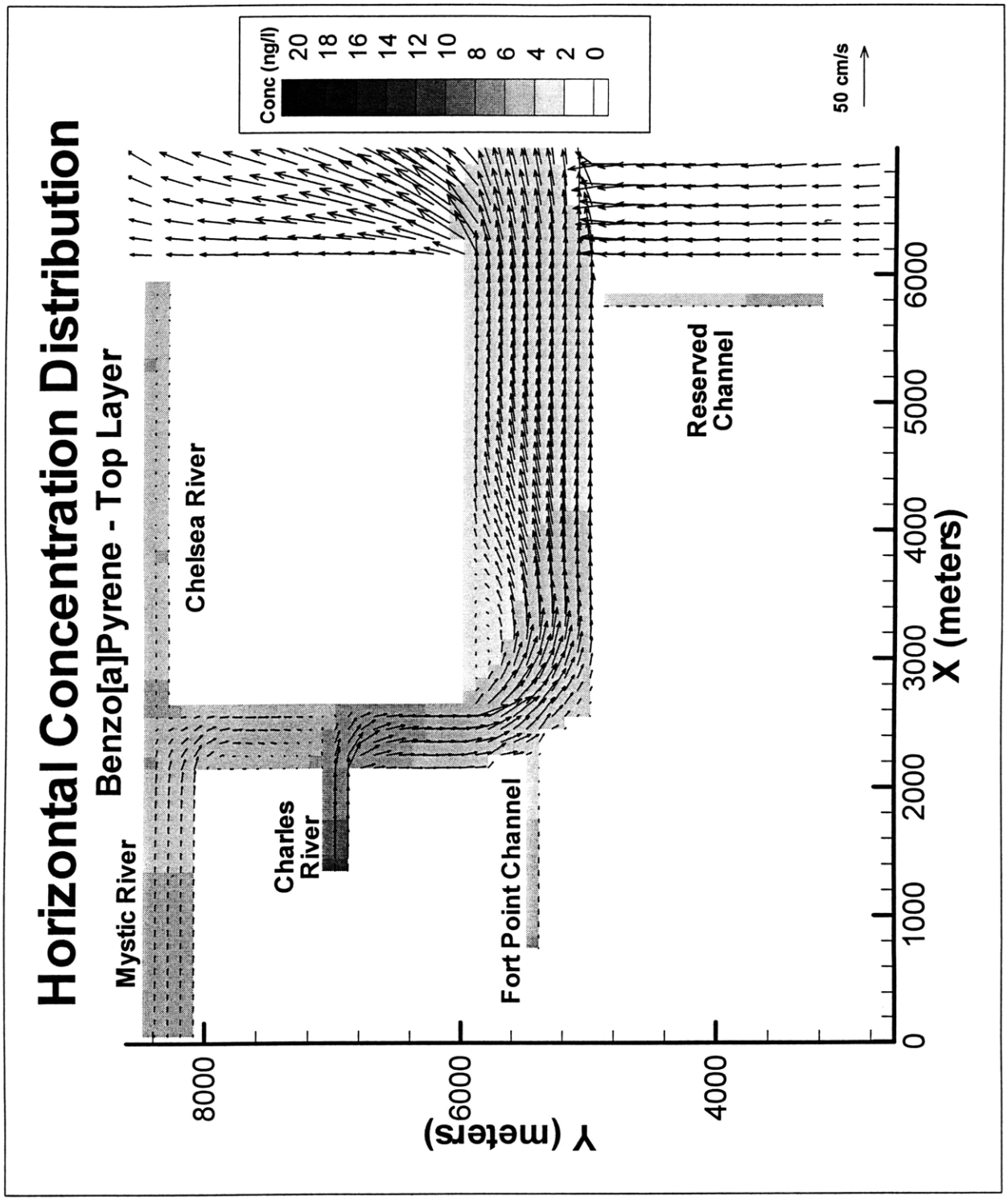

Figure D.4 – Flow and Concentration Distribution for Benzo[a]pyrene at the Surface at t= 123 hs (high tide)

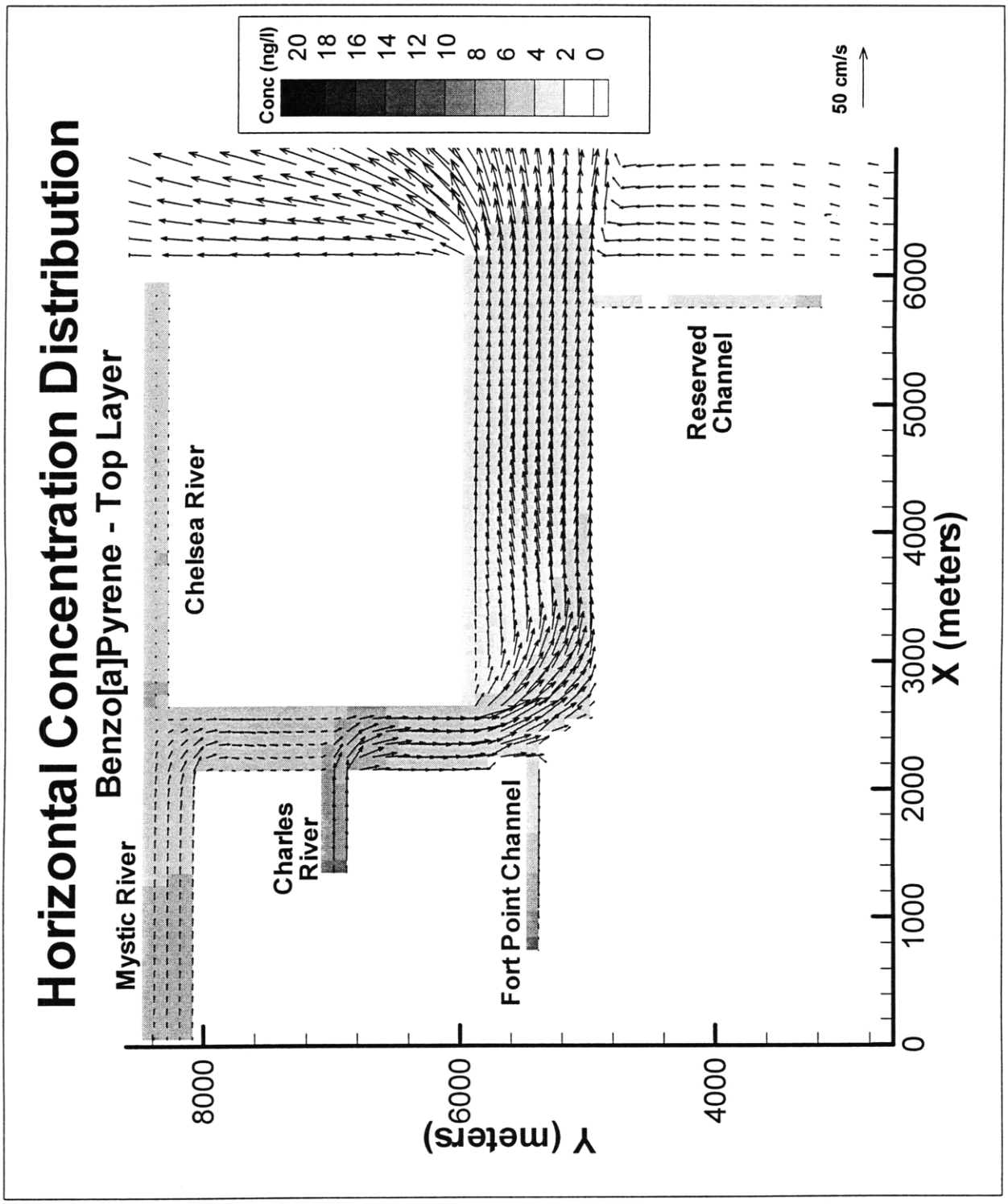

Figure D.5 – Flow and Concentration Distribution for Benzo[a]pyrene at the Surface at t = 126 hs (descending)

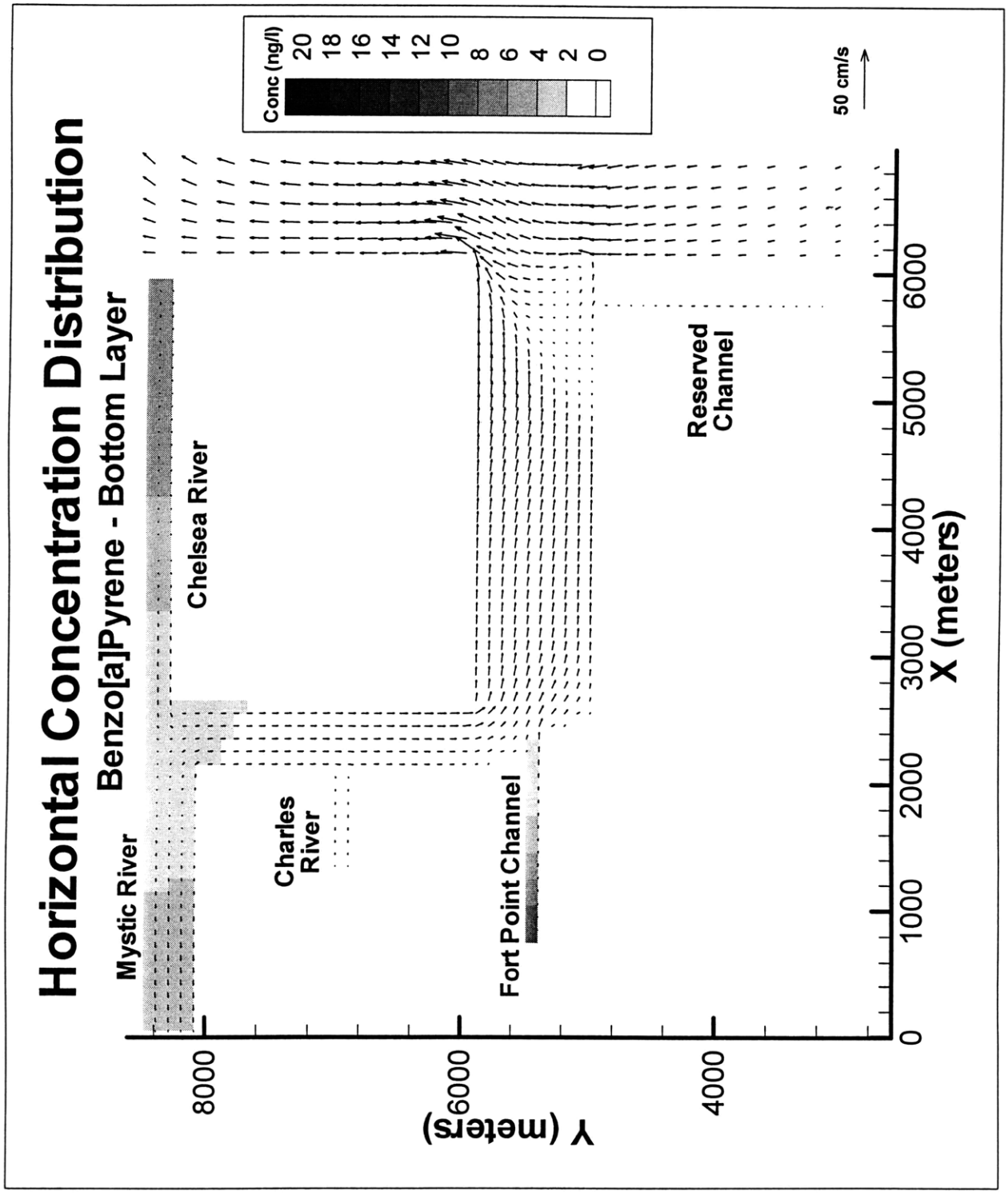

Figure D.6 – Flow and Concentration Distribution for Benzo[a]pyrene at about 1.5m from the Bottom at t = 114 hs (descending)

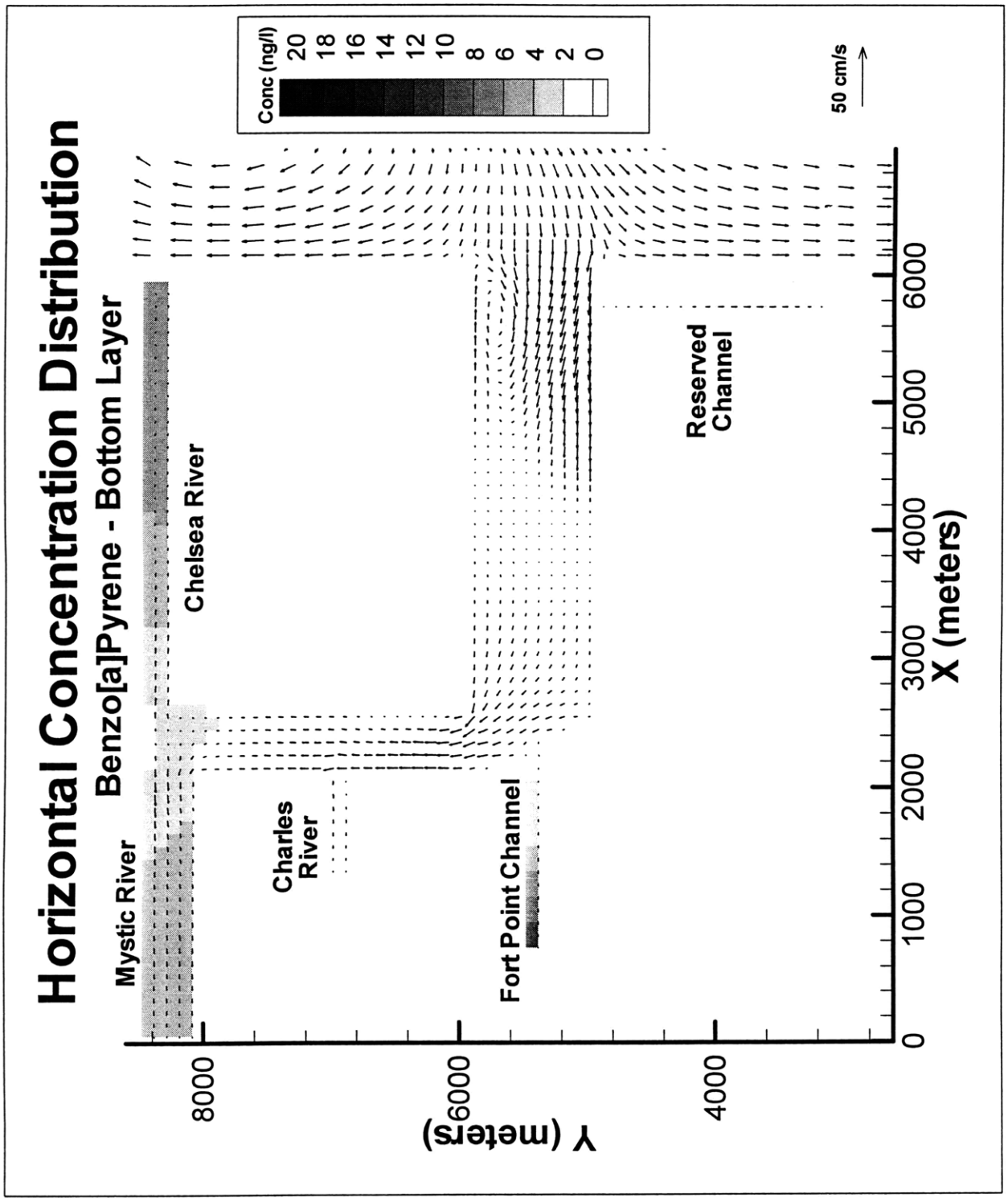

Figure D.7 – Flow and Concentration Distribution for Benzo[a]pyrene at about 1.5m from the Bottom at t = 117 hs (low tide)

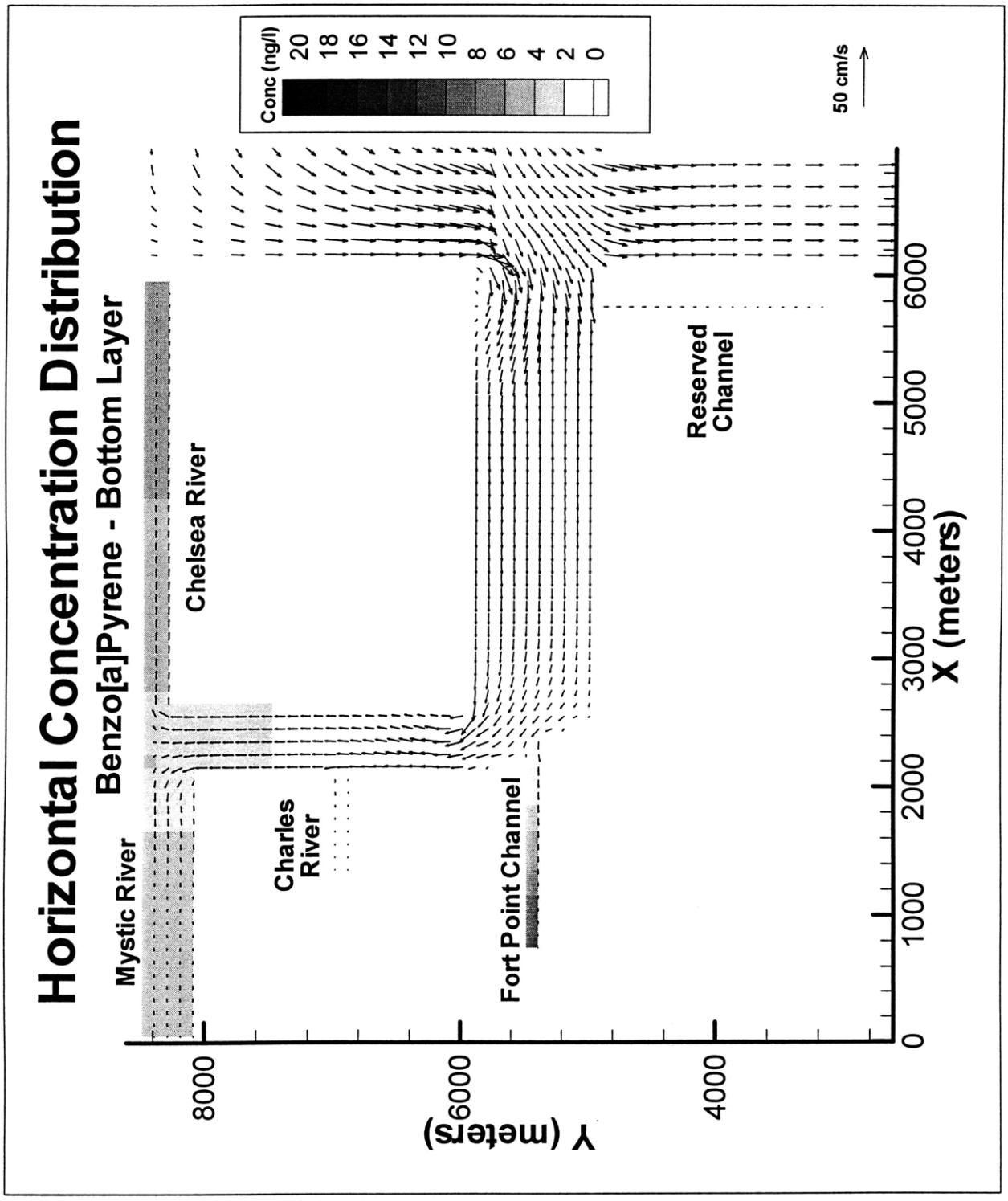

Figure D.8 – Flow and Concentration Distribution for Benzo[a]pyrene at about 1.5m from the Bottom at t = 120 hs (ascending)

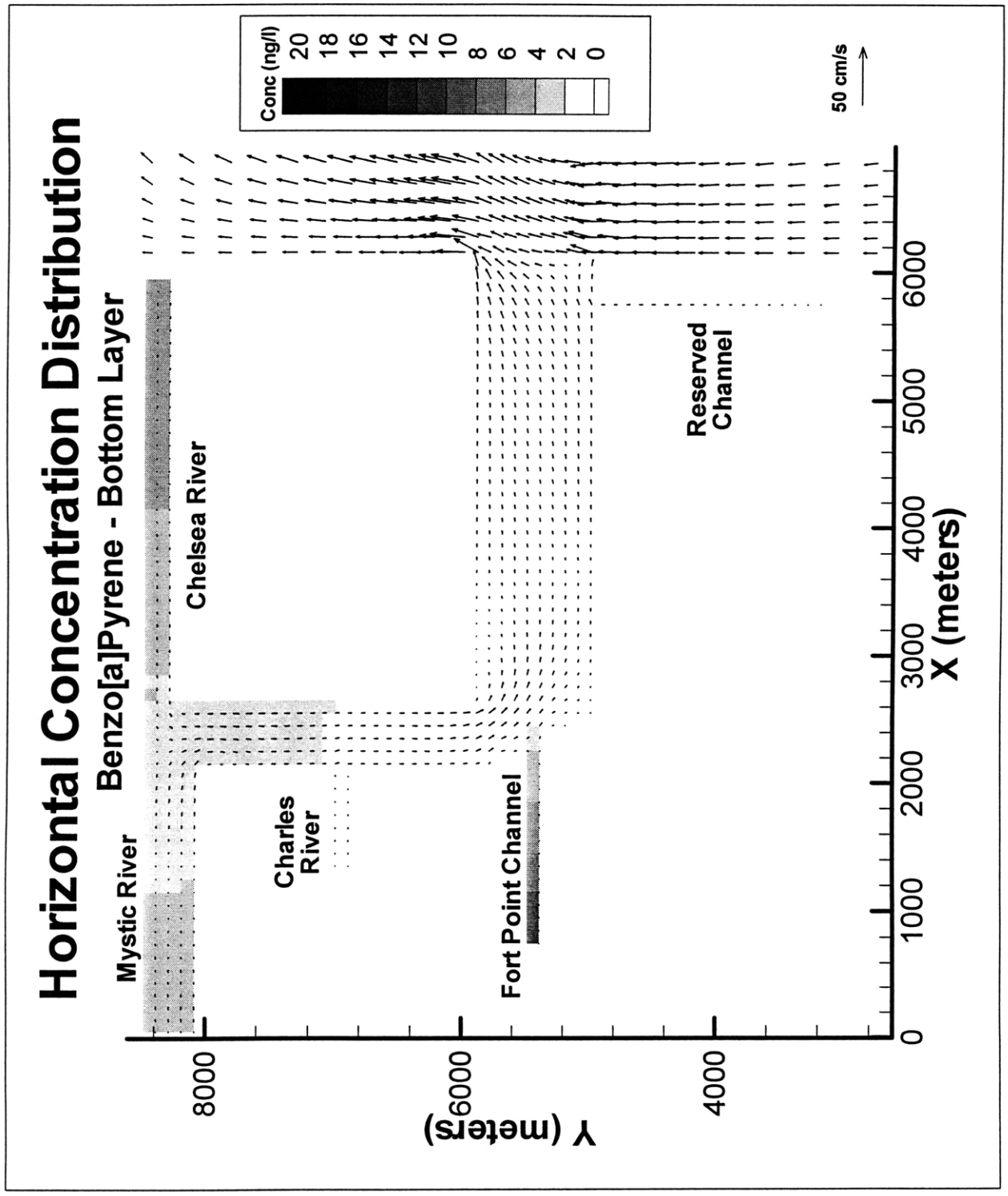

Figure D.9 – Flow and Concentration Distribution for Benzo[a]pyrene at about 1.5m from the Bottom at t = 123 hs (high tide)

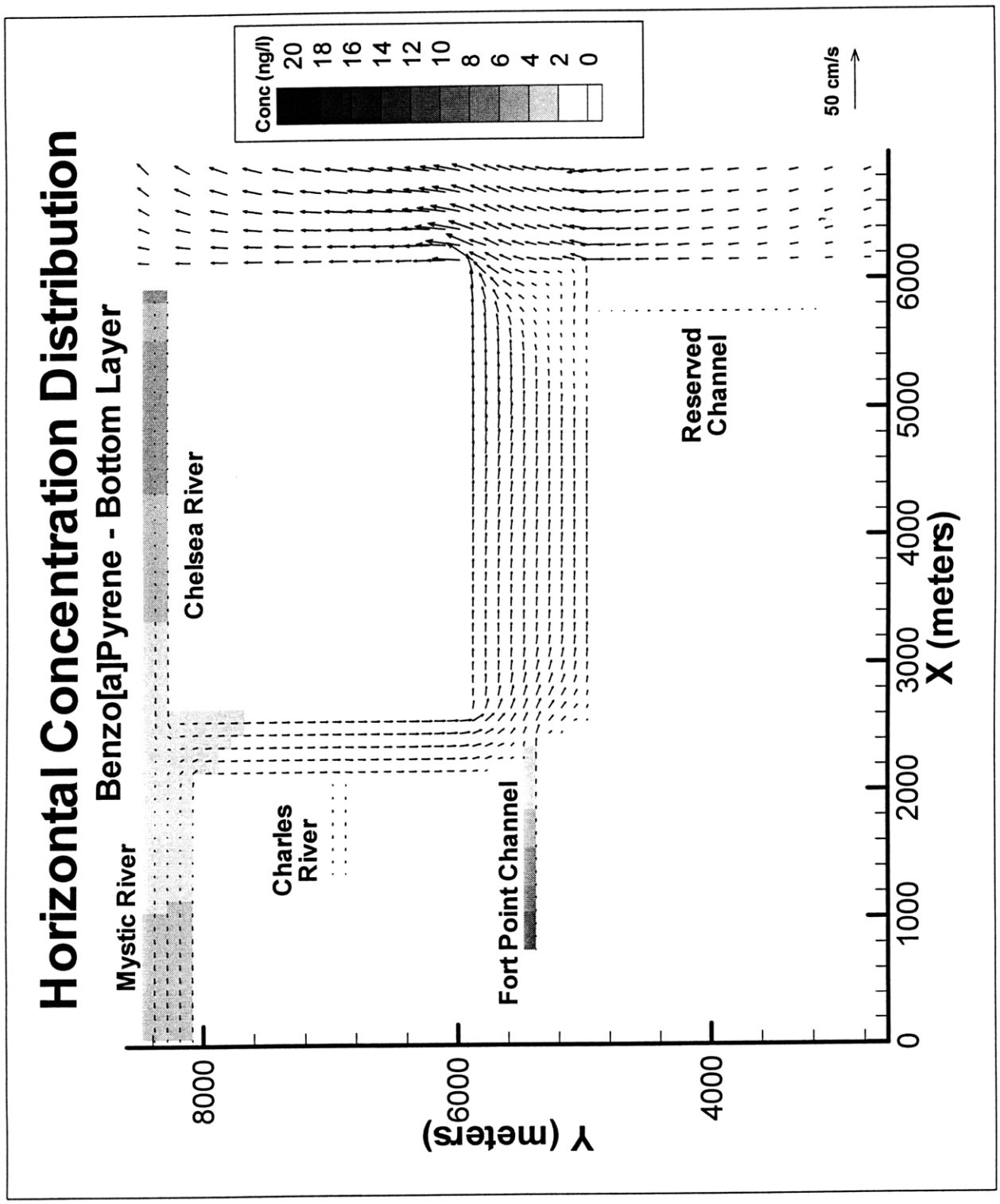

Figure D.10 – Flow and Concentration Distribution for Benzo[a]pyrene at about 1.5m from the Bottom at t = 126 hs (descending)